# The impact of mechanical stretch on the stability of desmosomes in epithelia

## Dissertation

zur

Erlangung des Doktorgrades (Dr. rer. nat)

der

Mathematisch-Naturwissenschaftlichen Fakultät

der

Rheinischen Friedrich-Wilhelms-Universität Bonn

vorgelegt von

**Pauline Laura Kinny** 

geb. Eichstedt

aus Hamburg

**Bonn, November 2024** 

Angefertigt mit Genehmigung der Mathematisch-Naturwissenschaftlichen Fakultät der Rheinischen Friedrich-Wilhelms-Universität Bonn

**Gutachter/Betreuer: Prof. Dr. Rudolf Merkel** 

**Gutachter: Prof. Dr. Ulrich Kubitschek** 

Tag der Promotion: 30.10.2025

Erscheinungsjahr: 2025

## **Abstract**

The mechanoresponse of epithelia is a well-known and essential process. Both cytoskeleton and cell adhesion sites react to mechanical stimuli, e.g. mechanical stretch. Cell adhesions like desmosomes act as connection sites in epithelia, they mediate cell-cell adhesion by providing mechanical strength and promoting an intercellular network by connecting the intermediate filaments between adjacent cells. Desmosomes are highly dynamic structures, which need to assemble and disassemble in order to adapt to an everchanging mechanical environment. This dynamic is put into excecution by protein exchange between the desmosomal structure and a pool of freely diffusing molecules in the cytoplasma. All in all, desmosomes are important sites of epithelial mechanoresponse, however, the research on desmosomes is predominantly based on experiments performed on static conditions. Therefore, little is known about the behaviour of desmosomal proteins, including their exchange kinetics upon mechanical stretch.

In order to address this knowledge gap, an experimental approach to analyse the responses of several desmosomal proteins to mechanical stretch was carried out within the scope of this thesis.

A monolayered epithelial system of MDCK (Madin-Darby Canine Kidney) cell lines stably expressing a fluorescently tagged desmosomal fusion protein was probed with FRAP (Fluorescence Recovery After Photobleaching) to analyse protein exchange kinetics of the desmosomal proteins DP (desmoplakin), PG (plakoglobin) and Dsc (desmocollin).

An experimental set-up with sealable silicone chambers was developed for cell stretching. The application of mechanical stretch was performed with a computer-controlled apparatus, the cell stretcher. Uniaxial, cyclic stretch with an 80 mHz (Millihertz) frequency was applied for a duration of 2 hours (h) to the analysed samples in live cell conditions.

The exchange kinetics of the desmosomal proteins DP, PG and Dsc were analysed at different time points after stretch in order to test the impact of mechanical stretch on the stability of desmosomes. The recovery curves displayed a biphasic ascent, indicating the presence of two distinct kinetic processes, free diffusion and exchange kinetics at the desmosomal sites.

To decide whether an exponential fit could be applied to the recovery curves, a straight was drawn between the first and the last point of the exponential fit while excluding the offset. If the maximum distance between this straight and the exponential fit was exceeding the standard deviation of the noise from the recovery curves this recovery curve was fitted with an exponential fit, otherwise, it was fitted with a linear fit.

This analysis has shown that, in the absence of mechanical stretch, the analysed desmosomal proteins are stable components of the desmosomal structure. Upon exposure to uniaxial, cyclic stretch PG and Dsc exhibit a reversible mechanoresponse, which expresses as an increase of their exchanging fraction. This mechanoresponse is not detectable 24 h after the stretching event.

In essence, this work analysed the exchange kinetic of desmosomal proteins under the influence of mechanical stretch.

# **Table of contents**

Abstract	V
Table of contents	vii
Abbreviations	ix
Figures	х
Tables	xiii
1. Introduction	1
1.1 Desmosomal structure and proteins	2
1.2 Adhesion and assembly of desmosomes	6
1.3 Protein exchange kinetics	7
1.4 Mechanical stretch and desmosomes	9
1.5 Aims of this thesis	11
2. Materials and methods	13
2.1 Materials and Devices	13
2.1.1 Consumables	13
2.1.2 Laboratory Devices	13
2.1.3 Imaging Equipment	14
2.1.4 Chemicals	14
2.1.5 Media & Buffers	16
2.1.6 Software	17
2.2 Methods	18
2.2.1 Cell culture	18
2.2.2 Western Blot	19
2.2.3. Cell stretching	22
2.2.4 Analysis of protein exchange kinetics	26
2.2.5 Data Analysis	33
3. Results	39
3.1 Desmocollin GFP is present as a fusion protein	42
3.2. Development of experimental set-up	43
3.2.1 Elastomer chambers	43
3.2.2. Cell lines	45
3.2.3 FRAP analysis	46
3.2.4 Correcting for artefacts	47

7 References	115
5. Outlook	
	110
4.2.2 The mechanoresponse of the desmosomal proteins is a reversible	
4.2.1 Upon uniaxial, cyclic stretch desmosomes adapt by an increase of the exfraction	xchanging 105
4.2 The desmosomal proteins PG, Dsc 2a NG and Dsc 2a GFP exhibit a mechano	oresponse
protein exchange	
4.1.1 Two kinetic processes shape the recovery of desmosomal proteins: Diffu	
4.1 In the absence of mechanical stretch, desmosomal proteins are stable comp	onents of
4. Discussion	
3.7.3 Desmosomal protein exchange kinetics after 24 h after mechanical stret	
3.7.1 Desmosomal protein exchange kinetics in the absence of mechanical stretch on desmosomal protein exchange kinetics	
3.7. Joint evaluation	
3.6.2 Fitted parameters	
3.6.1 Recovery curves	
3.6. Desmosomal protein exchange kinetics after 24 h after mechanical stretch	
3.5.2 Fitted parameters	
3.5.1 Recovery curves	
3.5. Effect of mechanical stretch on desmosomal protein exchange kinetics	66
3.4.2. Fitted parameters	60
3.4.1. Recovery curves	59
3.4. Desmosomal protein exchange kinetics in the absence of mechanical stretc	h59
3.3. Data Fit	50
3.2.5 Stretch	49

# **Abbreviations**

	Abbreviation
Airy Unit	AU
Desmocollin	Dsc
Desmoglein	Dsg
Desmoplakin	DP
Dublbecco's Modified Eagle's Medium	DMEM
Enhanced green fluorescent protein	EGFP
Fluorescence recovery after photobleaching	FRAP
Green fluorescent protein	GFP
Hertz	Hz
High calcium medium	НСМ
Hours	h
Kilodalton	kDa
Kilopascal	kPa
Laser scanning microscope	LSM
Low calcium medium	LCM
Lithium dodecyl sulfate	LDS
Madin-Darby Canine Kidney	MDCK
Millihertz	mHz
Minutes	min
NeonGreen	NG
Phosphate buffered saline	PBS
Plakoglobin	PG
Region of interest	ROI
Seconds	S
Sodium dodecyl sulfate – Polyacrylamid gel electrophoresis	SDS PAGE
United States	US

# **Figures**

The following figures where created with Biorender.com: Figure 1 to figure 25 and figure 47
Figure 1: The two morphological subunits of a desmosome
Figure 2: Desmosomal proteins5
Figure 3: Model of protein exchange at the desmosomal sites
Figure 4: Composition of a western blot
<b>Figure 5:</b> Elastomer chambers for cell cultivating, stretching and imaging of cellular monolayers. This graphic is a courtesy of J. Konrad22
Figure 6: Cell stretcher and chamber holder. This graphic is a courtesy of J. Konrad24
<b>Figure 7:</b> Workflow with the sealable elastomer chambers (part I). This graphic is a courtesy of J. Konrad
Figure 8: Workflow with the sealable elastomer chambers (part II). This graphic is a courtesy of J. Konrad
Figure 9: FRAP principle28
Figure 10: Experimental design of a FRAP analysis performed with MDCK Dsc 2a GFP cells32
Figure 11: Whittaker fit of the recovery curves
Figure 12: Protein identification of the Dsc 2a GFP cells by Western Blot
Figure 13: Elastomer chamber for FRAP experiments. This graphic is a courtesy of J. Konrad44
Figure 14: Imaging step of the experimental set-up. This graphic is a courtesy of J. Konrad44
<b>Figure 15:</b> Overview of continuous cellular monolayers of the different MDCK cell lines (PG, DP, Dsc 2a NG and Dsc 2a GFP)
<b>Figure 16:</b> An overview of a representative FRAP experiment with Dsc2a GFP cells in the absence of mechanical stretch
Figure 17: Details of the developed elastomer chamber within the experimental set-up50
<b>Figure 18:</b> Examples of the exponential as well as the linear fit with DP CTRL (above) and DP stretch (below) recovery curves
<b>Figure 19:</b> Examples of the exponential as well as the linear fit with DP CTRL+24 h (above) and DP stretch+24 h (below) recovery curves53

<b>Figure 20:</b> Examples of the exponential as well as the linear fit with Dsc2aNG CTRL (above) and Dsc2aNG stretch (below) recovery curves
<b>Figure 21:</b> Examples of the exponential as well as the linear fit with Dsc2aNG CTRL+24 h (above) and Dsc2aNG stretch+24 h (below) recovery curves
<b>Figure 22:</b> Examples of the exponential as well as the linear fit with Dsc2aGFP CTRL (above) and Dsc2aGFP stretch (below) recovery curves
<b>Figure 23:</b> Examples of the exponential as well as the linear fit with Dsc2aGFP CTRL+24 h (above) and Dsc2aGFP stretch+24 h (below) recovery curves
<b>Figure 24:</b> Examples of the exponential as well as the linear fit with PG CTRL (above) and PG stretch (below) recovery curves
<b>Figure 25:</b> Examples of the exponential as well as the linear fit with PG CTRL+24 h (above) and PG stretch+24 h (below) recovery curves
Figure 26: Recovery curves of the desmosomal proteins in absence of mechanical stretch
<b>Figure 27:</b> Boxplot of the offset of the desmosomal proteins DP, PG, Dsc 2a GFP and Dsc 2a NG in absence of mechanical stretch
<b>Figure 28:</b> Boxplot of the exchanging fraction of the desmosomal proteins DP, PG, Dsc 2a GFP and Dsc 2a NG in absence of mechanical stretch
<b>Figure 29:</b> Boxplot of the rate constant of the desmosomal proteins DP, PG, Dsc 2a GFP and Dsc 2a NG in absence of mechanical stretch
<b>Figure 30:</b> Boxplot of the lifetime of the desmosomal proteins DP, PG, Dsc 2a GFP and Dsc 2a NG in absence of mechanical stretch
<b>Figure 31:</b> Recovery curves of the desmosomal proteins DP, PG, Dsc 2a GFP and Dsc 2a NG after 2 h of mechanical stretch with a 50% amplitude at 80 mHz
<b>Figure 32:</b> Boxplot of the offset of the desmosomal proteins DP, PG, Dsc 2a GFP and Dsc 2a NG after 2 h of mechanical stretch with a 50% amplitude at 80 mHz
<b>Figure 33:</b> Boxplot of the exchanging fraction of the desmosomal proteins DP, PG, Dsc 2a GFP and Dsc 2a NG after 2 h of mechanical stretch with a 50% amplitude at 80 mHz70
<b>Figure 34:</b> Boxplot of the rate constant of the desmosomal proteins DP, PG, Dsc 2a GFP and Dsc 2a NG after 2 h of mechanical stretch with a 50% amplitude at 80 mHz72
<b>Figure 35:</b> Boxplot of the lifetime of the desmosomal proteins DP, PG, Dsc 2a GFP and Dsc 2a NG after 2 h of mechanical stretch with a 50% amplitude and 80 mHz.

<b>Figure 36:</b> Recovery curves of the desmosomal proteins 24 h after 2 h of mechanical stretch with a 50% amplitude at 80 mHz
<b>Figure 37:</b> Boxplot of the offset of the desmosomal proteins DP, PG, Dsc 2a GFP and Dsc 2a NG 24 h after 2 h of mechanical stretch with a 50% amplitude at 80 mHz77
<b>Figure 38:</b> Boxplot of the exchanging fraction of the desmosomal proteins DP, PG, Dsc 2a GFP and Dsc 2a NG 24 h after 2 h of mechanical stretch with an 50% amplitude at 80 mHz79
<b>Figure 39:</b> Boxplot of the rate constant of the desmosomal proteins DP, PG, Dsc 2a GFP and Dsc 2a NG 24 h after 2 h of mechanical stretch with an 50% amplitude at 80 mHz81
<b>Figure 40:</b> Boxplot of the lifetime of the desmosomal proteins DP, PG, Dsc 2a GFP and Dsc 2a NG 24 h after 2 h of mechanical stretch with an 50% amplitude at 80 mHz83
<b>Figure 41:</b> Boxplot of the joint offset of the desmosomal proteins DP, PG, Dsc 2a GFP and Dsc 2a NG in absence of mechanical stretch
<b>Figure 42:</b> Boxplot of the initial slope of the desmosomal proteins DP, PG, Dsc 2a GFP and Dsc 2a NG in absence of mechanical stretch
<b>Figure 43:</b> Boxplot of the joint offset of the desmosomal proteins DP, PG, Dsc 2a GFP and Dsc 2a NG after 2 h of mechanical stretch with a 50% amplitude at 80 mHz89
<b>Figure 44:</b> Boxplot of the initial slope of the desmosomal proteins DP, PG, Dsc 2a GFP and Dsc 2a NG after 2 h of mechanical stretch with a 50% amplitude at 80 mHz91
<b>Figure 45:</b> Boxplot of the joint offset of the desmosomal proteins DP, PG, Dsc 2a GFP and Dsc 2a NG 24 h after 2 h after mechanical stretch with a 50% amplitude at 80 mHz93
<b>Figure 46:</b> Boxplot of the initial slope of the desmosomal proteins DP, PG, Dsc 2a GFP and Dsc 2a NG 24 h after 2 h of mechanical stretch with an 50% amplitude at 80 mHz95
Figure 47: Model of diffusion and protein exchange at the desmosomal sites

# **Tables**

Table 1: MDCK cell lines provided by our cooperation partners	18
Table 2: Differences between MDCK cell lines during passaging	19
Table 3: Primary antibodies for Western Blot	21
Table 4: Secondary antibody for Western Blot.	21
<b>Table 5:</b> Number of independent samples and recovery curves of all desmosomal proteins and mechanical states	51
<b>Table 6:</b> Mean offset of the desmosomal proteins DP, PG, Dsc 2a NG and Dsc 2a GFP in the absence mechanical stretch, with their upper and lower confidence intervals (95%)	
<b>Table 7:</b> Mean exchanging fraction of the desmosomal proteins DP, PG, Dsc 2a NG and Dsc 2a GFP the absence of mechanical stretch, with their upper and lower confidence intervals (95%)	
<b>Table 8:</b> Mean rate constant of the desmosomal proteins DP, PG, Dsc 2a NG and Dsc 2a GFP in the absence of mechanical stretch, with their upper and lower confidence intervals (95%)	64
<b>Table 9:</b> Mean lifetime of the desmosomal proteins DP, PG, Dsc 2a NG and Dsc 2a GFP in the absent of mechanical stretch, with their upper and lower confidence intervals (95%)	
<b>Table 10:</b> Mean offset of desmosomal proteins DP, PG, Dsc 2a NG and Dsc 2a GFP after mechanical stretch (2 h, 50%, 80 mHz), with their upper and lower confidence intervals (95%)	
<b>Table 11:</b> Mean exchanging fraction of the desmosomal proteins DP, PG, Dsc 2a NG and Dsc 2a GFF after mechanical stretch (2 h, 50%, 80 mHz) with their upper and lower confidence intervals (95%)	
<b>Table 12:</b> Mean rate constant k of the desmosomal proteins DP, PG, Dsc 2a NG and Dsc 2a GFP after mechanical stretch (2 h, 50%, 80 mHz), with their upper and lower confidence intervals (95%)	
<b>Table 13:</b> Mean lifetime of the desmosomal proteins DP, PG, Dsc 2a NG and Dsc 2a GFP after mechanical stretch (2 h, 50%, 80 mHz), with their upper and lower confidence intervals (95%)	75
<b>Table 14:</b> Mean offset of the desmosomal proteins DP, PG, Dsc 2a GFP and Dsc 2a NG 24 h after mechanical stretch with their upper and lower confidence intervals (95%)	78
<b>Table 15:</b> Mean exchanging fraction of the desmosomal proteins DP, PG, Dsc 2a NG 24 h Dsc 2a GF 24 h after mechanical stretch (2 h, 50%, 80 mHz), with their upper and lower confidence intervals (95 mechanical stretch).	5%)
<b>Table 16:</b> Mean rate constant of the desmosomal proteins DP, PG, Dsc 2a NG and Dsc 2a GFP 24 h after mechanical stretch (2 h, 50%, 80 mHz), with their upper and lower confidence intervals (95%)	82

<b>Table 17:</b> Mean lifetime of the desmosomal proteins DP, PG, Dsc 2a NG, Dsc 2a GFP 24 h after mechanical stretch (2 h, 50%, 80 mHz), with their upper and lower confidence intervals (95%)84
Table 18: Mean joint offset of the desmosomal proteins DP, PG, Dsc 2a NG and Dsc 2a GFP, with their upper and lower confidence intervals (95%)
<b>Table 19:</b> Mean initial slope of the desmosomal proteins DP, PG, Dsc 2a NG and Dsc 2a GFP in the absence of mechanical stretch, with their upper and lower confidence intervals (95%)
<b>Table 20:</b> Mean joint offset of desmosomal proteins DP, PG, Dsc 2a NG and Dsc 2a GFP after mechanical stretch (2 h, 50%, 80 mHz), with their upper and lower confidence intervals (95%)90
<b>Table 21:</b> Mean initial slope of the desmosomal proteins DP, PG, Dsc 2a NG and Dsc 2a GFP after mechanical stretch (2 h, 50%, 80 mHz), with their upper and lower confidence intervals (95%)92
<b>Table 22:</b> Mean joint offset of the desmosomal proteins DP, PG, Dsc 2a GFP and Dsc 2a NG 24 h after mechanical stretch (2 h, 50%, 80 mHz), with their upper and lower confidence intervals (95%)94
<b>Table 23:</b> Mean initial slope of the desmosomal proteins DP, PG, Dsc 2a GFP and Dsc 2a NG 24 h after mechanical stretch (2 h, 50%, 80 mHz), with their upper and lower confidence intervals (95%)96

From an evolutionary perspective, epithelia provide tissue integrity to endure ever present mechanical stretch in the absence of a protective exoskeleton. This tissue integrity of epithelia is achieved by cell-cell contacts. Epithelia cells form two types of cell-cell-junctions, which have structural similarities but distinct molecular composition and functional properties: Adherens junctions and desmosomes<sup>1,2</sup>.

Adherens junctions are associated with the actin cytoskeleton and play an important role in the barrier function and adhesion of epithelia<sup>3</sup>. Desmosomes mediate cell-cell adhesion by providing mechanical strength and promoting an intercellular network by connecting the intermediate filaments between adjacent cells<sup>4,5</sup>. Compared to other cellular junctions, they are characterised by an extreme stability<sup>6</sup>. Therefore, desmosomes are predominantly found in mechanically challenged tissues, such as cardiac tissue or skin<sup>7</sup>. Loss of function, malfunctions or mutations of desmosomal proteins can entail severe diseases or disorders (<sup>8</sup>, reviewed in <sup>9</sup>), thus the correct functioning and stability of desmosomes is of substantial clinical importance.

Being the sites where mechanical stretch get transmitted throughout a tissue, desmosomes are subjected to substantial mechanical stretch. On the one hand, mechanical stretch acts as an important stimulus for a multitude of biological effects, i.e. cell differentiation, growth<sup>10</sup> and migration<sup>11</sup>. But on the other hand, exposition to excessive mechanical stretch leads to tissue damage<sup>12</sup> and pathological consequences<sup>13</sup>. Therefore, studying the stability of desmosomes without considering the influence of mechanical stretch limits the informative value of these investigations about the situation in vivo, because epithelial cells are constantly exposed to mechanical stretch. Mechanical stretch is known to alter desmosomal protein composition<sup>14</sup>, and more recent findings documented that mechanical stress also influences desmosomal stability which can further provoke the manifestation of disease phenotypes<sup>15</sup>. However, in the context of mechanical stretch and its impact on desmosomal stability, many questions remain unanswered.

In the following sections, the topics of desmosomes in relation to mechanical stretch is described further. Moreover, the underlying mechanism of protein exchange is charaterised, in order to provide a physicochemical basis for analysing the impact of mechanical stretch on desmosomal stability.

# 1.1 Desmosomal structure and proteins

Epithelia serve as protective barriers between the environment and an organism as well as between internal surfaces within an organism, not only concerning compounds and microorganism but also physical stimuli such as mechanical stretch<sup>16</sup>. Epithelia are mono- or multi-layered tissues characterised by a close formation of cells which are connected through various cell-cell contacts and often exhibit a polar differentiation between the apical and basal side<sup>17</sup>. Desmosomes are cell-cell contacts predominantly present in mechanically challenged tissues, such as cardiac tissue or skin<sup>7</sup> and appear as punctuate, intercellular structures on the plasma membrane<sup>18–20</sup>. The desmosomal structure itself is divided into two distinct morphological domains with their own unique protein composition<sup>21,22</sup> (Figure 1). The most important desmosomal proteins originate from three distinct gene families: The cadherins, armadillo proteins and plakins<sup>23</sup>.

- **1. The membrane core domain** mediates desmosomal adhesion between adjacent cells<sup>24</sup>. This domain is composed of transmembrane proteins termed cadherins and is bridging an intercellular space of 20-30 nm<sup>25</sup>. The desmosomal cadherins entail the transmembrane glycoproteins desmoglein (Dsg) and desmocollin (Dsc)<sup>26</sup>.
- **2. The cytoplasmic plaque** is located at the intracellular membrane, superjacent to the membrane core domain<sup>18</sup> and is responsible for the linkage to the intermediate filaments. The attachment to the intermediate filaments is mediated by DP, and the plaque proteins PG and plakophillin<sup>18,27</sup>.

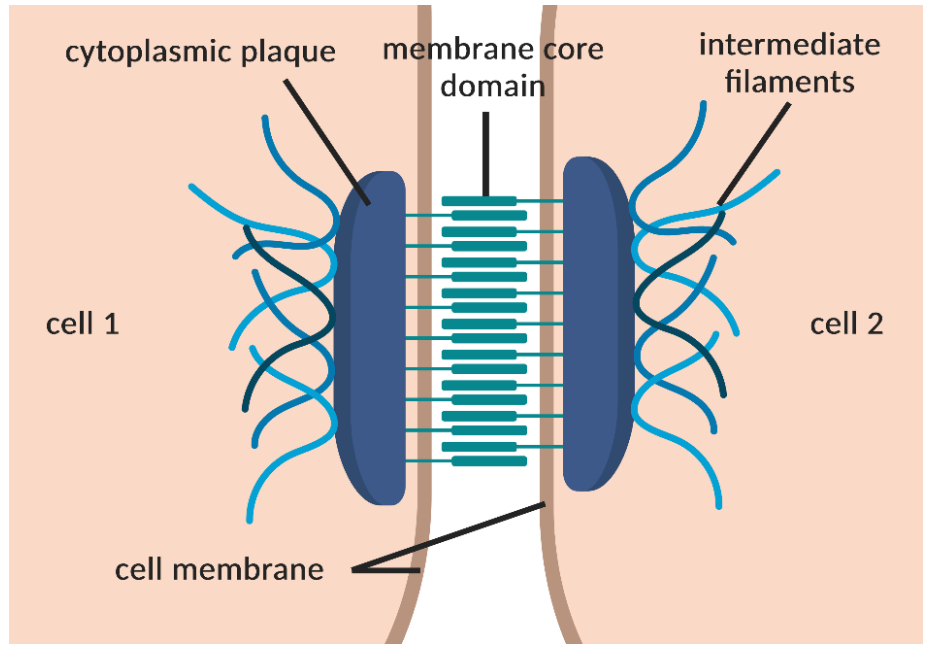


Figure 1: The two morphological subunits of a desmosome. The membrane core domain acts as a transmembrane domain and connects adjacent cells to one another. The cytoplasmic plaque is located at the intracellular membrane and conveys the linkage to the intermediate filaments.

The desmosomal cadherins Dsg and Dsc are calcium-dependent, glycosylated adhesion proteins with a tripartite structure<sup>28</sup>: The extracellular domain of Dsg and Dsc consists of multiple cadherin repeats, which are approximately 110 amino acids long, constitute the calcium dependent binding site. The binding sites of Dsg and Dsc adhere to each other via hetero- and homophillic interactions, although heterophilic interactions are preferred <sup>8,9,29,30</sup>. This interaction promotes the adhesive properties of the desmosomes<sup>31</sup>. While both Dsc and Dsg have a similar structure, their function seem to be more distinct, with Dsc being involved in the recruitment of other desmosomal proteins<sup>32</sup>. The desmosomal cadherins exist in different isoforms<sup>33</sup> and splice variants<sup>6</sup>, however, the isoforms Dsg 2 and Dsc 2 are the most common in humans<sup>33</sup>. All of the isoforms bind to the universal plaque protein PG.

Plaque proteins like PG convey the linkage between DP and the desmosomal cadherins<sup>34</sup>. Interestingly, PG is not a desmosomal specific protein, and is also present in adherens junctions<sup>35</sup>. PG has structural similarities to  $\beta$ -catenin, as both posess repeating amino acid motives termed armadillo-repeats<sup>36</sup> which give this type of

protein its name: armadillo proteins. The armadillo proteins include amongst others PG and plakophillin. PG binds to the intracellular domain of the desmosomal cadherins, including Dsc<sup>37</sup>.

DP is a member of the plakin family which is essential for the assembly of functional desmosomes<sup>38</sup>. DP mediates the linkage between the plaque proteins PG and plakophillin and the intermediate filaments<sup>39</sup>. Comparable to other proteins in the plakin family, DP is composed of a tripartite structure, consisting of a globular domain, a coiled-coil domain in the middle and a variable quantity of plakin-repeats<sup>40</sup>. Two predominant splice isoforms exist of DP<sup>41</sup>, which differ in slightly in their amino acid composition and molecular weight<sup>42</sup>. The localisation of the described proteins within the desmosomal structure is shown in figure 2.

The intermediate filament network is one of the three main cytoskeletal networks, which also include the actin filament network and microtubuli. The name refers to the average lenght of their filaments (10 nm), in comparison to the shorter actin filaments (7 nm) and longer microtubules (24 nm)<sup>43</sup>. Intermediate filaments are highly stable, as their main function is the preservation of tissue integrity and resistance to mechanical forces<sup>44</sup>. Interestingly, their response to mechanical stretch is force-dependent: Low forces and small extensions of the intermediate filaments result in an elastic response and high forces and bigger extension result in stiffening and hardening<sup>45</sup>. Intermediate filament proteins have a helical conformation which assemble in two-stranded coiled coils. As their composition within the intermediate filament network is tissue-specific, acidic and basic keratins are mainly expressed in epithelial cells<sup>46</sup>.

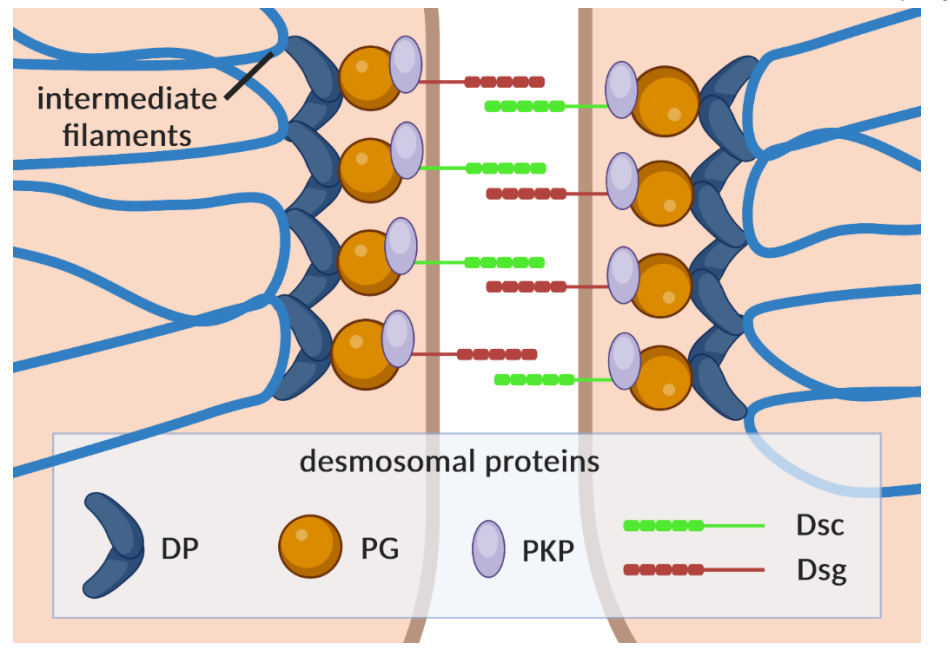


Figure 2: Desmosomal proteins. The transmembrane proteins Dsc and Dsg mediate the adhesion between the adjacent cells, the armadillo protein PG connects them to the other plaque proteins and DP conveys the linkage of the desmosomal structure to the intermediate filaments.

Adherens junctions are adhesive cell-cell-junctions that play in important role in the barrier function and rearrangement of epithelia<sup>47</sup> and also act as mechanosensors<sup>48</sup>. Analogous to desmosomes, adherens junctions are also compromised of a transmembrane domain linking the adjacent cells to one another, the cadherin-catenin complex, and plaque proteins which associate with the cytoskeleton. Additionally, the nectin-afadin complex takes on signalling as well as adhesive functions. However, this classification can merely serve as a rough distinction between the most prominent protein complexes required for the basic structure of adherens junctions<sup>3</sup>. Prominent adherens junction proteins include E-cadherin, p120, catenin,  $\beta$ -catenin,  $\alpha$ -catenin, nectin and afadin<sup>47</sup>. Adherens junctions are associated with the actin cytoskeleton, thus mediating cellular motility, migration, cytokinesis and phagocytosis<sup>49</sup>. This cytoskeletal network is comprised of the monomeric, globular G-actin wich polymerises into filaments, called F-actin<sup>50</sup>.

Even though desmosomes and adherens junctions are both independently associated with different cytoskeletal networks there is evidence of crosstalk between both cell-cell adhesions <sup>51–53</sup>.

# 1.2 Adhesion and assembly of desmosomes

In order to form desmosomal structures, the individual desmosomal proteins must be brought together. The desmosomal assembly occurs in a calcium dependent manner and is tunable by manipulating the extracellular calcium concentration<sup>54</sup>. Calcium ions bind to a binding site localized on the extracellular domain of desmosomal cadherins, resulting in a conformation change<sup>29</sup>. The desmosomal assembly can be induced by performing a calcium switch, thus, switching from low calcium medium (LCM, <0.05 mM calcium) to high calcium medium (HCM, 1.8 mM calcium)<sup>55</sup>.

Literature suggest that the assembly of desmosomal proteins into desmosomes is emanating upon a calcium switch from non-desmosomal protein pools<sup>56,57</sup> with kinetics which are unique to the respective proteins<sup>58</sup>. Depending on the desmosomal domain (cytoplasmic plaque and membrane core domain), the non-desmosomal pool is proposed to occur near the plasma membrane but still within the cytoplasm or within the plasma membrane<sup>9</sup>. For example, DP was shown to be present in the perinuclear region of cells cultivated in LCM and to be recruited within 1 h after a calcium switch to areas near the plasma membrane<sup>55</sup>. A similar distribution has been reported for Dsc and PG<sup>59</sup>. The recruitment of desmosomal proteins towards the desmosomal sites is coordinated by regulatory proteins<sup>60</sup>. Desmosomes are subjected to a constant circle of assembly and disassembly, which is regulated post-translationally<sup>61</sup>. Interestingly, the disassembled desmosomal proteins are not reutilised for the formation of new desmosomes<sup>56,62,63</sup>.

The calcium concentration plays an important role not only in the assembly of the desmosomal proteins, but also in the development of full adhesiveness. With regards to adhesiveness, the mere assembly of desmosomal proteins is not sufficient, and desmosmes undergo a process of maturation where desmosome adhesion eventually reaches a calcium independent state upon several days<sup>64</sup>. During this process of maturation, the desmosomal structure undergoes architectural changes<sup>65</sup>.

The extracellular calcium concentration is then no longer required to maintain intercellular adhesion. This calcium independent state is called hyperadhesion and – in contrast to adherens junctions – presents a unique feature of desmosomes<sup>33</sup>. Hyperadhesive desmosome have an enhanced intercellular adhesive strength<sup>66,67</sup>, and studies indicated that especially epithelia need hyperadhesion to resist the constant mechanical stresses to which they are subjected<sup>33</sup>.

# 1.3 Protein exchange kinetics

Desmosomes are highly dynamic structures, which need to assemble and disassemble in order to adapt to an everchanging mechanical environment. This dynamic is put into excecution by protein exchange between the desmosomal sites and a cytoplasmic pool. This protein exchange can be described with the following model in figure 3.

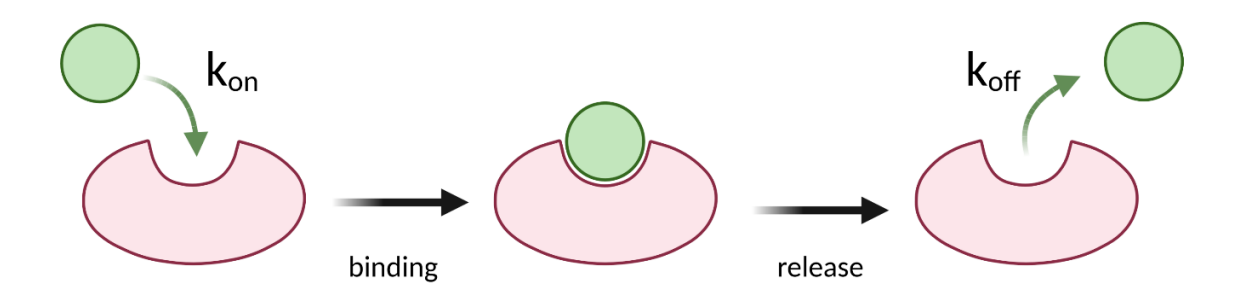


Figure 3: Model of protein exchange at the desmosomal sites. A freely moving desmosomal protein (green) occupies a binding site (red) with a specific exchange rate for the binding process ( $k_{on}$ ). Upon release, the protein leaves the binding site with a specific exchange rate for the unbinding (release) process ( $k_{off}$ ).

In this model, the desmosomal proteins (green) are freely moving in the cytoplasm until they eventually bind to immobile binding sites within the desmosomal structure (red). However, this model only holds true for the cytoplasmic plaque proteins. Membrane core proteins either diffuse within the plasmamembrane or are delivered via carriers<sup>9</sup>.

After binding, the binding sites are occupied. Upon release, these binding site are free to be occupied again. This cycle of binding and release is a random and time-dependent process and occurs at specific exchange rates, termed  $k_{on}$  for binding and

 $k_{off}$  for release. A mathematical approach for this model was presented by Lele et al., 2008.<sup>68</sup>. The probability for the binding of a protein to a binding site is dependent on  $k_{on}$ , the concentration c of the soluble protein and the ratio of available binding sites represented as 1-n, n being the fraction of binding sites which are occupied, which corresponds to a second-order reaction. The probability for release of a protein from a binding sites is dependent on  $k_{off}$ , and the number of occupied binding n. The change of n with time can be described as the ratio between occupied and total number of binding sites and can be calculated by following differential function:

$$\frac{\partial n(t)}{\partial t} = k_{on} * c * (1 - n(t)) - k_{off} n(t) \tag{1}$$

Upon integrating equation 1, the change of n over time can be described with the following function:

$$n(t) = \frac{k_{on} * c}{k_{on} * c + k_{off}} * (1 - e^{-(k_{on}*c + k_{off})*t})$$
 (2)

In this most general solution of equation 1 the exponential function is multiplied by a constant prefactor from the interval from 0 to 1. Due to the selected normalisation of the measured intensity (see section 2.2.5.1 for more details), this prefactor is 1. The ratio of free binding sites where a protein can bind with the rate constant k is described with the first term of equation 2 and termed  $\alpha$ . The rate constant k is described as  $k_{on}*c + k_{off}$ . Equation 2 can then be simplified to (equation 3):

$$n(t) = \alpha * (1 - e^{-k*t}) + \beta$$
 (3)

With

$$k = k_{on} * c + k_{off} \tag{4}$$

Equation 3 describes the exchange happening at the binding sites within the desmosomal structure. The desmosomal proteins present in the cytoplasmic pool on the other hand are freely moving in the cytoplasm of the cell. This process can be described with Einsteins diffusion equation<sup>69,70</sup>. The diffusion constant D indicates the mean square displacement of a protein assuming a three-dimensional Brownian

movement and the mean can be described with equation 5, with x being the distance along a linear axis (reviewed in  $^{71}$ ):

$$D = \frac{\langle x^2 \rangle}{6t} \tag{5}$$

These considerations regarding the protein exchange kinetics and diffusion are based on the assumption that these molecular interactions take place in a three dimensional space and that for other dimensionalities, other laws are applicable<sup>72</sup>. The protein exchange at the desmosomal sites can be linked to changes in their stability and adhesive properties<sup>73</sup>.

## 1.4 Mechanical stretch and desmosomes

In epithelial cells, mechanical stretch is processed through a perpetual "cycle of mechanosensing, mechanotransduction and mechanoresponse". The terms mechanosensing and mechanotransduction refer to the percipience and transduction of mechanical cues into a biochemical signals, often through mechanosensory proteins. Upon a mechanical stimulus, these proteins undergo conformational changes that expose phosphorylation or binding sites or allow allosteric regulation". Mechanical stimuli are transmitted to the nucleus and are then leading to a change in gene transcription". The mechanoresponse is then a functional feedback of the cell and can entail alterations in protein composition, cytoskeletal rearrangement and changes in cellular morphology.

On a cellular level, the mechanoresponse can look very differently depending on the nature of the mechanical stretch. For example, an immediate response to constant mechanical stretch can entail the lengthening of the body of the cell and reorientation in the direction of stretch<sup>77</sup>. Cyclic mechanical stretch on the other hand can cause the exact opposite, as cells tend to arrange themselves perpendicular to the direction of stretch<sup>78–80</sup> in order to reduce and intracellular mechanical stress and maintain cellular homeostasis<sup>81</sup>.

In this context, the duration of the mechanical stimulus is important: When exposed to short times of mechanical stretch – ranging from milliseconds to seconds – the cytoskletal networks often begin to rearrange themselves<sup>82,83</sup> whereas longlasting mechanical stretch leads to semi-permanent reorientation of the cell's morphology<sup>84</sup>.

Desmosomes act as connection sites of the intermediate filament cytoskeleton. Despite their prominent role in the transmission of mechanical stimuli, the potential mechanosensing role of desmosomes has not been fully explored yet<sup>85</sup>. Adherens junctions are well-known mechanosensing structures<sup>86</sup> which undergo alteration in response to internal and external mechanical stimuli<sup>87</sup>. They are therefore perceived as the "mechanosensing" cell-cell contact, whereas desmosomes were deemed to fulfill a more passive and safeguarding role by providing mechanical stability<sup>88,89</sup>. However, recent findings suggest an involvement in the process of mechanosensing and mechanotransduction of several desmosomal proteins<sup>90,91</sup> even though the underlying molecular mechanism remains unclear<sup>92</sup>.

## 1.5 Aims of this thesis

The previous sections described the role of desmosomes in the transmission of mechanical stretch in epithelia. Desmosomes have been characterised as important structures which maintain tissue integrity and stability. As desmosomes are very dynamic structures, desmosomal proteins are constantly exchanged at the desmosomal sites. In this thesis, the protein exchange kinetics of desmosomal proteins is used as a measure to investigate the stabilty of desmosomes under the impact of mechanical stretch.

As silicone substrates are a well established method to investigate mechanical stretch<sup>93–97</sup>, a similiar experimental set-up was chosen to conduct the experiments for this thesis. Sealable elastomer chambers were developed to address the technical requirements, e.g. imaging with an inverse laser scanning microscope (LSM). Cellular monolayer were seeded onto these elastomer chambers and were incubated 24 h for the desmosomes to mature. This incubation period was a compromise between the necessary maturation process of desmosomes (which can take up to a few days<sup>64</sup>) and the nessecity to reduce the risk of contamination within the samples.

The analysis of the protein exchange kinetics was limited to three different desmosomal proteins originating from the two major desmosomal domains (Dsc, PG and DP). These proteins were chosen due to their association as well as their position within the different morphological domains of the desmosomal structure and their unique functions: DP is the linker between desmosomal structure and intermediate filaments and has been found essential for desmosome formation<sup>98</sup>. PG mediates the attachement of the cytoplasmic plaque domain to the desmosomal cadherins of the membrane core domain and has therefore an important architectural role<sup>35</sup>. Dsc was selected as a representative of the desmosomal cadherins which constitute the membrane core domain. The cytoplasmic plaque domain and the membrane core domain are not only morphologically distinct. Due to their individual positions in the desmosmal architecture their exposure to mechanical stretch is different. This selection

of proteins contributes to a more thorough analysis in which the mechanical role of the desmosomes is represented in its entirety. In the experiments conducted for this thesis, MDCK cells were used as a model organism. Due to their many advantagous properties - fast growth-rate, high applicability for confocal imaging, their display of polarity in cell culture - these cells are a popular choice for the analysis not only of epithelial tissues<sup>99</sup>, but also desmosomes<sup>21,23,25,62,100,101,25</sup>. Within the scope of this thesis, these characteristics are as well sought-after. Obviously, a multilayered keratinocyte system, as described in Püllen et al. 102, would come closer of the situation in vivo compared to a monolayered MDCK system, however, were too fragile and too susceptible for contamination for the experiments planned in the scope of this thesis. Nevertheless, many essential research in the field of desmosomes and the intermediate has been conducted with monolayered MDCK cells<sup>56,103,104</sup>. As a monolayered MDCK system is a tried and tested model, it is suited for the purpose of this thesis: Analysing the of desmosomal exchange kinetics proteins investigate possible and mechanosensitivity.

The materials and devices utilised in the scope of this thesis are described in the following chapter.

# 2.1 Materials and Devices

## 2.1.1 Consumables

Product	Manufacturer
Syringe (2 mL)	B. Braun, Melsungen, Germany
6-well plate	Greiner Bio-one, Frickenhausen, Germany
Blotting paper for western Blot (7*10 cm)	VWR, Radnor, Pennsylvania, United States (US)
Cell culture flasks T25/T75	Corning, Corning, New York, US
Cell scraper with 18 cm handle	Corning, Corning, New York, US
Cover slip (ø 22 mm, #0)	Menzel, Braunschweig, Germany
Immersion oil W (2010)	Carl Zeiss, Jena, Germany
Western blot gels (Mini Protean TGX gels)	Bio-Rad, Hercules, California, US
Needle (100 sterican, 0.55*25mm)	B. Braun, Melsungen, Germany
Nitrocellulose blotting membrane	Cytiva, Little Chalfont, UK
Pipette tips (10 μL, 200 μL, 1250 μL)	StarLab, Hamburg, Germany
Reaction tube (1.5 mL, 2 mL)	Eppendorf, Wesseling/Berzdorf, Germany
Reaction tube (15 mL, 50 mL)	Corning, New York, US
Lens cleaning tissue (Whatman, 100*150 mm)	Global Life Sciences, Dassel, Germany

# 2.1.2 Laboratory Devices

Hardware	Company
Centrifuge (3-16L) with swing bucket rotor 11180	Sigma, Osterode, Germany
Centrifuge (5430 R)	Eppendorf, Wesseling/Berzdorf, Germany
Clean bench (HeraSafe KS)	Thermo Fisher Scientific, Waltham, US
Cell counter (Moxi Z Mini automated cell counter)	Biofrontier Technology, Singapore

## 14

## 2. Materials and methods

Hardware	Company
CO <sub>2</sub> - Incubator (Hera cell vios 160i)	Thermo Fisher Scientific, Waltham, US
Heating block (Dry Block heater)	Mettler-Toledo, Columbus, Ohio, US
Vacuum Pump (Integra Vacusafe)	Integra biosciences, Zizers, Switzerland
Western blot system (Mini Trans-Blot cell)	Bio-Rad, Hercules, California, US
Western blot system component (Mini-Protean tetra Systems)	Bio-Rad, Hercules, California, US
Osmometer (Osmomat 030)	Gonotec, Berlin, Germany
Power supply for electrophoresis (PowerPac Basic)	Bio-Rad, Hercules, California, US
Scale (new classic MF MS105DU)	Mettler-Toledo, Columbus, Ohio, US
Ultrapure Water System (Sartorius Arium PRO)	Thermo Fisher Scientific, Waltham, US
Vortex mixer	VWR, Radnor, Pennsylvania, US
Water bath (WNB-22)	Memmert, Schwabach, Germany

# 2.1.3 Imaging Equipment

Microscope	Company
Confocal Laser Scanning Microscope (LSM 880)	Carl Zeiss, Jena, Germany
Upright microscope (Axio Imager M2)	Carl Zeiss, Jena, Germany
Objective	Company
LD C-Apochromat 40x/1.1 W Korr M27	Carl Zeiss, Jena, Germany

## 2.1.4 Chemicals

Substance	Manufacturer
2-Amino-2(hydroxymethyl)-1,3-propanediol (Tris base)	Sigma, Taufkirchen, Germany
4x Laemmli sample buffer	Bio-Rad, Hercules, California, US
5-Bromo-4-chloro-3-indolyl phosphate/nitro blue tetrazolium (BCIP/NBT) liquid substrate system	Sigma, Taufkirchen, Germany
Calcium chloride dehydrate, GR for analysis	Merck, Darmstadt, Germany
Disodium phosphate, GR for analysis	Merck, Darmstadt, Germany

	Z. Materials and methods	
Substance	Manufacturer	
Dublbecco's Modified Eagle's Medium with high glucose	Thermo Fisher Scientific, Waltham,	
(DMEM 1x GlutaMAX –I)	Massachusetts, US	
Ethanol absolute, ACS reagent	Sigma, Taufkirchen, Germany	
Fetal Bovine Serum (FBS) Premium (South American origin)	Thermo Fisher Scientific, Waltham,	
	Massachusetts, US	
Glycine (suitable for electrophoresis, ≥99%)	Sigma, Taufkirchen, Germany	
Hibernate-E Medium	Thermo Fisher Scientific, Waltham, US	
Human fibronectin	Corning, Corning, New York, US	
Isopropanol, technical grade	LGC, Wesel, Germany	
Methanol, ACS reagent	VWR, Radnor, Pennsylvania, US	
Milk powder, blotting grade	Roth, Karlsruhe, Germany	
Penicillin-Streptomycin	Thermo Fisher Scientific, Waltham,	
	Massachusetts, US	
Potassium dihydrogen phosphate, GR for analysis	Merck, Darmstadt, Germany	
Protease inhibitor cocktail (P8340)	Sigma, Taufkirchen, Germany	
Protein ladder for electrophoresis (Precision Plus Protein	n Bio-Rad, Hercules, California, US	
Kaleidoscope)		
Radioimmunoprecipitation assay buffer (RIPA) buffer	Thermo Fisher Scientific, Waltham,	
	Massachusetts, US	
Silicone elastomer formulation (SORTA-Clear 12)	Smooth-on, Macungie, Pennsylvania, US	
Sodium chloride, p.a.	Sigma, Taufkirchen, Germany	
Sodium phosphate dibasic dodecahydrate, p.a.	Merck, Darmstadt, Germany	
Sulfuric acid 0.05 mol/L, GR for analysis	Merck, Darmstadt, Germany	
Trypsin-EDTA Solution (0.5 g porcine trypsin and 0.2 g EDTA)	Sigma, Taufkirchen, Germany	
β-mercaptoethanol, molecular biology grade	Merck, Darmstadt, Germany	

## 2.1.5 Media & Buffers

## **MDCK** cell medium

Components	Amount
DMEM 1x GlutaMAX –I	50 mL
FBS	10% (v/v)
Penicillin/Streptomycin	1% (v/v)

# **High calcium MDCK cell medium**

Components	Amount
DMEM 1x GlutaMAX –I	50 mL
FBS	10% (v/v)
Penicillin/Streptomycin	1% (v/v)
Calcium	1.8 mM

# Phospate-buffered saline (PBS) buffer for cell culture (10x), pH 8.0

Components	Amount
Sodium chloride	90 g/L
Potassium dihydrogen phosphate	14.4 g
Sodium phosphate dibasic dodecahydrate	10.63 g
Ultrapure water	Ad. 1 L
2M sodium hydroxide	For adjustment of pH value

## **Transfer buffer for western blot**

Components	Amount
Methanol	200 mL
Tris Base	3.03 g/L
Glycine	14.4 g/L
Ultrapure water	Ad. 1 L

# Laemmli buffer for western blot (10x)

Components	Amount
Tris Base	30.3 g/L
Glycine	14.1 g/L
SDS in ultrapure water	1% (v/v)
Ultrapure water	Ad. 1 L

# **Blocking solution for western blot**

Components	Amount
PBS	50 mL
Milk powder	5% or 1% (v/v), see section 2.2.2.4

## 2.1.6 Software

Software name	Company
Microscope control software (Zen black 2.3 SP1 FP3 2015)	Carl Zeiss, Jena, Germany
Microscope control software (Zen blue 2.3 lite 2011)	Carl Zeiss, Jena, Germany

## 2.2 Methods

#### 2.2.1 Cell culture

#### 2.2.1.1 Cells

MDCK cells expressing a stably incorporated fusion protein where a respective desmosomal protein is fluorescently tagged (either with Green Fluorescent Protein (GFP), Enhanced Green Fluorescent Protein (EGFP) or NeonGreen (NG)) were kindly provided by our cooperation partners (table 1 below). The MDCK cells were cultivated in MDCK cell medium at 37 °C, 5% CO<sub>2</sub> and humidified atmosphere.

Cell lines	Provided by
MDCK Desmocollin 2a GFP	Prof. Leube and Prof. Windoffer (Institute of Molecular and Cellular Anatomy, Uniklinik RWTH Aachen, Aachen)
MDCK Desmocollin 2a neon green	Prof. Ballestrem (Faculty of Biology, Medicine and Health, University of Manchester, Manchester)
MDCK Plakoglobin neon green  MDCK Desmoplakin EGFP	

Table 1: MDCK cell lines provided by our cooperation partners. More details can be found in the corresponding publications: For the Dsc 2a GFP cells, please refer to Windoffer et al.  $2002^{59}$ , and for the Dsc 2a NG, as well as the PG and DP cells, to Fülle et al., $2021^{105}$ .

## 2.2.1.2 Passaging of MDCK cells

Except for varying trypsin incubation times and concentration while re-seeding (table 2), the different MDCK cell lines were treated the same during passaging. The MDCK cells were passaged every 3 days or when they reached 90-100% confluency. For passaging, the MDCK medium was removed from the flask and the cell monolayer washed twice with 1 mL PBS to remove detached cells and serum protein residues present in the medium. To detach the cells from the flask, 1 mL trypsin (concentration 0.05% in PBS) was added and the flask was incubated for 8 – 18 minutes (min) depending on the cell line. After incubation, 3 mL MDCK medium was added to neutralize the trypsin and the detached cells were suspended and transferred to a new Falcon tube using a 5 mL pipette. After centrifugation at 122 g for 5 min a number of

300 000 – 500 000 cells (depending on the cell line) was determined using a Moxi Z Mini automated cell counter, suspended with MDCK cell medium and transferred into a new T25 flask. For cultivation on elastomer chambers, a density of 100 000 cells was seeded per chamber. The designated area has a 248 mm<sup>2</sup> surface. In order for the desmosomes to fully develop, freshly prepared high calcium MDCK medium was used for this step.

Cell type	Trypsin incubation time [min]	Cell count during re-seeding
MDCK Desmocollin GFP	8-10	500 000/T25 flask
MDCK Desmocollin 2a neon green	12-14	300 000/T25 flask
MDCK Plakoglobin neon green	16-18	300 000/T25 flask
MDCK Desmoplakin EGFP	16-18	300 000/T25 flask

Table 2: Differences between MDCK cell lines during passaging.

#### 2.2.2 Western Blot

To determine if the expected fusion protein was present in the cell line, the Dsc 2a GFP cells were analysed with western blotting.

### 2.2.2.1 Isolation of Dsc 2a GFP proteins

For the isolation of the Dsc 2a GFP proteins, the MDCK medium was subtracted from a T25 flask and the cell monolayer washed twice with ice-cold PBS to remove detached cells and serum protein residues. All subsequent steps were then performed on ice. The lysis buffer (RIPA buffer) containing 1:100 proteinase inhibitor cocktail was then added to the flask and the cell monolayer was removed with a cell scraper. The proteinase inhibitor cocktail and the refrigeration prevents the cellular proteases from digesting its own proteins. The cell suspension was then transferred into a 1.5 mL Eppendorf tube and pipetted up and down using a 2 mL syringe to break down the cell membrane and dissolves the proteins in the suspension. To remove cell debris, the suspension was centrifuged at 10 000 g for 10 min at 4°C and the supernatant then transferred into another 1.5 mL Eppendorf tube. Afterwards, 4x Lämmli buffer and  $\beta$ -mercaptoethanol were added and heated at 95 °C for 5 min. The heat as well as the lithium dodecyl

sulfate (LDS) contained in the 4x Lämmli buffer causes the proteins to denature, whereas the  $\beta$ -mercaptoethanol disrupts disulphide bonds and breaks up the tertiary and secondary structure of the proteins. The LDS accumulates at the thereby linearized proteins which causes them to be negatively charged. The protein suspension was either stored at -20 °C or immediately used in Sodium Dodecyl Sulfate – PolyAcrylamid Gel Electrophoresis (SDS-PAGE).

#### 2.2.2.2 SDS-PAGE

Prior to loading the proteins onto the gel, the wells were flushed twice with Lämmli buffer (see section 2.1.5) to remove remaining buffer. The outer wells were used for the protein ladder. During SDS gel electrophoresis, the linearized and negatively charged proteins migrate through the gel dependent on their size. SDS gel electrophoresis was performed for 10 min at 80 V to first achieve an accumulation of the proteins, then followed by 1 hour at 120 V for optimal separation.

#### 2.2.2.3 Transfer on nitrocellulose membrane

After completion of the SDS-PAGE, a western blot was conducted to transfer the proteins inside the gel onto a nitrocellulose membrane. In order to execute the western blot two sponges, two Whatman filter papers, a SDS gel and a nitrocellulose membrane facing the anode were assembled figure 4.

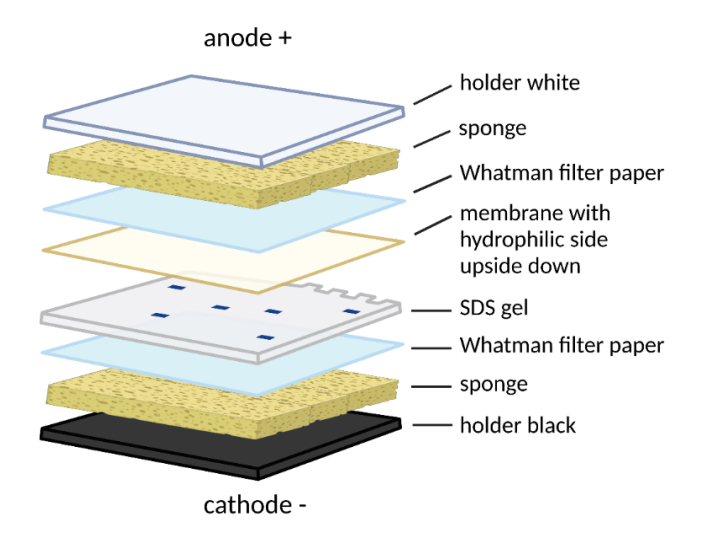


Figure 4: Composition of a western blot. From anode to cathode, one blot sponge, one Whatman filter paper, the nitrocellulose membrane with the hydrophilic side facing the cathode, the SDS gel followed by another Whatman filter paper and another sponge were assembled.

The western blot was performed for 90 min at 4 °C in freshly prepared transfer buffer (see section 2.1.5) to transfer the proteins onto the nitrocellulose membrane. After blotting, the nitrocellulose membrane was placed overnight in blocking solution containing 5% milk powder (see section 2.1.5) for blocking unspecific binding sites.

## 2.2.2.4 Immunological staining of protein bands

Incubation with the primary antibody directed against the target protein was performed with a 1:1000 or 1:500 dilution in blocking solution containing 1% milk powder for 24 h at 4 °C (table 3 below). The membrane was washed with PBS three times for 5 min each. Incubation with the secondary antibody directed against the host species of the primary antibody was performed with a 1:1000 dilution in blocking solution containing 1% milk powder for 1 hour at room temperature (table 4 below). After incubation with the secondary antibody, the washing step was repeated, and the membrane developed with BCIP/NBT liquid substrate system. The alkaline phosphatase coupled to the secondary antibody induces a reaction where BCIP is hydrolysed resulting in a blue coloured substrate. NBT concurrently gets reduced to a final product which appears blue. After 10 min, the reaction was stopped by discarding the BCIP/NBT liquid substrate system and washing twice the membrane with ultrapure water. The resulting bands were documented and analysed qualitatively after drying the membrane.

Target	Antibody	Host species	Dilution
Dsc 2	Anti-Desmocollin 2 antibody (ab23003a from abcam,	rabbit	1:1000
	Cambridge, UK)		
GFP	Anti-GFP polyclonal antibody (A-11122 from invitrogen at	rabbit	1:500
	Thermo Fisher Scientific, Waltham, USA)		

Table 3: Primary antibodies for Western Blot.

Antibody	Host species	Dilution
Anti rabbit (A3812 from Sigma, Osterode, Germany)	goat	1:1000

Table 4: Secondary antibody for Western Blot.

#### 2.2.3 Cell stretching

To investigate the reaction upon mechanical stretch of the desmosomal proteins, cellular monolayers were seeded on elastomer chambers and exposed to uniaxial cyclic stretch using a computer-controlled apparatus, the cell stretcher, as previously described in Faust et. al., 2011<sup>106</sup>. The monolayer which is attached to the bottom of the elastomer chamber is subjected to mechanical stretch of defined parameters in terms of amplitude, frequency and duration in live cell conditions.

#### 2.2.3.1 Elastomer chambers

The design of the elastomer chambers as described in Faust et. al., 2011<sup>106</sup> was adapted to the specific requirements of the experiments performed for this thesis with technical support by J. Konrad (IBI-2, Forschungszentrum Jülich). The revised elastomer chambers have a sealable compartment and can therefore be turned upside down for imaging (figure 5). A detailed description of the development of the elastomer chambers and its application is given in section 3.2. For the stretching experiments, the elastomer chambers were mounted in chamber holders, which are described in more detail in the next section.

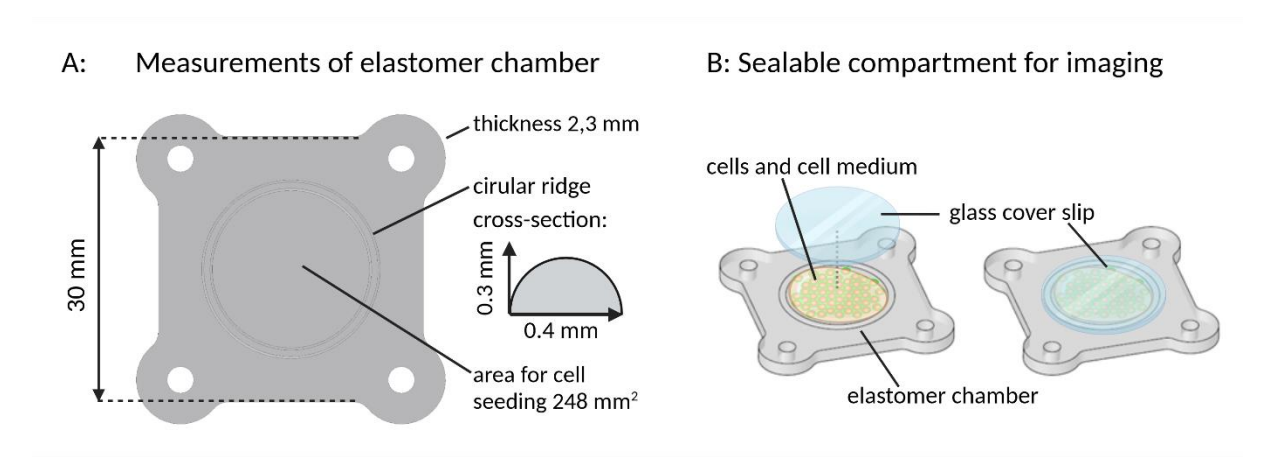


Figure 5: Elastomer chambers for cell cultivating, stretching and imaging of cellular monolayers. Measurements of elastomer chamber (A). Sealable compartment for imaging in which the cells (supplemented with cell medium) are sealed in with a glass cover slip (B). This graphic is a courtesy of J. Konrad.

#### 2.2.3.2 Cell Stretcher

The cell stretcher was initially developed inhouse by W. Rubner (hardware) and W. Hürrtlen (software). Further technical development was conducted by J. Konrad, all IBI, at Forschungszentrum Jülich. A description of stretcher and standard accessories is given in Püllen et. al, 2023<sup>102</sup>. The two main components of the cell stretcher are the computer controlled linear translation stage and the insert for elastomer chambers. The elastomer chambers were mounted onto a chamber holder to hold the elastomer chamber during incubation, stretching and imaging. The chamber holder consists of two fixating elements and a frame made of anodized aluminium. The purpose of the rods on the upper part of the fixating elements is pinning all four corners of the elastomer chamber. The elastomer chamber is installed with the circular ridge facing upwards and fixed from below with two additional barbell-shaped aluminium elements. Lastly, these elements are screwed to the rods of the fixating elements with two screws each (figure 6A). The fixating elements are interconnected with screws to a frame, which can be adjusted to an optimal position. To avoid sagging, the elastomer chamber was stretched 5 mm from its original position and this position was fixed with the frame. This particular position was defined as *prestretch*. The assembled chamber holder (figure 6B) was inserted in the cell stretcher (figure 6C). The linear transition stage device is motorised and thereby stretches the elastomer chamber uniaxially with programmed parameters (for more details, see appendix page XXXIV).

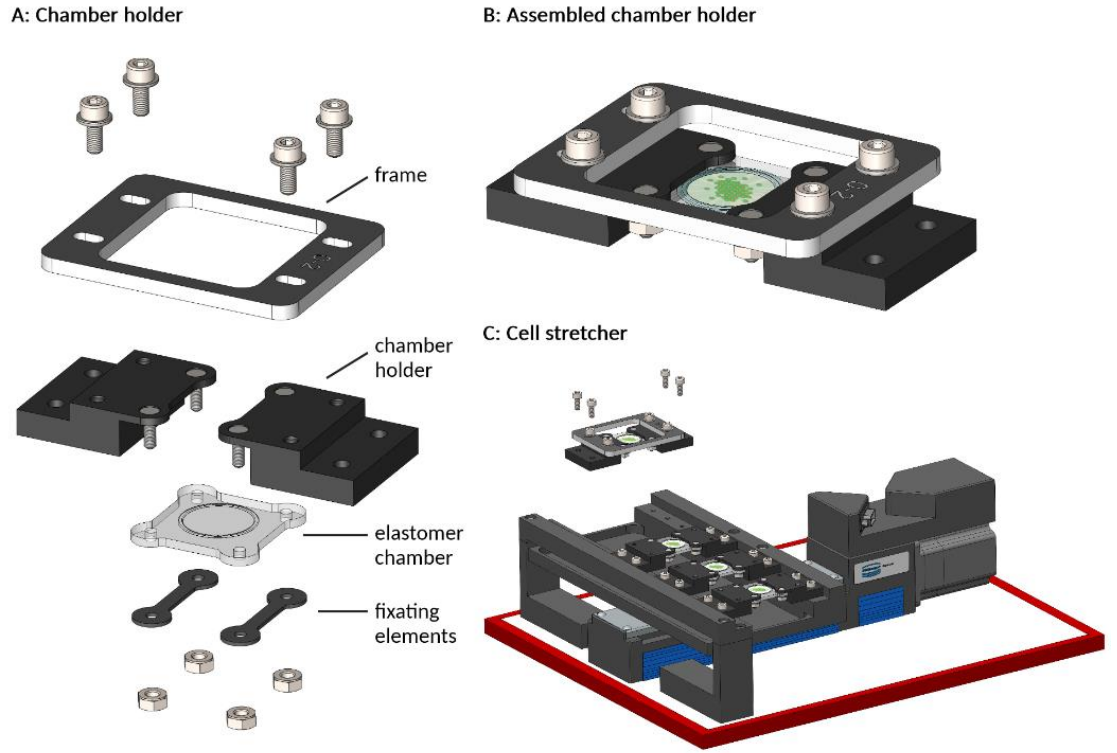


Figure 6: Cell stretcher and chamber holder. For cell stretching, the elastomer chambers are mounted onto a chamber holder (A). Once assembled (B), the chamber holder can be placed in the cell stretcher (C). This graphic is a courtesy of J. Konrad.

# 2.2.3.3 Workflow of stretching experiments

To analyse protein exchange kinetics, MDCK cells were seeded onto the elastomer chambers which were fixed in a chamber holder in *prestretch* position. For cell seeding, the surface inside the perimeter of the circular ridge was coated with 500 µl PBS containing 0.02 mg/mL fibronectin for 30 min at 37 °C. MDCK cells are seeded in 500 µl high calcium MDCK cell medium (100 000 cells per chamber, figure 7A). The MDCK cells were allowed to form a confluent monolayer overnight. The elastomer chambers were then installed in the stretcher. For cell stretching, a strain amplitude of 50% and a frequency of 80 mHz was chosen, which corresponded to a total traverse path of 19.5 mm. The traverse path for each stretch and release movement was completed within 3.4 s (seconds), and the stretcher paused 2.7 s in between each manoeuvre. All in all, a single stretching cycle lasted 12.2 s and a stretching experiment had a total duration of 2 h. All stretching experiments were performed under sterile conditions, at 37 °C and in a humidified atmosphere of 5% CO<sub>2</sub>. After a completed stretching

experiment, the chamber holder was stopped in the *prestretch* position. Excess medium was removed until the level of the remaining cell medium was in plane with the circular rim (figure 7B). A cover glass with a diameter of 22 mm was placed to seal the compartment of the MDCK cells on the elastomer chamber. An additional cover glass at the bottom of the elastomer chamber provided additional stability (figure 7C).

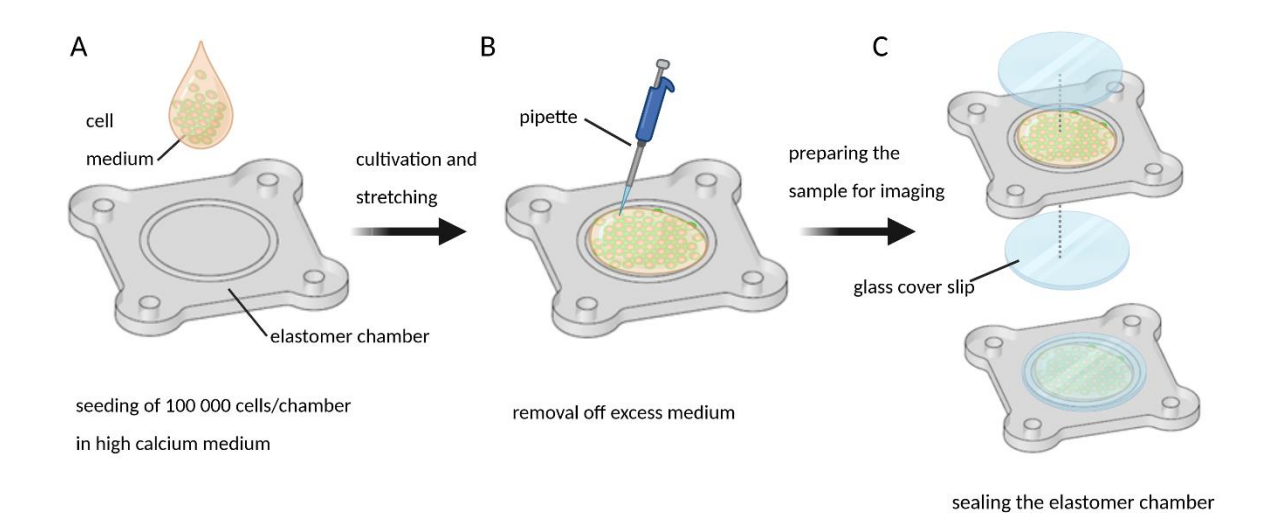


Figure 7: Workflow with the sealable elastomer chambers (part I). Workflow includes of cell seeding (A), cultivation, stretching and preparing the sample for imaging by removing excess medium (B) and sealing the elastomer chamber with a glass cover slip (C). One additional glass cover slip is added for stability. This graphic is a courtesy of J. Konrad.

The frame was mounted onto the chamber holder and the chamber holder then detached from the stretcher (figure 8A). For imaging, the position of the frame needed to be changed and another frame therefore mounted in reverse on the chamber holder (figure 8B). The original chamber holder could then be removed. The prepared sample could then be transferred to a microscope for imaging. To place the chamber holder onto the microscope stage, a fitting stage was designed and 3D printed by J. Konrad (figure 8C). The process of preparing the sample and transferring it onto the microscope for imaging results in a lag time ranging from 12 to 45 min between stretching and the analysis of the exchange kinetics. The FRAP analysis was carried out for 2 h and discarded afterwards. Samples that were analysed again after an additional 24 h of incubation had their glas coverslip removed and the cells were supplied with

500 µl of fresh MDCK HCM. The chamber holder was then wiped with ethanol and put away for an additional 24 h of incubation before another FRAP analysis was carried out. As control samples, MDCK cells were cultivated in elastomer chambers and analysed after 24 h or 48 h without being stretched. The latter also underwent a medium change after 26 h of incubation.

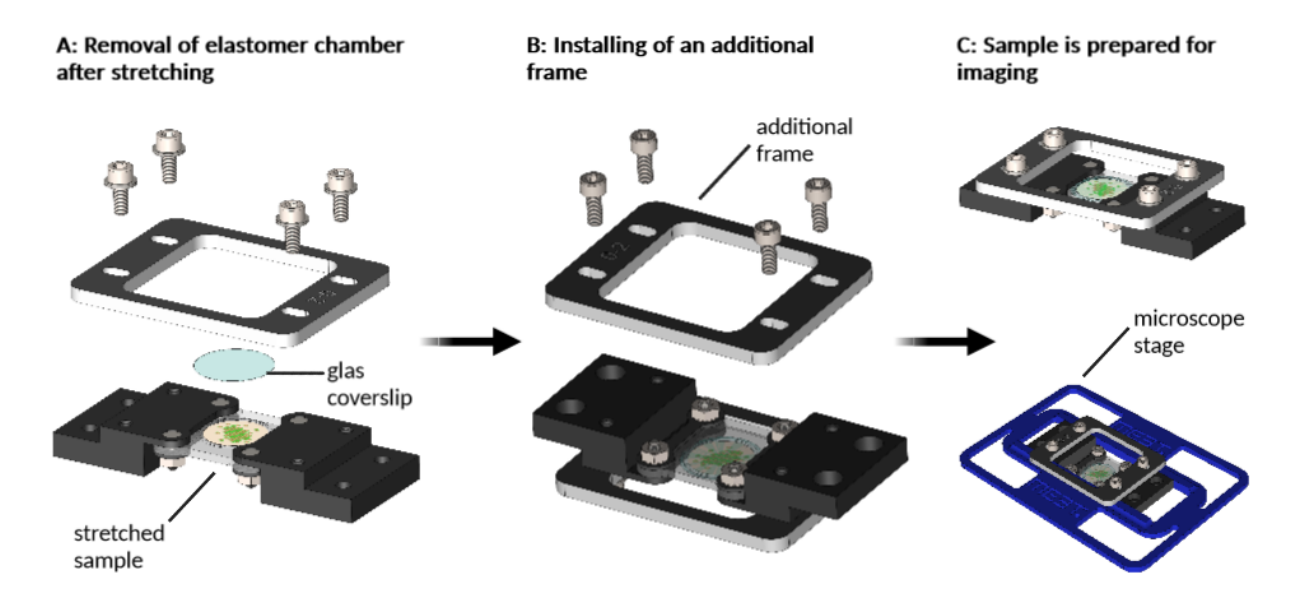


Figure 8: Workflow with the saelable elastomer chambers (part II). Workflow includes removing the chamber holder from the cell stretcher (A), preparing chamber holder for imaging by adding an additional frame (B) and imaging the sample with a confocal microscope (C). This graphic is a courtesy of J. Konrad.

#### 2.2.4 Analysis of protein exchange kinetics

#### 2.2.4.1 Confocal Laser Scanning Microscopy

Confocal laser scanning microscopy is a widely used method to image fluorescently labelled samples in diverse biological applications<sup>107</sup>. The basic principle of confocal microscopy involves scanning a sample with a diffraction limited spot and collecting the emitted light through a pinhole aperture. Emitted light originating from other planes than the focal plane is therefore eliminated, resulting in improved optical sectioning and allowing for imaging thin sections in a non-invasive manner.

Confocal LSMs are typically equipped with different excitation lasers. With a dichroic mirror, the light of different lasers can be superimposed. A scanning mirror directs the laser beam onto a fluorescently labelled sample, where it scans the sample with a grid

like fashion. The period of time the laser beam remains on one pixel before moving on to the next is determined through the pixel dwell time. The scanning speed is specified in lines on the grid per second, and is therefore given in Hertz (Hz). The number of grid lines results together with the number of pixels per grid line in the total number of pixels per scanned image.

In the course of this scanning process fluorescence excitation occurs. The light emitted by the sample is collected by a lens before it returns via the same path through the scanning mirrors and dichroic beam splitter, while the laser light is blocked by a filter. The light then reaches the pinhole, which functions as an aperture. In combination with the resolution of the respective objective and the wavelength of the light used, the diameter of the pinhole determines the thickness of the optical section. The opening of the pinhole is also indicated in Airy Units (AU), a measurement unit that refers to the intensity distribution of light passing a circular aperture. One AU corresponds to the pinhole diameter where the majority of the light reflected by the focal plane passes through, whereas light originating from other higher and lower planes in the sample is mostly blocked. If the pinhole is opened more than one AU, the light from other planes than the focal plane is resulting in blurry images. The light passing through the pinhole subsequently hits a photomultiplier, which converts the incoming photons into an electrical signal and lastly, renders a digital image.

## 2.2.4.2 Fluorescence Recovery After Photobleaching

Fluorescent reporter proteins are a powerful tool for analysing protein exchange kinetics<sup>108–110</sup>. Microscopy based methods such as FRAP are well established since the 1970s<sup>111</sup>. In the scope of this thesis, the analysis of protein exchange kinetics was performed via FRAP (figure 9). FRAP is a light microscopy based method that harnesses the fact that fluorophores are photosensitive agents. Fluorophores are coupled to a protein of interest (figure 9A), and are then irreversibly bleached in a limited area with a high-intensity pulse of light in a process called photobleaching. The result is a local decrease of the fluorescence intensity in the bleached region (Figure 9B). Unbleached fluorophores from the surroundings will enter the ROI whereas bleached fluorophores

exit the ROI (figure 9C). Subsequently, the fluorescence intensity in this region of interest (ROI) will recover at a rate that depends on the mobility of the molecules. This process continues until an equilibrium is reached (figure 9D). The lifetime indicates the time span until half the intensity of the equilibrium is reached and is an important parameter when comparing recovery curves. It is also of interest to note that, if all the proteins of interest were completely mobile, the final fluorescence intensity after a sufficiently long time after the bleaching will reach the same intensity level as before bleaching. A discrepancy between the final and the initial fluorescence intensity is therefore indicative of a fraction of the bleached proteins being immobile.

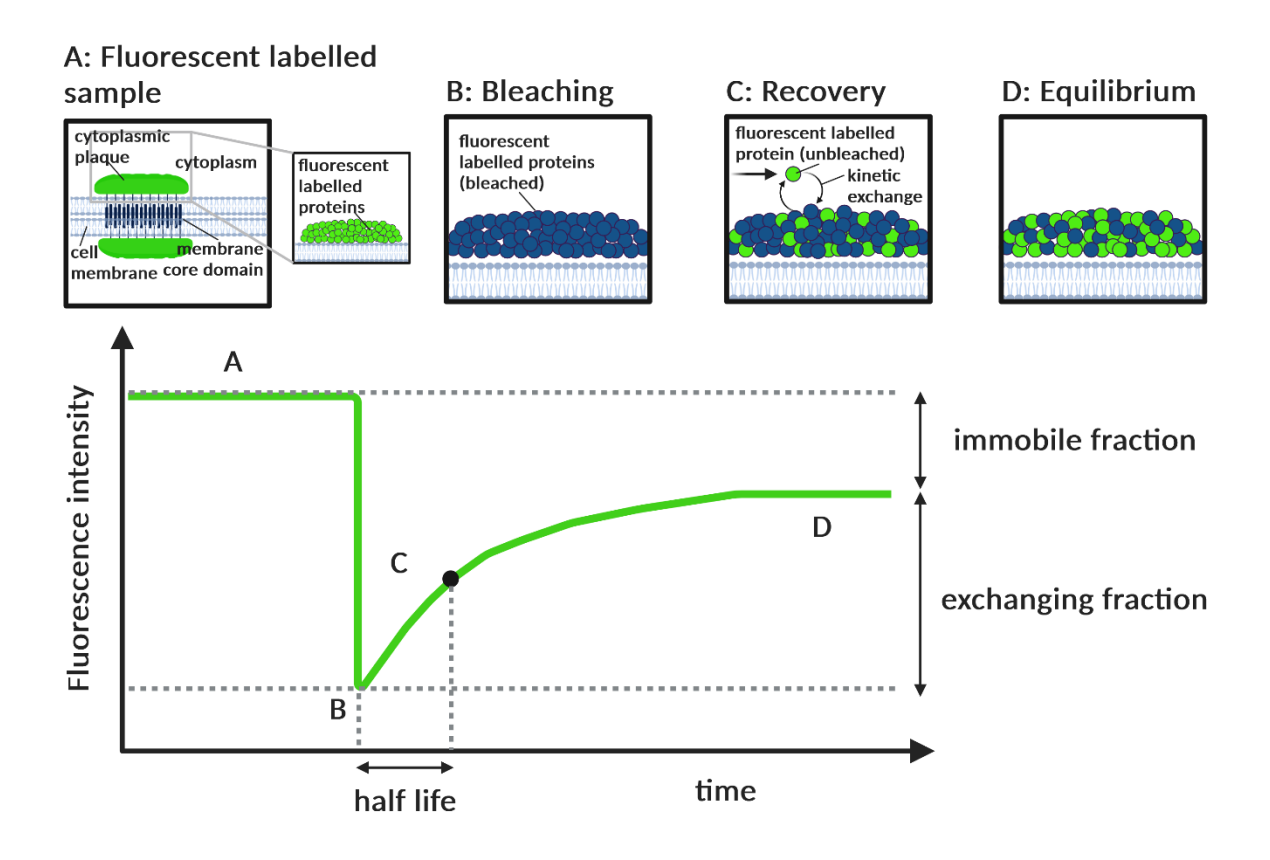


Figure 9: FRAP principle. A MDCK cell line, where a cytoplasmic plaque protein is tagged with GFP, is shown as an exemplary fluorescently labelled sample (A). The fluorescently labelled sample is then bleached with an intense laser pulse (B) and the recovery of the intensity is recorded over time (C) until it reaches an equilibrium (D). The resulting recovery curves provide information including the ratio of the immobile and exchanging fraction and the half-life of the cytoplasmic plaque protein.

The intensity in the ROI is measured over time to analyse which kinetic processes underlie the behaviour of the observed protein. Performing FRAP at a confocal LSM is

advantageous because a very thin optical sectioning can be achieved. Nevertheless, FRAP experiments can be disrupted by several artefacts which can deteriorate the correct measurement of the intensity in a ROI:

- **1. Bleaching** refers to the irreversible loss of fluorescence signal due to photo degradation of fluorophores. The FRAP technique itself relies on this effect, and usually high laser intensities are chosen to distinctly bleach the fluorophores in a limited area. But during imaging, bleaching is unwanted since it results in a continuous diminished emission of the fluorophore. Bleaching during imaging can be minimised by choosing a very low laser intensity for imaging. Another approach is the use of reference regions to assess and correct for the exact amount of bleaching over time, as described in section 2.2.6.1. A low laser intensity is also advantageous for preventing cell damage.
- **2. Cellular dynamics** results in a displacement of the originally bleached area against a ROI. During analysis, a ROI is a fixed structure in the image section. Cellular movements can lead to a distortion of the overall intensity measured in a ROI, which then rather reflects these movements than the protein exchange kinetics because fluorescent parts of the sample that have not been bleached are moved into the ROI, whereas bleached parts exit the ROI. Cellular dynamics occur naturally due to metabolic processes inside the cell and rearrangement of inter- and intracellular networks. These movements can occur in all three dimensions, horizontally within the current focal plane (dynamics in x- and y- direction) or vertically (in z- direction) in an unregularly fashion. The effect of cellular dynamics can be minimized by strategically shaping and placing ROIs (for cellular dynamics in x- and y- direction) and by widening the pinhole (for cellular dynamics in z-direction).
- **3. Focus drift** occurs when the whole sample is dislocated upwards or downwards in the focal plane (drift in z-direction). In contrast to cellular dynamics, drift is an even, unidirectional movement. Focus drift can be caused the (re-) adjustment of the elastomer chamber once the chamber holder is placed into the microscope. Focus drift can be avoided by allowing the sample to equilibrate before starting an analysis. The

influence of sample drift on the overall intensity can also be minimised to a certain amount by widening the pinhole.

In the scope of this thesis, the exchange kinetics of the desmosomal proteins DP, PG and Dsc were analysed. For this purpose, stably transfected MDCK cell lines were utilised where the respective desmosomal protein is coupled to a green fluorophore (either neon green or GFP as described in section 2.2.1.1). The use of stable transfected cell lines is advantageous, because they typically form uniformly luminous monolayers and cells are not subjected to constant stress resulting from repeated transfection processes. The presence of a fluorescent tag is not believed to alter protein exchange dynamics<sup>112</sup>.

Since desmosomes are subjected to constant assembly and disassembly all desmosomal proteins are present in both cytoplasm and desmosome at some point of the desmosomal life cycle. Therefore, the fluorescence recovery measured with FRAP is likely caused by two separate molecular processes: Diffusion and bond kinetics.

- **1. Diffusion** is caused by proteins dissolved in the cytoplasm. They diffuse freely in and out of the bleached ROI.
- **2. Bond kinetics** refers to proteins that directly interact with the desmosomal structure. When bound to the desmosomal structure, these proteins occupy binding sites. Upon release, these binding site are free to be occupied again. This cycle of binding and release is a random and time-dependent process.

If both of these processes are actually present, both the intensity of the fluorescent cytoplasmic proteins as well as the intensity of the fluorescent desmosomal bound proteins are contributing to the overall intensity measured in a ROI. Another strategy to distinguish between the effects of diffusion and binding is to develop an experimental set-up were these are separated as far as possible. Therefore ROIs that overlie only the area of cell-cell contacts were employed.

#### 2.2.4.3 Experimental set-up

The experimental design of the FRAP measurements had to factor in artefacts like bleaching, cellular dynamics and focus drift. To avoid confounding between the artefact bleaching and bleaching as part of FRAP measurement, the latter is referred to as photobleaching. MDCK cells were highly mobile within their monolayer, often resulting in changes of cell shape and placement. In order to prevent cellular dynamic in x- and y- direction, a rectangular ROI for photobleaching with the dimensions  $3.7 \times 12 \, \mu m$  was placed perpendicular on the cell-cell contacts (Figure 10). In order to minimize cellular dynamics, an applicable distance was kept to any other structures which could interfere with the analysis of the intensity in this ROI. For intensity analysis, a smaller ROI with the dimensions  $1.6 \times 3.7 \, \mu m$  was superimposed on the photobleaching ROI. Analysis was performed in a total of five different ROIs with these dimensions, were the average intensity was recorded over time (Figure 10).

The ROI intended to record the bleaching ( $I_{bleach}$ , red) and three as references to account for bleaching artefacts ( $I_{ref_i}$  blue, green, yellow). From these three references two were chosen based on how closely their intensity resembles the initial intensity in the bleaching ROI over time and their intensities averaged. One additional reference was recorded to analyse the intensity of the cytoplasm ( $I_{cyt_i}$  turqouise). Imaging was performed every second for a total duration of 5 min, resulting in a total of 300 cycles. Bleaching was performed after the first 10 cycles. Multiple FRAP experiments were performed on an individual sample, while respecting a minimum distance of 50  $\mu$ m – 100  $\mu$ m to the next photobleaching site.

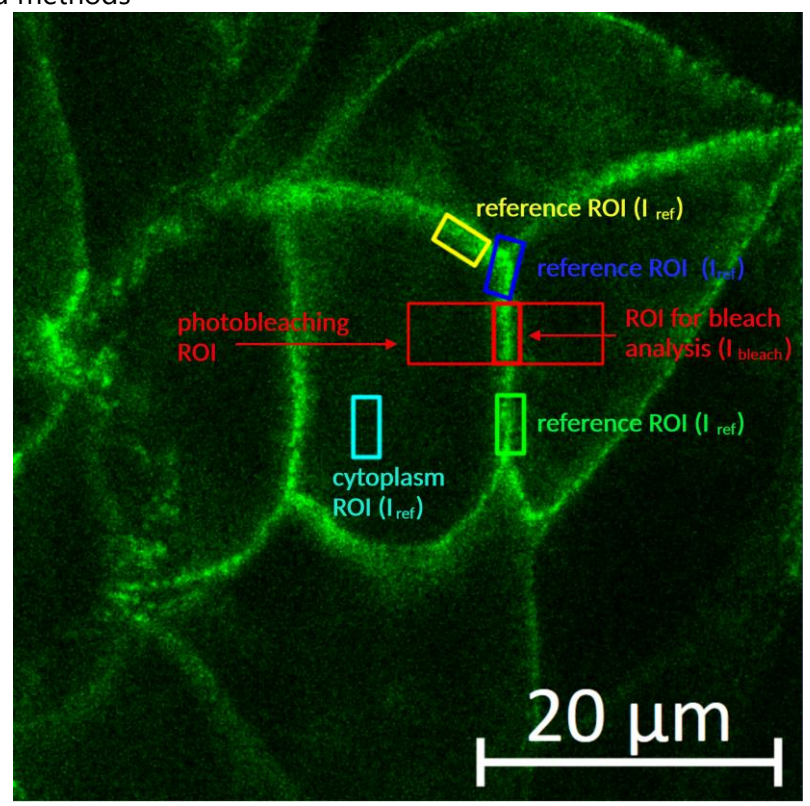


Figure 10: Experimental design of a FRAP analysis performed with MDCK Dsc 2a GFP cells. Image was taken with an LD C-Apochromat 40x/1.1 W Korr M27 objective at an LSM 880 using the 488 nm argon laser at 3% intensity. The emitted light was recorded between 493 nm and 550 nm with a gain of 500, a pinhole size of 5.07 AU and a pixel dwell time of 1.62 μs.

#### 2.2.4.4 Microscopy set up

Imaging and photobleaching was performed using an inverse Zeiss LSM 880 confocal microscope with an LD C-Apochromat 40x (1.1 NA) immersion objective. A 488 nm argon laser was employed for excitation. Different laser intensities were chosen for imaging and bleaching in order to minimize light stress for the cells for the different experiments. Imaging was performed at a 3% laser intensity while bleaching was performed at a 100% laser intensity with seven iterations. The emitted light was then recorded between 493 nm and 550 nm with a gain of 500 and a pinhole size of 200.8 µm in diameter (corresponding to 5.07 AUs). The pixel dwell time was set to 1.62 µs. The resulting image had a size of 488x488 pixels and a total scan time of 0.60 s. A twofold zoom was used to observe the cell-cell contacts. To compare intensities between different desmosomal proteins, all imaging settings were kept constant.

#### 2.2.5 Data Analysis

#### 2.2.5.1 Raw data processing

The values to the intensities measured in the ROIs were processed in order to obtain recovery curves of the respective desmosomal protein. To exclude the cytoplasmic background and eliminate the effect of bleaching, the intensity measured in the cytoplasm ( $I_{cyt}$ ) was subtracted from the intensity of the references ( $I_{ret}$ ) as well as from the intensity of the bleached region ( $I_{bleach}$ ). The intensity of the bleached region, thus cleared of the cytoplasmic background, was then put into relation with the averaged references to account for changes of the intensity over time due to possible artefacts as discussed in section 2.2.4.2 (equation 5):

$$I_{recovery}(t) = \frac{I_{bleach}(t) - I_{cyt}(t)}{\frac{1}{n} \sum_{i=1}^{n} I_{ref}(t)_i - I_{cyt}(t)}$$

$$(5)$$

In a next step, the values for the intensity of the bleached region were normalised for better comparability (equation 6). The mean was taken of the intensity values which were recorded before bleaching (bl = number of intensity values pre-bleach). The intensity measured directly after bleaching (time point bl+1) was set as the new zero point and subtracted from the intensity values of the bleaching process as well as from the averaged initial intensity:

$$I_{normalised\ recovery} = \frac{I_{Ad}(t) - I_{Ad}(t_{bl+1})}{\frac{1}{bl} \sum_{i=1}^{bl} I_{Ad}(t_i) - I_{Ad}(t_{bl+1})}$$
(6)

The therewith obtained values for the intensity of the bleached region result in recovery curves which are unique for the respective proteins.

#### 2.2.5.2 Data Fit

By fitting a mathematical model to the recovery curve the behaviour of a respective protein can be described by quantitative parameters. Saturation processes, as e.g. protein exchange kinetics, can often be described with an exponential function. The kinetic model described in section 2.2.5.3 was complemented by the observation of a visually striking offset present in some recovery curves. Therefore, the preterm (a) was added to the exponential function represented in equation 3. The prefactor b corresponds to the value on which the system settles in equilibrium which is termed exchanging fraction in the section 2.2.5.2. The following exponential function was deemed to best describe the obtained recovery curves and was developed by Prof. R. Merkel (equation 7):

$$f(t) = a + b * (1 - e^{-k*t})$$
(7)

This exponential function was fitted to the obtained recovery curves with a program written by G. Dreissen and Dr. R. Springer. The employed routine is based on the method of least squares and was executed in python with the command *scipy.optimize import curve\_fit* (SciPy Version 1.11.1). Prior to fitting, the last 39 images were omitted from the evaluation, since the recovery of the analysed proteins was completed amply in the 5 min of analysing. To calculate the lifetime of a respective protein, the offset a was deemed to be 0 and the exchanging fraction b was deemed to be 1. Based on equation 7, the lifetime  $t_{1/2}$  was then calculated with the following equation 8:

$$t_{1/2} = \frac{\ln 2}{k} \tag{8}$$

During this process, some recovery curves appeared to have a linear rather than an exponential curve progression, suggesting a very slow exchange kinetic that could not be fully depicted during the duration of a FRAP experiment. In these cases, an exponential fit could not provide sensible values for the parameters a,b and k. A common denominator in those recovery curves was a certain amount of noise. To better distinguish between a curve progression where noise covered an otherwise

exponential appearance and linear curve progression covered by noise, an objective criterion was needed. In order to reveal the underlying pattern in the noisy and fluctuating recovery curves a Whitaker baseline correction fit (Whitaker fit) was performed by Dr. R. Springer. The Whittaker fit is based on the Whittaker smoothing function which is a non-parametric technique for smoothing data points, also referred to as penalized least square<sup>113</sup>. Originally, the Whittaker fit is used to refer data to a baseline. Here, it was employed as a centreline fit, to obtain the value of the noise fluctuating around the x-axis.

To decide whether an exponential fit can be applied to the recovery curves, a straight was drawn between the first and the last point of the exponential fit while excluding the offset. If the maximum distance between this straight and the exponential fit was exceeding the standard deviation of the noise originating from the recovery curves (figure 11A), this recovery curve was deemed to be best fitted with the exponential fit (equation 7). Otherwise, even though the recovery curve was still deemed to be exponential, the duration of a FRAP experiment would not depict the completed recovery due to very slow exchange kinetic. Therefore, a linear fit deemed to be the best approximation to fit these incomplete recovery curves (figure 11B). This procedure is described in the next section.

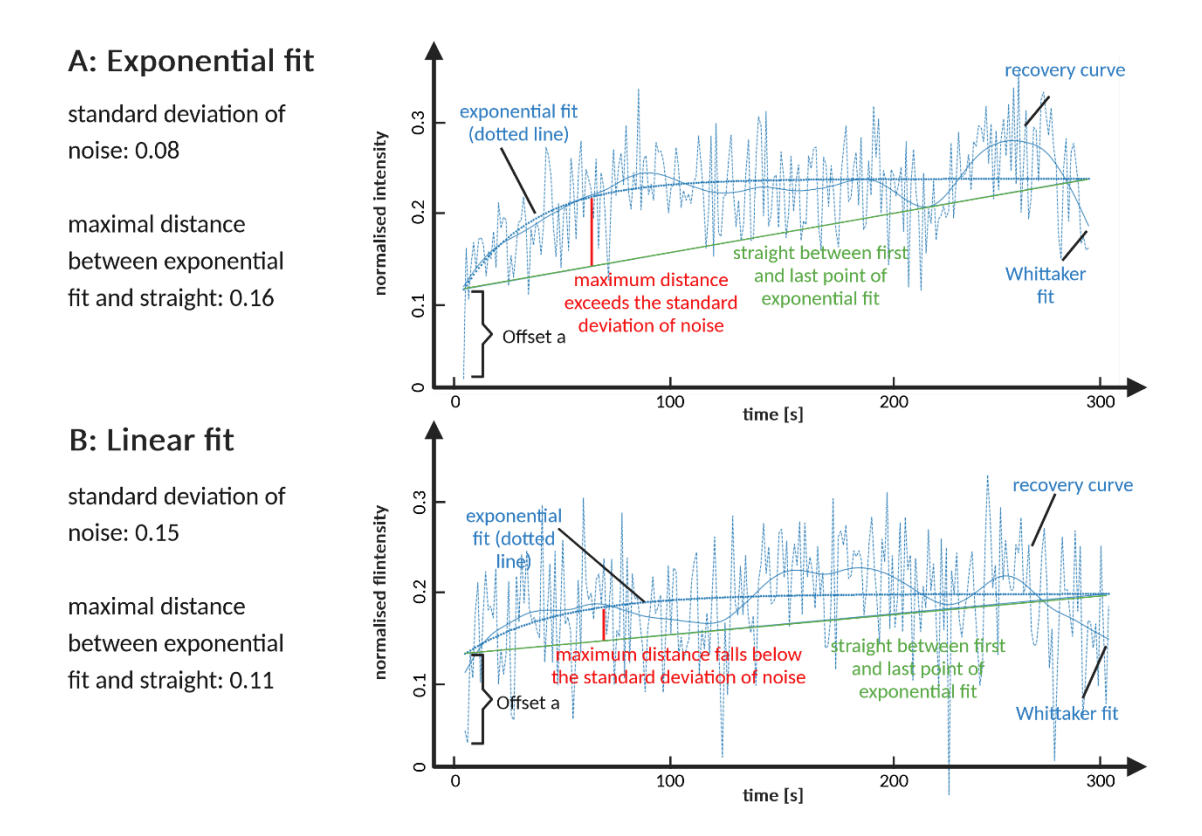


Figure 11: Whittaker fit of the recovery curves. To determine whether the recovery curves could be fitted with an exponential or a linear fit, the maximum distance between the exponential fit and a straight drawn between the first and last point of the exponential fit was exmined. If this distance was exceeding the standard deviation of the noise originating from the recovery curves, the exponential fit was used for describing the recovery curve (A), otherwise, a linear fit was used (B).

With the development of the Taylor series<sup>114</sup> for  $e^x$  at the position  $x \to 0$  (equation 9), a linear function can be derivated.

$$e^{x} = \sum_{n=0}^{\infty} \frac{x^{n}}{n!} = 1 + x + \frac{x^{2}}{2!} + \frac{x^{3}}{3!} + \dots$$
 (9)

By the substitution of x to -k\*t and inserting the above equation 9, equation 10 was obtained:

$$1 - e^{-k*t} = 1 - \left(1 - k*t + \frac{(k*t)^2}{2!} - \frac{(k*t)^3}{3!} + \cdots\right)$$
 (10)

Neglecting all higher order terms (quadratic or higher) the following equation is obtained (equation 11):

$$1 - e^{-k*t} \approx k * t \tag{11}$$

The following linear simplification is then obtained for the equation 11 (equation 12):

$$f(t) \approx a + b * k * t \tag{12}$$

However, the product b\*k is now a common factor and therefore, the exchanging fraction b and the rate constant k can not be analysed independently in this linear form. Ultimately, if the recovery curve is deemed to be linear du to the procedure above, the following equation 13 is applied to the corresponding recovery curves.

$$f(t) = a_{lin} + b_{lin} * t \tag{13}$$

For a joint analysis of the exponential and the linear fitted recovery curves, the parameter  $b_{lin}$ , which corresponds to the common factor b\*k originating from the linearised function (equation 12) can be compared to the product b\*k (product of two individual parameters) from the exponential fit (equation 7). With this approach, the exponentially fitted recovery curves can be evaluated together with the lineary fitted recovery curves of a first approximation regarding the initial slope of the recovery curves.

In order to depict the desmosomal protein kinetics realistically, all values and errors for the parameters a, b, k,  $a_{lin}$  and  $b_{lin}$  as well as b\*k would have to have values significantly smaller than 1. Therefore, all recovery curves where the value of a parameter or an error is greater than 1 are deemed unrealistic and were not taken into account. With this approach, outliers are removed from the evaluation.

#### 2.2.5.3 Error analysis

In order to carry out an error analysis of the determined parameters a bootstrap procedure was performed by Dr. R. Springer. Bootstrapping<sup>115</sup> is a statistical method based on resampling with replacement. During resampling with replacement, randomly selected data points from the original data set are returned to the data set before a next selection. Through this process, a new synthetic data set is created that mimics the properties of the original data set. Resampling was repeated for 1000 iterations for the the parameters a, b, k,  $a_{lin}$  and  $b_{lin}$ . This approach represents the error of these in a

more accurate way than the 95% confidence interval, which only indicates the uncertainty of the results of an individual fit and does not account for intercellular differences. For the error analysis of the product b\*k, which is required for the joint evalutation of the exponential and the linear fitted recovery curves, the standard deviation sb\*k was determined using quadratic propagation of error<sup>116</sup> for independent and uncorrelated variables (equation 14).

$$s_{b*k} = \sqrt{(\frac{\partial b * k}{\partial b})^2 * s_b^2 + (\frac{\partial b * k}{\partial b})^2 * s_b^2} = \sqrt{(\bar{k})^2 * s_b^2 + (\bar{b})^2 * s_k^2}$$
(14)

#### 2.2.5.6 Statistical analysis

The bootstrapped data for the parameters a, b and k were tested for normality using the Shapiro-Wilk test<sup>117</sup>. For normally distributed data, the Levene<sup>118</sup> test was utilised to test the equality of the variances. Otherwise, the Fligner-Kileen<sup>119</sup> test was utilised. Depending on the normality and the homoscedasticity respectively the heteroscedasticity of the data, following test were used to compare the data sets originating from the stretched samples to their correspondent controls: If the data was normally distributed, the two-tailed t-test was used for equal variances while the Welch test was used for unequal variances. If however the data was not normally distributed, the Wilcoxon was used for equal variances while the Kolmogorov Smirnoff test was used for unequal variances<sup>120,121</sup>. All experiments were repeated independently three times. The significance level  $\alpha$  was defined as follows:

$$\alpha \ge 0.05$$
 not significant (ns)  
 $\alpha < 0.05$  significant (\*)

Desmosomes act as connection sites for intermediate filaments and transmit forces throughout the tissue. In order to analyse their response to mechanical stretch, desmosomal protein exchange kinetics were probed. For this purpose, different MDCK cell lines were used as model organsisms, in each of which a respective desmosomal protein was fluorescently tagged with either GFP, EGFP or NG. Three different MDCK cell desmosomal proteins were analysed: DP, PG and Dsc2a NG and Dsc2a GFP with FRAP. To perform these kinds of experiments, an already existing stretching system<sup>102,106</sup> was complemented with a new elastomer chamber. For the specific requirements of the FRAP analysis at an inverse microscope, this new elastomer chamber features a sealable compartement for imaging. The results are described in six subsections that are outlined in the following:

To detect the fusion protein Dsc2a GFP, a western blot was performed. The results of the western blot are given in **section 3.1**.

In **section 3.2**, the experimental set-up is described in detail. An elastomer chamber for FRAP application was developed to cultivate and stretch cellular monolayers and to subsequently perform FRAP analysis at an inverse microscope. The MDCK cell lines used in this experiments are also discussed in more detail here.

With this experimental set-up, the exchange kinetics of the desmosomal proteins DP, PG, Dsc 2a GFP and Dsc 2a NG were probed in three mechanical states with FRAP: The samples were analysed after 2 h of mechanical stretch with a 50% amplitude at 80 mHz (mechanical state termed stretch) and after an additional 24 h of incubation (mechanical state termed stretch+24 h). Unstretched samples were utilised as controls and treated identically in regards to incubation times. These controls were termed CTRL and CTRL+24 h.

Either an exponential (equation 7) or a linear (equation 13) fit function was fitted to the resulting recovery curves (see section 2.2.5.2). In the **section 3.3.**, the execution of

both data fits is presented. Following the data fit, a bootstrap procedure was performed by Dr. R. Springer in order to determine the 95% confidence interval of the obtained parameters (see section 2.2.5.3).

The following three sections are subdivided according to the analysed mechanical states: In order to determine a baseline, desmosomal exchange kinetics were examined first in the absence of mechanical stretch after 24 h of incubation (**section 3.4**). These results were used as a control for the stretched samples presented in the next section and are termed *CTRL*-samples. The impact of mechanical stretch on desmosomal exchange kinetics is outlined in **section 3.5**. These samples are termed *stretch*-samples. To examine the longevity of the effect mechanical stress had on desmosomal exchange kinetics, FRAP analysis were performed again on the *stretch*-samples 24 h after stretch (**section 3.6**). These samples are now termed *stretch+24 h*-samples. Unstretched sample were incubated for 48 h and used as a control. These samples are termed *CTRL+24 h*-samples. For better differentiation, the following colour code was used for the graphics presented in these sections: The recovery curves of the *CTRL*-samples are depicted in green, the recovery curves of the *stretch* as well as of the *stretch+24 h*-samples are both depicted in red and the recovery curves of the *CTRL+24 h*-samples are depicted in blue.

In each of these sections, the recovery curves of all four desmosomal proteins (DP, PG, Dsc 2a GFP and Dsc 2a NG) and their fitted parameters yielding from the exponential fit are presented. These are the parameters a, b, and k, which correspond to the offset, the exchanging fraction and the rate constant, as well as the lifetime, which was calculated from the latter. Additionally, a joint evaluation of the offset as well as of the initial slope of the recovery curves was conducted. For this purpose, the parameter  $a_{lin}$  originating from the linear fit (equation 13) was analysed together with the parameter a originating from the exponential fit (equation 7). Additionally, the parameter  $b_{lin}$ , which corresponds to the common factor b\*k originating from the linearised function (equation 12) was analysed together with the product b\*k, product of the two

individual parameters from the exponential fit (equation 7). These pair of parameters give comparable conclusions of the offset as well as of the initial slope (see section 2.2.5.2 for more details). These results are also subdivided according to the analysed mechanical state and are presented in **section 3.7**.

# 3.1 Desmocollin GFP is present as a fusion protein

Whether the fusion protein was present in the Dsc 2a GFP cells provided by our cooperation partner Prof. Leube was qualitatively analysed with Western Blot (Figure 12). The size of the fusion protein consisting of Dsc 2a and GFP is calculated to be 121 kilo Dalton (kDa), due to the size of its two components, Dsc 2a (94 kDa) and GFP (27 kDa). The western blot membrane stained against Dsc 2 showed two distinct bands in the range of approximately 130-150 kDa, estimated to be around 120 kDa for the lower and 150 kDa for the upper band. Additionally, there was a blurry section ranging from approximately 130 kDa down to approximately 80 kDa. The western blot membrane stained against GFP showed one distinct band around 130-140 kDa. The presence of one band in each staining at approximately 130 kDa within both stainings indicate the presence of the fusion protein in the Dsc 2a GFP cells. The less clear, merged bands below the 130 kDa mark are deemed to be degradation products. This result is in accordance with Windoffer et. al<sup>59</sup>, where the analysis via Western Blot provided a similar result.

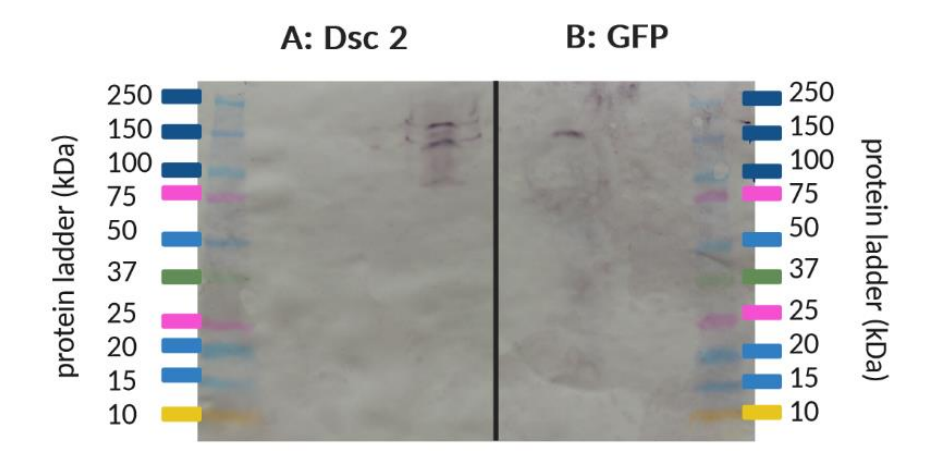


Figure 12: Protein identification of the Dsc 2a GFP cells by Western Blot. Western Blot membrane stained against Dsc 2 (A) and against GFP (B). The size of the protein ladder is indicated in kDa.

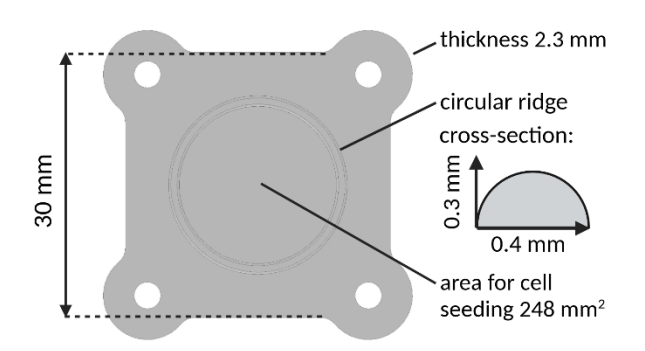
# 3.2. Development of experimental set-up

#### 3.2.1 Elastomer chambers

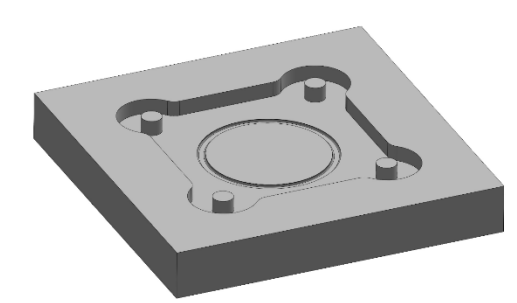
The stretching system previously described in Faust et. al., 2011<sup>106</sup> is an application for use at an upright microscope. To probe cellular monolayers on elastomer chambers with FRAP at an inverse microscope, a new elastomer chambers was developed. This new stretching system features a sealable compartment on the elastomer chamber which can be turned upside down for imaging at an inverse microscope. The elastomer chambers are rimless and a 0.3 mm ridge encircles a 248 mm<sup>2</sup> area (Figure 13A). Cells can be seeded into this ciruclar well and be supplemented with medium for cultivation and stretching. This area can be sealed by placing a glas coverslip on top of the circular ridge and the whole elastomer chamber can now be turned upside down for imaging at an inverse microscope. The adhesive properties of the material used prevent the glas coverslip from falling off.

The elastomer chambers were manufactured using SORTA-clear 12 (Smooth-on, Macungie, Pennsylvania, US), a two-component polydimethylsiloxan elastomer with a high biocompatibility and tensile strength. The elasticity is tunable via the ratio of its two components A and B. The components were weighed in a 2.66:1 ratio resulting in a modulus of elasticity of 50 kPa. The mixture was well stirred for 10 min and degased to prevent air bubbles from interfering with cross linking. 3.4 mL of the mixture were then poured into molds made of polyvinyl chloride (Figure 13B) and cured at 60 °C for 16 h. The hardened elastomer chamber can be detached from the mold with isopropanol and stored until stretching. For the stretching experiments, the elastomer chambers were mounted in chamberholders and afterwards placed in a cell stretcher (described in section 2.2.3.2). Compared to the elastomer chambers described in Faust et. al., 2011<sup>106</sup>, the elastomer chambers used here were not coverable due to their rimless design. This resulted in occasional contaminations with funghi or bacteria when cultivated longer than 24 h. Therefore, one medium change was performed on the samples that were analysed after 48 h of incubation (see section 2.2.3.3).

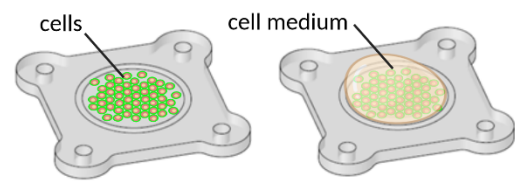
#### A: Measurement of elastomer chamber



#### B: Elastomer chamber mold



#### C: Applications of elastomer chambers



imaging with sealed elastomer chamber

glass cover slip

cultivation and stretching

Figure 13: Elastomer chamber for FRAP experiments. Measurements of elastomer chamber (A). The circular ridge enclosing the area for cell seeding is 0.4 mm wide and 0.3 mm high. Mold of the elastomer chamber (B) and applications e.g. cultivation, stretching and imaging (C). This graphic is a courtesy of J. Konrad.

Imaging occurred through the glas coverslip at the bottom of the elastomer chamber (Figure 14). The gap between monolayer and glas coverslip was 300  $\mu$ m, thus an LD C-Apochromat 40x (1.1 NA) immersion objective with a water immersion lens was used.

# A: Imaging at an inverse microscope B: Sealable compartment for imaging sealed elastomer chamber LD C-Apochromat 40x (1.1 NA) immersion objective

Figure 14: Imaging step of the experimental set-up. The imaging is performed at an inverse microscope (LSM 880) with a 3D printed microscopic stage (A). The sealable compartement is approached from below with an LD C-Apochromat 40x (1.1 NA) immersion objective. (B). This graphic is a courtesy of J. Konrad.

#### 3.2.2. Cell lines

Utilizing the elastomer chambers described in the preceding section, FRAP analysis could be conducted using an upright microscope. For analysis, four different MDCK cell lines stably expressing a fluorescently tagged desmosomal fusion protein (either DP, PG, Dsc2a NG or Dsc2a GFP) were used (Figure 15).

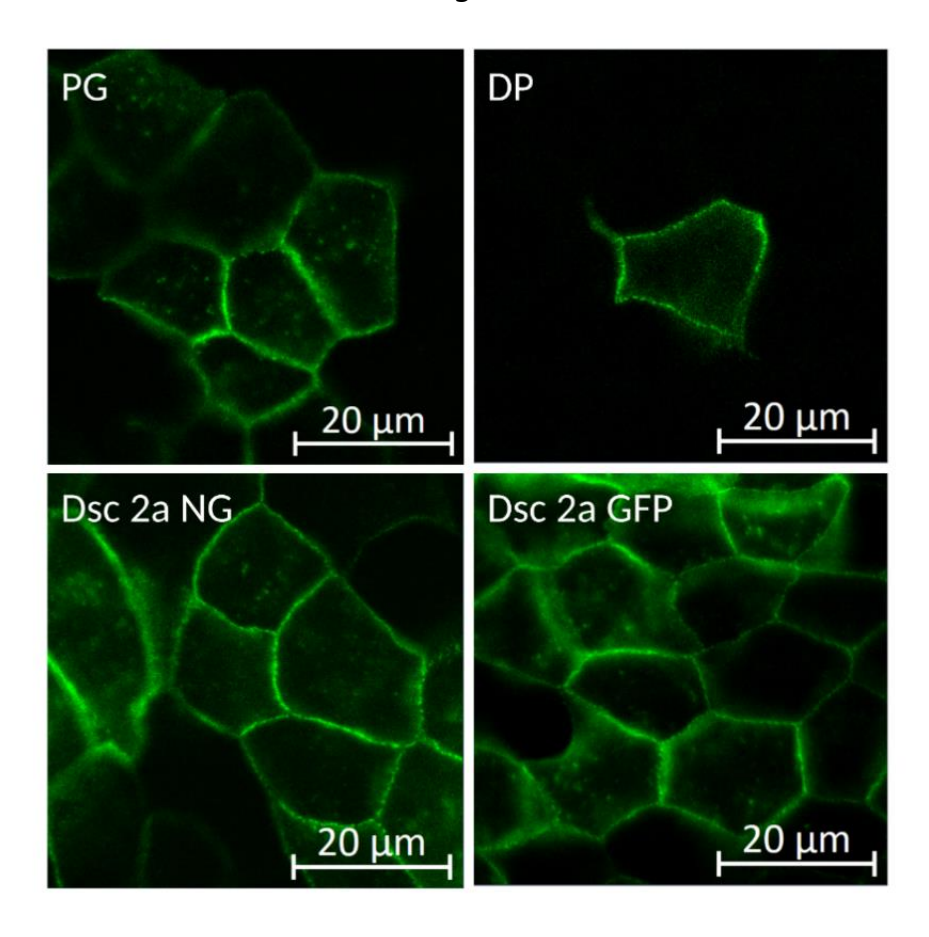


Figure 15: Overview of continuous cellular monolayers of the different MDCK cell lines (PG, DP, Dsc 2a NG and Dsc 2a GFP). Image was taken with an LD C-Apochromat 40x/1.1 W Korr M27 objective at an LSM 880 using the 488 nm argon laser at 3% intensity. The emitted light was recorded between 493 nm and 550 nm with a gain of 500, a pinhole size of 5.07 AU and a pixel dwell time of 1.62 µs.

The desmosomal maturation was induced with the increase of the calcium concentration 24 h prior to the first FRAP analysis. Upon imaging, differences in the quantity of fluorescent cells and and overall brightness between the analysed cell lines became apparent. The fluoresecence signal of all cell lines intensified around the cell-cell contacts, indicating that the desmosomal proteins accumulated there. If the desmosomes align perpendiculary in the optical plane, the cell-cell contact appears as

a continuous line. Otherwise, the individual desmosomes appear as sharply defined roundish structures distributed over a larger area. Depending on the cell type and luminosity, a faint fluorescence signal was also present in the cytoplasm and appeared as a greenish fog filling the cell.

As described in section 2.2.5.2, there were notable differences in terms of overall brightness and transfection efficiency between the cell lines. At their maximum, the raw fluorescence intensities of PG, Dsc2a NG and Dsc2a GFP were tenfold higher than the raw fluorescence intensities of DP. Since the brightness between the analysed cell lines differed so much, the normalisation of the fluorescence intensity (section 2.2.5.1) was an important step in processing of the data.

As a result of the varying condition of the MDCK cell lines, the appearance of the recovery curves differ distinctly and artefacts like bleaching, cellular dynamics and focus drift also presented themselves differently.

#### 3.2.3 FRAP analysis

With FRAP, protein exchange kinetics were probed in different mechanical states. In order to determine a baseline, desmosomal exchange kinetics were examined in the absence of mechanical stretch.

The total duration of the FRAP analysis was determined with pilot experiments. An analysis duration of 5 min with an imaging frequency of 1 picture per second was chosen to reflect the complete recovery of the respective desmosomal proteins. During analysis, the overall intensity was recorded in ROIs with specific dimensions (see section 2.2.5.3). The ROI in which the bleaching occurred depicted the uncorrected recovery curve of the respective protein. To assess and correct for bleaching over time three reference regions were employed. Two of these were chosen based on how closely their intensity resembles the initial intensity in the bleaching ROI over time and their intensities averaged. In order to record the intensity of the cytoplasm, one additional reference was analysed. The raw data of the recorded intensities from a representative FRAP experiment with Dsc2a GFP cells are shown in Figure 16.

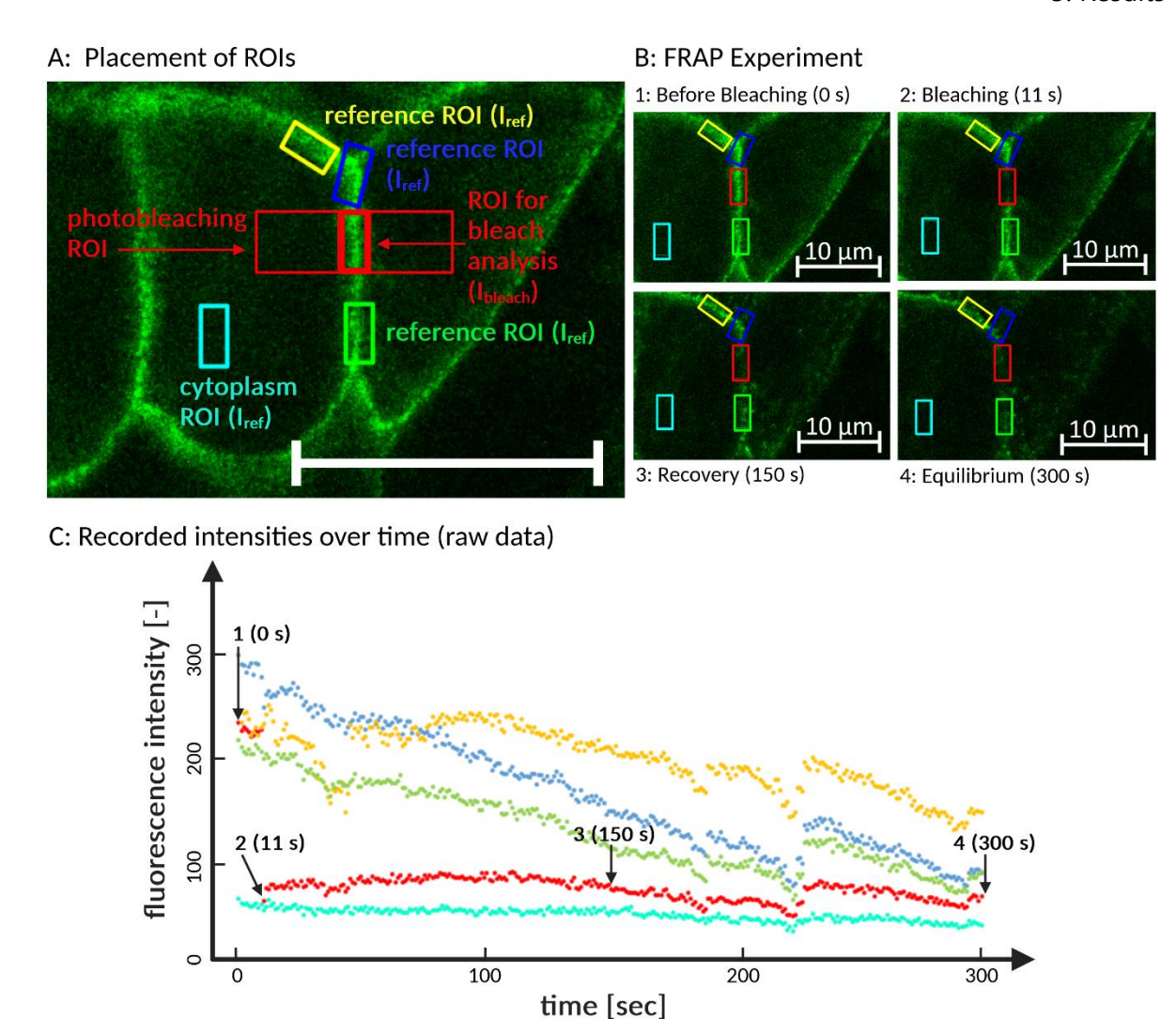


Figure 16: An overview of a representative FRAP experiment with Dsc2a GFP cells in the absence of mechanical stretch. The placement of the five ROIs before analysis (A, scale bar  $20 \mu m$ ). Photobleaching was performed in the "photobleaching ROI" and the fluorescence intensity was recorded in the "ROI for bleach analysis". Four characteristic time points during a FRAP experiment (B): (1) Before bleaching (0 s), (2) bleaching (11 s), (3) recovery (150 s) and (4) equilibrium (300 s). The recorded intensities of the FRAP experiment shown as raw data (C). The four characteristic time points shown in (B) are indicated with arrows. Images were taken with an LD C-Apochromat 40x/1.1 W Korr M27 objective at an LSM 880 using the 488 nm argon laser at 3% intensity. The emitted light was recorded between 493 nm and 550 nm with a gain of 500, a pinhole size of 5.07 AU and a pixel dwell time of 1.62  $\mu$ s.

#### 3.2.4 Correcting for artefacts

Upon inspection of the raw data it becomes apparent that artefacts influence the recovery curve (for more details see section 2.2.4.2). The most distinct artefacts during the FRAP analysis were cellular dynamics and focus drift. Cellular dynamics occur due to the very active monolayers formed by the MDCK cell lines, resulting the originally

bleached area to shift outside the ROI. The reactangluar shape of the ROI was attenuating cellular dynamics in a limited fashion: If this displacement occurred alongside the longer side of the ROI, the overall intensity in the ROI would remain the same. The same applies for small or cyclic cellular movements, where the originally bleached area remains in place only have a marginal impact on the overall intensity in the ROI.

Focus drift occurred in most of the performed FRAP measurements to varying extent and becomes apparent as a continuous decrease of the overall fluorescence intensity in a ROI. Even though sample equilibration is a proven method to reduce this artefact, the goal of the performed experiments was to limit the lag time between stretching and imaging. Therefore, the sample was only equilibrated for a few minutes before analysing started. However, moderate focus drift still occurred throughout the duration of a FRAP measurement, probably due to the agitation of the elastomer chambers while displacing the microscope objective during different measurements. To diminish the effect of focus drift on the recorded intensity, the pinhole was opened to 5 AU. The recovery curve of the brighter cell lines were less impacted by focus drift. During the second step of data processing, the data was normalised for better comparability of the recovery curves. This step was crucial, especially with regards to the differences in brightness between the MDCK cell lines.

In addition, normalising the data (as described in section 2.2.5.1) proved to be a suitable method to reduce any steady-going motion and could also reduce the effects of both moderate cellular dynamics and focus drift. Nevertheless, measurements with either too pronounced cellular dynamics or focus drift (or both) had to be discarded.

The least noticeable artefact was bleaching, since cellular dynamics and focus drift would overlay this effect if present. In retrospective, it was unfeasible to tell if bleaching was present at all. To prevent potential bleaching, a low intensity (3%) was kept for the imaging laser. All in all, cellular dynamics and focus drift both impact the recovery curves and are different to separate. However, all artefacts added up during

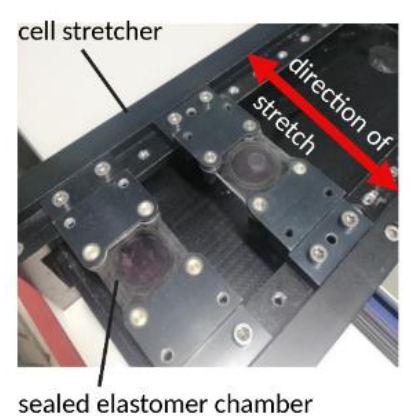
the course of the experiment and resulted in an increasing scatter overlying the recovery curves. Since the recovery of all analysed proteins was completed amply in the 5 min of analysing, the last 39 images were omitted before fitting the data with equation 7 (see section 2.2.5.2).

#### 3.2.5 Stretch

The experimental set-up was developed around the prerequisite of analysing mechanical stretch (Figure 17). For this purpose, cellular monolayers were seeded on elastomer chamber and stretched for 2 h with a 50% amplitude at 80 mHz. The experimental set-up consisting of a separate stretching and imaging facility resulted in a lag time between stretching and imaging ranging from 12 to 45 min. Thus, a relaxation of unknown extent back to the unstretched state will have taken place during the lag time and therefore, only an attenuated effect could be observed.

Pilot experiments with Dsc2a GFP cells showed that amplitudes ranging from 11% to 25% resulted in small kinetic changes which were not consistently measureable due to the occuring artefacts. In order to allow this effect stand out more clearly, higher amplitudes were tested. With these increasing amplitudes, the material requirements needed to be adjusted. The material previously (50 kPa Sylgard, manufactured with Sylgard 184 silicone elastomer kit, Dow Corning, Wiesbaden, Germany) used in the pilot experiments was replaced by SORTA-clear 12. With a 50% amplitude, kinetic changes could be observed more distinctly and was therefore set to perform the experiments described in the following sections.

A: Elastomer chambers installed in the cell stretcher



B: Elastomer chamber installed in chamber holder

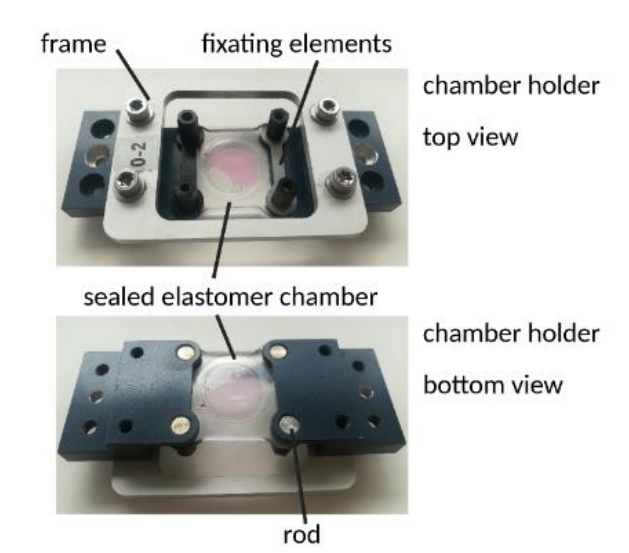


Figure 17: Details of the developed elastomer chamber within the experient that set-up. The sealed elastomer chambers installed in the cell stretcher after the stretching process (A) and the chamber holders viewed from top and bottom (B).

#### 3.3. Data Fit

With the experimental set-up described in section 3.2, 171 recovery curves were recorded and primarily fitted with both fit functions, the exponential fit (equation 7) and the linear fit (equation 13). Recovery curves with parameter or error values for *a* or *b* exceeding 1 were excluded from further evaluation.

All in all, 158 recovery curves were then evaluated (all individual recovery curves are displayed in the appendix pages I to XVII). In order to decide which fit – exponential or linear - described the recovery curve best, the standard deviation from the noise of the recovery curves was used as a criterion (for more details see section 2.2.5.2). Therefore, the parameter  $f_{max}$  was calculated for each recovery curve. This parameter represents the maximum distance between the exponential fit and the straight drawn between the first and the last point of the exponential fit. If  $f_{max}$  was exceeding the standard deviation of the noise originating from the recovery curve, the recovery curve was fitted with the exponential fit (equation 7). Otherwise, it was fitted with the linear fit (equation 13).

The classification of all recovery curves is presented in the table *fit function* (appendix page XVIII to XXIII). The parameter values of the corresponding fits for all recovery curves are presented in the table *parameter values* (for the exponential fits see appendix pages XIV to XXVIII and for the linear fits see appendix page XXIX). All in all, 139 recovery curves were deemed to be best fitted with the exponential fit and 19 recovery curves were deemed to be best fitted with the linear fit (Table 5 below).

Desmosonal protein	Mechanical state	N independent samples	N recovery curves (total)	N exponential fits	N linear fits
DP	CTRL	5	9	5	4
	stretch	3	10	5	5
	stretch+24 h	3	7	4	3
	CTRL+24 h	3	10	8	2
PG	CTRL	4	7	7	0
	stretch	4	10	10	0
	stretch+24 h	3	9	8	1
	CTRL+24 h	4	9	7	2
Dsc 2a NG	CTRL	3	10	10	0
	stretch	3	16	16	0
	stretch+24 h	3	11	11	0
	CTRL+24 h	3	11	11	0
Dsc 2a GFP	CTRL	3	10	9	1
	stretch	3	10	10	0
	stretch+24 h	4	11	10	1
	CTRL+24 h	3	8	8	0

Table 5: Number of independent samples and recovery curves of all desmosomal proteins and mechanical states.

Recovery curves which could not be fitted with the exponential fit were fitted with the linear fit.

During this procedure it became apparent that throughout all proteins and mechanical states, but primarily with DP recovery curves, recovery curves that required linear fitting occurred. The parameter  $b_{lin}$  corresponds to the common factor b\*k originating from the linearised function (equation 12) and can therefore be compared to the product of b\*k from the exponential fit (equation 7, see section 2.2.5.2).

With this approach, the exponentially fitted recovery curves could be evaluated together with the linerary fitted recovery curves. The parameter values of this joint

analysis are presented in the table *parameter values for joint evaluation* (see appendix pages XXX to XXXIV). In order to document how the respective fit described the recovery curves, exemplary fits –exponential and linear if available- of all desmosomal protein and mechanical states are shown in the Figure 18-25.

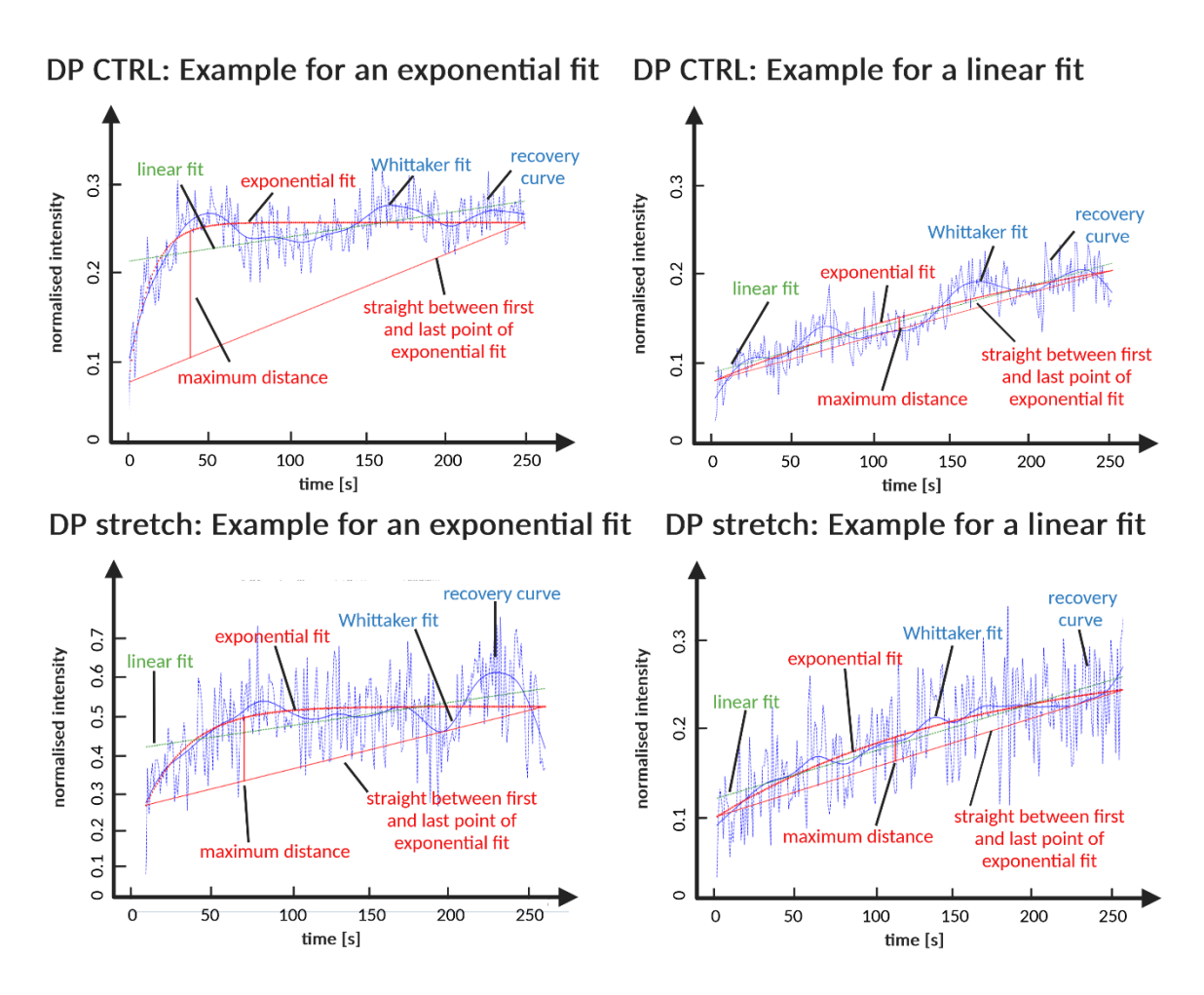


Figure 18: Examples of the exponential as well as the linear fit with DP CTRL (above) and DP stretch (below) recovery curves. DP CTRL: For the exponential fit, the standard deviation was 0.024 and the  $f_{max}$  was 0.16 and for the linear fit, the standard deviation was 0.038 and the  $f_{max}$  was 0.028. DP stretch: For the exponential fit, the standard deviation was 0.080 and the  $f_{max}$  was 0.16 and for the linear fit, the standard deviation was 0.041 and the  $f_{max}$  was 0.028. For more details on the fit functions as well as the Whittaker fit see section 2.2.5.2.

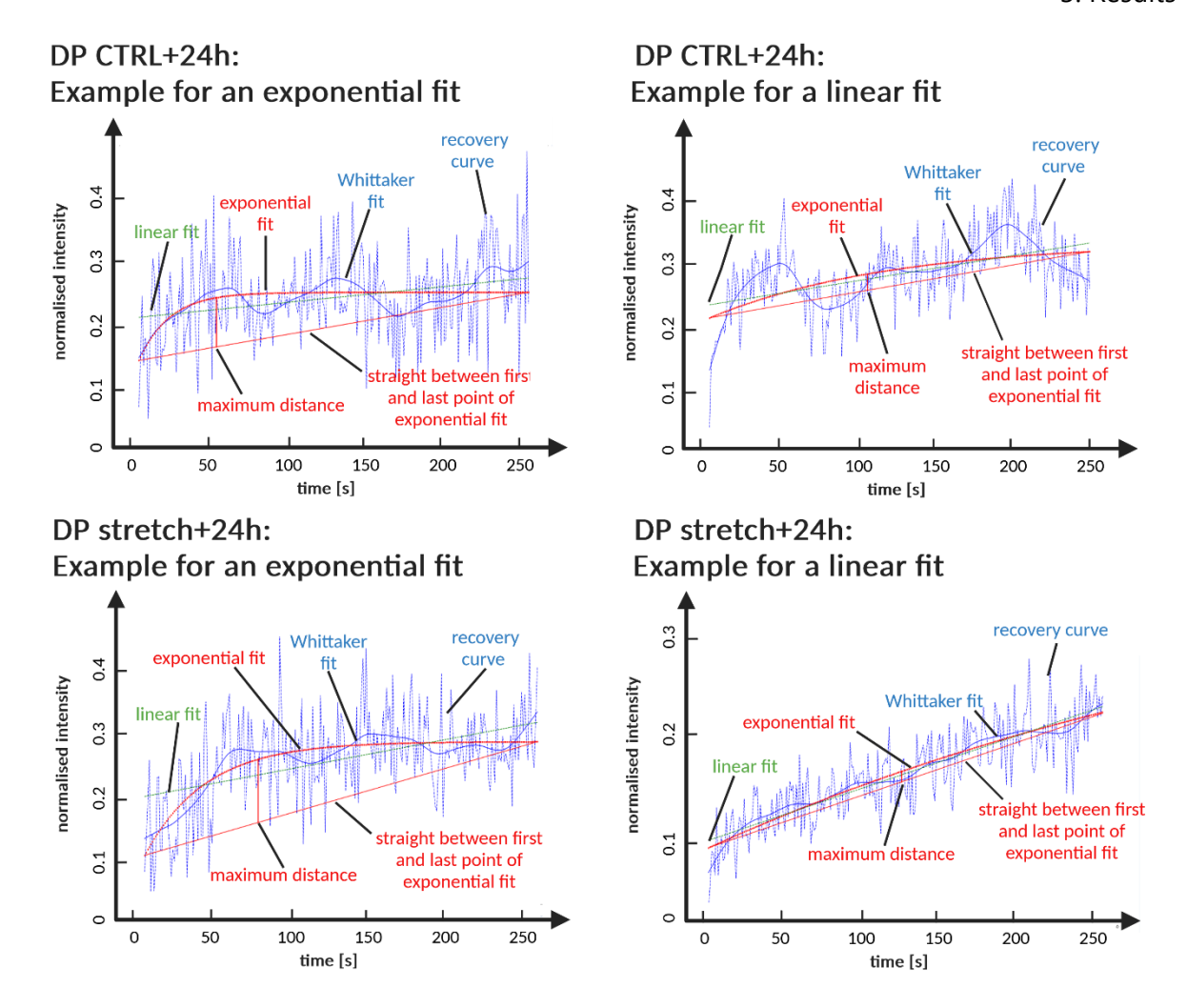


Figure 19: Examples of the exponential as well as the linear fit with DP CTRL+24 h (above) and DP stretch+24 h (below) recovery curves. DP CTRL+24 h: For the exponential fit, the standard deviation was 0.069 and the  $f_{max}$  was 0.089 and for the linear fit, the standard deviation was 0.041 and the  $f_{max}$  was 0.028. DP stretch+24 h: For the exponential fit, the standard deviation was 0.070 and the  $f_{max}$  was 0.13 and for the linear fit, the standard deviation was 0.025 and the  $f_{max}$  was 0.011. For more details on the fit functions as well as the Whittaker fit see section 2.2.5.2.

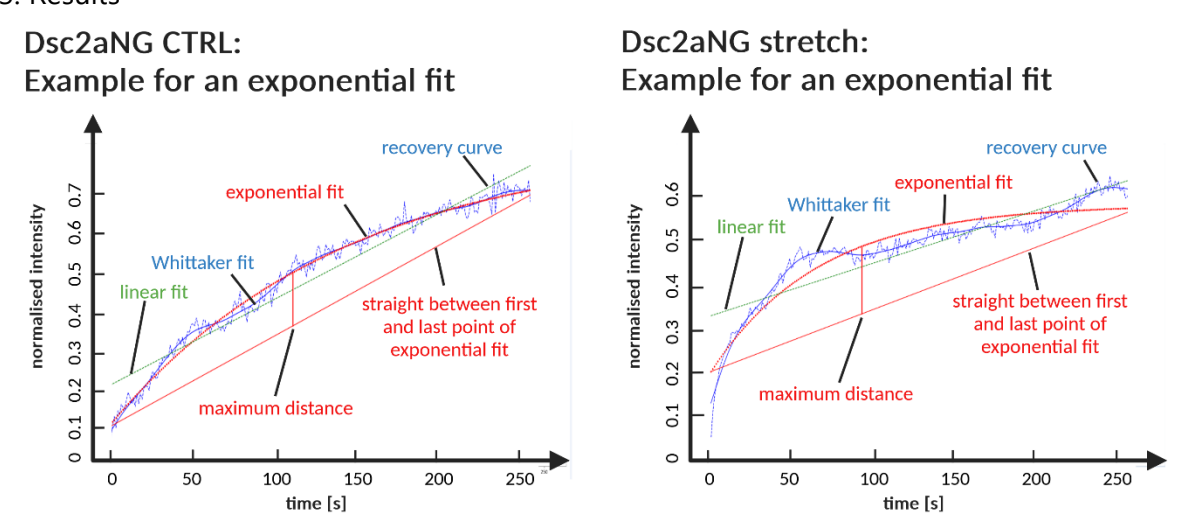


Figure 20: Examples of the exponential as well as the linear fit with Dsc2aNG CTRL (above) and Dsc2aNG stretch (below) recovery curves. Dsc2aNG CTRL: For the exponential fit, the standard deviation was 0.016 and the  $f_{max}$  was 0.13. Dsc2aNG stretch: For the exponential fit, the standard deviation was 0.016 and the  $f_{max}$  was 0.18. For more details on the fit functions as well as the Whittaker fit see section 2.2.5.2.

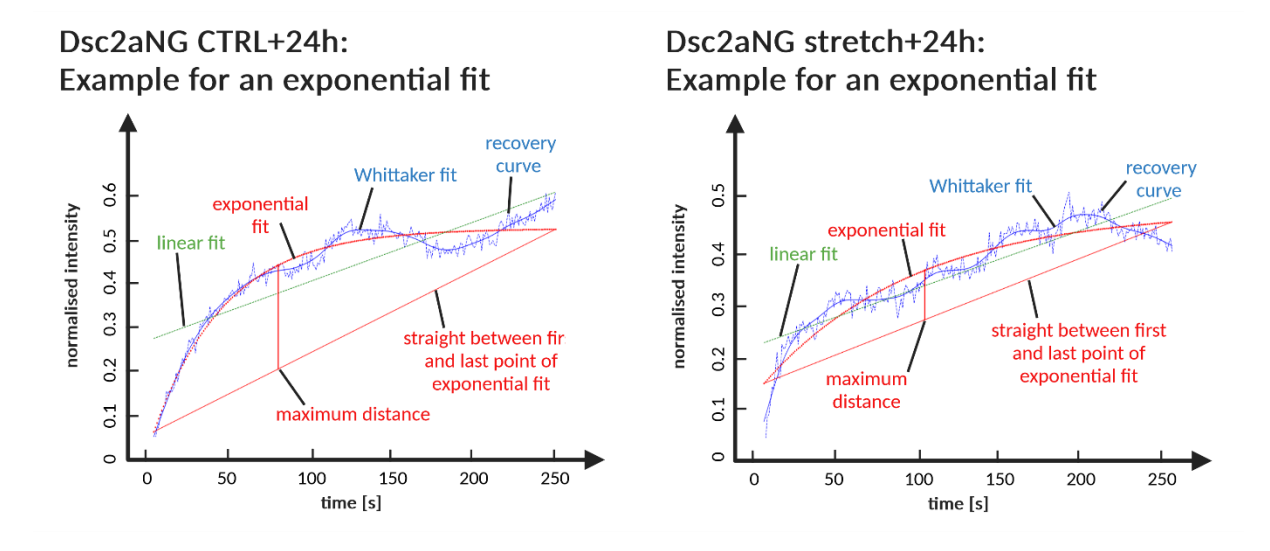
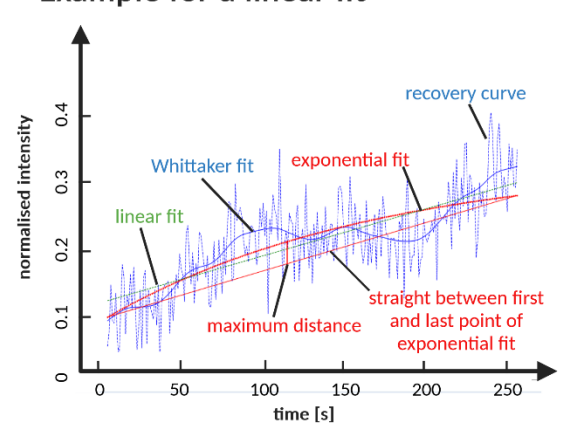


Figure 21: Examples of the exponential as well as the linear fit with Dsc2aNG CTRL+24 h (above) and Dsc2aNG stretch +24 h (below) recovery curves. Dsc2aNG CTRL+24 h: For the exponential fit, the standard deviation was 0.014 and the  $f_{max}$  was 0.25. Dsc2aNG stretch+24 h: For the exponential fit, the standard deviation was 0.017 and the  $f_{max}$  was 0.098. For more details on the fit functions as well as the Whittaker fit see section 2.2.5.2.

# Dsc2aGFP CTRL: Example for an exponential fit

#### Whittaker 0.3 recovery curve exponential normalised intensity 0.2 0.1 straight between first and last point of exponential fit maximum distance 50 100 150 200 250 time [s]

## Dsc2aGFP CTRL: Example for a linear fit



# Dsc2aGFP stretch: Example for an exponential fit

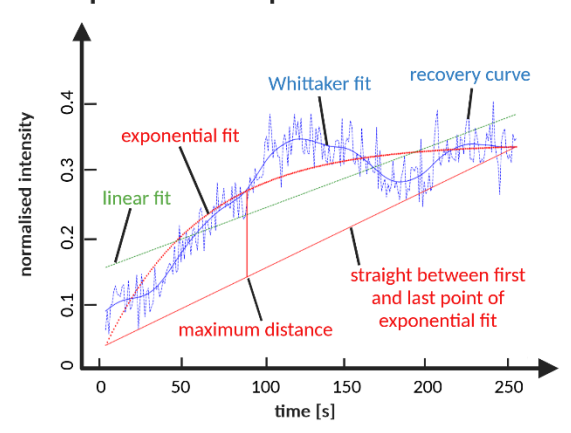
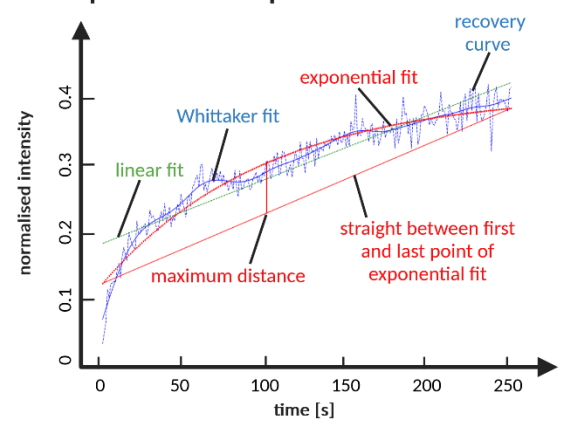
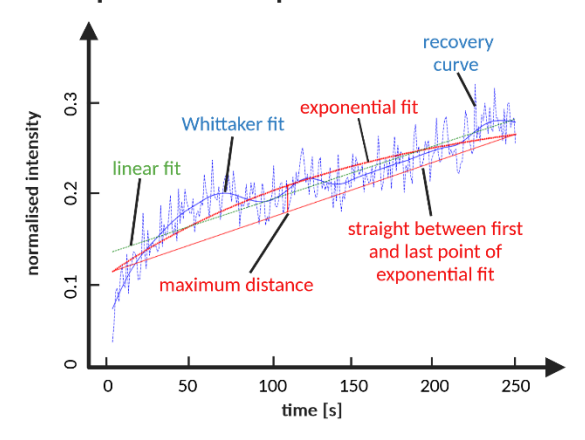


Figure 22: Examples of the exponential as well as the linear fit with Dsc2aGFP CTRL (above) and Dsc2aGFP stretch recovery curves (below). For the exponential fit, the standard deviation was 0.011 and the  $f_{max}$  was 0.11 and for the linear fit, the standard deviation was 0.045 and the  $f_{max}$  was 0.037. Dsc2aGFP stretch: For the exponential fit, the standard deviation was 0.027 and the  $f_{max}$  was 0.15. For more details on the fit functions as well as the Whittaker fit see section 2.2.5.2.

# Dsc2aGFP CTRL+24h: Example for an exponential fit



## Dsc2aGFP stretch+24h: Example for an exponential fit



# Dsc2aGFP stretch+24h: Example for a linear fit

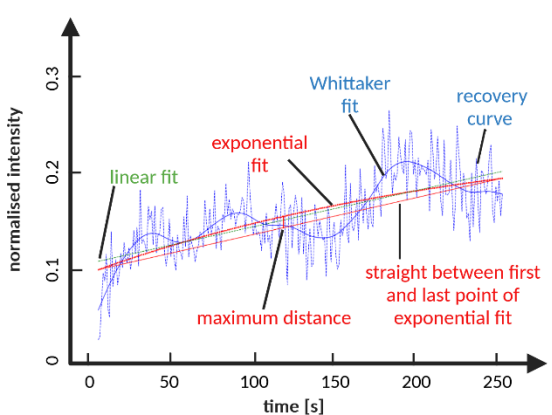


Figure 23: Examples of the exponential as well as the linear fit with Dsc2aGFP CTRL+24 h (above) and Dsc2aGFP stretch+24 h (below) recovery curves. Dsc2aGFP CTRL+24 h: For the exponential fit, the standard deviation was 0.015 and the  $f_{max}$  was 0.073. Dsc2aGFP stretch+24 h: For the exponential fit, the standard deviation was 0.019 and the  $f_{max}$  was 0.033 and for the linear fit, the standard deviation was 0.025 and the  $f_{max}$  was 0.013. For more details on the fit functions as well as the Whittaker fit see section 2.2.5.2.

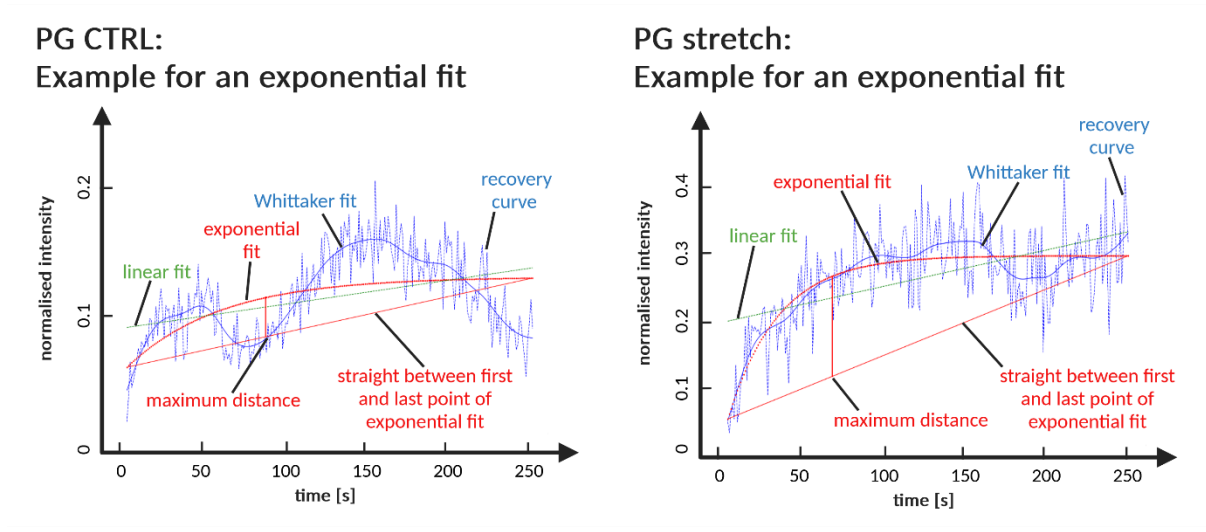


Figure 24: Examples of the exponential as well as the linear fit with PG CTRL (above) and PG stretch (below) recovery curves. PG CTRL: For the exponential fit, the standard deviation was 0.019 and the  $f_{max}$  was 0.037. PG stretch: For the exponential fit, the standard deviation was 0.055 and the  $f_{max}$  was 0.19. For more details on the fit functions as well as the Whittaker fit see section 2.2.5.2.

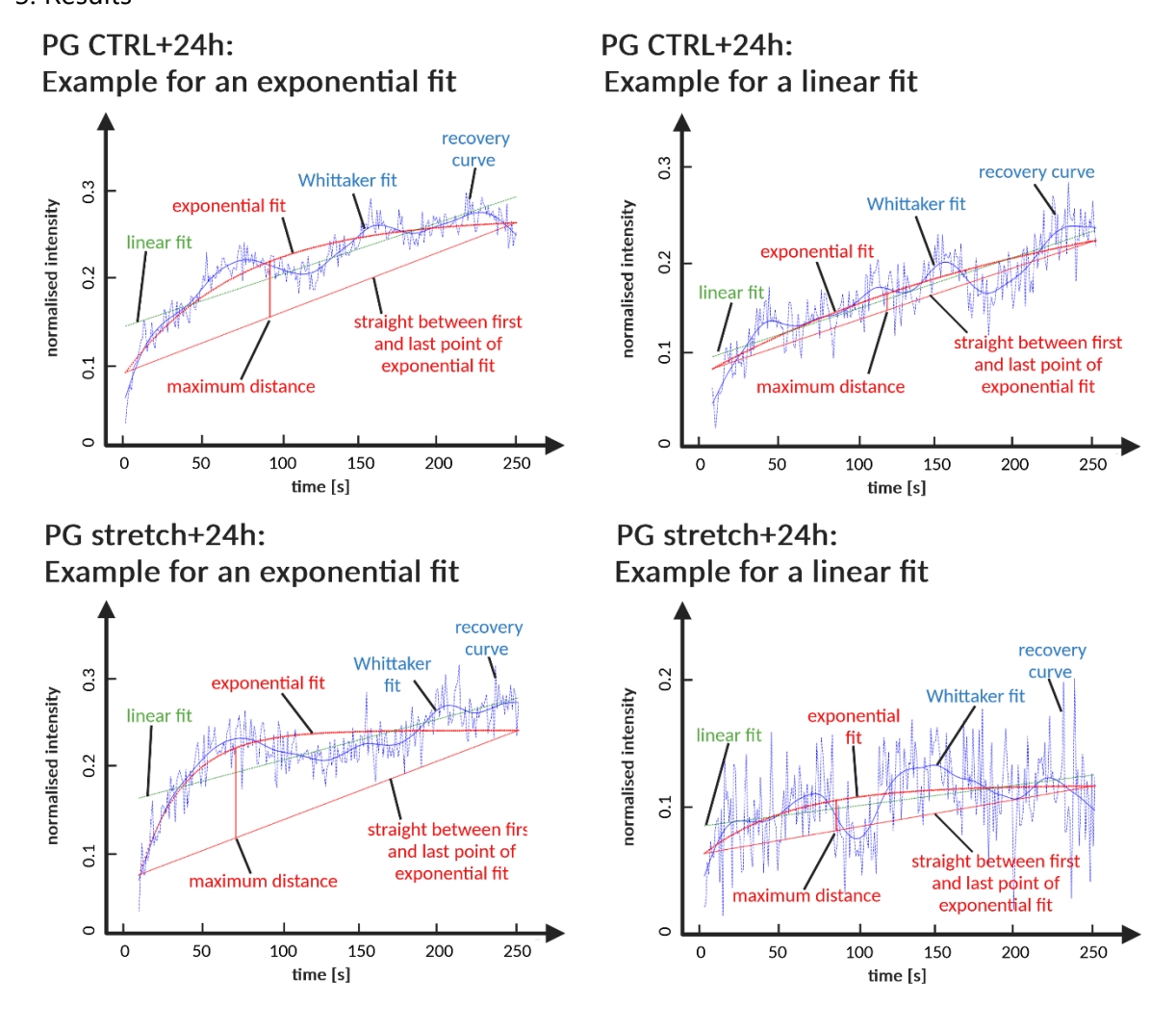


Figure 25: Examples of the exponential as well as the linear fit with PG CTRL+24 h (above) and PG stretch+24 h (below) recovery curves. PG CTRL+24 h: For the exponential fit, the standard deviation was 0.013 and the  $f_{max}$  was 0.072 and for the linear fit, the standard deviation was 0.021 and the  $f_{max}$  was 0.020. PG stretch+24 h: For the exponential fit, the standard deviation was 0.020 and the  $f_{max}$  was 0.11 and for the linear fit, the standard deviation was 0.031 and the  $f_{max}$  was 0.027. For more details on the fit functions as well as the Whittaker fit see section 2.2.5.2.

# 3.4. Desmosomal protein exchange kinetics in the absence of mechanical stretch

## 3.4.1. Recovery curves

Analysing the desmosomal protein exchange kinetics in the absence of mechanical stretch provided a baseline for the stretched samples. For DP, PG, Dsc 2a GFP and Dsc 2a NG, three respectively four independent samples were analysed. With each sample, 10 or 11 measurements could be conducted (figure 26) below.

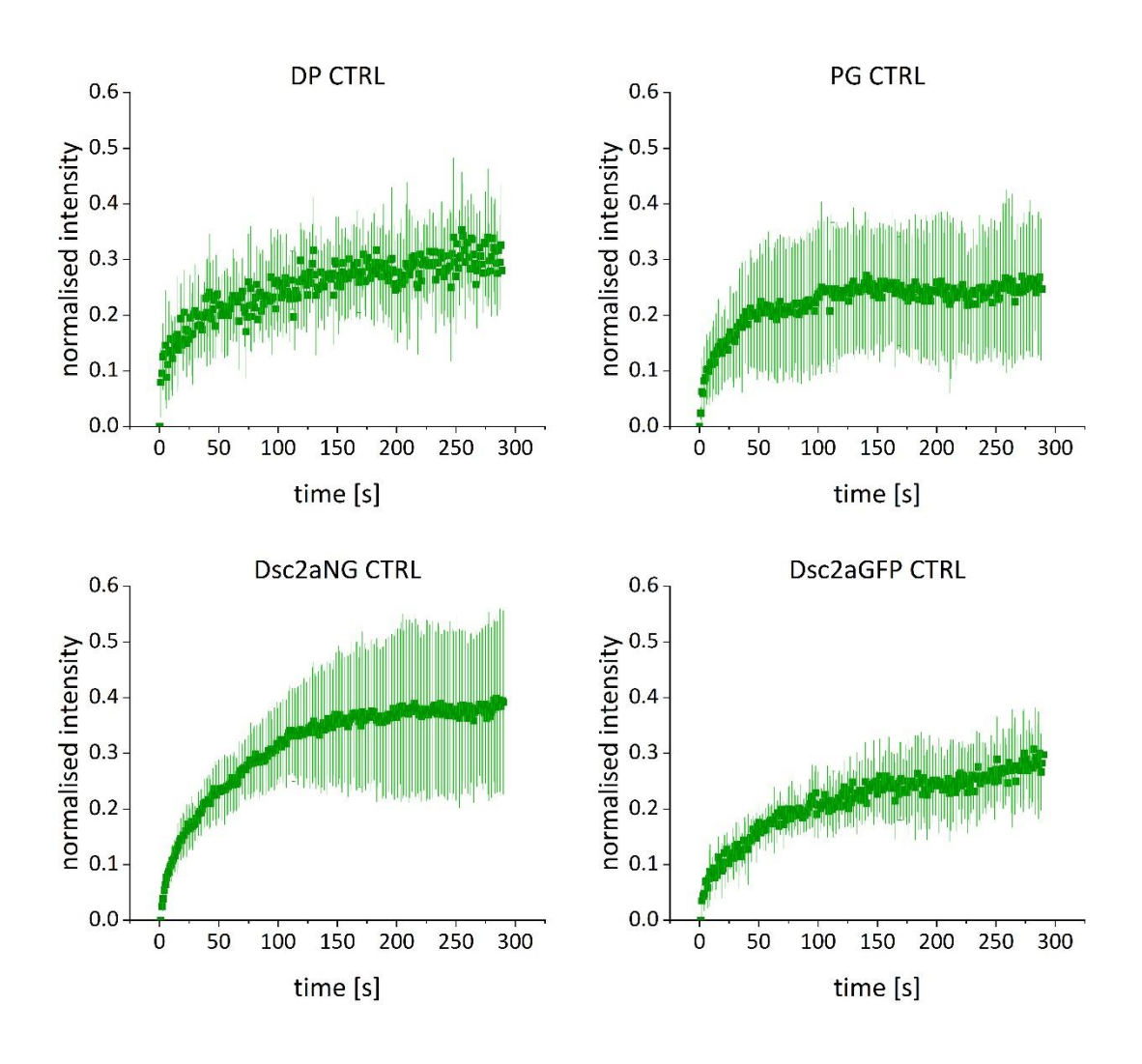


Figure 26: Recovery curves of the desmosomal proteins in absence of mechanical stretch. Mean recovery and standard deviation of DP (N=9, from five independent samples), PG (N=7, from four independent samples), Dsc2a NG (N=10, from three independent samples) and Dsc2a GFP (N=10, from three independent samples). The normalisation procedure is described in section 2.2.5.1. The individual recovery curves can be found in the appendix, pages I to XVII.

## 3.4.2. Fitted parameters

Upon closer examination, it became apparent that some recovery curves display a visually noticeable increase in intensity in the first second after bleaching. Although the experimental set-up already largely discriminated against the cytoplasmic background, there seems to be some diffusive fraction in the cytoplasm influencing the recovery curves and creating this offset. Moreover, the height of the offset differs between the cell lines. In the exponential fit described with equation 7, this offset is taken into account and is represented by the parameter *a*. The offset of DP, PG, Dsc 2a GFP and Dsc 2a NG in the absence of mechanical stretch is shown in figure 27 below.

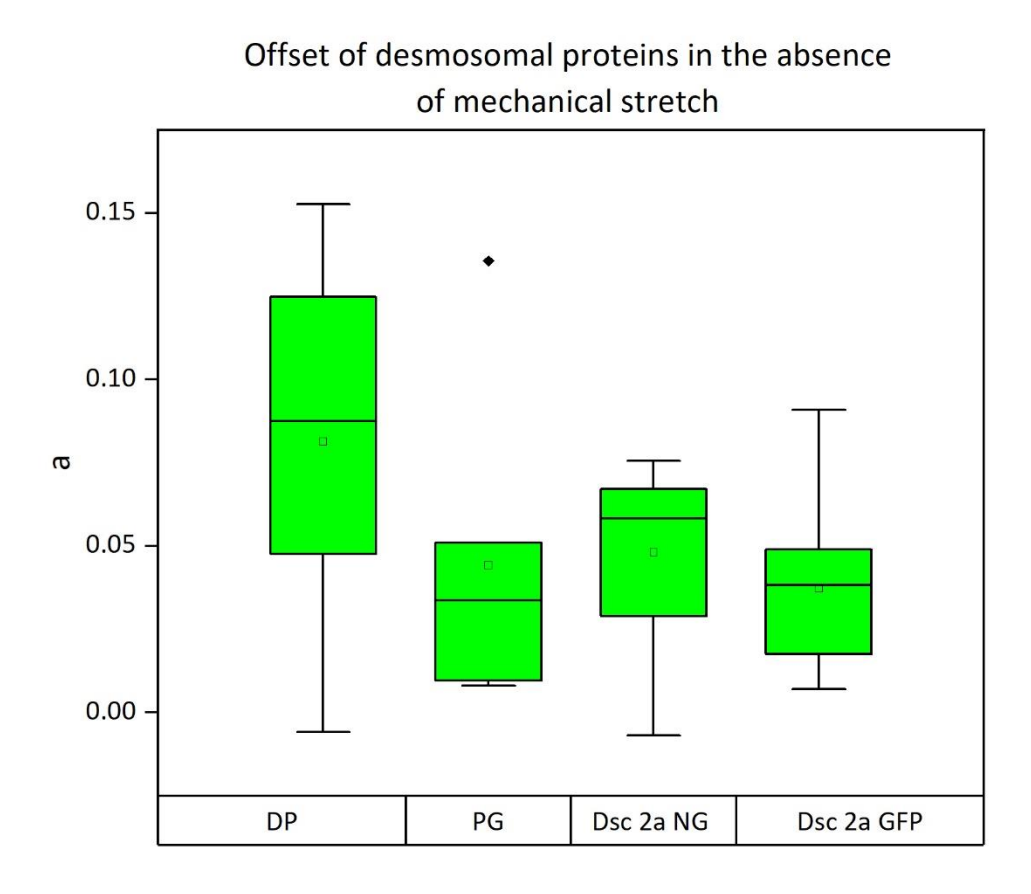


Figure 27: Boxplot of offset of the desmosomal proteins DP, PG, Dsc 2a GFP and Dsc 2a NG in absence of mechanical stretch. The number of fits included in the evaluation were N=5 for DP (from five independent samples), N=7 for PG (from four independent samples), N=10 for Dsc 2a NG (from three independent samples) and N=9 for Dsc 2a GFP (from three independent samples). The boxplot indicates the mean (square), the median (line), 25-75% of the data distribution (box) and potential outliers (rhombus) for each data set.

In the absence of mechanical stretch, the mean offset was 0.081 for DP, 0.044 for PG, 0.048 for Dsc 2a NG and 0.037 for Dsc 2a GFP. The bootstrapped confidence intervals (95%) for these values can be found in the table 6 below (for details see section 2.2.5.3).

Offset in the abscence of mechanical stretch			
Desmosomal protein	mean	upper	lower
DP	0.081	0.13	0.034
PG	0.044	0.069	0.012
Dsc 2a NG	0.048	0.065	0.033
Dsc 2a GFP	0.037	0.052	0.020

Table 6: Mean offset of the desmosomal proteins DP, PG, Dsc 2a GFP and Dsc 2a NG in the absence of mechanical stretch, with their upper and lower confidence intervals (95%). The number of fits included in the evaluation were N=5 for DP (from five independent samples), N=7 for PG (from four independent samples), N=10 for Dsc 2a NG (from three independent samples) and N=9 for Dsc 2a GFP (from three independent samples).

In the exponential fit (equation 7) the parameter *b* indicates the exchanging fraction. The exchanging fractions of DP, PG, Dsc 2a GFP and Dsc 2a NG are shown in figure 28 below.

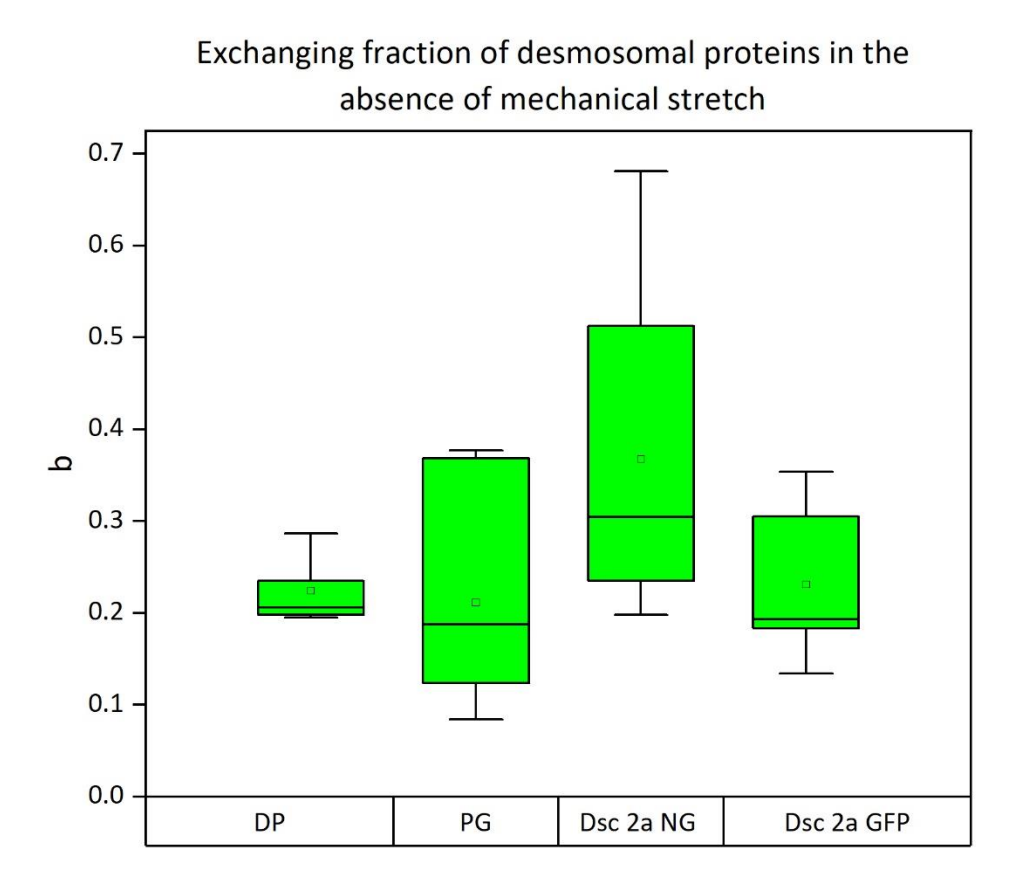


Figure 28: Boxplot of the exchanging fraction of the desmosomal proteins DP, PG, Dsc 2a GFP and Dsc 2a NG in absence of mechanical stretch. The number of fits included in the evaluation were N=5 for DP (from five independent samples), N=7 for PG (from four independent samples), N=10 for Dsc 2a NG (from three independent samples) and N=9 for Dsc 2a GFP (from three independent samples). The boxplot indicates the mean (square), the median (line), 25-75% of the data distribution (box) and potential outliers (rhombus) for each data set.

In the absence of mechanical stretch, the mean exchanging fraction was 0.22 for DP, 0.21 for PG, 0.37 for Dsc 2a NG and 0.23 for Dsc 2a GFP. The bootstrapped confidence intervals (95%) for these values can be found in table 7 on the next page.

Exchanging fraction in the abscence of mechanical stretch			
Desmosomal protein	mean	upper	lower
DP	0.22	0.25	0.19
PG	0.21	0.28	0.13
Dsc 2a NG	0.37	0.46	0.27
Dsc 2a GFP	0.23	0.28	0.18

Table 7: Mean exchanging fraction of the desmosomal proteins DP, PG, Dsc 2a GFP and Dsc 2a NG in the absence of mechanical stretch, with their upper and lower confidence intervals (95%). The number of fits included in the evaluation were N=5 for DP (from five independent samples), N=7 for PG (from four independent samples), N=10 for Dsc 2a NG (from three independent samples) and N=9 for Dsc 2a GFP (from three independent samples).

In the exponential fit, the rate constant is indicated by parameter k (equation 7). The rate constant of DP, PG, Dsc 2a GFP and Dsc 2a NG is shown in figure 29 below.

## Rate constant of desmosomal proteins in the absence of mechanical stretch

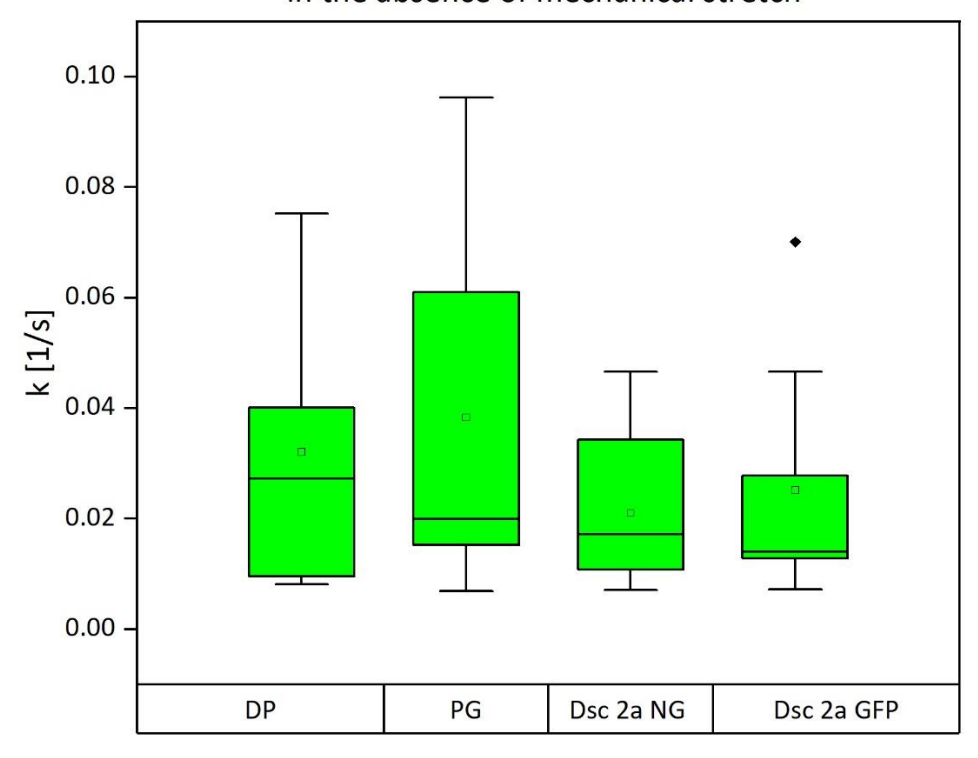


Figure 29: Boxplot of the rate constant of the desmosomal proteins DP, PG, Dsc 2a GFP and Dsc 2a NG in absence of mechanical stretch. The number of fits included in the evaluation were N=5 for DP (from five independent samples), N=7 for PG (from four independent samples), N=10 for Dsc 2a NG (from three independent samples) and N=9 for Dsc 2a GFP (from three independent samples). The boxplot indicates the mean (square), the median (line), 25-75% of the data distribution (box) and potential outliers (rhombus) for each data set.

In the absence of mechanical stretch, the mean rate constant was 0.032 1/s for DP, 0.038 1/s for PG, 0.021 1/s for Dsc 2a NG and 0.025 1/s for Dsc 2a GFP. The bootstrapped confidence interval (95%) for these values can be found in table 8 below (for details see section 2.2.5.3).

Rate constant in the abscence of mechanical stretch [1/s]						
Desmosomal protein mean upper lower						
DP	0.032	0.051	0.093			
PG	0.038	0.059	0.015			
Dsc 2a NG	0.021	0.029	0.012			
Dsc 2a GFP	0.025	0.036	0.012			

Table 8: Mean rate constant of the desmosomal proteins DP, PG, Dsc 2a GFP and Dsc 2a NG in the absence of mechanical stretch, with their upper and lower confidence intervals (95%). The number of fits included in the evaluation were N=5 for DP (from five independent samples), N=7 for PG (from four independent samples), N=10 for Dsc 2a NG (from three independent samples) and N=9 for Dsc 2a GFP (from three independent samples).

The lifetime of the desmosomal proteins is calculated based on the rate constant (equation 8) and corresponds to the time point at which half of the intensity of the exchanging fraction is reached. The lifetime,  $t_{1/2}$ , of the desmosomal proteins DP, PG, Dsc 2a GFP and Dsc 2a NG in the abscence of mechanical stretch is shown in figure 30 on the next page.

# Lifetime of desmosomal proteins in the absence of mechanical stretch

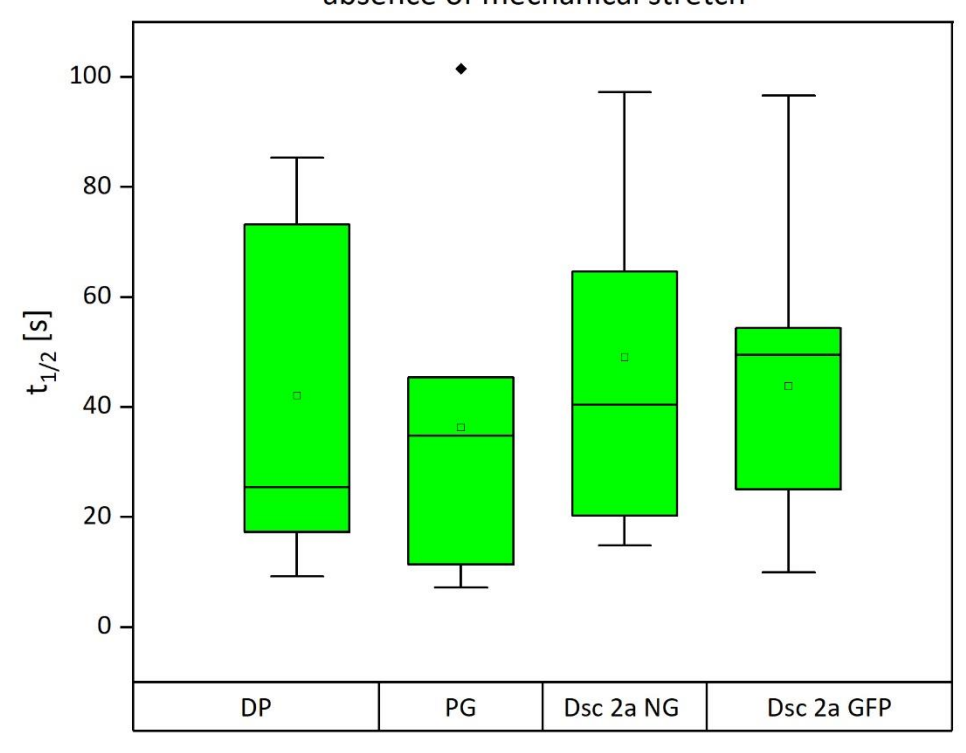


Figure 30: Boxplot of the lifetime of the desmosomal proteins DP, PG, Dsc 2a GFP and Dsc 2a NG in absence of mechanical stretch. The number of fits included in the evaluation were N=5 for DP (from five independent samples), N=7 for PG (from four independent samples), N=10 for Dsc 2a NG (from three independent samples) and N=9 for Dsc 2a GFP (from three independent samples). The boxplot indicates the mean (square), the median (line), 25-75% of the data distribution (box) and potential outliers (rhombus) for each data set.

In the absence of mechanical stretch, the mean lifetime was 42 s for DP, 36 s for PG, 49 s for Dsc 2a NG and 44 s for Dsc 2a GFP. The bootstrapped confidence intervals (95%) for these values can be found in table 9 on the next page (for details see section 2.2.5.3).

Lifetime in the abscence of mechanical stretch [s]			
Desmosomal protein	mean	upper	lower
DP	42	68	15
PG	36	56	13
Dsc 2a NG	49	67	31
Dsc 2a GFP	44	60	26

Table 9: Mean lifetime of the desmosomal proteins DP, PG, Dsc 2a GFP and Dsc 2a NG in the absence of mechanical stretch with their upper and lower confidence intervals (95%). The number of fits included in the evaluation were N=5 for DP (from five independent samples), N=7 for PG (from four independent samples), N=10 for Dsc 2a NG (from three independent samples) and N=9 for Dsc 2a GFP (from three independent samples).

# 3.5. Effect of mechanical stretch on desmosomal protein exchange kinetics

## 3.5.1 Recovery curves

To analyse the effect of mechanical stretch on desmosomal protein exchange kinetics, different MDCK cell lines where one respective desmosomal protein was fluorescently tagged were analysed with FRAP after mechanical stretch. For DP, PG, Dsc 2a GFP and Dsc 2a NG, three respectively four independent samples were analysed after 2 h of mechanical stretch with a 50% amplitude at 80 mHz. With each sample, 10 or 16 measurements could be conducted (figure 31 on the next page).

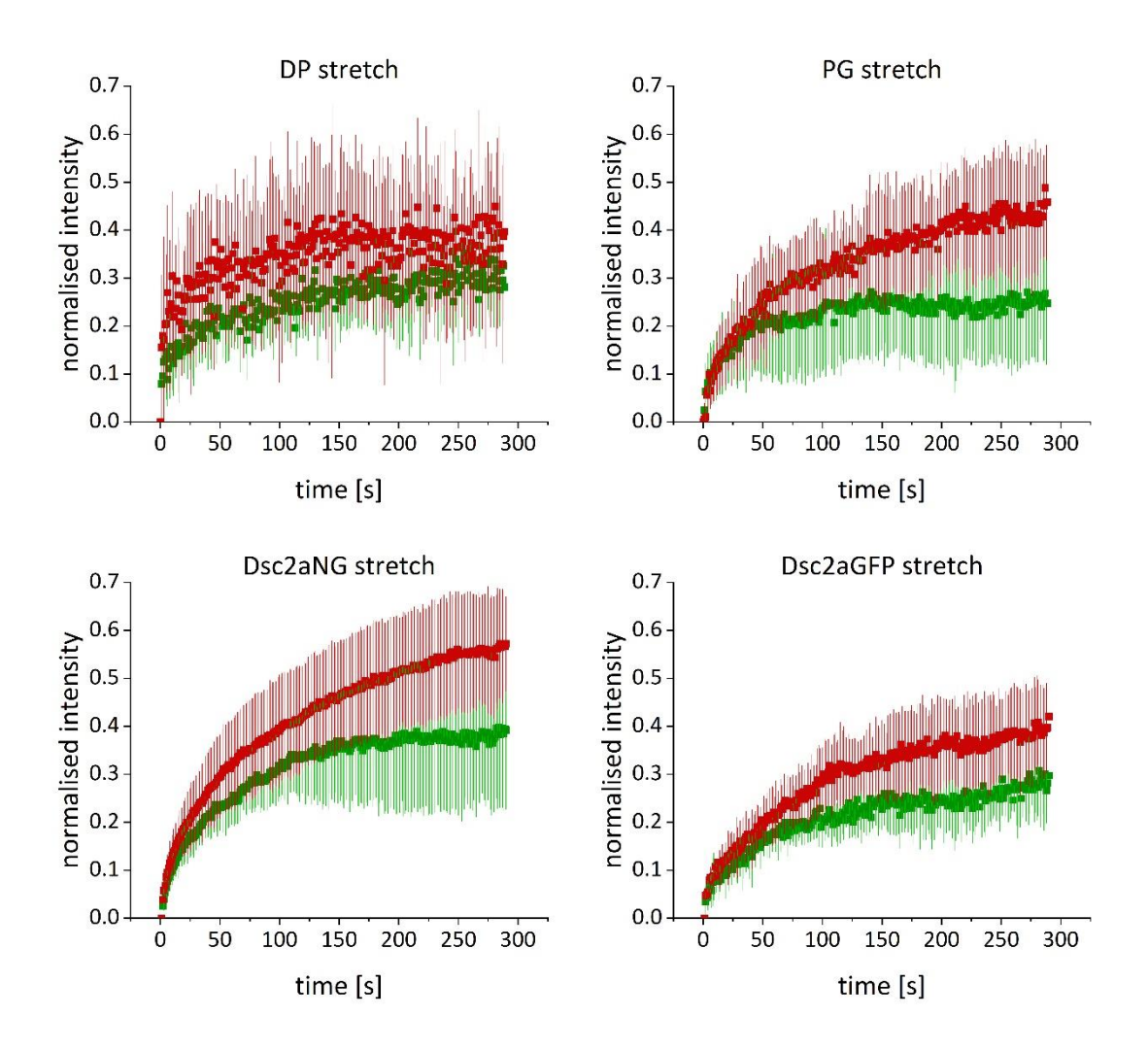


Figure 31: Recovery curves of the desmosomal proteins DP, PG, Dsc 2a GFP and Dsc 2a NG after 2 h of mechanical stretch with a 50% amplitude at 80 mHz. Mean recovery and standard deviation (red) of DP (N=10, from three independent samples), Dsc2a NG (N=16, from three independent samples) and Dsc2a GFP (N=10, from three independent samples). CTRL in absence of mechanical stretch (green) is shown in figure 26. The normalisation procedure is described in section 2.2.5.1. The individual recovery curves can be found in the appendix, pages I to XVII.

#### 3.5.2 Fitted parameters

The offsets of the desmosomal proteins DP, PG, Dsc 2a GFP and Dsc 2a NG after 2 h, 50% and 80 mHz of mechanical stretch are compared to unstretched controls and shown in figure 32 on the next page.

# Offset of desmosomal proteins after mechanical stretch (2h, 50%, 80 mHz)

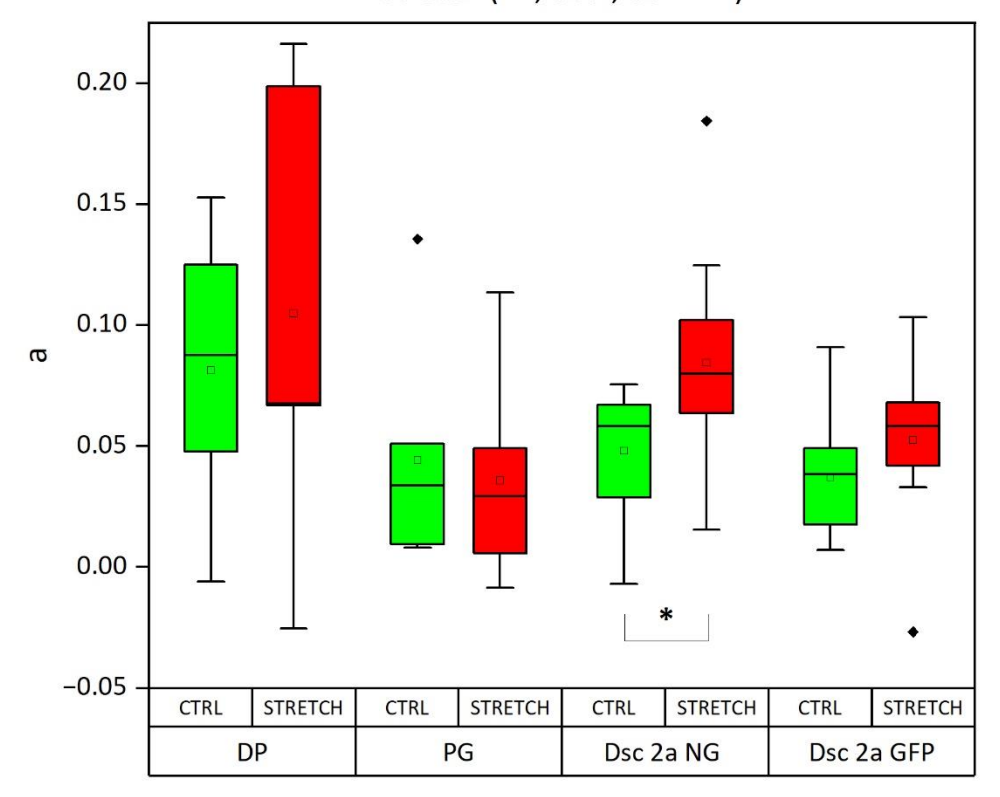


Figure 32: Boxplot of the offset of the desmosomal proteins DP, PG, Dsc 2a GFP and Dsc 2a NG after 2 h of mechanical stretch with a 50% amplitude at 80 mHz (red) in comparison with the unstretched control (green, shown in figure 27). The number of fits included in the evaluation were N=5 for DP (from five independent samples), N=7 for PG (from four independent samples), N=10 for Dsc 2a NG (from three independent samples) and N=9 for Dsc 2a GFP (from three independent samples) for the unstretched controls, and N=5 for DP (from three independent samples), N=10 for PG (from four independent samples), N=16 for Dsc 2a NG (from three independent samples) and N=10 for Dsc 2a GFP (from three independent samples) for the stretched samples. The boxplot indicates the mean (square), the median (line), 25-75% of the data distribution (box) and potential outliers (rhombus) for each data set. Significant results (two-tailed t-test with significance level  $\alpha < 0.05$ ) are highlighted with an asterisk.

After stretch, the mean offset was 0.10 for DP, 0.036 for PG, 0.085 for Dsc 2a NG and 0.052 for Dsc 2a GFP. Compared to the unstretched control, the offset increase of the Dsc 2a NG cells was found to be significantly (determined with the two tailed t-test, significance level  $\alpha$ =0.05). For DP, PG and Dsc 2a GFP, no significant increase was found. The mean offsets of the desmosomal proteins and the bootstrapped confidence interval (95%) for these values can be found in the table 10 on the next page (for details see section 2.2.5.3).

Offset after mechanical stretch			
Desmosomal protein	mean	upper	lower
DP CTRL	0.081	0.13	0.034
DP stretch	0.10	0.19	0.027
PG CTRL	0.044	0.069	0.012
PG stretch	0.036	0.055	0.012
Dsc 2a NG CTRL	0.048	0.065	0.033
Dsc 2a NG stretch	0.085	0.10	0.067
Dsc 2a GFP CTRL	0.037	0.052	0.020
Dsc 2a GFP stretch	0.052	0.072	0.035

Table 10: Mean offset of desmosomal proteins DP, PG, Dsc 2a NG and Dsc 2a GFP after mechanical stretch (2 h, 50%, 80 mHz), with their upper and lower confidence intervals (95%). The number of fits included in the evaluation were N=5 for DP (from five independent samples), N=7 for PG (from four independent samples), N=10 for Dsc 2a NG (from three independent samples) and N=9 for Dsc 2a GFP (from three independent samples) for the unstretched controls, and N=5 for DP (from three independent samples), N=10 for PG (from four independent samples), N=16 for Dsc 2a NG (from three independent samples) and N=10 for Dsc 2a GFP (from three independent samples) for the stretched samples.

The exchanging fractions of the desmosomal proteins DP, PG, Dsc 2a GFP and Dsc 2a NG after 2 h, 50% and 80 mHz of mechanical stretch is shown in figure 33 on the next page.

# Exchanging fraction of desmosomal proteins after mechanical stretch (2h, 50%, 80 mHz)

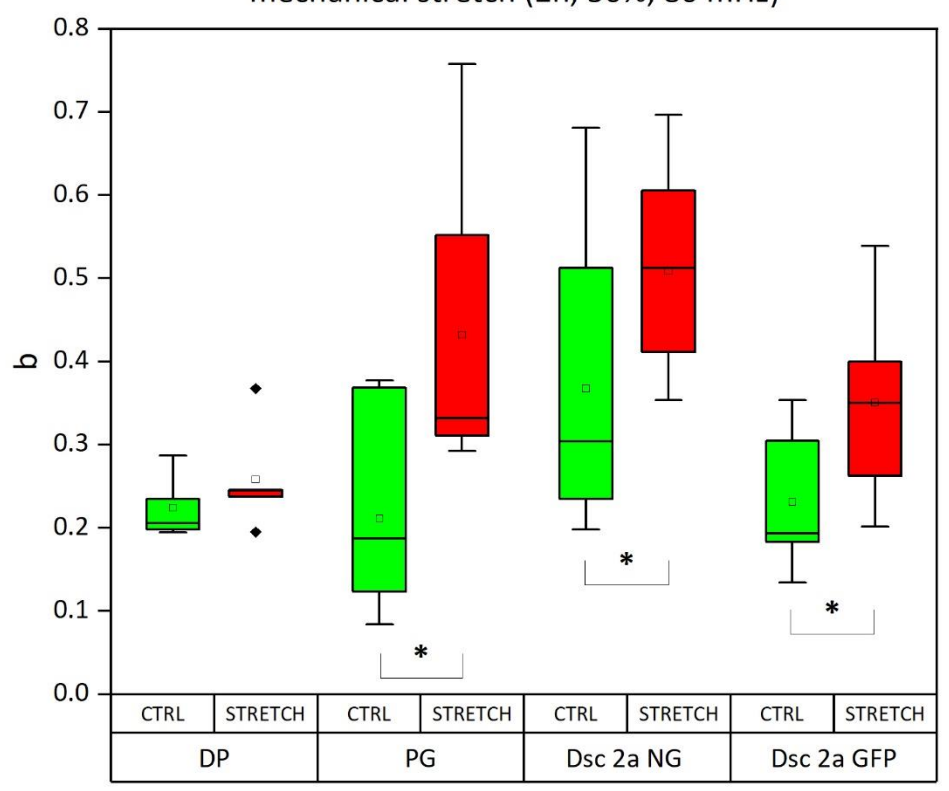


Figure 33: Boxplot of the exchanging fraction of the desmosomal proteins DP, PG, Dsc 2a GFP and Dsc 2a NG after 2 h of mechanical stretch with a 50% amplitude at 80 mHz (red) in comparison to the unstretched control (green, shown in figure 28). The number of fits included in the evaluation were N=5 for DP (from five independent samples), N=7 for PG (from four independent samples), N=10 for Dsc 2a NG (from three independent samples) and N=9 for Dsc 2a GFP (from three independent samples) for the unstretched controls, and N=5 for DP (from three independent samples), N=10 for PG (from four independent samples), N=16 for Dsc 2a NG (from three independent samples) and N=10 for Dsc 2a GFP (from three independent samples) for the stretched samples. The boxplot indicates the mean (square), the median (line), 25-75% of the data distribution (box) and potential outliers (rhombus) for each data set. Significant results (Wilcoxon rank sum test (PG) respectively two tailed t-test (Dsc 2a GFP and Dsc 2a NG), all with significance level  $\alpha$ <0.05) are highlighted with an asterisk.

After stretch, the mean exchanging fraction was 0.26 for DP, 0.43 for PG, 0.51 for Dsc 2a NG and 0.35 for Dsc 2a GFP. Compared to the unstretched control, the exchanging fraction of PG, Dsc 2a NG and Dsc 2a GFP increased significantly (determined with the Wilcoxon rank sum test (PG) respectively the two tailed t-test (Dsc 2a GFP and Dsc 2a NG) with a significance level  $\alpha$ =0.05). The exchanging fraction of DP did not change significantly after stretch. The mean exchanging fractions of the

desmosomal proteins and the bootstrapped confidence interval (95%) for these values can be found in the table 11 below (for details see section 2.2.5.3).

Exchanging fraction after mechanical stretch			
Desmosomal protein	mean	upper	lower
DP CTRL	0.22	0.25	0.19
DP stretch	0.26	0.30	0.20
PG CTRL	0.21	0.28	0.13
PG stretch	0.43	0.53	0.33
Dsc 2a NG CTRL	0.37	0.46	0.27
Dsc 2a NG stretch	0.51	0.56	0.45
Dsc 2a GFP CTRL	0.23	0.28	0.18
Dsc 2a GFP stretch	0.35	0.41	0.29

Table 11: Mean exchanging fraction of the desmosomal proteins DP, PG, Dsc 2a NG and Dsc 2a GFP after mechanical stretch (2 h, 50%, 80 mHz), with their upper and lower confidence intervals (95%). The number of fits included in the evaluation were N=5 for DP (from five independent samples), N=7 for PG (from four independent samples), N=10 for Dsc 2a NG (from three independent samples) and N=9 for Dsc 2a GFP (from three independent samples) for the unstretched controls, and N=5 for DP (from three independent samples), N=10 for PG (from four independent samples), N=16 for Dsc 2a NG (from three independent samples) and N=10 for Dsc 2a GFP (from three independent samples) for the stretched samples.

The rate constants of the desmosomal proteins DP, PG, Dsc 2a GFP and Dsc 2a NG after 2 h, 50% and 80 mHz of mechanical stretch is shown in figure 34 on the next page.

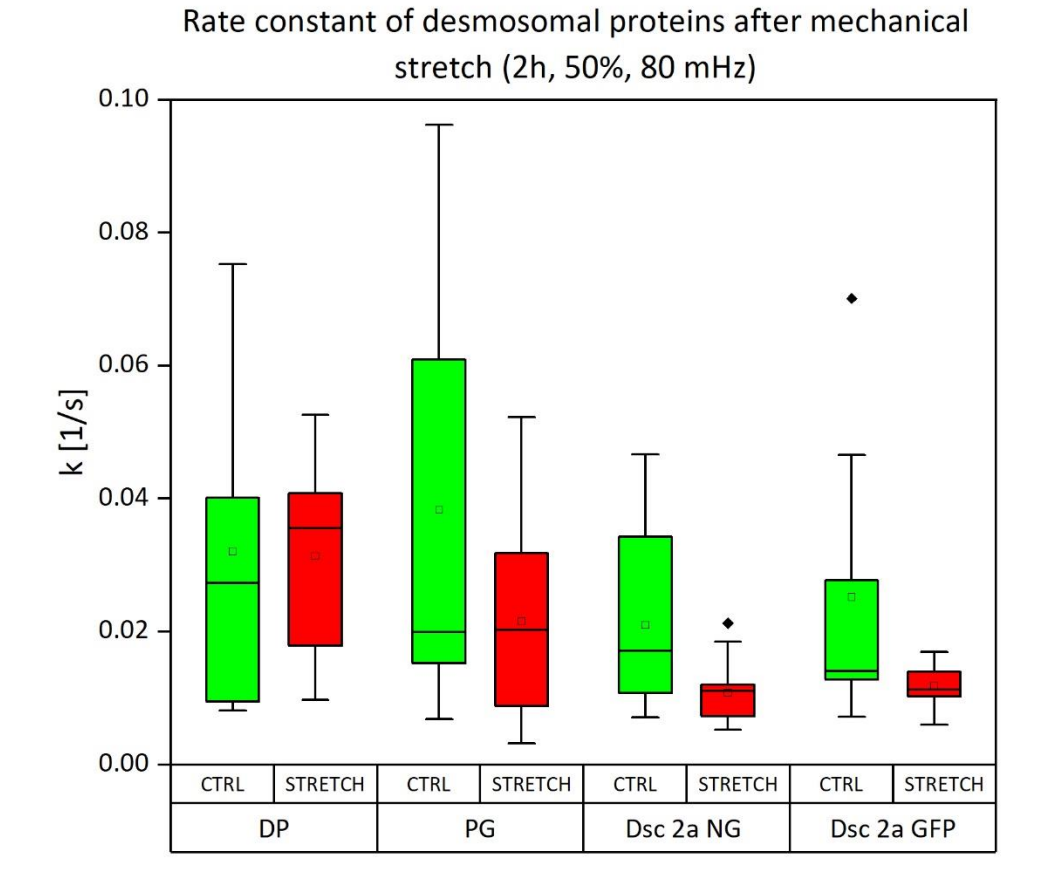


Figure 34: Boxplot of the rate constant of the desmosomal proteins DP, PG, Dsc 2a GFP and Dsc 2a NG after 2 h of mechanical stretch with a 50% amplitude at 80 mHz for the (red) in comparison with the unstretched control (green, shown in figure 29). The number of fits included in the evaluation were N=5 for DP (from five independent samples), N=7 for PG (from four independent samples), N=10 for Dsc 2a NG (from three independent samples) and N=9 for Dsc 2a GFP (from three independent samples) for the unstretched controls, and N=5 for DP (from three independent samples) and N=10 for Dsc 2a GFP (from three independent samples) for the stretched samples. The boxplot indicates the mean (square), the median (line), 25-75% of the data distribution (box) and potential outliers (rhombus) for each data set.

After stretch, the mean rate constant was 0.031 1/s for DP, 0.022 1/s for PG, 0.011 1/s for Dsc 2a NG and 0.012 1/s for Dsc 2a GFP. For all desmosomal proteins, there were no significant changes between the stretched and the unstretched samples. The mean rate constants of the desmosomal proteins and the bootstrapped confidence interval (95%) for these values can be found in the table 12 on the next page (for details see section 2.2.5.3).

Rate constant after mechanical stretch [1/s]			
Desmosomal protein	mean	upper	lower
DP CTRL	0.032	0.051	0.093
DP stretch	0.031	0.049	0.019
PG CTRL	0.038	0.059	0.015
PG stretch	0.022	0.030	0.013
Dsc 2a NG CTRL	0.021	0.029	0.012
Dsc 2a NG stretch	0.011	0.013	0.0086
Dsc 2a GFP CTRL	0.025	0.036	0.012
Dsc 2a GFP stretch	0.012	0.014	0.010

Table 12: Mean rate constant k of the desmosomal proteins DP, PG, Dsc 2a NG and Dsc 2a GFP after mechanical stretch (2 h, 50%, 80 mHz), with their upper and lower confidence intervals (95%). The number of fits included in the evaluation were N=5 for DP (from five independent samples), N=7 for PG (from four independent samples), N=10 for Dsc 2a NG (from three independent samples) and N=9 for Dsc 2a GFP (from three independent samples) for the unstretched controls, and N=5 for DP (from three independent samples), N=10 for PG (from four independent samples), N=16 for Dsc 2a NG (from three independent samples) and N=10 for Dsc 2a GFP (from three independent samples) for the stretched samples.

The lifetimes of the desmosomal proteins DP, PG, Dsc 2a GFP and Dsc 2a NG after 2 h, 50% and 80 mHz of mechanical stretch is shown in figure 35 below.

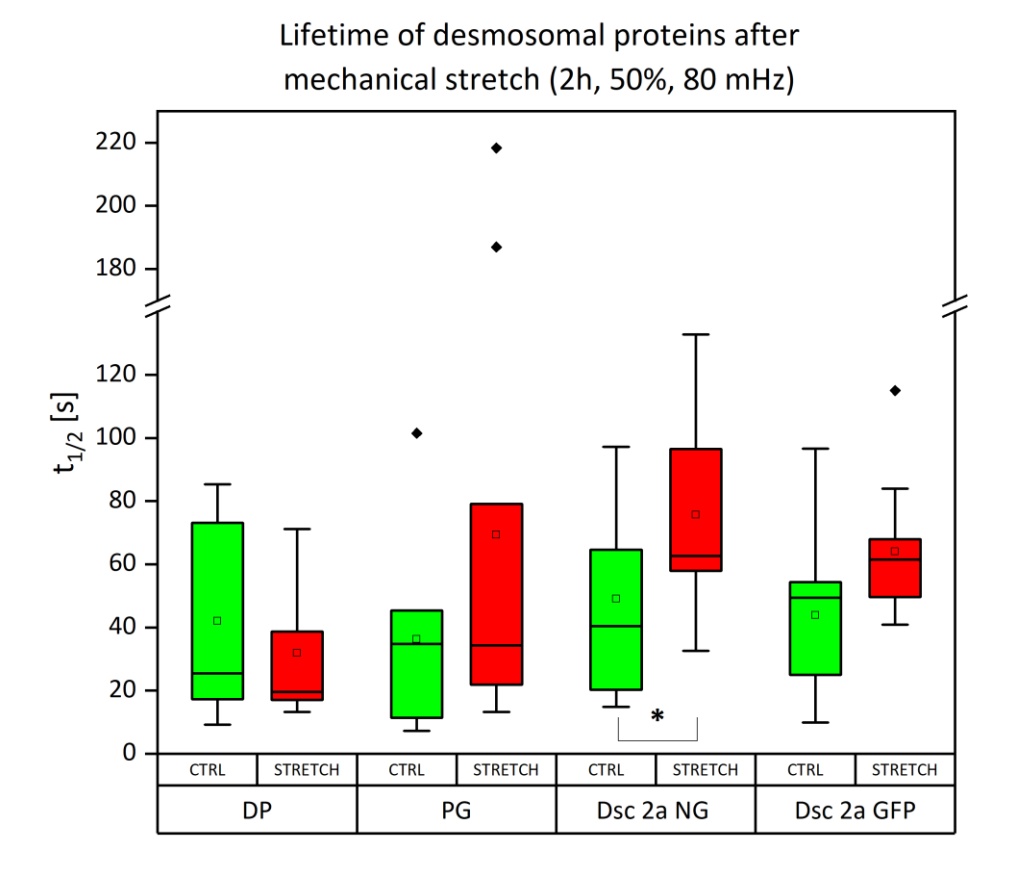


Figure 35: Boxplot of the lifetime of the desmosomal proteins DP, PG, Dsc 2a GFP and Dsc 2a NG after 2 h of mechanical stretch with a 50% amplitude and 80 mHz (red) in comparison with the unstretched control (green, shown in figure 30). The number of fits included in the evaluation were N=5 for DP (from five independent samples), N=7 for PG (from four independent samples), N=10 for Dsc 2a NG (from three independent samples) and N=9 for Dsc 2a GFP (from three independent samples) for the unstretched controls, and N=5 for DP (from three independent samples), N=10 for PG (from four independent samples), N=16 for Dsc 2a NG (from three independent samples) and N=10 for Dsc 2a GFP (from three independent samples) for the stretched samples. The boxplot indicates the mean (square), the median (line), 25-75% of the data distribution (box) and potential outliers (rhombus) for each data set. Significant results (two tailed t-test with significance level  $\alpha$ <0.05) are highlighted with an asterisk.

After stretch, the mean lifetime was 32 s for DP, 69 s for PG, 76 s for Dsc 2a NG and 64 s for Dsc 2a GFP. Compared to the unstretched control, the mean lifetime of Dsc 2a NG increased significantly (determined with the two tailed t-test at a significance level  $\alpha$ =0.05). The lifetimes of DP, PG and Dsc 2a GFP did not change significantly after stretch. The mean lifetime of the desmosomal proteins and the

bootstrapped confidence intervals for these values can be found in the table 13 below (for details see section 2.2.5.3).

Lifetime after mechanical stretch [s]			
Desmosomal protein	mean	upper	lower
DP CTRL	42	68	15
DP stretch	32	48	12
PG CTRL	36	56	13
PG stretch	69	110	19
Dsc 2a NG CTRL	49	67	31
Dsc 2a NG stretch	76	89	61
Dsc 2a GFP CTRL	44	60	26
Dsc 2a GFP stretch	64	75	50

Table 13: Mean lifetime of the desmosomal proteins DP, PG, Dsc 2a NG and Dsc 2a GFP after mechanical stretch (2 h, 50%, 80 mHz), with their upper and lower confidence intervals (95%). The number of fits included in the evaluation were N=5 for DP (from five independent samples), N=7 for PG (from four independent samples), N=10 for Dsc 2a NG (from three independent samples) and N=9 for Dsc 2a GFP (from three independent samples) for the unstretched controls, and N=5 for DP (from three independent samples), N=10 for PG (from four independent samples), N=16 for Dsc 2a NG (from three independent samples) and N=10 for Dsc 2a GFP (from three independent samples) for the stretched samples.

# 3.6. Desmosomal protein exchange kinetics after 24 h after mechanical stretch

## 3.6.1 Recovery curves

To investigate the reversibility of the effect induced by mechanical stretch, the stretched samples were re-examined after 24 h. For DP, PG, Dsc 2a GFP and Dsc 2a NG, three respectively four independent samples were analysed again 24 h after 2 h of mechanical stretch (50% amplitude, 80 mHz frequency). With each sample, 10 or 16 measurements could be conducted (figure 36) on the next page.

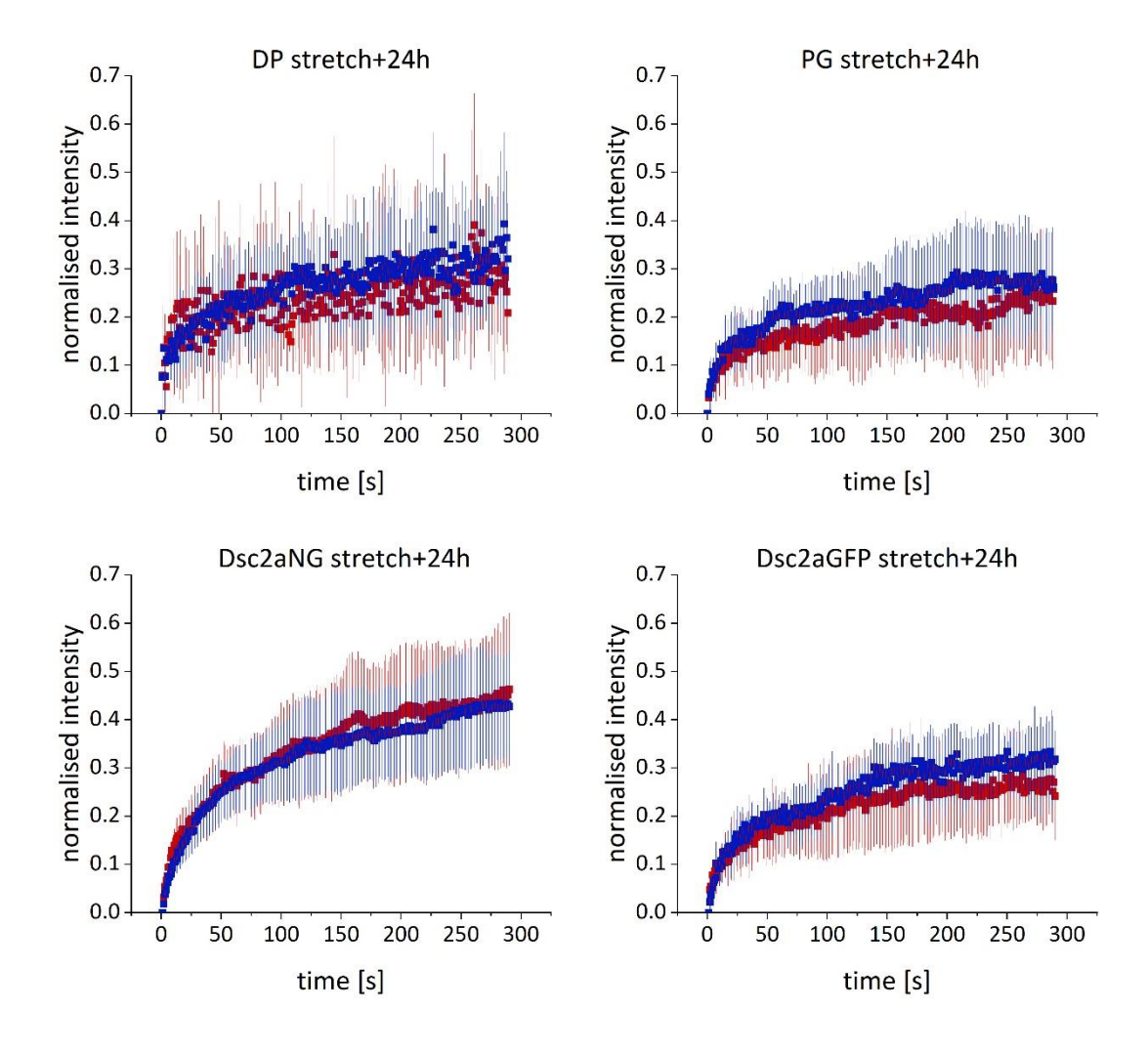


Figure 36: Recovery curves of the desmosomal proteins DP, PG, Dsc 2a GFP and Dsc 2a NG 24 h after 2 h of mechanical stretch with a 50% amplitude at 80 mHz. Mean recovery and standard deviation (red) of DP (N=7, from three independent samples), PG (N=9, from three independent samples), Dsc2a NG (N=11, from three independent samples) and Dsc2a GFP (N=8, from four independent samples). An unstretched control was analysed after 48 h of incubation (blue) insuring the same level of maturity for both stretched samples as well as control samples. Mean recovery and standard deviation of the CTRL of DP (N=10, from three independent samples), PG (N=9, from 4 independent samples), Dsc2a NG (N=11, from three independent samples) and Dsc2a GFP (N=8, from 3 independent samples). The normalisation procedure is described in section 2.2.5.1. The individual recovery curves can be found in the appendix, pages I to XVII.

### 3.6.2 Fitted parameters

The offsets of the desmosomal proteins DP, PG, Dsc 2a GFP and Dsc 2a NG 24 h after 2 h, 50% and 80 mHz of mechanical stretch are compared to unstretched controls and shown in figure 37 on the next page.

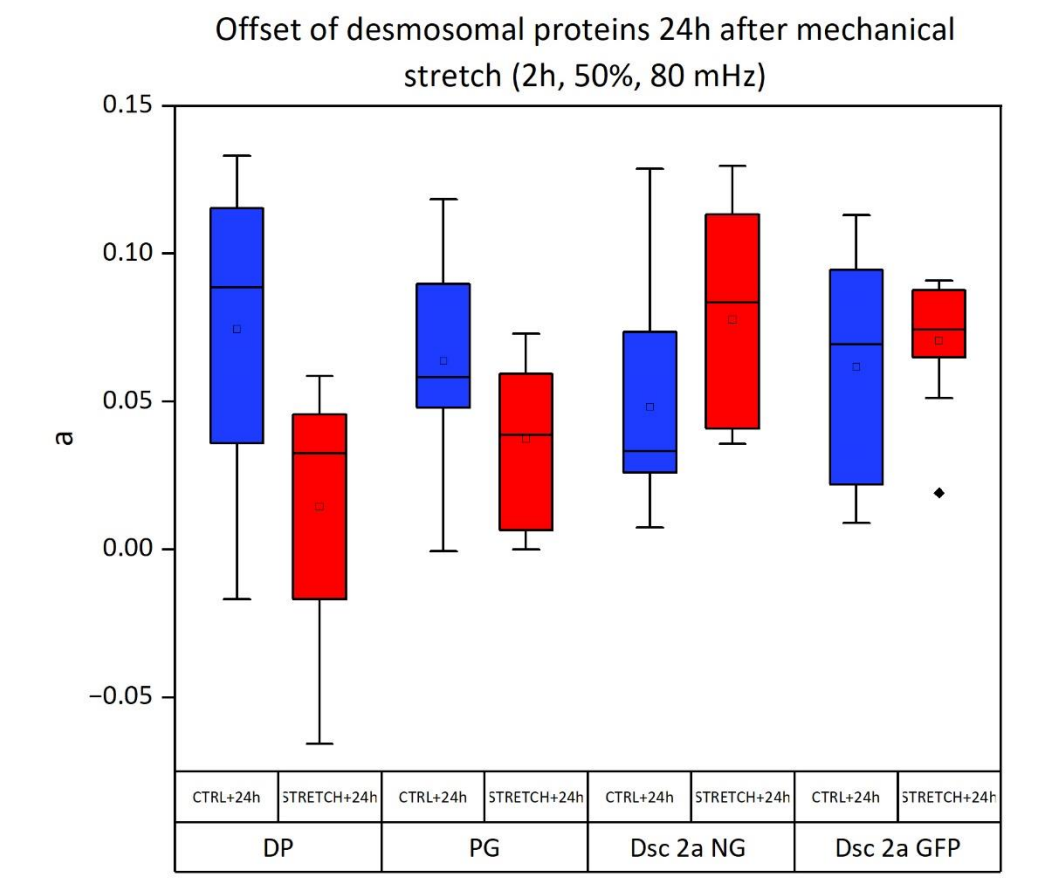


Figure 37: Boxplot of the offset of the desmosomal proteins DP, PG, Dsc 2a GFP and Dsc 2a NG 24 h after 2 h of mechanical stretch with a 50% amplitude at 80 mHz (red) in comparison with the unstretched control (blue). The number of fits included in the evaluation were N=8 for DP (from three independent samples), N=7 for PG (from four independent samples), N=11 for Dsc 2a NG (from three independent samples) and N=8 for Dsc 2a GFP (from three independent samples) for the unstretched controls, and N=4 for DP (from three independent samples), N=8 for PG (from three independent samples), N=11 for Dsc 2a NG (from three independent samples) and N=10 for Dsc 2a GFP (from four independent samples) for the stretched samples. The boxplot indicates the mean (square), the median (line), 25-75% of the data distribution (box) and potential outliers (rhombus) for each data set.

24 h after stretch, the mean offset was 0.014 for DP, 0.037 for PG, 0.078 for Dsc 2a NG and 0.071 for Dsc 2a GFP, whereas the unstretched control displayed a mean offset of 0.075 for DP, 0.064 for PG, 0.048 for Dsc 2a NG and 0.062 for Dsc 2a GFP. For all desmosomal proteins, there were no significant changes between the stretched and the unstretched samples 24 h after stretch. The mean offsets of the desmosomal proteins and the bootstrapped confidence intervals (95%) for these values can be found in the table 14 on the next page (for details see section 2.2.5.3).

Offset 24 h after mechanical stretch			
Desmosomal protein	mean	upper	lower
DP CTRL+24 h	0.075	0.11	0.043
DP stretch+24 h	0.014	0.070	-0.023
PG CTRL+24 h	0.064	0.086	0.040
PG stretch+24 h	0.037	0.055	0.018
Dsc 2a NG CTRL+24 h	0.048	0.067	0.026
Dsc 2a NG stretch+24 h	0.078	0.10	0.057
Dsc 2a GFP CTRL+24 h	0.062	0.088	0.036
Dsc 2a GFP stretch+24 h	0.071	0.084	0.059

Table 14: Mean offset of the desmosomal proteins DP, PG, Dsc 2a GFP and Dsc 2a NG 24 h after mechanical stretch (2 h, 50%, 80 mHz), with their upper and lower confidence intercals (95%). The number of fits included in the evaluation were N=8 for DP (from three independent samples), N=7 for PG (from four independent samples), N=11 for Dsc 2a NG (from three independent samples) and N=8 for Dsc 2a GFP (from three independent samples) for the unstretched controls, and N=4 for DP (from three independent samples), N=8 for PG (from three independent samples), N=11 for Dsc 2a NG (from three independent samples) and N=10 for Dsc 2a GFP (from four independent samples) for the stretched samples.

The exchanging fraction of the desmosomal proteins DP, PG, Dsc 2a GFP and Dsc 2a NG 24 h after 2 h, 50% and 80mHz of mechanical stretch is shown in figure 38 on the next page.

# Exchanging fraction of desmosomal proteins 24h after mechanical stretch (2h, 50%, 80 mHz)

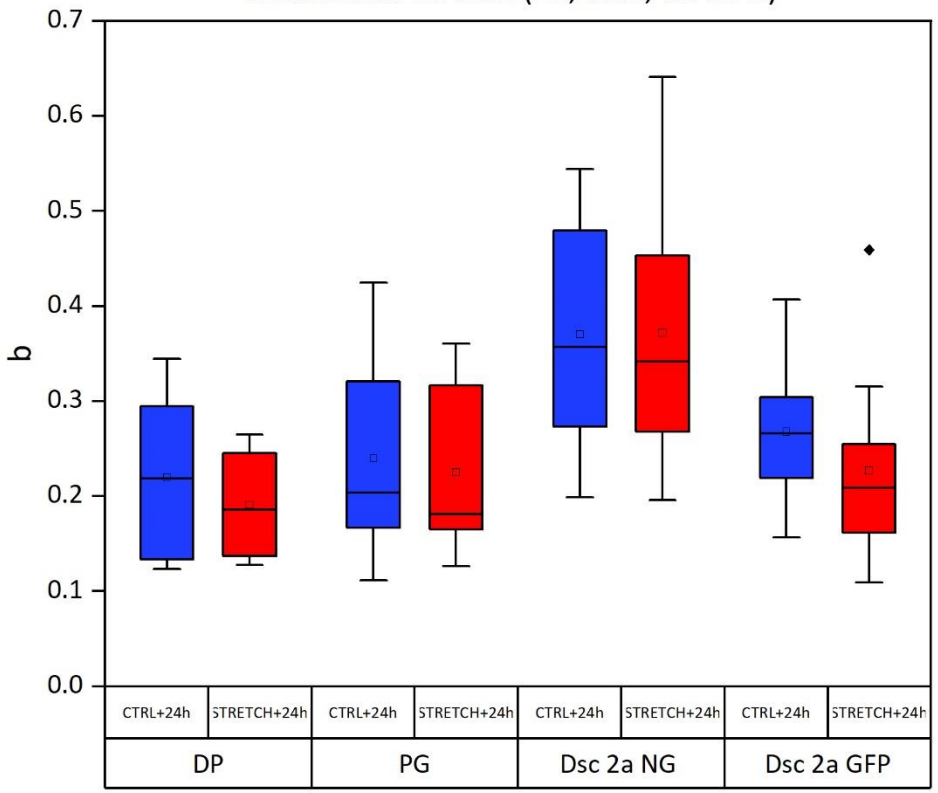


Figure 38: Boxplot of the exchanging fraction of the desmosomal proteins DP, PG, Dsc 2a GFP and Dsc 2a NG 24 h after 2 h of mechanical stretch with an 50% amplitude at 80 mHz for (red) in comparison with the unstretched control (blue). The number of fits included in the evaluation were N=8 for DP (from three independent samples), N=7 for PG (from four independent samples), N=11 for Dsc 2a NG (from three independent samples) and N=8 for Dsc 2a GFP (from three independent samples) for the unstretched controls, and N=4 for DP (from three independent samples) and N=10 for Dsc 2a GFP (from three independent samples) and N=10 for Dsc 2a GFP (from four independent samples) for the stretched samples. The boxplot indicates the mean (square), the median (line), 25-75% of the data distribution (box) and potential outliers (rhombus) for each data set.

24 h after stretch, the mean exchanging fraction was 0.19 for DP, 0.23 for PG, 0.37 for Dsc 2a NG and 0.23 for Dsc 2a GFP. The unstretched controls were examined after 48 h of incubation and displayed a mean exchanging fraction of 0.22 for DP, 0.24 for PG, 0.37 for Dsc 2a NG and 0.27 for Dsc 2a GFP. For all desmosomal proteins, there were no significant changes between the stretched and the unstretched samples 24 h after stretch. The mean exchanging fractions of the desmosomal proteins and the bootstrapped confidence intervals (95%) for these values can be found in the table 15 on the next page (for details see section 2.2.5.3).

Exchanging fraction 24 h after mechanical stretch			
Desmosomal protein	mean	upper	lower
DP CTRL+24 h	0.22	0.27	0.16
DP stretch+24 h	0.19	0.24	0.14
PG CTRL+24 h	0.24	0.31	0.17
PG stretch+24 h	0.23	0.28	0.16
Dsc 2a NG CTRL+24 h	0.37	0.43	0.30
Dsc 2a NG stretch+24 h	0.37	0.45	0.29
Dsc 2a GFP CTRL+24 h	0.27	0.31	0.22
Dsc 2a GFP stretch+24 h	0.23	0.28	0.16

Table 15: Mean exchanging fraction of the desmosomal proteins DP, PG, Dsc 2a GFP 24 h after mechanical stretch (2 h, 50%, 80 mHz), with their upper and lower confidence intercals (95%). The number of fits included in the evaluation were N=8 for DP (from three independent samples), N=7 for PG (from four independent samples), N=11 for Dsc 2a NG (from three independent samples) and N=8 for Dsc 2a GFP (from three independent samples) for the unstretched controls, and N=4 for DP (from three independent samples), N=8 for PG (from three independent samples), N=11 for Dsc 2a NG (from three independent samples) and N=10 for Dsc 2a GFP (from four independent samples) for the stretched samples.

The rate constants of the desmosomal proteins DP, PG, Dsc 2a GFP and Dsc 2a NG 24 h after 2 h, 50% and 80mHz of mechanical stretch is shown in figure 39 below.

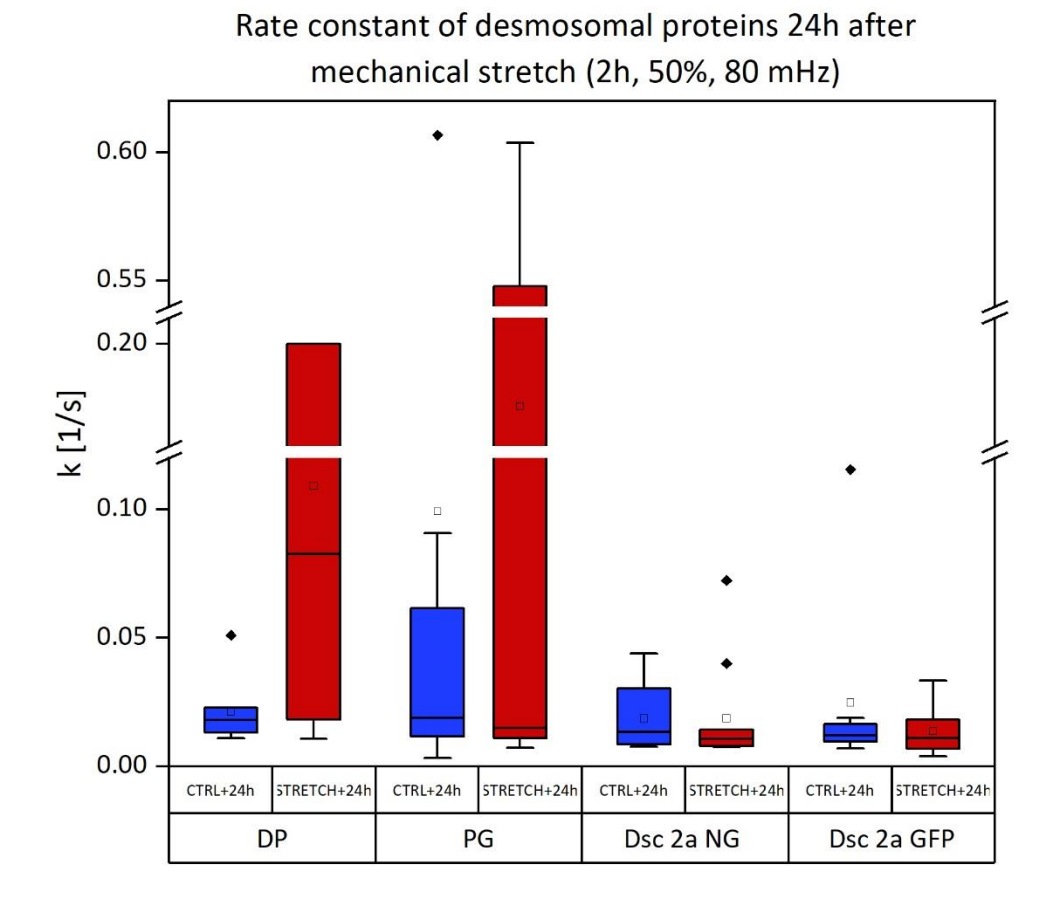


Figure 39: Boxplot of the rate constant of the desmosomal proteins DP, PG, Dsc 2a GFP and Dsc 2a NG 24 h after 2 h of mechanical stretch with an 50% amplitude at 80 mHz for (red) in comparison with the unstretched control (blue). The number of fits included in the evaluation were N=8 for DP (from three independent samples), N=7 for PG (from four independent samples), N=11 for Dsc 2a NG (from three independent samples) and N=8 for Dsc 2a GFP (from three independent samples) for the unstretched controls, and N=4 for DP (from three independent samples), N=8 for PG (from three independent samples), N=11 for Dsc 2a NG (from three independent samples) and N=10 for Dsc 2a GFP (from four independent samples) for the stretched samples. The boxplot indicates the mean (square), the median (line), 25-75% of the data distribution (box) and potential outliers (rhombus) for each data set.

24 h after stretch, the mean rate constant was 0.11 1/s for DP, 0.18 1/s for PG, 0.019 1/s for Dsc 2a NG and 0.014 1/s for Dsc 2a GFP, whereas the unstretched control displayed a mean rate constant of 0.021 1/s for DP, 0.099 1/s for PG, 0.019 1/s for Dsc 2a NG and 0.025 1/s for Dsc 2a GFP. For all desmosomal proteins, there were no significant changes between the stretched and the unstretched samples 24 h after stretch. Negative values given by the bootstrap procedure were set to zero as negative values

for the rate constant are physicochemically meaningless. The mean rate constant of the desmosomal proteins and the bootstrapped confidence intervals (95%) for these values can be found in the table 16 below (for details see section 2.2.5.3).

Rate constant 24 h after mechanical stretch [1/s]			
Desmosomal protein	mean	upper	lower
DP CTRL+24 h	0.021	0.028	0.012
DP stretch+24 h	0.11	0.20	0.016
PG CTRL+24 h	0.099	0.18	0
PG stretch+24 h	0.18	0.34	0
Dsc 2a NG CTRL+24 h	0.019	0.025	0.012
Dsc 2a NG stretch+24 h	0.019	0.028	0.0071
Dsc 2a GFP CTRL+24 h	0.025	0.039	0
Dsc 2a GFP stretch+24 h	0.014	0.0082	0.018

Table 16: Mean rate constant of the desmosomal proteins DP, PG, Dsc 2a GFP 24 h after mechanical stretch (2 h, 50%, 80 mHz), with their upper and lower confidence intercals (95%). The number of fits included in the evaluation were N=8 for DP (from three independent samples), N=7 for PG (from four independent samples), N=11 for Dsc 2a NG (from three independent samples) and N=8 for Dsc 2a GFP (from three independent samples) for the unstretched controls, and N=4 for DP (from three independent samples), N=8 for PG (from three independent samples), N=11 for Dsc 2a NG (from three independent samples) and N=10 for Dsc 2a GFP (from four independent samples) for the stretched samples.

The lifetime of the desmosomal proteins DP, PG, Dsc 2a GFP and Dsc 2a NG 24 h after 2 h, 50% and 80mHz of mechanical stretch is shown in figure 40 below.

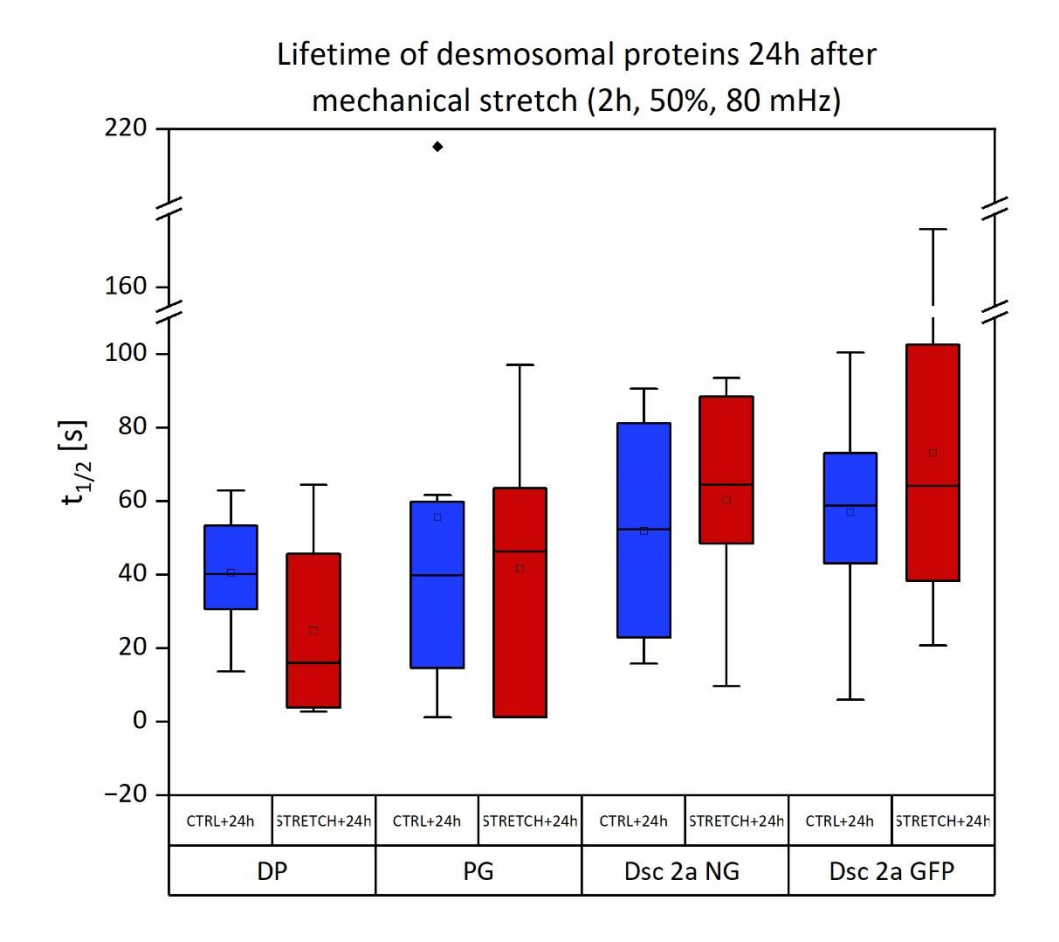


Figure 40: Boxplot of the lifetime of the desmosomal proteins DP, PG, Dsc 2a GFP and Dsc 2a NG 24 h after 2 h of mechanical stretch with an 50% amplitude at 80 mHz for (red) in comparison with the unstretched control (blue). The number of fits included in the evaluation were N=8 for DP (from three independent samples), N=7 for PG (from four independent samples), N=11 for Dsc 2a NG (from three independent samples) and N=8 for Dsc 2a GFP (from three independent samples) for the unstretched controls, and N=4 for DP (from three independent samples), N=8 for PG (from three independent samples) and N=10 for Dsc 2a GFP (from four independent samples) for the stretched samples. The boxplot indicates the mean (square), the median (line), 25-75% of the data distribution (box) and potential outliers (rhombus) for each data set.

24 h after stretch, the mean lifetime was 25 s for DP, 42 s for PG, 60 s for Dsc 2a NG and 73 s for Dsc 2a GFP, whereas the unstretched control displayed a mean lifetime of 41 s for DP, 56 s for PG, 52 s for Dsc 2a NG and 57 s for Dsc 2a GFP. For all desmosomal proteins, there were no significant changes between the stretched and the unstretched samples 24 h after stretch. The mean lifetime of the desmosomal proteins and the

# 3. Results bootstrapped confidence intervals for these values can be found in the table 17 below (for details see section 2.2.5.3).

Lifetime 24 h after mechanical stretch [s]			
Desmosomal protein	mean	upper	lower
DP CTRL+24 h	41	53	30
DP stretch+24 h	25	46	0
PG CTRL+24 h	56	90	6.8
PG stretch+24 h	42	64	19
Dsc 2a NG CTRL+24 h	52	67	37
Dsc 2a NG stretch+24 h	60	76	46
Dsc 2a GFP CTRL+24 h	57	76	39
Dsc 2a GFP stretch+24 h	73	96	43

Table 17: Mean lifetime of the desmosomal proteins DP, PG, Dsc 2a GFP 24 h after mechanical stretch (2 h, 50%, 80 mHz), with their upper and lower confidence intercals (95%). The number of fits included in the evaluation were N=8 for DP (from three independent samples), N=7 for PG (from four independent samples), N=11 for Dsc 2a NG (from three independent samples) and N=8 for Dsc 2a GFP (from three independent samples) for the unstretched controls, and N=4 for DP (from three independent samples), N=8 for PG (from three independent samples), N=11 for Dsc 2a NG (from three independent samples) and N=10 for Dsc 2a GFP (from four independent samples) for the stretched samples.

## 3.7. Joint evaluation

The parameter a represents the offset within the exponential fit (equation 7) whereas the parameter  $a_{lin}$  represents the offset in the linear fit (equation 13). The initial slope consists of the parameter  $b_{lin}$  (which corresponds to b\*k from the linearised function, equation 12), and the product b\*k, the product of the two individual parameters from the exponential fit. The results of these joint evaluations are presented in this section.

### 3.7.1 Desmosomal protein exchange kinetics in the absence of mechanical stretch

The joint offset of DP, PG, Dsc 2a GFP and Dsc 2a NG directly in the abscence of mechanical stretch are shown in figure 41 below.

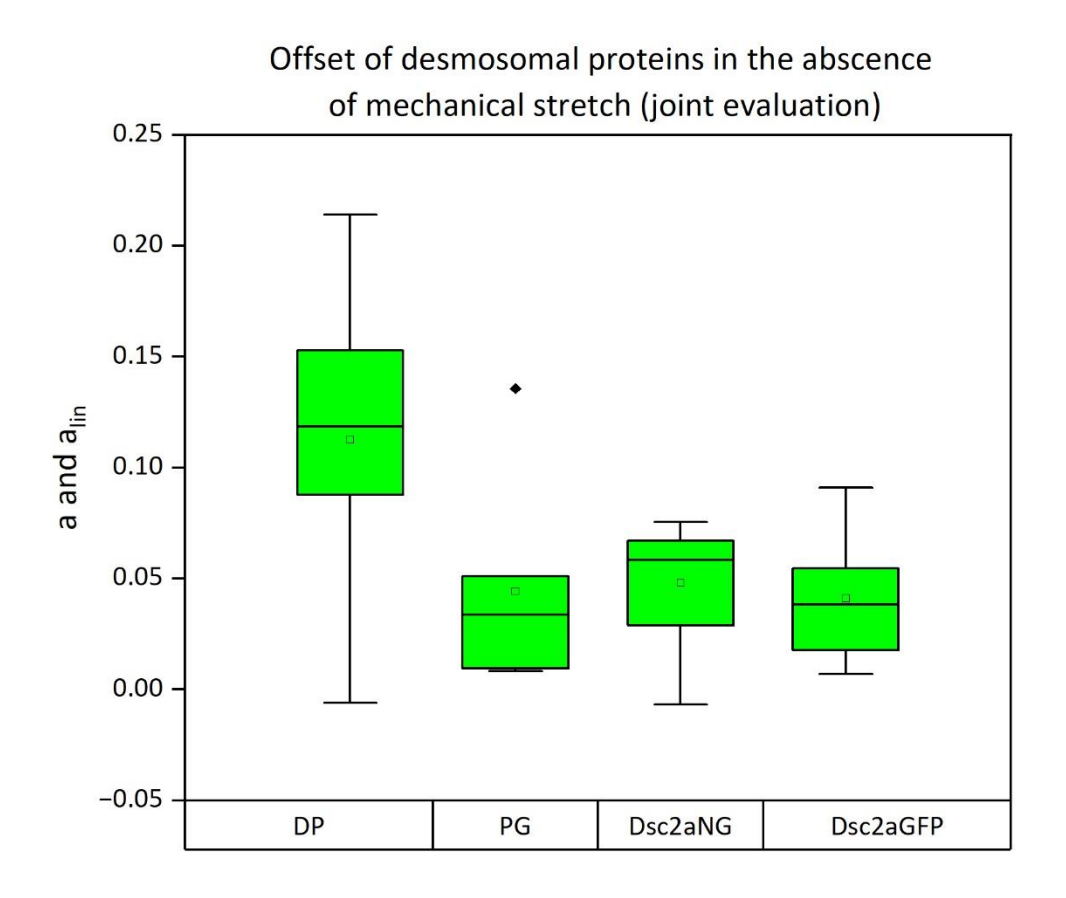


Figure 41: Boxplot of the joint offset of the desmosomal proteins DP, PG, Dsc 2a NG and Dsc 2a GFP in absence of mechanical stretch. The number of fits included in this joint evaluation was N=9 (N=5 exponential fits, N=4 linear fits) for DP (from five independent samples), N=7 (all exponential fits) for PG (from four independent samples), N=10 (all exponential fits) for Dsc 2a NG (from three independent samples) and N=10 (N=9 exponential fits, N=1 linear fits) for Dsc 2a GFP (from three independent samples). The boxplot indicates the mean (square), the median (line), 25-75% of the data distribution (box) and potential outliers (rhombus) for each data set.

The mean joint offset was 0.11 for DP, 0.044 for PG, 0.048 for Dsc 2a NG and 0.041 for Dsc 2a GFP. The bootstrapped confidence intervals (95%) for these values can be found in the table 18 below (for details see section 2.2.5.3).

Joint offset in the abscence of mechanical stretch			
Desmosomal protein	mean	upper	lower
DP	0.11	0.16	0.0073
PG	0.044	0.068	0.012
Dsc 2a NG	0.048	0.065	0.033
Dsc 2a GFP	0.041	0.055	0.026

Table 18: Mean joint offset of the desmosomal proteins DP, PG, Dsc 2a NG and Dsc 2a GFP in the absence of mechanical stretch, with their upper and lower confidence intervals (95%). The number of fits included in this joint evaluation was N=9 (N=5 exponential fits, N=4 linear fits) for DP (from five independent samples), N=7 (all exponential fits) for PG (from four independent samples), N=10 (all exponential fits) for Dsc 2a NG (from three independent samples) and N=10 (N=9 exponential fits, N=1 linear fits) for Dsc 2a GFP (from three independent samples).

The initial slope of the desmosomal proteins DP, PG, Dsc 2a GFP and Dsc 2a NG in the absence of mechanical stretch is shown in figure 42 below.

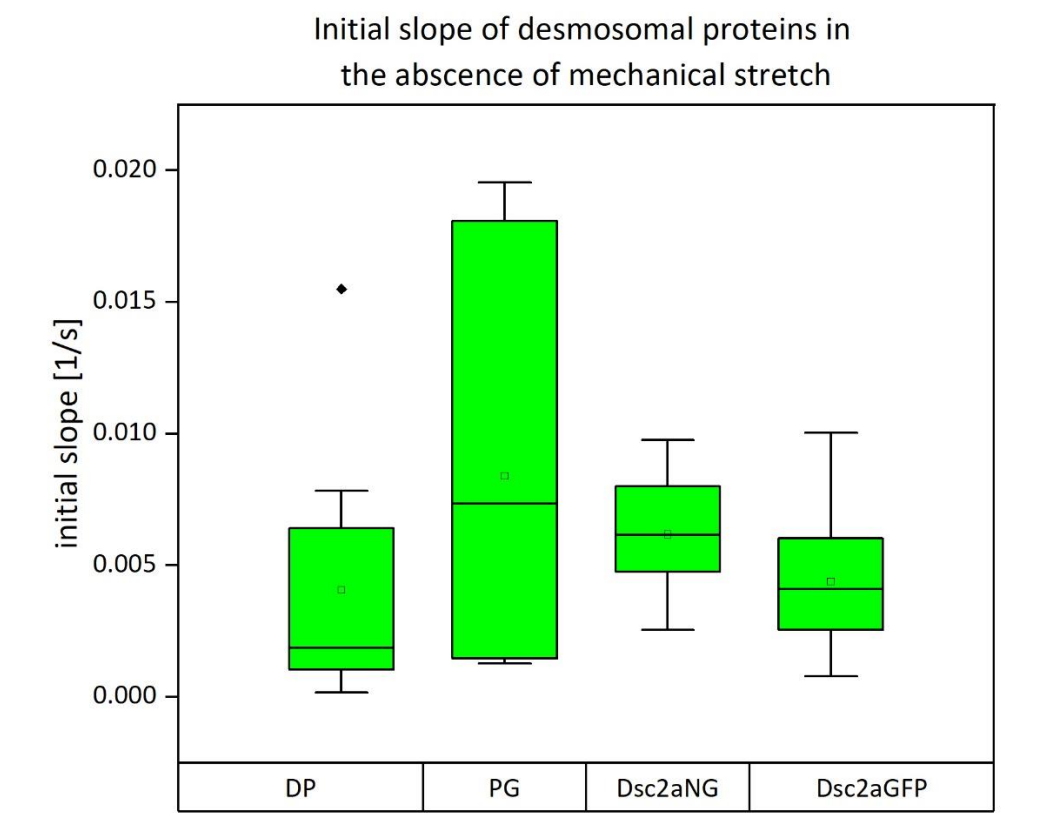


Figure 42: Boxplot of the initial slope of the desmosomal proteins DP, PG, Dsc 2a GFP and Dsc 2a NG in absence of mechanical stretch. The number of fits included in this joint evaluation was N=9 (N=5 exponential fits, N=4 linear fits) for DP (from five independent samples), N=7 (all exponential fits) for PG (from four independent samples), N=10 (all exponential fits) for Dsc 2a NG (from three independent samples) and N=10 (N=9 exponential fits, N=1 linear fits) for Dsc 2a GFP (from three independent samples). The boxplot indicates the mean (square), the median (line), 25-75% of the data distribution (box) and potential outliers (rhombus) for each data set.

In the absence of mechanical stretch, the initial slope was 0.0041 1/s for DP, 0.0084 1/s for PG, 0.0062 1/s for Dsc 2a NG and 0.0044 1/s for Dsc 2a GFP. The bootstrapped confidence interval for these values can be found in the table 19 on the next page (for details see section 2.2.5.3).

Initial slope in the abscence of mechanical stretch [1/s]			
Desmosomal protein	mean	upper	lower
DP	0.0041	0.0084	0.0066
PG	0.0084	0.013	0.0031
Dsc 2a NG	0.0062	0.0075	0.0048
Dsc 2a GFP	0.0044	0.0060	0.0027

Table 19: Mean initial slope of the desmosomal proteins DP, PG, Dsc 2a NG and Dsc 2a GFP in the absence of mechanical stretch, with their upper and lower confidence intervals (95%). The number of fits included in this joint evaluation was N=9 (N=5 exponential fits, N=4 linear fits) for DP (from five independent samples), N=7 (all exponential fits) for PG (from four independent samples), N=10 (all exponential fits) for Dsc 2a NG (from three independent samples) and N=10 (N=9 exponential fits, N=1 linear fits) for Dsc 2a GFP (from three independent samples).

## 3.7.2 Effect of mechanical stretch on desmosomal protein exchange kinetics

The joint offsets of the desmosomal proteins DP, PG, Dsc 2a GFP and Dsc 2a NG after 2 h, 50% and 80 mHz of mechanical stretch are compared to unstretched controls and shown in figure 43 on the next page.

# Offset of desmosomal proteins after mechanical stretch (2h, 50%, 80 mHz), joint evaluation

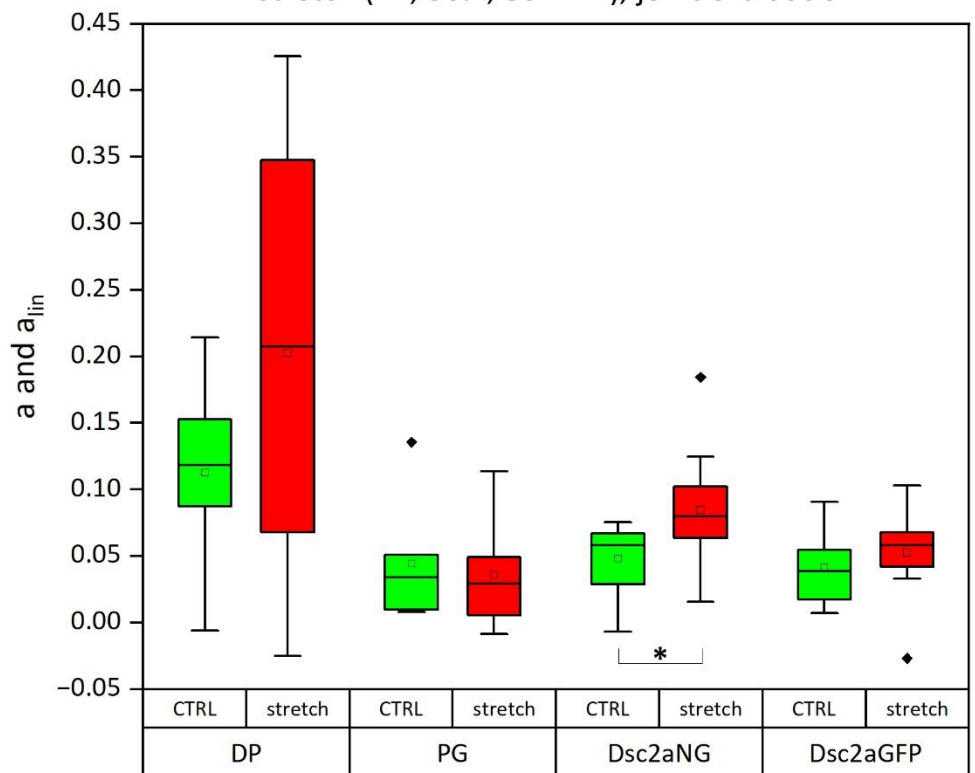


Figure 43: Boxplot of the joint offset of the desmosomal proteins DP, PG, Dsc 2a GFP and Dsc 2a NG after 2 h of mechanical stretch with a 50% amplitude at 80 mHz (red) in comparison with the unstretched control (green). The number of fits included in this joint evaluation was N=9 (N=5 exponential fits, N=4 linear fits) for DP (from five independent samples), N=7 (all exponential fits) for PG (from four independent samples), N=10 (all exponential fits) for Dsc 2a NG (from three independent samples) and N=10 (N=9 exponential fits, N=1 linear fits) for Dsc 2a GFP (from three independent samples) for the unstretched controls, and N=10 (N=5 exponential fits, N=5 linear fits) for DP (from three independent samples), N=10 (all exponential fits) for PG (from four independent samples), N=16 (all exponential fits) for Dsc 2a NG (from three independent samples) and N=10 (all exponential fits) for Dsc 2a GFP (from three independent samples) for the stretched samples. The boxplot indicates the mean (square), the median (line), 25-75% of the data distribution (box) and potential outliers (rhombus) for each data set. Significant results (two-tailed t-test with significance level  $\alpha$ <0.05) are highlighted with an asterisk.

After stretch, the joint mean offset was 0.20 for DP, 0.036 for PG, 0.085 for Dsc 2a NG and 0.052 for Dsc 2a GFP. Compared to the unstretched control, the offset increase of the Dsc 2a NG cells was found to be significantly (determined with the two tailed t-test, significance level  $\alpha$ =0.05). For DP, PG and Dsc 2a GFP, no significant increase was found. The mean offsets of the desmosomal proteins and the bootstrapped confidence

3. Results

interval for these values can be found in the table 20 below (for details see section 2.2.5.3).

Joint offset after mechanical stretch			
Desmosomal protein	mean	upper	lower
DP CTRL	0.11	0.16	0.073
DP stretch	0.20	0.29	0.11
PG CTRL	0.044	0.068	0.012
PG stretch	0.036	0.057	0.012
Dsc 2a NG CTRL	0.048	0.065	0.033
Dsc 2a NG stretch	0.085	0.10	0.067
Dsc 2a GFP CTRL	0.041	0.055	0.026
Dsc 2a GFP stretch	0.052	0.075	0.035

Table 20: Mean joint offset of desmosomal proteins DP, PG, Dsc 2a NG and Dsc 2a GFP after mechanical stretch (2 h, 50%, 80 mHz), with their upper and lower confidence intervals (95%). The number of fits included in this joint evaluation was N=9 (N=5 exponential fits, N=4 linear fits) for DP (from five independent samples), N=7 (all exponential fits) for PG (from four independent samples), N=10 (all exponential fits) for Dsc 2a NG (from three independent samples) and N=10 (N=9 exponential fits, N=1 linear fits) for Dsc 2a GFP (from three independent samples) for the unstretched controls, and N=10 (N=5 exponential fits, N=5 linear fits) for DP (from three independent samples), N=10 (all exponential fits) for PG (from four independent samples), N=16 (all exponential fits) for Dsc 2a NG (from three independent samples) and N=10 (all exponential fits) for Dsc 2a GFP (from three independent samples)

The initial slope of the desmosomal proteins DP, PG, Dsc 2a GFP and Dsc 2a NG after 2 h, 50% and 80 mHz of mechanical stretch is shown in figure 44 on the next page.

# Initial slope of desmosomal proteins in after mechanical stretch (2h, 50%, 80 mHz)

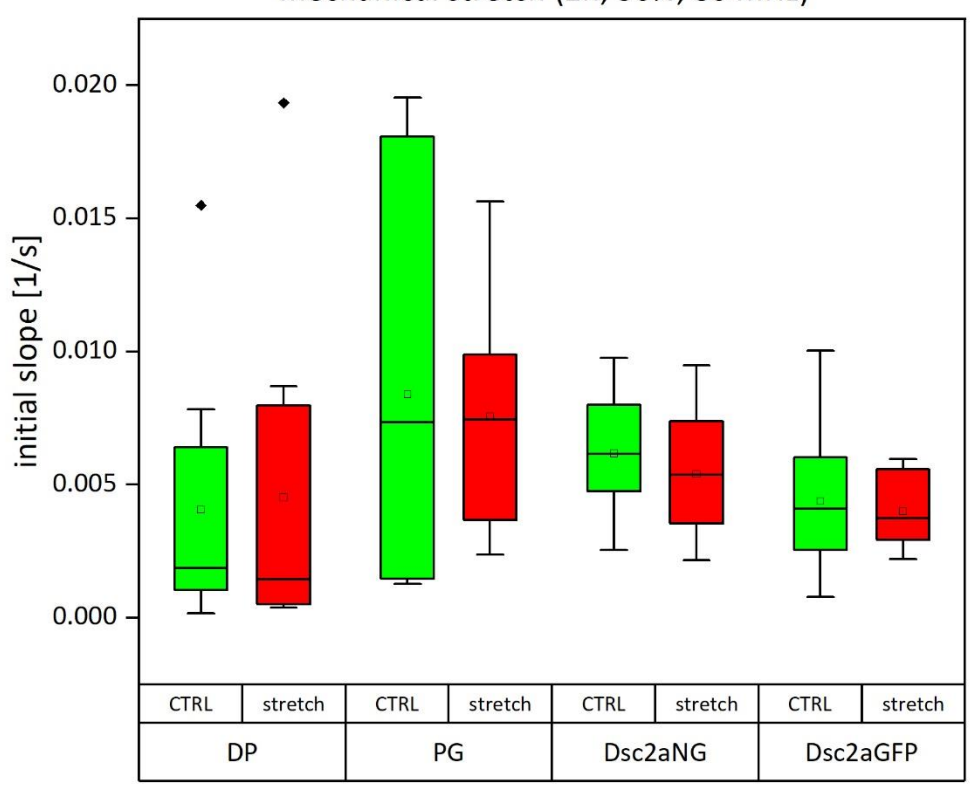


Figure 44: Boxplot of the initial slope of the desmosomal proteins DP, PG, Dsc 2a GFP and Dsc 2a NG 24 h after 2 h of mechanical stretch with a 50% amplitude at 80 mHz (red) in comparison with the unstretched control (green). The number of fits included in this joint evaluation was N=9 (N=5 exponential fits, N=4 linear fits) for DP (from five independent samples), N=7 (all exponential fits) for PG (from four independent samples), N=10 (all exponential fits) for Dsc 2a NG (from three independent samples) and N=10 (N=9 exponential fits, N=1 linear fits) for Dsc 2a GFP (from three independent samples) for the unstretched controls, and N=10 (N=5 exponential fits, N=5 linear fits) for DP (from three independent samples), N=10 (all exponential fits) for PG (from four independent samples), N=16 (all exponential fits) for Dsc 2a NG (from three independent samples) and N=10 (all exponential fits) for Dsc 2a GFP (from three independent samples) for the stretched samples. The boxplot indicates the mean (square), the median (line), 25-75% of the data distribution (box) and potential outliers (rhombus) for each data set.

After stretch, the mean initial slope was 0.0045 1/s for DP, 0.0076 1/s for PG, 0.0054 1/s for Dsc 2a NG and 0.0040 1/s for Dsc 2a GFP. For all desmosomal proteins, there were no significant changes between the stretched and the unstretched samples. The mean initial slope of the desmosomal proteins and the bootstrapped confidence interval for these values can be found in the table 21 on the next page (for details see section 2.2.5.3).

Initial slope after mechanical stretch [1/s]			
Desmosomal protein	mean	upper	lower
DP CTRL	0.0041	0.0066	0.00084
DP stretch	0.0045	0.0076	0.00067
PG CTRL	0.0084	0.013	0.0031
PG stretch	0.0076	0.010	0.0047
Dsc 2a NG CTRL	0.0062	0.0075	0.0048
Dsc 2a NG stretch	0.0054	0.0065	0.0043
Dsc 2a GFP CTRL	0.0044	0.0060	0.0027
Dsc 2a GFP stretch	0.0040	0.0047	0.0032

Table 21: Mean initial slope of the desmosomal proteins DP, PG, Dsc 2a NG and Dsc 2a GFP after mechanical stretch (2 h, 50%, 80 mHz), with their upper and lower confidence intervals (95%). The number of fits included in this joint evaluation was N=9 (N=5 exponential fits, N=4 linear fits) for DP (from five independent samples), N=7 (all exponential fits) for PG (from four independent samples), N=10 (all exponential fits) for Dsc 2a NG (from three independent samples) and N=10 (N=9 exponential fits, N=1 linear fits) for Dsc 2a GFP (from three independent samples) for the unstretched controls, and N=10 (N=5 exponential fits, N=5 linear fits) for DP (from three independent samples), N=10 (all exponential fits) for PG (from four independent samples), N=16 (all exponential fits) for Dsc 2a NG (from three independent samples) and N=10 (all exponential fits) for Dsc 2a GFP (from three independent samples) for the stretched samples.

### 3.7.3 Desmosomal protein exchange kinetics after 24 h after mechanical stretch

The joint offsets of the desmosomal proteins DP, PG, Dsc 2a GFP and Dsc 2a NG 24 h after 2 h, 50% and 80 mHz of mechanical stretch are compared to unstretched controls and shown in figure 45 on the next page.

# Offset of desmosomal proteins 24h after mechanical stretch (2h, 50%, 80 mHz, joint evaluation

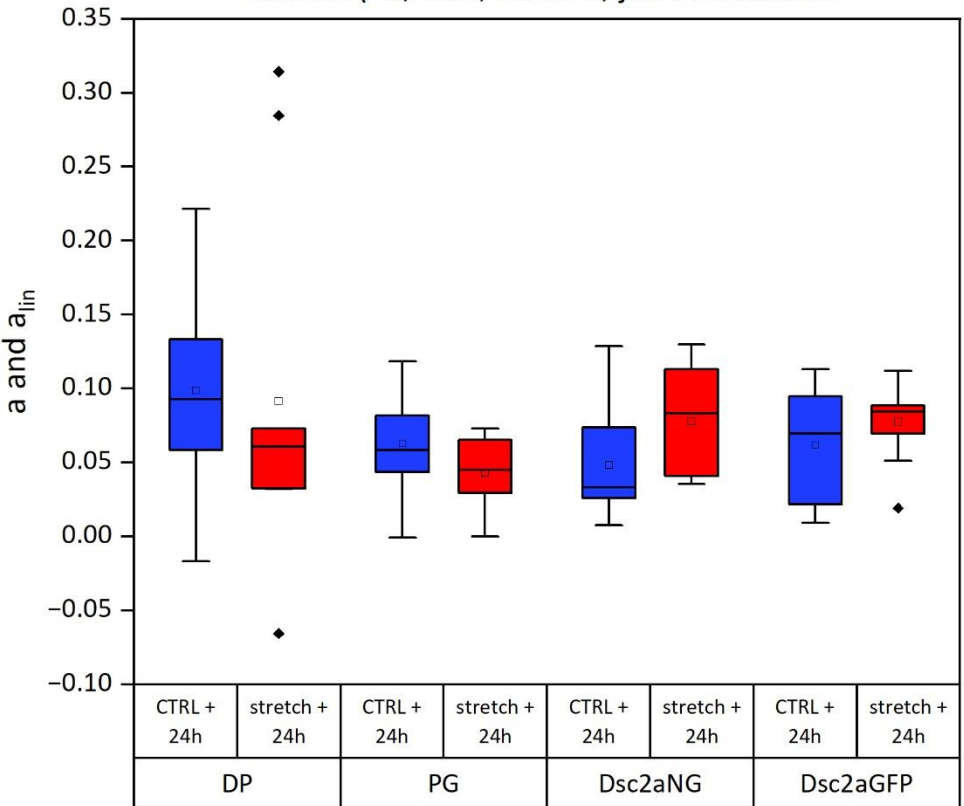


Figure 45: Boxplot of the joint offset of the desmosomal proteins DP, PG, Dsc 2a NG and Dsc 2a GFP 24 h after 2 h after mechanical stretch with a 50% amplitude at 80 mHz (red) in comparison with the unstretched control (blue). The number of fits included in the evaluation were N=10 (N=8 exponential fits and N=2 linear fits) for DP (from three independent samples), N=9 (N=7 exponential fits and N=2 linear fits) for PG (from four independent samples), N=11 (all exponential fits) for Dsc 2a NG (from three independent samples) and N=8 (all exponential fits) for Dsc 2a GFP (from three independent samples) for the unstretched controls, and N=7 (N=4 exponential fits and N=3 linear fits) for DP (from three independent samples), N=9 (N=8 exponential fits and N=1 linear fits) for PG (from three independent samples), N=11 (all exponential fits) for Dsc 2a NG (from three independent samples) and N=11 (N=10 exponential fits and N=1 linear fits) for Dsc 2a GFP (from four independent samples) for the stretched samples. The boxplot indicates the mean (square), the median (line), 25-75% of the data distribution (box) and potential outliers (rhombus) for each data set. Significant results (two-tailed t-test with significance level  $\alpha$ <0.05) are highlighted with an asterisk.

24 h after stretch, the mean joint offset was 0.10 for DP, 0.040 for PG, 0.078 for Dsc 2a NG and 0.072 for Dsc 2a GFP, whereas the unstretched control displayed a mean joint offset of 0.10 for DP, 0.061 for PG, 0.048 for Dsc 2a NG and 0.062 for Dsc 2a GFP. For all desmosomal proteins, there were no significant changes between the stretched and the unstretched samples 24 h after stretch. The mean joint offsets of

the desmosomal proteins and the bootstrapped confidence interval (95%) for these values can be found in the table 22 below (for details see section 2.2.5.3).

Joint offset 24 h after mechanical stretch			
Desmosomal protein	mean	upper	lower
DP CTRL+24 h	0.10	0.15	0.062
DP stretch+24 h	0.10	0.20	-0.0045
PG CTRL+24 h	0.061	0.084	0.038
PG stretch+24 h	0.040	0.056	0.024
Dsc 2a NG CTRL+24 h	0.048	0.067	0.027
Dsc 2a NG stretch+24 h	0.078	0.097	0.057
Dsc 2a GFP CTRL+24 h	0.062	0.088	0.037
Dsc 2a GFP stretch+24 h	0.072	0.086	0.062

Table 22: Mean joint offset of the desmosomal proteins DP, PG, Dsc 2a GFP and Dsc 2a NG 24 h after mechanical stretch (2 h, 50%, 80 mHz), with their upper and lower confidence intervals (95%). The number of fits included in the evaluation were N=10 (N=8 exponential fits and N=2 linear fits) for DP (from three independent samples), N=9 (N=7 exponential fits and N=2 linear fits) for PG (from four independent samples), N=11 (all exponential fits) for Dsc 2a NG (from three independent samples) and N=8 (all exponential fits) for Dsc 2a GFP (from three independent samples) for the unstretched controls, and N=7 (N=4 exponential fits and N=3 linear fits) for DP (from three independent samples), N=11 (all exponential fits) for Dsc 2a NG (from three independent samples) and N=1 (N=10 exponential fits and N=1 linear fits) for Dsc 2a GFP (from four independent samples) for the stretched samples.

The initial slope of the desmosomal proteins DP, PG, Dsc 2a GFP and Dsc 2a NG 24 h after 2 h, 50% and 80mHz of mechanical stretch is shown in figure 46 on the next page.

# Initial slope of desmosomal proteins 24h after mechanical stretch (2h, 50%, 80 mHz)

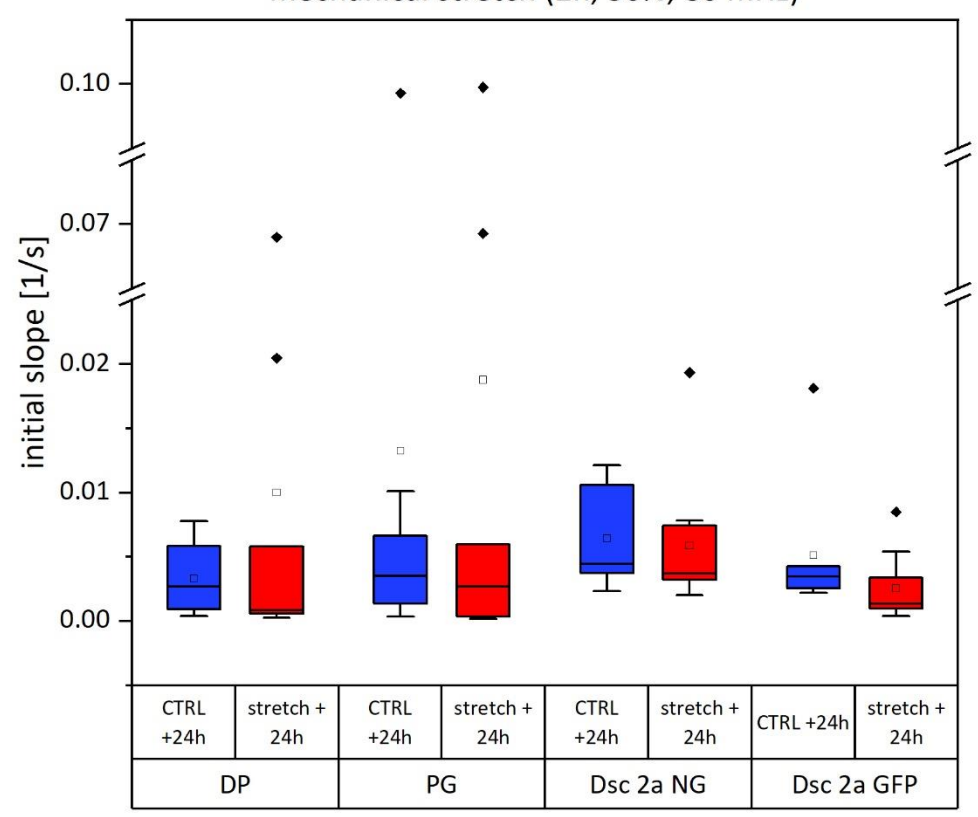


Figure 46: Boxplot of the initial slope of the desmosomal proteins DP, PG, Dsc 2a NG and Dsc 2a GFP 24 h after 2 h of mechanical stretch with an 50% amplitude at 80 mHz for (red) in comparison with the unstretched control (blue). The number of fits included in the evaluation were N=10 (N=8 exponential fits and N=2 linear fits) for DP (from three independent samples), N=9 (N=7 exponential fits and N=2 linear fits) for PG (from four independent samples), N=11 (all exponential fits) for Dsc 2a NG (from three independent samples) and N=8 (all exponential fits) for Dsc 2a GFP (from three independent samples) for the unstretched controls, and N=7 (N=4 exponential fits and N=3 linear fits) for DP (from three independent samples), N=9 (N=8 exponential fits and N=1 linear fits) for PG (from three independent samples), N=11 (all exponential fits) for Dsc 2a NG (from three independent samples) and N=11 (N=10 exponential fits and N=1 linear fits) for Dsc 2a GFP (from four independent samples) for the stretched samples. The boxplot indicates the mean (square), the median (line), 25-75% of the data distribution (box) and potential outliers (rhombus) for each data set.

24 h after stretch, the mean initial slope was 0.014 1/s for DP, 0.0021 1/s for PG, 0.0059 1/s for Dsc 2a NG and 0.0029 1/s for Dsc 2a GFP, whereas for the unstretched control, the mean initial slope was 0.0036 1/s for DP, 0.015 1/s for PG, 0.0065 1/s for Dsc 2a NG and 0.0051 1/s for Dsc 2a GFP. For all desmosomal proteins, there were no significant changes between the stretched and the unstretched samples. The mean initial slope of the desmosomal proteins and the bootstrapped confidence intervals

3. Results (95%) for these values can be found in the table 23 below (for details see section 2.2.5.3).

Initial slope 24 h after mechanical stretch [1/s]						
Desmosomal protein	mean	upper	lower			
DP CTRL+24 h	0.0036	0.0051	0.0021			
DP stretch+24 h	0.014	0.027	-0.0053			
PG CTRL+24 h	0.015	0.027	-0.0065			
PG stretch+24 h	0.0021	0.040	-0.0076			
Dsc 2a NG CTRL+24 h	0.0065	0.0086	0.0043			
Dsc 2a NG stretch+24 h	0.0059	0.0080	0.0028			
Dsc 2a GFP CTRL+24 h	0.0051	0.0074	0.0013			
Dsc 2a GFP stretch+24 h	0.0029	0.0041	0.0014			

Table 23: Mean initial slope of the desmosomal proteins DP, PG, Dsc 2a NG and Dsc 2a GFP 24 h after mechanical stretch (2 h, 50%, 80 mHz), with their upper and lower confidence intervals (95%). The number of fits included in the evaluation were N=10 (N=8 exponential fits and N=2 linear fits) for DP (from three independent samples), N=9 (N=7 exponential fits and N=2 linear fits) for PG (from four independent samples), N=11 (all exponential fits) for Dsc 2a NG (from three independent samples) and N=8 (all exponential fits) for Dsc 2a GFP (from three independent samples) for the unstretched controls, and N=7 (N=4 exponential fits and N=3 linear fits) for DP (from three independent samples), N=11 (all exponential fits) for Dsc 2a NG (from three independent samples) and N=1 linear fits) for Dsc 2a NG (from three independent samples) and N=11 (N=10 exponential fits and N=1 linear fits) for Dsc 2a GFP (from four independent samples) for the stretched samples.

# 4. Discussion

In the scope of this thesis, a sealable elastomer chamber was developed for the stretching and imaging of MDCK monolayers in order to analyse the stability of desmosomes. With this experimental set-up, different MDCK cell lines, in each of which one of the desmosomal proteins DP, PG and Dsc2a was fluorescently tagged with either GFP, EGFP or NG were analysed with FRAP. Uniaxial, cyclic stretch was applied for 2 h with a 50% amplitude at 80 mHz and the exchange kinetics of the desmosomal proteins DP, PG, Dsc 2a NG and Dsc 2a GFP were then probed in three mechanical states, unstretched, stretched and 24 h after stretch.

Depending on the standard deviation of the noise of the recorded signal, either an exponentital (equation 7) or a linear (equation 12) fit was fitted to the resulting recovery curves (see section 2.2.5.2). The recovery curves displayed a biphasic ascent, which was most pronounced for the protein DP in the abscence of mechanical stretch and after stretch. This biphasic ascent is indicating the presence of two distinct kinetic processes, diffusion and exchange at the desmosomal sites. The analysis of the exchanging fraction of the desmosomal proteins revealed that, in the absence of mechanical stretch, all desmosomal proteins are a stable component of the desmosomal structure. Furthermore, the increase of the exchanging fraction recorded after stretching followed by a decline after 24 h of additional incubation desmonstrated a reversible mechanoresponse of the proteins PG and Dsc.

In this chapter, the discussion of the results is organised in the following sections:

In **section 4.1**, the situation in the absence of mechanical stretch is discussed, including The mechanoresponse of the desmosomal proteins DP, PG, Dsc 2a GFP and Dsc 2a NG is discussed in **section 4.2**.

Taken together, the results suggests a special, yet unknown mechanical role for the desmosomal proteins DP, which is briefly discussed in **section 4.3.** 

# 4.1 In the absence of mechanical stretch, desmosomal proteins are stable components of the desmosomal structure

Desmosomes are extremely stable structures that can withstand many mechanical stresses. In the abscence of mechanical stretch exchanging fractions of 0.22 for DP (lower confidence interval 0.19, upper confidence interval 0.25), 0.21 for PG (lower confidence interval 0.13, upper confidence interval 0.28), 0.37 for Dsc 2a NG (lower confidence interval 0.27, upper confidence interval 0.46) and 0.23 for Dsc 2a GFP (lower confidence interval 0.18, upper confidence interval 0.28) were determined. Overall, these values for the exchanging fractions of these desmosomal proteins were lower then values determined in earlier studies. For the exchanging fraction of DP, Fülle et al. found exchanging fractions of 50.2%, 37.7% for the exchanging fraction of PG and 35.7% the exchanging fraction of for Dsc2a<sup>105</sup>. Windoffer et a. found an exchanging fraction of 60±20% for Dsc2a after a total of 30 min of recovery<sup>59</sup>. These discrepancies could be due to even minor differences in handling conditions as well as higher passaging numbers, which has been found to cause chromose drift and thus alter the cell lines properties<sup>122</sup>. Moreover, differences in data analysis probably led to varying values for the exchanging fraction, e.g. the biphasic ascent found in the scope of this thesis (see section 4.1.1. for more details.).

The exchanging fractions determined in the absence of mechanical stretch within the scope of this thesis reinforce the notion that this stability is reflected by desomosmal proteins remaining for the larger part immobile within the desmosomal sites. These results align with the literature, where the high stability of desmosomes is unanimously described and the low protein exchange kinetics at the desmosomal sites is believed to ensure this stability<sup>123–125</sup>.

In addition, two other interesting aspects of the recovery curves recorded in the absence of mechanical stretch became apparent: The biphasic ascent of some recorded recovery curves as well as a striking difference of the mean exchanging fraction

between the two MDCK cell lines where Dsc is fluorescently tagged (Dsc 2a GFP and Dsc 2a NG).

All in all, the analysed desmosomal proteins DP, PG, Dsc 2a GFP and Dsc 2a NG are, due to their low exchanging fraction - very stable components of the desmosomal structure in the abscence of mechanical stretch.

# 4.1.1 Two kinetic processes shape the recovery of desmosomal proteins: Diffusion and protein exchange

The shapes of some recorded recovery curves indicated a biphasic ascent, and therefore suggest the involvement of another kinetic process in the first second of this exchange: Diffusion. Usually, diffusion of proteins in aqueous solution occurs many times faster than the kinetic exchange of the desmosomal proteins<sup>126</sup>. If the protein exchange at the desmosomal sites is considerably slower than the diffusion process, the diffusion remains perceptible on its own under the condition that the bleached area is not too large.

The time scale of the diffusion is composed of the dimension of the respective bleaching area squared divided by twice the diffusion constant (see equation 5, described in more detail in section 1.3):

$$D = \frac{\langle x^2 \rangle}{6t} \tag{5}$$

The diffusion coefficent is typically below  $10 \ \mu m^2 * s^{-1}$  for proteins associated with the plasma membrane 127,128, with very low values of ~0.02  $\mu m^2 * s^{-1}$  documented for Dsc2 127. Diffusion coefficents ranging from  $3 \ \mu m^2 * s^{-1}$  to  $30 \ \mu m^2 * s^{-1}$  (reviewed in 129) and  $30 \ \mu m^2 * s^{-1}$  to  $50 \ \mu m^2 * s^{-1}$  for cytosolic proteins 130. The smaller dimension chosen for the bleaching areas within the experimental set-up (see section 2.2.4.3) was 3.7  $\mu m$ , thus resulting in time scales of a second to a few seconds for the completed diffusion within the bleaching area. The actual protein exchange afterwards on the other hand takes minutes to be completed. These findings align with the literature, where

#### 4. Discussion

diffusion-driven increase of the intensity of the recovery curve usually appears in the first few seconds, whereas the cycle of binding and release happens within minutes<sup>131</sup>.

These two kinetic processes are illustrated in the following model (figure 47). The intensity in the bleached area (figure 47A) is composed of the intensity of the desmosomal structure itself and the intensity of the diffusive protein pool above (figure 47A/A1). Upon bleaching, the protein in both desmosomal structure and diffusive protein pool are bleached (figure 47B). The bleached proteins present in the cytoplasm leave the perimeters of the bleached area in the matter of a few seconds due to diffusion within the cell (figure 47C). Due to the large volume of the cell – which can assumed to be much larger than the bleached area, as even smaller cells have an approximate volume of 15 000  $\mu$ m<sup>3</sup>– the reservoir of unbleached proteins is, even with half the bleach field being within one cell, virtually infinite. Once this diffusion process is completed (figure 47C/C1) the actual protein exchange – here termed recovery – can be observed within the bleached area (figure 47D) until an equilibrium is reached (figure 47E). All in all, this model fits very well with the observation that the first part of the biphasic ascent from the recovery curves can be attributed to diffusion.

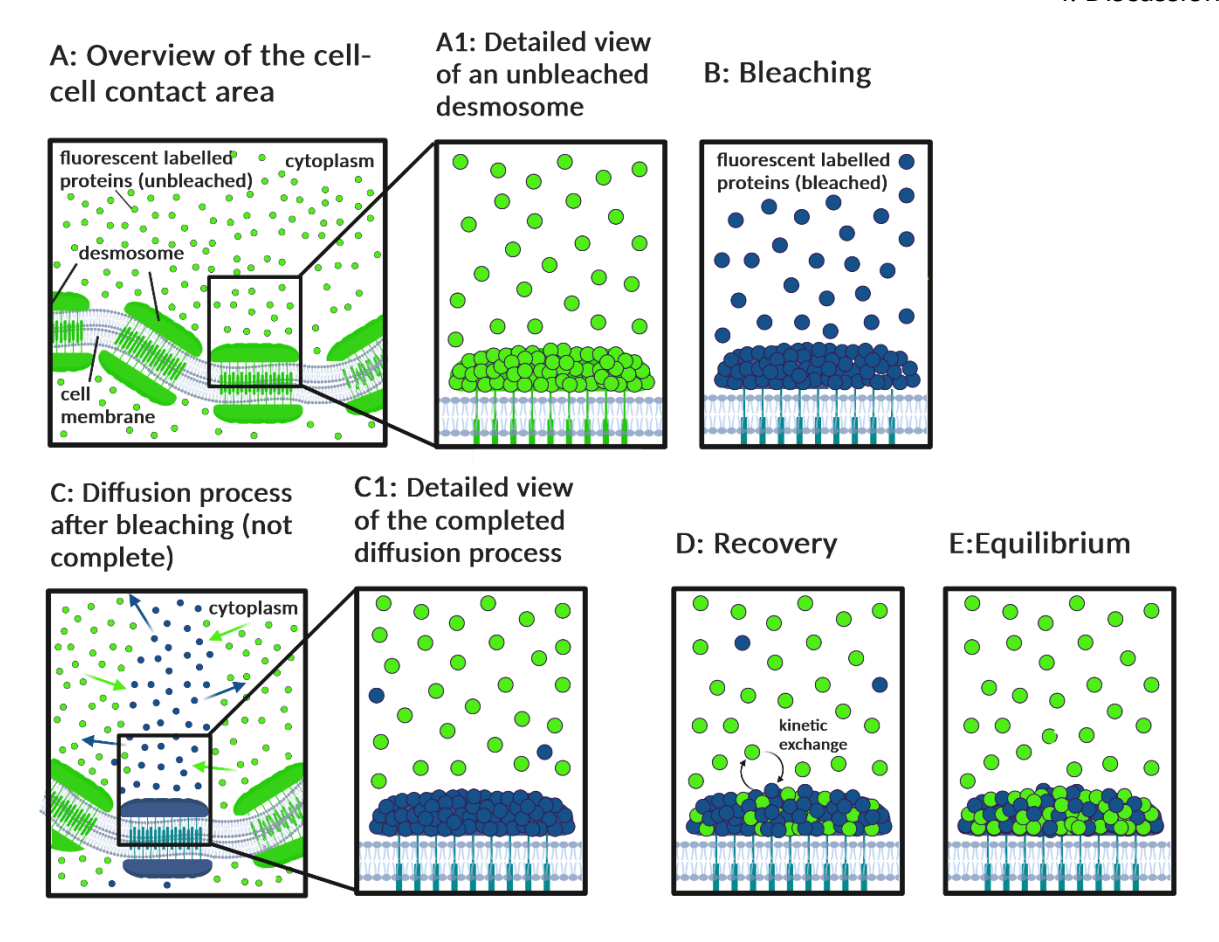


Figure 47: Model of diffusion and protein exchange at the desmosomal sites. Overview of the cell-cell contact area (A) and bleaching process (B). Detailed view of the completed diffusion process (C). Recovery process of the protein kinetic exchange at the desmosomal sites (D) and equilibrium (E). For the sake of simplicity the intermediate filament network connected to the desmosomes is not shown.

# 4.1.2. Differences in expression levels lead to differing exchanging fractions

The mean exchanging fractions in the absence of mechanical stretch were similar across the desmosomal proteins with one interesting exception. Surprisingly, the biggest difference ocurred between the two MDCK cell lines, where the same protein, Dsc 2a, was fluorescently tagged with NG or GFP (exchanging fraction of 0.37 for Dsc 2a NG (lower confidence interval 0.27, upper confidence interval 0.46) and 0.23 for Dsc 2a GFP (lower confidence interval 0.18, upper confidence interval 0.28)). The external appearance of the two cell lines in terms of overall fluorescence could provide an explanation for this.

#### 4. Discussion

The Dsc 2a NG displays overall expression levels of 80%-90%, while the Dsc 2a GFP cell line displays an expression level of 100%. This circumstance could be attributed to different transfection levels of the MDCK cells. It is well known that observed dissociation kinetics of immobilised receptor-ligand complexes depends on the concentration of ligand in solution<sup>132</sup>.

In both cell lines, the probability for a binding sites to be occupied within the desmosomal structure (the number of occupied binding sites is indicated with the symbol g) is dependent of the number of said binding sites, the concentration of available ligands I (in this case, fluorescently tagged Dsc°2a proteins) as well as their specific exchange rates,  $k_{on}$  for binding and  $k_{off}$  for release. This relationship can be represented by the following equation (equation 15).

$$\dot{g} = -g * k_{off} + (1 - g) * k_{on} * l \tag{15}$$

Without FRAP, the number of the fluorescent proteins is not subjected to any change over time, the system of exchanging proteins at the binding sites is therefore in equilibrium (equation 16). Based on this assumption, equation 15 can be solved for g, which was termed  $g_e$  in for g this equilibrium state (equation 17.1 and 17.2).

$$\dot{g} = 0 \tag{16}$$

$$g_e * k_{off} + g_e * k_{on} * l = k_{on} * l$$
 (17.1)

$$g_e = \frac{k_{on} * l}{k_{off} + k_{on} * l} \tag{17.2}$$

After bleaching, this system presents itself differently: The total number of occupied binding sites is now composed of a time-invariant constant  $g_e$  and a varying part that will decay to zero  $g_v$ . (equation 18).

$$g = g_e + g_v \tag{18}$$

With equation 15 taken into account, the change of the occupied binding sites over time presents itself as follows (equation 19.1), which and can then be further simplified to equation 19.2.

4. Discussion

$$\frac{d}{dt}(g_e + g_v) = -(g_e + g_v) * k_{off} + (l - g_e - g_v) * k_{on} * l$$
 (19.1)

$$\dot{g} = \left(-k_{off} - k_{on} * l\right) * g_v \tag{19.2}$$

Which can also be represented as

$$\frac{dg}{dt} = \frac{dg_v}{dt} \tag{19.2}$$

Equation 19.2. can then be solved for  $g_{\nu}$  based on equation 7 (see section 2.2.5.2), the result is (equation 20):

$$g_v = a * e^{-k*t} \tag{20}$$

The observed rate constant k can then be indicated with equation 21:

$$k = k_{off} + k_{on} * l (21)$$

During the FRAP experiments, the non-exchanging, thus immobile fraction was recorded (see figure 9 in section 2.2.4). Due to a higher concentration of available ligands before bleaching (equation 17), the Dsc 2a GFP cell line displays a higher overall fluorescence compared to the Dsc 2a NG cell line. Therefore, the mean exchanging fractions in absence of mechanical stretch differ between the two cell lines even if the same protein was fluorescently tagged. If we take these considerations into account, the observed protein exchange kinetics of these two cell lines do not contradict each other.

# 4.2 The desmosomal proteins PG, Dsc 2a NG and Dsc 2a GFP exhibit a mechanoresponse

The analysis of the protein exchange kinetic after mechanical stretch resulted in a significant change of the exchanging fraction of the desmosomal proteins PG, Dsc 2a NG and Dsc 2a GFP (for PG the exchanging fraction increased from 0.21 (lower confidence interval 0.13, upper confidence interval 0.28) to 0.43 (lower confidence interval 0.33, upper confidence interval 0.53), for Dsc 2a NG from 0.37 (lower confidence interval 0.45, upper confidence interval 0.46) to 0.51 (lower confidence interval 0.45, upper confidence interval 0.56) and for Dsc 2a GFP from 0.23 (lower confidence interval 0.29, upper confidence interval 0.28) to 0.35 (lower confidence interval 0.29, upper confidence interval 0.41)). This mechanoresponse is probably directly triggered by the stretching of the intermediate filaments, as the mechanical stretch is transmitted mainly through them to the desmosomes.

Unfortunately, the experimental set-up left no other option than to stretch and image separately. However, this lag time (ranging from 12 to 45 min) between stretching and imaging has been the major limitation of the analysis performed for this thesis, because the adaptation to mechanical stretch is not recorded in real time. As this mechanoresponse was later found to be reversible, the inital effect is presumed to be more pronounced and the recorded intensities only represent an extenuated adaptation to mechanical stretch.

Therefore, the fact that the exchanging fraction of some desmosomal proteins is still significantly increased even after a lag time, indicates the impact of mechanical stretch on the stablity of desmosomes to be substantial. Taken together with the results of the FRAP analysis performed after an aditional 24 h of incubation, a reversible mechanoresponse of some desmosomal upon uniaxial, cyclic stretch proteins was shown.

# 4.2.1 Upon uniaxial, cyclic stretch desmosomes adapt by an increase of the exchanging fraction

Provdiding mechanical stability for tissues is one of the core function of desmosomes. In literature, the stability of desmosomes is perceived to stem from a slow recovery and/or a low exchanging fractions<sup>133</sup>. In this context, Windoffer et al. raised the interesting question whether "desmosome stability is reflected by the long residence times of its constituents or is maintained through the continuous exchange of its molecular components"<sup>59</sup>.

These results, which demonstrated a significant change of the exchanging fraction of the desmosomal proteins PG, Dsc 2a NG and Dsc 2a GFP, encourages the latter notion. Changes of the exchanging fraction of desmosomal proteins have been hypothesised to be - similar to the constant assembly and disassembly – a mechanism cells regulate their adhesive properties due to mechanical cues<sup>134</sup>, but on the whole, due to difficult experimental conditions, this mechanoresponse is still not well characterised.

For other cell-cell contacts, this kind of mechanoresponse has already been outlined. For example, Samak et al. described a stretch-induced redistribution of two adherens junction proteins, E-cadherin and  $\beta$ -catenin, from the actual cell-cell contact structure into intracellular compartements<sup>135</sup> and de Beco et al. described a quicker turnover for E-cadherin, a mechanosensitive adherens junction protein, upon uniacial, however not cyclic, stretch<sup>101</sup>. Furthermore, there is evidence that the rate constant  $k_{off}$  of zyxin, a focal adhesion proteins – postulated as mechanosensors - is sensitive to mechanical forces<sup>136,137</sup>.

Interestingly, it has been recently described for DP<sup>138</sup>, the only protein which did not exhibit an significant increase of its exchanging fraction (the potential role of DP in the mechanoresponse of desmosomes upon mechanical stretch will be discussed in the chapter 4.3.).

Concerning this adaptation process to mechanical stretch, many aspects remain speculative. Analogous to the unstretched state, the exchanged desmosomal proteins

# 4. Discussion

are likely to originate from a non-desmosomal protein pools in the cytoplasm and at the plasma membrane. Is this exchange in any way circular, with proteins going back and forth between the desmosomal structure and the non-desmosomal protein pools? Or are the proteins PG and Dsc 2a, once removed from the desmosomal structure, headed for degradation? The literature suggests that particles and parts of the dismantled desmosomal structure are not reutilised for the formation of new desmosomes <sup>56,62,63</sup>.

The assumption that the desmosomal proteins PG and Dsc 2a are only exchanged once at the desmosomal sites would entail an increased de novo synthesis on the one hand and on the other hand an equally increased need for the degradation of the exchanged proteins. However, the situation here could present itself differently, as the desmosmal structure remains intact and only individual proteins get exchanged.

The question regarding the reason why the proteins PG, Dsc 2a NG and Dsc 2a GFP are exchanged to a greater extent than DP in the event of uniaxial, cyclic stretch also leaves room for speculation. Is it possible that the exchange of these respective proteins is elevated due to stretchdependent structural changes? It is already known that mechanical stretch can expose bindings sites of mechanosensitive proteins in adherens junctions, which then recruit other proteins 139,140. This phenomenon has already been documented for desmosomal cadherins 141 and PG 142 but many aspects still remain unknown. The architecture of the protein is hypothesised to provide more insight 143.

The increase of the exchanging fraction could also be connected to post-translational modifications like phosphorylation. Phosphorylation of desmosomal proteins have been described to regulate desmosomal assembly and maturation (reviewed in<sup>9</sup>). For example, phosphorylation events (in interplay with arginine methylation) mediate the interaction between DP and the intermediate filaments<sup>144</sup>, but only in static conditions. Phophorylation in general has been linked to events of mechanical stress in the context of other cell-cell contact proteins as well as cytoskeletal components such as intermediate filaments<sup>145</sup>, but phosphoralytion events of particular desmosomal

proteins and their influence on exchange kinetics in the context of mechanical stretch is still not well characterised. In static conditions however, phosphorylation has been reported to regulate the protein exchange kinetic of focal adhesion protein vinculin during maturation<sup>146,147</sup>.

Surprisingly, the transmembrane protein Dsc 2a behaves similarly to the plaque protein PG, even though they originate from morphologically distinct domains. The fact that the exchanging fraction of these proteins both increased in a similar fashion despite those differences raises many more questions about this sort of mechanoresponse, especially regarding its uniqueness throughout the desmosomal structure. Conversely, the exchanging fraction of DP did not increase significantly, possibly another indicator for a special mechanical role of this protein.

Across the literature, differing protein exchange rates have been reported for the same desmosomal proteins in static conditions. These differences can be attributed to a multitude of factors such as the use of different cell lines, maturation times and conditions and different approaches in FRAP analysis and evaluation. Additionally, seemingly understated differences in transfection intensity - as discussed in chapter 4.1.2 – can have a substantial impact on the exchanging fraction. Therefore the most noticeable observation is less the absolute value of the recovery curves than the relative change of the exchanging fraction upon mechanical stretch.

#### 4.2.2 The mechanoresponse of the desmosomal proteins is reversible

Since pilot experiments (see section 3.2.3-3.2.5) suggested a certain volatileness of the mechanoresponse to mechanical stretch, questions about the longevity of this effect arose. Therefore, a FRAP analysis of the desmosomal proteins DP, PG, Dsc 2a NG and Dsc 2a GFP was performed after an additional 24 h of incubation after stretching.

The analysis of the protein exchange kinetic 24 h after mechanical stretch resulted in no significant change of the exchanging fraction of all desmosomal proteins when compared to the unstretched control (for DP, the exchanging fraction of the unstretched control was 0.22 (lower confidence interval 0.16, upper confidence interval

#### 4. Discussion

0.27) and 0.19 for the stretched sample after 24 h of additional incubation (lower confidence interval 0.14, upper confidence interval 0.24), for PG, the exchanging fraction of the unstretched control was 0.24 (lower confidence interval 0.17, upper confidence interval 0.31) and 0.23 for the stretched sample after 24 h of additional incubation (lower confidence interval 0.16, upper confidence interval 0.28), for Dsc 2a NG, the exchanging fraction of the unstretched control was 0.37 (lower confidence interval 0.30, upper confidence interval 0.43) and 0.37 for the stretched samples after 24 h of additional incubation (lower confidence interval 0.29, upper confidence interval 0.45) and for Dsc 2a GFP, the exchanging fraction of the unstretched control was 0.27 (lower confidence interval 0.22, upper confidence interval 0.31) and 0.23 for the stretched samples after 24 h of additional incubation (lower confidence interval 0.16, upper confidence interval 0.28)). Thus, the effects of mechanical stretch on the exchanging fraction can indeed be considered as reversible. This observation is going well along with other studies having described reversible, or at least partially reversible<sup>148</sup>, mechanoresponses in the context of mechanical stretch.

With the additional 24 h of incubation time, the desmosomes continued to mature. The affect of maturation and hyperadhesion could also potentially influence the level of the exchanging fraction, as hyperadhesion ultimatively leads to an even further decrease of the exchanging fraction of the desmosomal proteins DP, PG and Dsc 2a compared to the calcium dependent state<sup>105</sup>.

As hyperadhesion has not been inspected in the scope of this thesis, no certain statement can be made to a potential calcium-independence of the analysed samples. The examined samples have been incubated in HCM for a total of 48 h. MDCK cells exhibited to form desmosomes rather quickly<sup>56</sup>, but as is also known, desmosomes continue to mature after initial assembly<sup>64</sup>. However, Fülle et al. previously reported the cell lines DP, PG and Dsc 2a NG reaching hyperadhesion after 3 days of confluent culture and the values for the exchanging fraction are similar when taking into account that they indicated their recovery curves without an offset<sup>105</sup>. Taken together with the

results from Bartle et al., who showed that the exchanging fraction of desmosomal cadherins can be halved when entering a hyperadhesive state<sup>73</sup>, these cell lines are deemed to be still calcium-dependent at the time of the second FRAP analysis.

The aspect of desmosomal maturation in the context of mechanical stretch can further entail interesting speculations. In large parts, maturation is perceived as a linear process with the decrease of the exchanging fraction being linked to an ongoing maturation. Possibly this perception is incomplete. A similar concept was also suggested for the phosphorylation in focal adhesions. Phosphorylation levels have been described to regulate focal adhesion maturation<sup>146</sup>, indicating that different maturation stages correspond to different phophorylation patterns. Interestingly, the phosphorylation patterns seemed to be related to the maturation stages as well as to the decline of protein exchange kinetics. If this realtionship is transferable to desmosomes, the aspect of a reversible mechanoresponse could suggest a delay or alteration in the advancement of the maturation.

# 4.3 DP has a potentially special, yet unknown role in the mechanoresponse of desmosomes

The non-significant results obtained in the examination of the DP exchange kinetics raise several potential explanations. The most likely explanation appears to be related to the specific DP cell line used in this study. The DP cell line showed a particularly faint fluorescence signal and low transfection levels (described in section 3.3.2). These characteristics could - under the applied experimental conditions- be masking any potential changes in its exchange kinetics, giving the impression that the protein exchange kinetics remain constant.

In addition, two alternative explanations warrant brief consideration. One possibility is that the lag time between stretching and imaging with FRAP (up to 45 min, described in section 3.2.5) already was sufficient to allow the system to return to equilibrium. Thus, any transient alterations in DP exchange kinetics induced by mechanical stretch could have dissipated by the time of analysis. In future studies, a setup enabling real-time FRAP during could mitigate this issue and help capture any fleeting changes in DP protein exchange kinetics. Another explanation is that the exchange kinetics of DP might not change at all under the experimental conditions applied. While this is an intriguing hypothesis, it appears less likely based on the current understanding of DP function in mechanotransduction. If the kinetics of DP truly remain unchanged, it could possibly indicate that stretching affects other regulatory processes - such as DP synthesis or degradation - rather than its exchange kinetics directly. Interestingly, some evidence suggests that DP is involved in mediating desmosomal hyperadhesion 149.

However, given the characteristics of the used DP cell line, the most plausible conclusion remains that the DP cell line itself is responsible for the lack of significant results. Moving forward, further studies could benefit from the use of cell lines that express a fluorescently tagged DP at higher levels. Additionally, varying experimental parameters (e.g. stretching amplitudes and time intervals between stretching and FRAP analysis) could offer further insights.

# 5. Outlook

In the scope of this thesis, the protein exchange kinetics of different desmosomal proteins were analysed under different mechanical states with an experimental approach. With FRAP, the recovery of the desmosomal proteins DP, PG and Dsc 2a (fluorescently tagged with either GFP, EGFP or NG) were documented under the influence of uniaxial, cyclic stretch (2 h, 50%, 80 mHz). These experiments were sought to explore the impact of mechanical stretch on the stability of epithelial tissues as desmosomes play a prominent role in their transmission of mechanical stretch. For this purpose, sealable elastomer chambers made of silicone were developed. This experimental set-up allowed for consecutive stretching, imaging and FRAP analysis of monolayered epithelial systems of MDCK cells. Taken together, the obtained data demonstrated a reversible mechanoresponse of PG and Dsc 2a NG upon uniaxial, cyclic stretch. Interestingly, DP exhibited no such mechanoresponse, supposedly due to its unique position within the desmosomal structure.

Due to the technical limitations of the experimental set-up, certain conditions, especially after stretch, could not be tested. Thus the mechanoresponse of the analysed desmosomal proteins could not be described in it's entity. The lag time between imaging and FRAP analysis certainly resulted in such a loss of information, because the adaptation to mechanical stretch was not recorded in real time. The collected recovery curves can therefore only be interpreted as an "echo" of the actual adaptation of desmosomes to mechanical stretch, as this adaptation was found to be reversible. Pilot experiments already indicated that shorter lag times led to even more pronounced increases of the exchanging fraction. A thorough analysis of the impact of mechanical stretch on the stability of desmosomes will not be able to avoid an experimental set-up in which stretching and imaging are possible simultaneously.

Beyond that, many other issues regarding the mechanoresponse of desmosomal proteins upon mechanical stretch were raised. In this context, one of the most important question is the one regaring the life cycle of desmosomal proteins in the

#### 5. Outlook

context of mechanical stretch. For example, the origin of the desmosomal proteins exchanged in the event of mechanical stretch remains unclear. Does the exchanging fraction increase due to a larger supply of freely diffusing proteins or has the binding constant (of the desmosomal protein itself or of its binding partners) changed, possibly through modification (e.g. phosphorylation)? Analysing the protein exchange kinetics in combination with agents blocking the de-novo synthesis could be a suitable approach, and in this context, previous studies demonstrated the use of clycloheximide<sup>64</sup>. To investigate a possible degradation, the usage of agents blocking the lysosomal and/or proteasomal degradation could provide more insights in this respect, chloroquine and/or respectively MG132 could be utilised<sup>150</sup>.

As the reversibility of the desmosomal mechanoresponse was analysed, the question arose whether desmosomal maturation could also be affected – or involved – in this process. Possibly because maturation was oftentimes analysed under static conditions, maturation is perceived as a linear process with the decrease of the exchanging fraction being linked to an ongoing maturation. Taking into account the reversibility of the increased exchanging fraction found here for several desmosomal proteins, a certain adaptability, delay or alteration in the advancement of the maturation appears probable, giving mechanical stretch a substantial impact on the long-term stability of tissues.

All in all, the results found in the scope of this thesis demonstrated that the desmosomal proteins PG and Dsc 2a are mechanosensitive as they react to uniaxial, cyclic stretch. Further investigation of the interplay between desmosomes and mechanical stretch could provide more insight about the mechanobiology of epithelial tissues. Considering that the presence of mechanical stimuli of any kind is the rule and not the exception in the context of living tissues emphasises the importance of further mechanobiological investigations.

# 6. Acknowledgements

My time as a doctoral researcher was a challenging and instructive experience, and completing this doctoral thesis would not have been possible without the support of valued supervisors, colleagues and loved ones.

First of all, I would like to express my thanks to my supervisor **Prof. Dr. Rudolf Merkel** for the oppurtunity to conduct my scientific research at the IBI-2. I am very grateful for his assistance and guidance during countless hours of experiment planning, data evaluation and scientific discussions. It has been a bliss working alongside someone who always puts science first!

I would also like to thank **PD Dr. Bernd Hoffmann** for his support. I am grateful for him spontaneously stepping into the role as my "unofficial supervisor" and providing me advice in my day-to-day work in the lab.

As I spent a significant amount of time developping and implementing my experimental set-up, **Jens Konrad** has been of tremendous help I am very grateful for. Also many thanks to **Georg Dreissen** and **Dr. Ronald Springer** for their support with data fitting and data evaluation. I want to thank them for their kind and patient assistance with the statistical analysis of my data – and any IT related troubles that I have encountered over the years.

Being a member of the ME3T (Mechanobiology in Epithelial 3D Tissue Constructs) graduate school was an incredibly insightful experience. The ME3T graduate school enabled me to participate in lectures, talks and conferences. Even though the curriculum was exceptional, it is the amazing community I am most grateful for. Thanks to all my fellow ME3Tees for the time we spent together discussing, celebrating and supporting each other. I would like to thank **Prof. Dr. Rudolf Leube** not only for the oppurtunity to be part of the first cohort of ME3T, but especially for his efforts cosupervising my thesis. Additionally, I want to thank him and **Prof. Dr. Reinhard Windoffer** for providing me with a MDCK cell line.

#### 6. Acknowledgements

I would further like to thank **Dr. Judith Fülle** and **Prof. Dr. Christoph Ballestrem** from the University of Manchester also for providing me with MDCK cell lines and useful advice during my experiment planning.

It makes me happy to know that parts of my research will be continued within the PhD project of **Hajaani Manoharan**. I would like to thank her for an enjoyable and collegial passing of the baton in the lab!

Many (former and actual) members of the **IBI-2** have contributed to a welcoming and inspiring atmosphere in both lab and breakroom, even during a global pandemic. Thank you for making my time at Forschungszentrum Jülich as pleasant as it has been! Specifically, I want to thank **Claudia Klamandt** for her administrative help and sympathetic ear.

Many thanks to my second reviewer, **Prof. Dr. Ulrich Kubitscheck**, for taking the time to revise my thesis and assess my scientific work. I would also like to thank the other members of my thesis committee, **Prof. Dr. Arne Lützen and Prof. Dr. Jörg Höhfeld**, for their time and commitment.

Lastly, I would like to express my special gratitude to my friends and family without whoose support I would not have come this far. Many thanks to my parents **Françoise**Baritaud and Manfred Eichstedt for their assistance and faith, and to Dieter

Begemann for making sure I never run out of freshly baked cookies.

I am beyond grateful for my very dear friends, especially **Claudia Reichelt** and **Erik Röcher**, for their loving encouragement and comfort during difficult times. Last but not least, I would like to thank my wonderful husband **Sebastian Kinny** for being my companion through the highs and the lows of (PhD-) life.

- 1 Fletcher DA, Mullins RD. Cell mechanics and the cytoskeleton. Nature 2010; 463(7280): 485–92.
- 2 Kowalczyk AP, Rubenstein DS, Garrod DR *et al.* Milestones in Investigative Dermatology: The Desmosome. *Journal of Investigative Dermatology* 2007; **127:** E1.
- Niessen CM. Tight junctions/adherens junctions: basic structure and function. *J Invest Dermatol* 2007; **127**(11): 2525–32.
- 4 Green KJ, Simpson CL. Desmosomes: new perspectives on a classic. *J Invest Dermatol* 2007; **127**(11): 2499–515
- Garrod DR, Chidgey M. Desmosome structure, composition and function. *Biochim Biophys Acta* 2007; **1778**(3): 572–87.
- 6 Garrod DR, Merritt AJ, Nie Z. Desmosomal cadherins. Current opinion in Cell Biology 2002; 14: 537–45.
- 7 Cheng X, Den Z, Koch PJ. Desmosomal cell adhesion in mammalian development. *Eur J Cell Biol* 2005; **84**(2-3): 215–23.
- 8 Dusek RL, Attardi LD. Desmosomes: new perpetrators in tumor suppression. *Nature reviews cancer* 2011; **11:** 317–23
- 9 Nekrasova O, Green KJ. Desmosome assembly and dynamics. Trends Cell Biol 2013; 23(11): 537–46.
- 10 Cui Y, Hameed FM, Yang B *et al.* Cyclic stretching of soft substrates induces spreading and growth. *Nat Commun* 2015: **6:** 6333.
- 11 Ingber DE. Tensegrity II. How structural networks influence cellular information processing networks. *J Cell Sci* 2003; **116**(Pt 8): 1397–408.
- Dabboue H, Builles N, Frouin É *et al.* Assessing the Impact of Mechanical Damage on Full-Thickness Porcine and Human Skin Using an In Vitro Approach. *Biomed Res Int* 2015; **2015**: 434623.
- 13 Cabrera-Benítez NE, Parotto M, Post M *et al*. Mechanical stress induces lung fibrosis by epithelial-mesenchymal transition. *Crit Care Med* 2012; **40**(2): 510–7.
- Weber GF, Bjerke MA, DeSimone DW. A mechanoresponsive cadherin-keratin complex directs polarized protrusive behavior and collective cell migration. *Dev Cell* 2012; **22**(1): 104–15.
- Bliley JM, Vermeer MC, Duffy RM *et al.* Dynamic loading of human engineered heart tissue enhances contractile function and drives a desmosome-linked disease phenotype. *Science Translational medicine* 2021;
- 16 Powell DW. Barrier function of epithelia. Am J Physiol Gastrointest Liver Physiol 1981; 4(241): 275–88.
- 17 Gerhard Aumüller, Gabriela Aust, Jürgen Engele, Joachim Kirsch, Giovanni Maio. *Duale Reihe Anatomie*. 5th ed. Thieme, 2020.
- Overton J. Desmosome Development in Normal and Reassociating Cells in the Early Chick Blastoderm. Developmental Biology 1962; **47:** 532–48.
- 19 McNutt NS, Weinstein RS. Membran ultrastructure at mammalian intercellular junctions. *Progress in Biophysics and Molecular Biology* 1973; (26): 45–101.
- Cowin P, Kapprell H-P, Franke WW. The Complement of Desmosomal Plaque Proteins in Different Cell Types. *The Journal of Cell Biology* 1985; **101:** 1442–54.
- 21 Suhrbier A, Garrod DR. An investigation of the molecular components of desmosomes in epithelial cells of five vertebrates. *J Cell Sci* 1986; **81:** 223–42.
- Miller K, Mattey DL, Measures H *et al.* Localisation of the protein and glycoprotein components of bovine nasal epithelial desmosomes by immunoelectron microscopy. *The EMBO Journal* 1987; **6**(4): 885–9.

- Huber O. Structure and function of desmosomal proteins and their role in development and disease. *Cellular and molecular life sciences* 2003; **60**(9): 1872–90.
- 24 Overton J. Cell Junctions and Their Development. Progress in Surface and Membrane Science 1974: 161–208.
- 25 Ian D.J. Burdett. Aspects of the Structure and Assembly of Desmosomes. *Micron* 1998; **29**(4): 309–28.
- 26 Cowin P, Garrod DR. Antibodies to epithelial desmosomes show wide tissue and species cross-reactivity. Nature 1983; 302(10): 148-150.
- 27 Drochmans P, Freudenstein C, Wanson JC *et al.* Structure and bio- chemical composition of desmosome and tonofilaments isolated from calf muzzle epidermis. *J. Cell Biology* 1978; **79:** 427–43.
- Twiss F, Rooij J de. Cadherin mechanotransduction in tissue remodeling. *Cellular and molecular life sciences* 2013; **70**(21): 4101–16.
- 29 Harrison OJ, Brasch J, Lasso G *et al.* Structural basis of adhesive binding by desmocollins and desmogleins. *Proc Natl Acad Sci U S A* 2016; **113**(26): 7160–5.
- 30 Nie Z, Merritt A, Rouhi-Parkouhi M *et al.* Membrane-impermeable cross-linking provides evidence for homophilic, isoform-specific binding of desmosomal cadherins in epithelial cells. *J Biol Chem* 2011; **286**(3): 2143–54.
- Cowin P, Mattey DL, Garrod DR. Distribution of desmosomal components in the tissues of vertebrates, studied by fluorescent antibody staining. *J Cell Sci* 1984; **66:** 119–32.
- Lowndes M, Rakshit S, Shafraz O *et al.* Different roles of cadherins in the assembly and structural integrity of the desmosome complex. *J Cell Sci* 2014; **127**(Pt 10): 2339–50.
- Garrod DR, Kimura TE. Hyper-adhesion: a new concept in cell-cell adhesion. *Biochem Soc Trans* 2008; **36**: 195–201.
- Kowalczyk AP, Hatzfeld M, Bornslaeger EA *et al.* The head domain of plakophilin-1 binds to desmoplakin and enhances its recruitment to desmosomes. Implications for cutaneous disease. *J Biol Chem* 1999; **274**(26): 18145–8.
- Cowin P, Kapprell H-P, Franke WW *et al.* Plakoglobin: A Protein Common to Different Kinds of Intercellular Adhering Junctions. *Cell* 1986; **46:** 1063–73.
- 36 Stokes DL. Desmosomes from a structural perspective. Current opinion in Cell Biology 2007; 19(5): 565–71.
- Witcher LL, Collins R, Puttagunta S *et al.* Desmosomal cadherin binding domains of plakoglobin. *J Biol Chem* 1996; **271**(18): 10904–9.
- Vasioukhin V, Ethan Bowers, Bauer C *et al.* Desmoplakin is essential in epidermal sheet formation. *Nat Cell Biol* 2001; **3:** 1076–85.
- Leung CL, Green KJ, Liem RK. Plakins: a family of versatile cytolinker proteins. *Trends Cell Biol* 2002; **12**(1): 37–45.
- Jefferson JJ, Leung CL, Liem RKH. Plakins: goliaths that link cell junctions and the cytoskeleton. *Nat Rev Mol Cell Biol* 2004; **5**(7): 542–53.
- 41 Green KJ, Parry DA, Steinert PM *et al.* Structure of the human desmoplakins. Implications for function in the desmosomal plaque. *Journal of Biological Chemistry* 1990; **265**(5): 2603–12.
- O'Keefe EJ, Erickson HP, Bennett V. Desmoplakin I and desmoplakin II. *Journal of Biological Chemistry* 1989; **264**(14): 8310–8.
- 43 Etienne-Manneville S. Cytoplasmic Intermediate Filaments in Cell Biology. *Annu Rev Cell Dev Biol* 2018; **34:** 1–28.
- Sapra KT, Medalia O. Bend, Push, Stretch: Remarkable Structure and Mechanics of Single Intermediate Filaments and Meshworks. *Cells* 2021; **10**(8).

- Block J, Schroeder V, Pawelzyk P *et al.* Physical properties of cytoplasmic intermediate filaments. *Biochim Biophys Acta* 2015; **1853**(11 Pt B): 3053–64.
- Herrmann H, Aebi U. Intermediate Filaments: Structure and Assembly. *Cold Spring Harb Perspect Biol* 2016; **8**(11).
- 47 Takeichi M. Dynamic contacts: rearranging adherens junctions to drive epithelial remodelling. *Nat Rev Mol Cell Biol* 2014; **15**(6): 397–410.
- 48 Maiden SL, Hardin J. The secret life of  $\alpha$ -catenin: moonlighting in morphogenesis. *The Journal of Cell Biology* 2011; **195**(4): 543–52.
- 49 Rasool S, Geethakumari AM, Biswas KH. Role of Actin Cytoskeleton in E-cadherin-Based Cell–Cell Adhesion Assembly and Maintenance. *J Indian Inst Sci* 2021; **101**(1): 51–62.
- Tobacman LS, Korn ED. The kinetics of actin nucleation and polymerization. *Journal of Biological Chemistry* 1983; **258**(5): 3207–14.
- Godsel LM, Dubash AD, Bass-Zubeck AE *et al.* Plakophilin 2 Couples Actomyosin Remodeling to Desmosomal Plaque Assembly via RhoA. *Molecular Biology of the Cell* 2010; **21:** 2844–59.
- Pasdar M, Li Z. Disorganization of microfilaments and intermediate filaments interferes with the assembly and stability of desmosomes in MDCK epithelial cells. *Cell Motility and the Cytoskeleton* 1993; **26**(2): 163–80.
- Roberts BJ, Pashaj A, Johnson KR, Wahl JK. Desmosome dynamics in migrating epithelial cells requires the actin cytoskeleton. *Exp Cell Res* 2011; **317**(20): 2814–22.
- Duden R, Franke WW. Organization of Desmosomal Plaque Proteins in Cells Growing at Low Calcium Concentrations. *Journal of Cell Biology* 1988; **107:** 1049–63.
- Jones JC, Goldmann RD. Intermediate filaments and the initiation of desmosome assembly. The Journal of Cell Biology 1985; 101: 506–17.
- Mattey DL, Garrod DR. Calcium-induced desmosome Formation in cultured kidney epithelial cells. *J Cell Sci* 1986; (85): 95–111.
- 57 Penn EJ, Burdett ID, Hobson C et al. Structure and Assembly of Desmosome Junctions: Biosynthesis and Turnover of the Major Desmosome Components of Madin-Darby Canine Kidney Cells in Low Calcium Medium. The Journal of Cell Biology 1987; **105:** 2327–34.
- Pasdar M, Nelson JW. Regulation of Desmosome Assembly in Epithelial Cells: Kinetics of Synthesis, Transport, and Stabilization of Desmoglein I, a Major Protein of the Membrane Core Domain. *The Journal of Cell Biology* 1989; (109): 163–77.
- Windoffer R, Borchert-Stuhlträger M, Leube RE. Desmosomes: interconnected calcium-dependent structures of remarkable stability with significant integral membrane protein turnover. *J Cell Sci* 2002; **115**(8): 1717–32.
- 60 Pasdar M, Nelson JW. Kinetics of Desmosome Assembly in Madin-Darby Canine Kidney Epithelial Cells: Temporal and Spatial Regulation of Desmoplakin Organization and Stabilization upon Cell-Cell Contact. I. Biochemical Analysis. *The Journal of Cell Biology* 1988; **106:** 677–85.
- 41 Yin T, Green KJ. Regulation of desmosome assembly and adhesion. Semin Cell Dev Biol 2004; **15**(6): 665–77.
- Mattey DL, Garrod DR. Splitting and internalization of the desmosomes of cultured kidney epithelial cells by reduction in calcium concentration. *J Cell Sci* 1986; (85): 113–24.
- 63 Burdett ID. Internalisation of desmosomes and their entry into the endocytic pathway via late endosomes in MDCK cells Possible mechanisms for the modulation of cell adhesion by desmosomes during development. *J Cell Sci* 1993; **106:** 1115–30.
- 64 Mattey DL, Burdge G, Garrod DR. Development of desmosomal adhesion between MDCK cells following calcium switching. *J Cell Sci* 1990; **97:** 689–704.

- Beggs RR, Rao TC, Dean WF *et al.* Desmosomes undergo dynamic architectural changes during assembly and maturation. *Tissue Barriers* 2022; **10**(4): 2017225.
- Thomason HA, Scothern A, McHarg S, Garrod DR. Desmosomes: adhesive strength and signalling in health and disease. *Biochem J* 2010; **429**(3): 419–33.
- 67 Kimura TE, Merritt AJ, Garrod DR. Calcium-independent desmosomes of keratinocytes are hyper-adhesive. *J Invest Dermatol* 2007; **127**(4): 775–81.
- Lele TP, Thodeti CK, Pendse J, Ingber DE. Investigating complexity of protein-protein interactions in focal adhesions. *Biochem Biophys Res Commun* 2008; **369**(3): 929–34.
- 69 Einstein A. Theoretische Bemerkungen über die Brownsche Bewegung. *Zeitschrift für Elektrochemie* 1907; **13**(6): 41–8.
- 70 Einstein A. Elementare Theorie der Brownschen Bewegung. Zeitschrift für Elektrochemie 1908; (17): 235–9.
- 71 Islam M. Einstein-Smoluchowski Diffusion Equation: A Discussion. Physica Scripta 2004; 70: 120-5.
- Gennes PG de. Kinetics of diffusion-controlled processes in dense polymer systems. I. Nonentangled regimes. *The Journal of Chemical Physics* 1982; **76**(6): 3316–21.
- Bartle EI, Rao TC, Beggs RR *et al.* Protein exchange is reduced in calcium-independent epithelial junctions. *The Journal of Cell Biology* 2020; **219**(6).
- 74 Vogel V, Sheetz M. Local force and geometry sensing regulate cell functions. *Nat Rev Mol Cell Biol* 2006; **7**(4): 265–75.
- Vogel V, Sheetz MP. Cell fate regulation by coupling mechanical cycles to biochemical signaling pathways. *Current opinion in Cell Biology* 2009; **21**(1): 38–46.
- 76 Cooper J, Giancotti FG. Integrin Signaling in Cancer: Mechanotransduction, Stemness, Epithelial Plasticity, and Therapeutic Resistance. *Cancer Cell* 2019; **35**(3): 347–67.
- 77 Collinsworth AM, Torgan CE, Nagda SN *et al.* Orientation and length of mammalian skeletal myocytes in response to a unidirectional stretch. *Cell Tissue Res* 2000; **302**(2): 243–51.
- Hayakawa K, Sato N, Obinata T. Dynamic reorientation of cultured cells and stress fibers under mechanical stress from periodic stretching. *Exp Cell Res* 2001; **268**(1): 104–14.
- 79 Dartsch PC, Betz E. Response of cultured endothelial cells to mechanical stimulation. *Basic Research in Cardiology* 1989; **84**(3): 268–81.
- Noethel B, Ramms L, Dreissen G *et al.* Transition of responsive mechanosensitive elements from focal adhesions to adherens junctions on epithelial differentiation. *Molecular Biology of the Cell* 2018; **29:** 2317–25.
- Chien S. Mechanotransduction and endothelial cell homeostasis: the wisdom of the cell. *Am J Physiol Heart Circ Physiol* 2007; **292**(3): H1209–H1224.
- 82 Zielinski A, Linnartz C, Pleschka C et al. Reorientation dynamics and structural interdependencies of actin, microtubules and intermediate filaments upon cyclic stretch application. Cytoskeleton 2018; 75(9): 385–94.
- Hoffman BD, Massiera G, van Citters KM, Crocker JC. The consensus mechanics of cultured mammalian cells. *Proc Natl Acad Sci U S A* 2006.
- Dave Ahrens. Biomechanische Untersuchungen zur Rolle des Zytoskeletts für die mechanische Anisotropie und Dehnbarkeit von Monolagen epithelialer Zellen [Dissertation]. Bonn: Rheinische Friedrich-Wilhelms-Universität Bonn; 2019.
- Green KJ, Roth-Carter Q, Niessen CM, Nichols SA. Tracing the Evolutionary Origin of Desmosomes. *Curr Biol* 2020; **30**(10): R535-R543.
- Muhamed I, Wu J, Sehgal P *et al.* E-cadherin-mediated force transduction signals regulate global cell mechanics. *J Cell Sci* 2016; **129**(9): 1843–54.

- 87 Cronin NM, DeMali KA. Dynamics of the Actin Cytoskeleton at Adhesion Complexes. *Biology (Basel)* 2021; **11**(1).
- Hatzfeld M, Keil R, Magin TM. Desmosomes and Intermediate Filaments: Their Consequences for Tissue Mechanics. *Cold Spring Harb Perspect Biol* 2017; **9**(6).
- Price AJ, Cost A-L, Ungewiß H *et al.* Mechanical loading of desmosomes depends on the magnitude and orientation of external stress. *Nat Commun* 2018; **9**(1): 5284.
- Broussard JA, Koetsier JL, Hegazy M, Green KJ. Desmosomes polarize and integrate chemical and mechanical signaling to govern epidermal tissue form and function. *Curr Biol* 2021; **31**(15): 3275-3291.e5.
- 91 Broussard JA, Jaiganesh A, Zarkoob H *et al.* Scaling up single-cell mechanics to multicellular tissues the role of the intermediate filament-desmosome network. *J Cell Sci* 2020; **133**(6).
- 92 Angulo-Urarte A, van der Wal T, Huveneers S. Cell-cell junctions as sensors and transducers of mechanical forces. Biochim Biophys Acta Biomembr 2020; 1862(9): 183316.
- 93 Sawada Y, Nakamura K, Doi K *et al.* Rap1 and cell stretching-initiated p38 activation. *J Cell Sci* 2001; **114:** 1221–7.
- 94 Kaunas R, Nguyen P, Usami S, Cien S. Cooperative effects of Rho and mechanical stretch on stress fiber organization. *Proc Natl Acad Sci U S A* 2005; **102**(44): 15895–900.
- Peussa H. Characterization of a stretching and compression device and it's application on epithelial cells [Masterarbeit]: Tampere Univversity; 2020.
- 96 Mori N, Morimoto Y, Takeuchi S. Perfusable and stretchable 3D culture system for skin-equivalent. *Biofabrication* 2019; **11**(1).
- 97 Zhou C, Bette S, Babendreyer A *et al.* Stretchable electrical cell-substrate impedance sensor platform for monitoring cell monolayers under strain. *Sensors and Actuators B: Chemical* 2021; **336:** 129656.
- 98 Wanuske M-T, Brantschen D, Schinner C *et al.* Clustering of desmosomal cadherins by desmoplakin is essential for cell-cell adhesion. *Acta Physiol (Oxf)* 2021; **231**(4): e13609.
- 99 Dukes JD, Whitley P, Chalmers AD. The MDCK variety pack: choosing the right strain. BMC Cell Biol 2011; 12.
- 100 Baddam SR, Arsenovic PT, Narayanan V *et al.* The Desmosomal Cadherin Desmoglein-2 Experiences Mechanical Tension as Demonstrated by a FRET-Based Tension Biosensor Expressed in Living Cells. *Cells* 2018; **7**(7).
- 101 Beco S de, Perney J-B, Coscoy S, Amblard F. Mechanosensitive Adaptation of E-Cadherin Turnover across adherens Junctions. *PLoS ONE* 2015; **10**(6): e0128281.
- Püllen R, Konrad J, Hoffmann B, Merkel R. Cell Stretcher Assay to Analyze Mechanoresponses to Cyclic Stretching [Zaidel-Bar, Ronen (editor)]. *Mechanobiology: Methods and Protocols* 2023; **2600:** 91–105.
- 103 Rothen-Rutishauser B, Kraemer SD, Braun A *et al.* MDCK Cell Cultures as an Epithelial In Vitro Model: Cytoskeleton and Tight Junctions as Indicators for the Definition of Age-Related Stages by Confocal Microscopy. *Pharmaceutical Research* 1998; **15**(7).
- 104 Nagatomi J. *Mechanobiology Handbook*. CRC Press, 2011.
- Fülle JB, Huppert H, Liebl D *et al.* Desmosome dualism most of the junction is stable, but a plakophilin moiety is persistently dynamic. *J Cell Sci* 2021; **134**(21).
- 106 Faust U, Hampe N, Rubner W *et al.* Cyclic Stress at mHz Frequencies Aligns Fibroblasts in Direction of Zero Strain. *PLoS ONE* 2011; **6**(12): 1-16. URL https://journals.plos.org/plosone/article/file?id=10.1371/journal.pone.0028963&type=printable.
- 107 James B.Pawley. Biological Confocal Microscopy. Springer Science+Business Media, LLC, 2006.
- 108 Lorén N, Hagman J, Jonasson JK *et al.* Fluorescence recovery after photobleaching in material and life sciences: putting theory into practice. *Q Rev Biophys* 2015; **48**(3): 323–87.

- 109 Barden AO, Goler AS, Humphreys SC *et al.* Tracking individual membrane proteins and their biochemistry: The power of direct observation. *Neuropharmacology* 2015; **98:** 22–30.
- Reits EA, Neefjes JJ. From fixed to FRAP: measuring protein mobility and activity in living cells. *Nat Cell Biol* 2001; **3**(6): E145-E147.
- 111 Axelrod D, Koppel DE, J. Schlessinger *et al.* Mobility measurement by analysis of fluorescence photobleaching recovery kinetics. *Biophys J* 1976; **16:** 1055–69.
- 112 Gloushankova NA, Wakatsuki T, Troyanovsky RB *et al.* Continual assembly of desmosomes within stable intercellular contacts of epithelial A-431 cells. *Cell Tissue Res* 2003; **314**(3): 399–410.
- 113 Edmund T. Whittaker. *On a new method of graduation*. Proceedings of the Edinburgh Mathematical Society, 1922
- 114 Engel A. *Taylorentwicklung, Jacobi-Matrix, V, δ(x) und Co.: Rechenmethoden für Studierende der Physik.* 1st ed. Springer Spektrum, 2020.
- 115 Bradley E, Tibshirani RJ. An Introduction to the Bootstrap. 1st ed. Chapman and Hall/CRC, 1994.
- 116 Bevington PR, Robinson DK. *Data Reduction and Error Analysis for the Physical Sciences*. New York: McGraw Hill, 2003.
- 117 Shapiro SS, Wilk MB. An Analysis of Variance Test for Normality. Biometrika 1965; 52(3/4): 591–611.
- 118 Gastwirth JL, Gel YR, Miao W. The Impact of Levene's Test of Equality of Variances on Statistical Theory and Practice. *Statist. Sci.* 2009; **24**(3).
- 119 Fligner MA, Killeen TJ. Distribution-free two-sample tests for scale. *Journal of the American Statistical Association* 1976; **71**(353): 210–3.
- 120 Weiß C. Basiswissen Medizinische Statistik. 7th ed. Springer Lehrbuch, 2019.
- 121 Hedderich J, Sachs L. Angewandte Statistik: Methodensammlung mit R. 17th ed. Springer Spektrum, 2021.
- 122 Cassio D. Long term culture of MDCK strains alters chromosome content. BMC Research Notes 2013; 6(162).
- Jordan K, Solan JL, Dominguez M *et al.* Trafficking, Assembly, and Function of a Connexin43-Green Fluorescent Protein Chimera in Live Mammalian Cells. *Molecular Biology of the Cell* 1999; **10:** 2033–50.
- Windoffer R, Beile B, Leibold A *et al.* Visualization of gap junction mobility in living cells. *Cell Tissue Res* 2000; **299**(3): 347–62.
- Foote HP, Sumigray KD, Lechler T. FRAP analysis reveals stabilization of adhesion structures in the epidermis compared to cultured keratinocytes. *PLoS ONE* 2013; **8**(8): 1-7.
- 126 Lippincott-Schwartz J, Snapp E, Kenworthy A. Studying protein dynamics in living cells. *Nat Rev Mol Cell Biol* 2001; **2:** 444–56.
- 127 Resnik N, Luca GMR de, Sepčić K *et al.* Depletion of the cellular cholesterol content reduces the dynamics of desmosomal cadherins and interferes with desmosomal strength. *Histochem Cell Biol* 2019; **152**(3): 195–206.
- Weiß K, Neef A, Van Q *et al.* Quantifying the diffusion of membrane proteins and peptides in black lipid membranes with 2-focus fluorescence correlation spectroscopy. *Biophys J* 2013; **105**(2): 455–62.
- Mogre SS, Brown AI, Koslover EF. Getting around the cell: physical transport in the intracellular world. *Phys Biol* 2020; **17**(6): 61003.
- 130 Verkmann AS. Solute and macromolecule diffusion in cellular aqueous compartments. *Trends in Biochemical Sciences* 2002; **27**(1).
- 131 Wu J, Fang Y, Zarnitsyna VI *et al.* A coupled diffusion-kinetics model for analysis of contact-area FRAP experiment. *Biophys J* 2008; **95**(2): 910–9.

- O'Shannessy DJ, Brigham-Burke M, Soneson KK *et al.* Determination of Rate and Equilibrium Binding Constants for Macromolecular Interactions Using Surface Plasmon Resonance: Use of Nonlinear Least Squares Analysis Methods. *Analytical Biochemistry* 1993; **212:** 457–68.
- 133 Sprague BL, McNally JG. FRAP analysis of binding: proper and fitting. Trends Cell Biol 2005; 15(2): 84–91.
- Hiermaier M, Kliewe F, Schinner C *et al.* The Actin-Binding Protein  $\alpha$ -Adducin Modulates Desmosomal Turnover and Plasticity. *J Invest Dermatol* 2021; **141**(5): 1219-1229.e11.
- 135 Samak G, Gangwar R, Crosby LM *et al.* Cyclic stretch disrupts apical junctional complexes in Caco-2 cell monolayers by a JNK-2-, c-Src-, and MLCK-dependent mechanism. *Am J Physiol Gastrointest Liver Physiol* 2014; **306**(11): G947-58.
- 136 Lele TP, Pendse J, Kumar S *et al.* Mechanical forces alter zyxin unbinding kinetics within focal adhesions of living cells. *J Cell Physiol* 2006; **207**(1): 187–94.
- 137 Sigaut L, Bilderling C von, Bianchi M *et al.* Live cell imaging reveals focal adhesions mechanoresponses in mammary epithelial cells under sustained equibiaxial stress. *Sci Rep* 2018; **8**(1): 9788.
- 138 Uttagomol J, Ahmad US, Rehman A *et al.* Evidence for the Desmosomal Cadherin Desmoglein-3 in Regulating YAP and Phospho-YAP in Keratinocyte Responses to Mechanical Forces. *Int J Mol Sci* 2019; **20**(24).
- 139 Del Rio A, Perez-Jimenez R, Liu R *et al.* Stretching single talin rod molecules activates vinculin binding. *Science* 2009; **323**(5914): 638–41.
- 140 Massou S, Nunes Vicente F, Wetzel F *et al.* Cell stretching is amplified by active actin remodelling to deform and recruit proteins in mechanosensitive structures. *Nat Cell Biol* 2020; **22**(8): 1011–23.
- 141 Yonemura S, Wada Y, Watanabe T *et al.* α-Catenin as a tension transducer that induces adherens junction development. *Nat Cell Biol* 2010; **12**(6): 533–42.
- Daday C, Kolšek K, Gräter F. The mechano-sensing role of the unique SH3 insertion in plakin domains revealed by Molecular Dynamics simulations. *Sci Rep* 2017; **7**(1): 11669.
- 143 Goult BT, Essen M von, Hytönen VP. The mechanical cell the role of force dependencies in synchronising protein interaction networks. *J Cell Sci* 2022; **135**(22).
- 144 Albrecht LV, Zhang L, Shabanowitz J et al. GSK3- and PRMT-1-dependent modifications of desmoplakin control desmoplakin-cytoskeleton dynamics. *The Journal of Cell Biology* 2015; **208**(5): 597–612.
- 145 Flitney EW, Kuczmarski ER, Adam SA, Goldman RD. Insights into the mechanical properties of epithelial cells: the effects of shear stress on the assembly and remodeling of keratin intermediate filaments. *FASEB J* 2009; **23**(7): 2110–9.
- Möhl C, Kirchgeßner N, Schäfer C *et al.* Becoming stable and strong The interplay between vinculin exchange dynamics and adhesion strength during adhesion site maturation. *Cell Motility and the Cytoskeleton* 2009; **66:** 350–64.
- 147 Küpper K, Lang N, Möhl C *et al.* Tyrosine phosphorylation of vinculin at position 1065 modifies focal adhesion dynamics and cell tractions. *Biochem Biophys Res Commun* 2010; **399**(4): 560–4.
- Lutz A, Jung D, Diem K *et al.* Acute effects of cell stretch on keratin filaments in A549 lung cells. *FASEB J* 2020; **34**(8): 11227–42.
- Hobbs RP, Green KJ. Desmoplakin regulates desmosome hyperadhesion. *J Invest Dermatol* 2012; **132**(2): 482–5.
- 150 Lövenich L. Dehnungsinduzierte Mechanosensitivität in Abhängigkeit der RhoA-induzierten Zellkontraktilität und BAG3-vermittelter Autophagie [Dissertation]. Bonn: Rheinische Friedrich-Wilhelms-Universität Bonn; 2022.

# **Appendix**

# Individual recovery curves

In the following section, the individual recovery curves of the FRAP experiments performed for this thesis are presented sorted by desmosomal protein and mechanical state.

### **DP** CTRL-samples

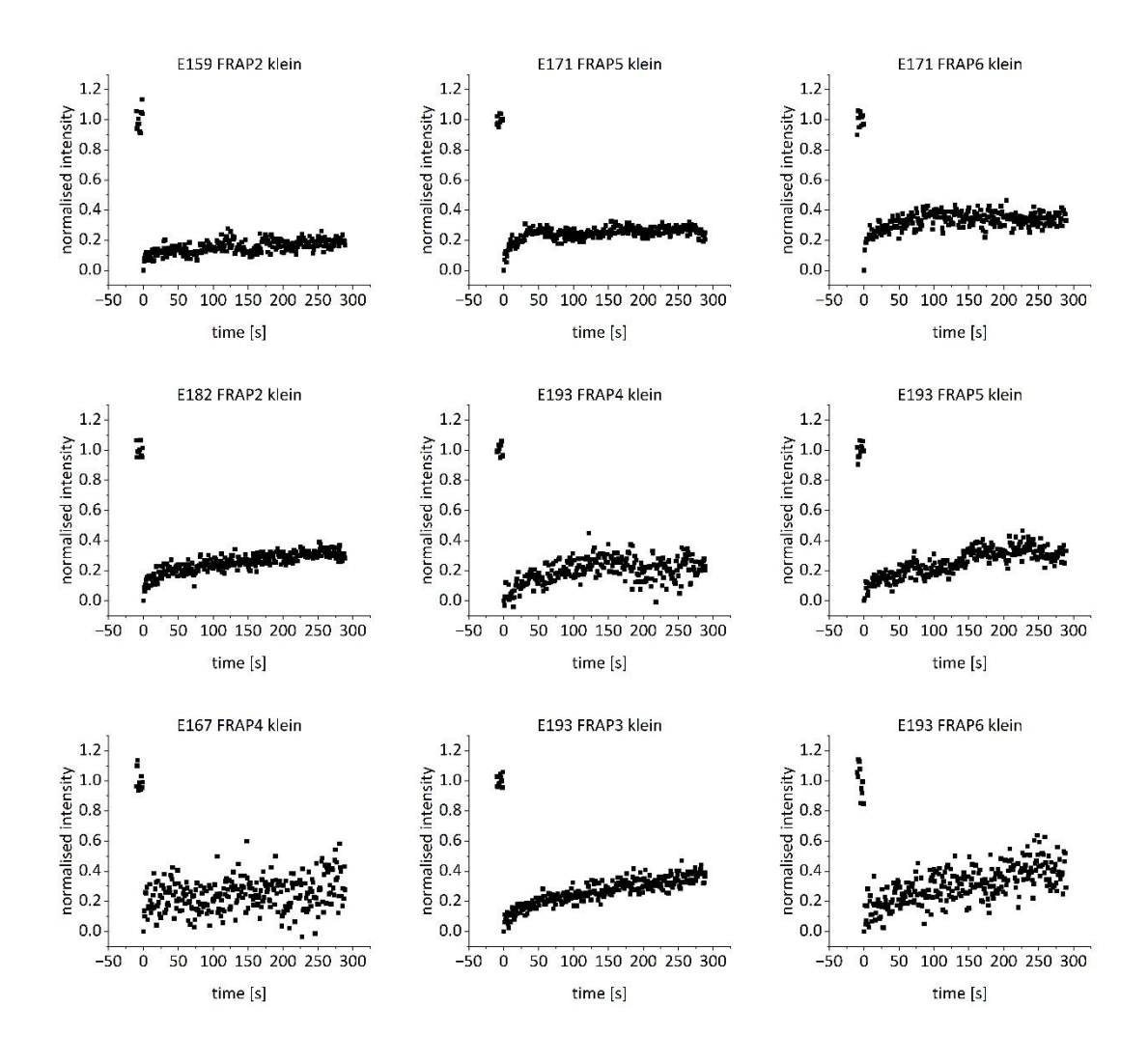


Figure 1: The individual recovery curves of the DP CTRL FRAP experiments. The recovery curves E159 FRAP2 klein, E167 FRAP4 klein, E193 FRAP5 klein and E193 FRAP6 klein were fitted with the linear fit. E171 FRAP5 klein, E171 FRAP6 klein, E182 FRAP2 klein, E193 FRAP3 klein and E193 FRAP3 klein were fitted with the exponential fit.

# **DP** stretch-samples

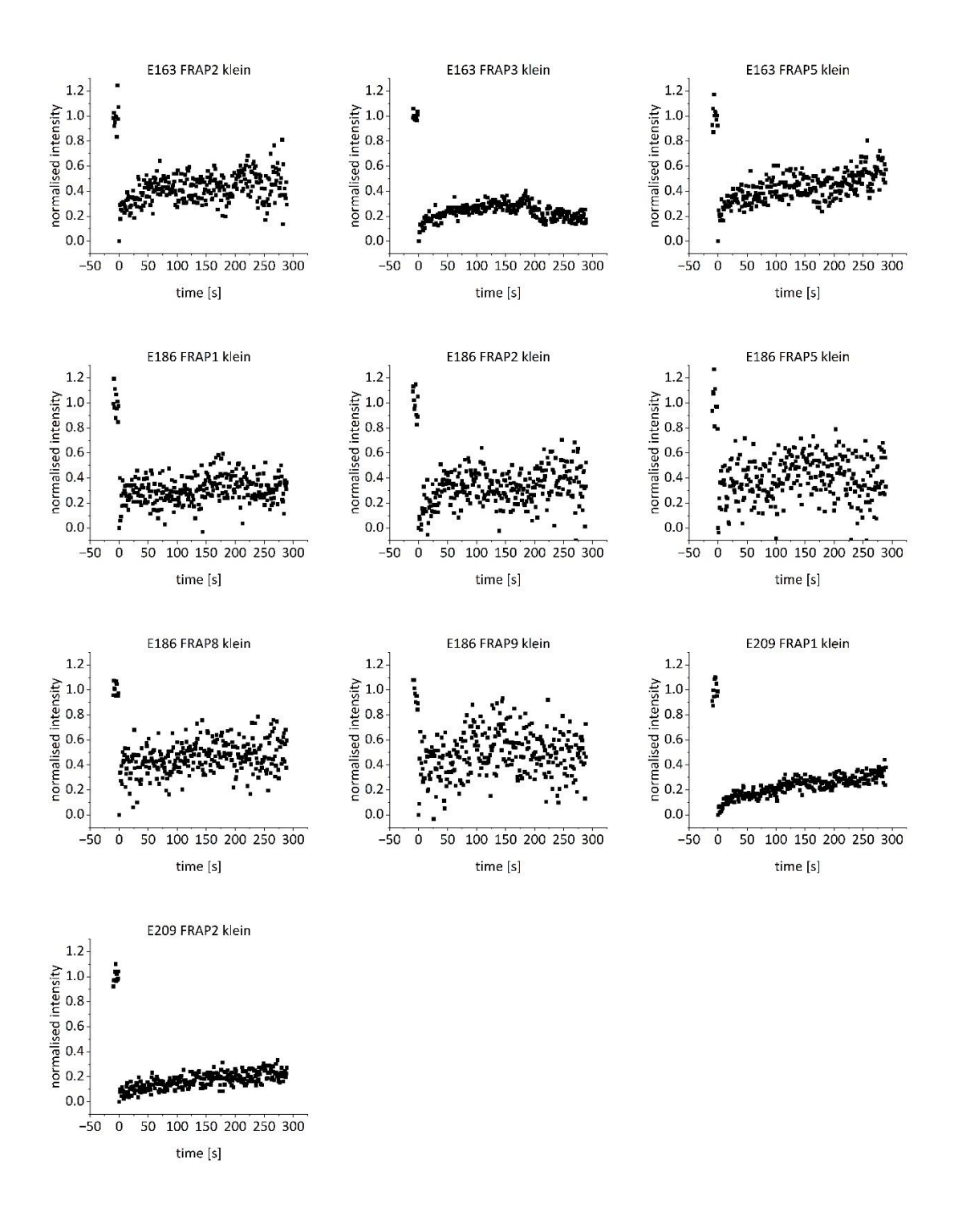


Figure 2: The individual recovery curves of the DP stretch FRAP experiments. The recovery curves E186 FRAP1 klein, E186 FRAP8 klein, E186 FRAP9 klein and E209 FRAP2 klein were fitted with the linear fit. The recovery curves E163 FRAP2 klein, E163 FRAP3 klein, E163 FRAP5 klein, E186 FRAP2 klein and E209 FRAP1 klein were fitted with the exponential fit.

# DP stretch+24 h-samples

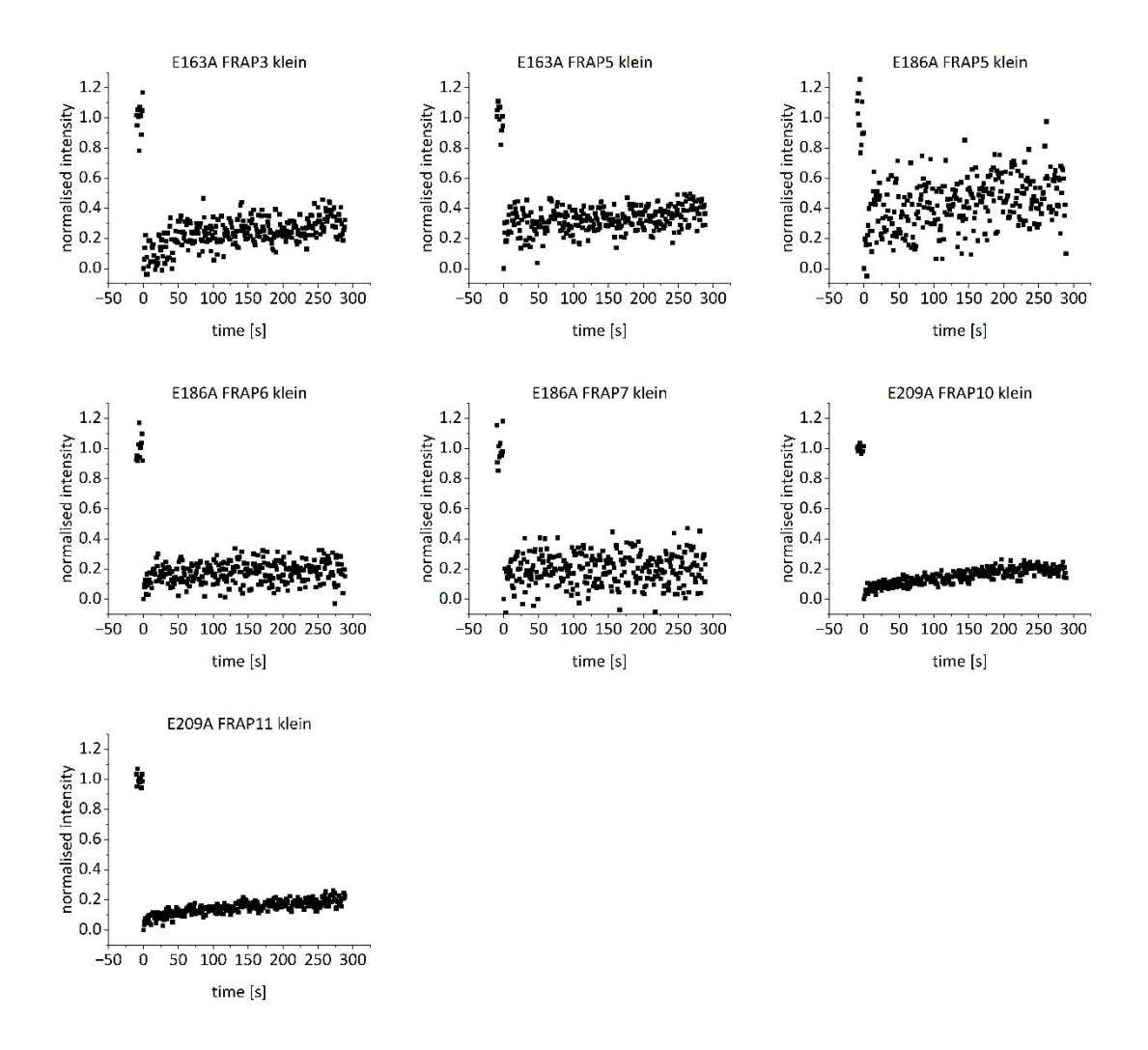


Figure 3: The individual recovery curves of the DP stretch+24h FRAP experiments. The recovery curves E163A FRAP5 klein, E186A FRAP5 klein and E209A FRAP10 klein were fitted with the linear fit. The recovery curves were E163A FRAP3 klein, E186A FRAP6 klein, E186A FRAP7 klein and E209A FRAP11 klein fitted with the exponential fit.

# DP CTRL+24 h-samples

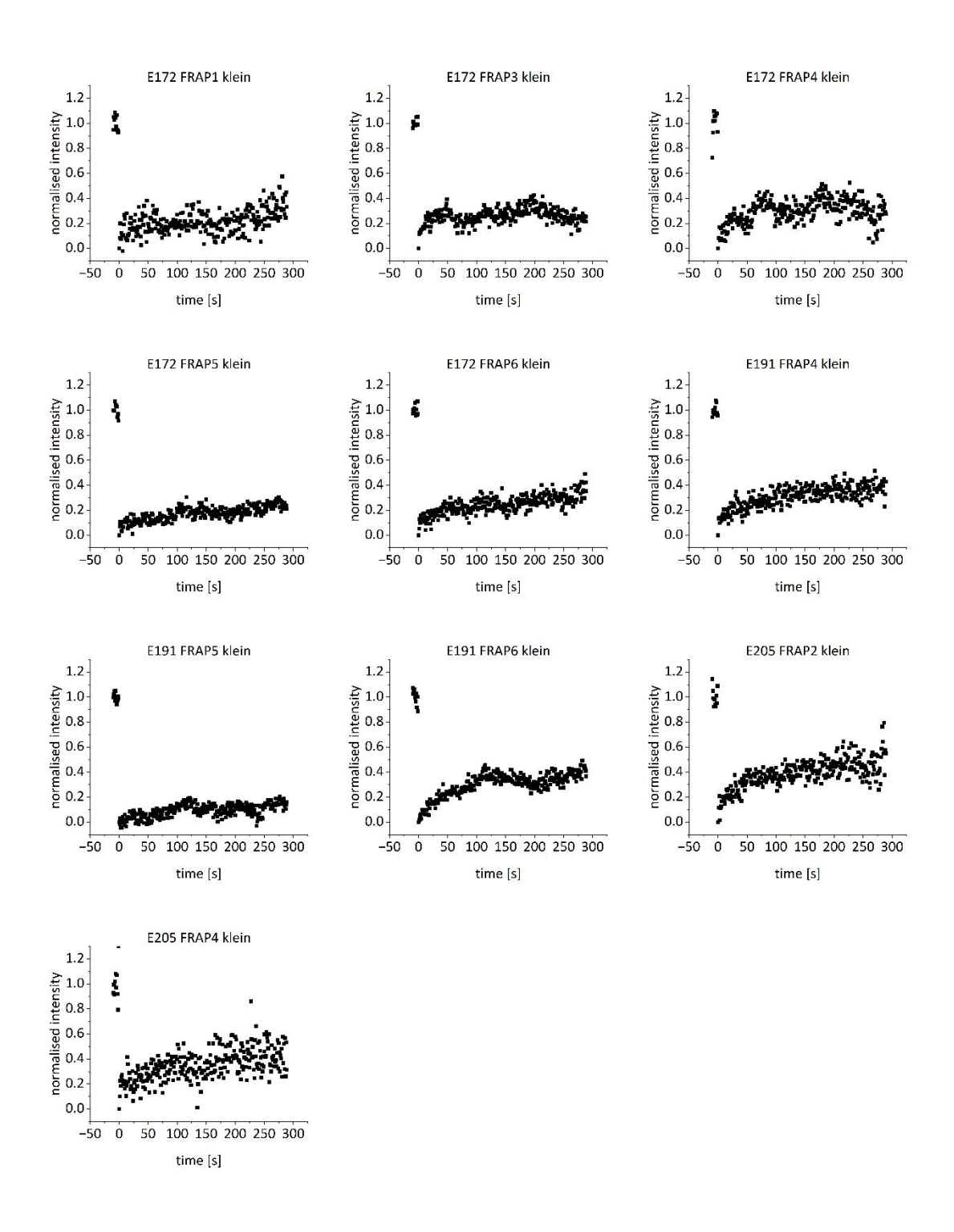


Figure 4: The individual recovery curves of the DP CTRL+24h FRAP experiments. The recovery curves E172 FRAP3 klein and E205 FRAP4 klein were fitted with the linear fit. The recovery curves E172 FRAP1 klein, E172 FRAP4 klein, E172 FRAP4 klein, E191 FRAP5 klein, E191 FRAP6 klein and E205 FRAP2 klein were fitted with the exponential fit.

# PG CTRL-samples

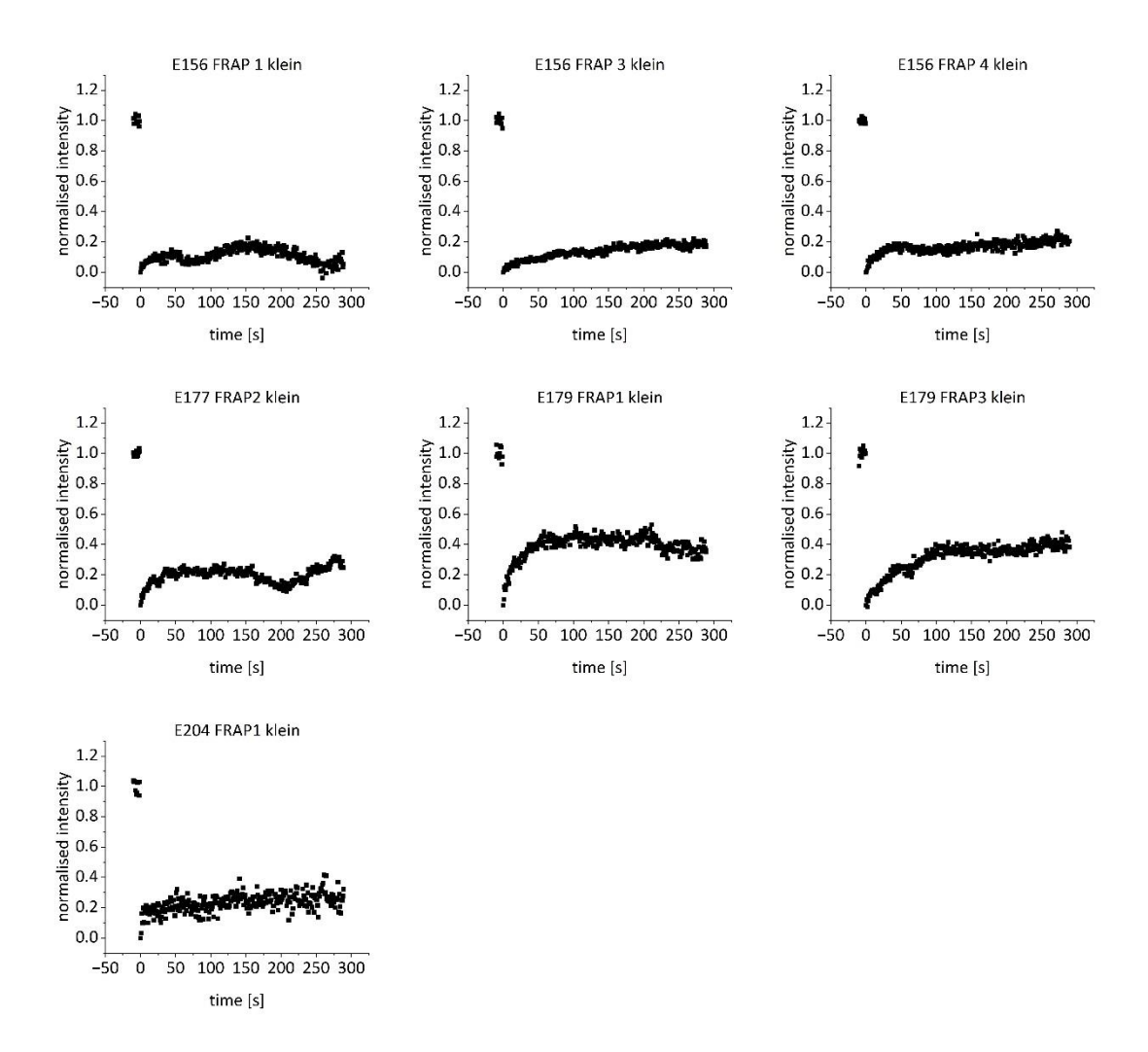


Figure 5: The individual recovery curves of the PG CTRL FRAP experiments. All recovery curves were fitted with the exponential fit.

# PG stretch-samples

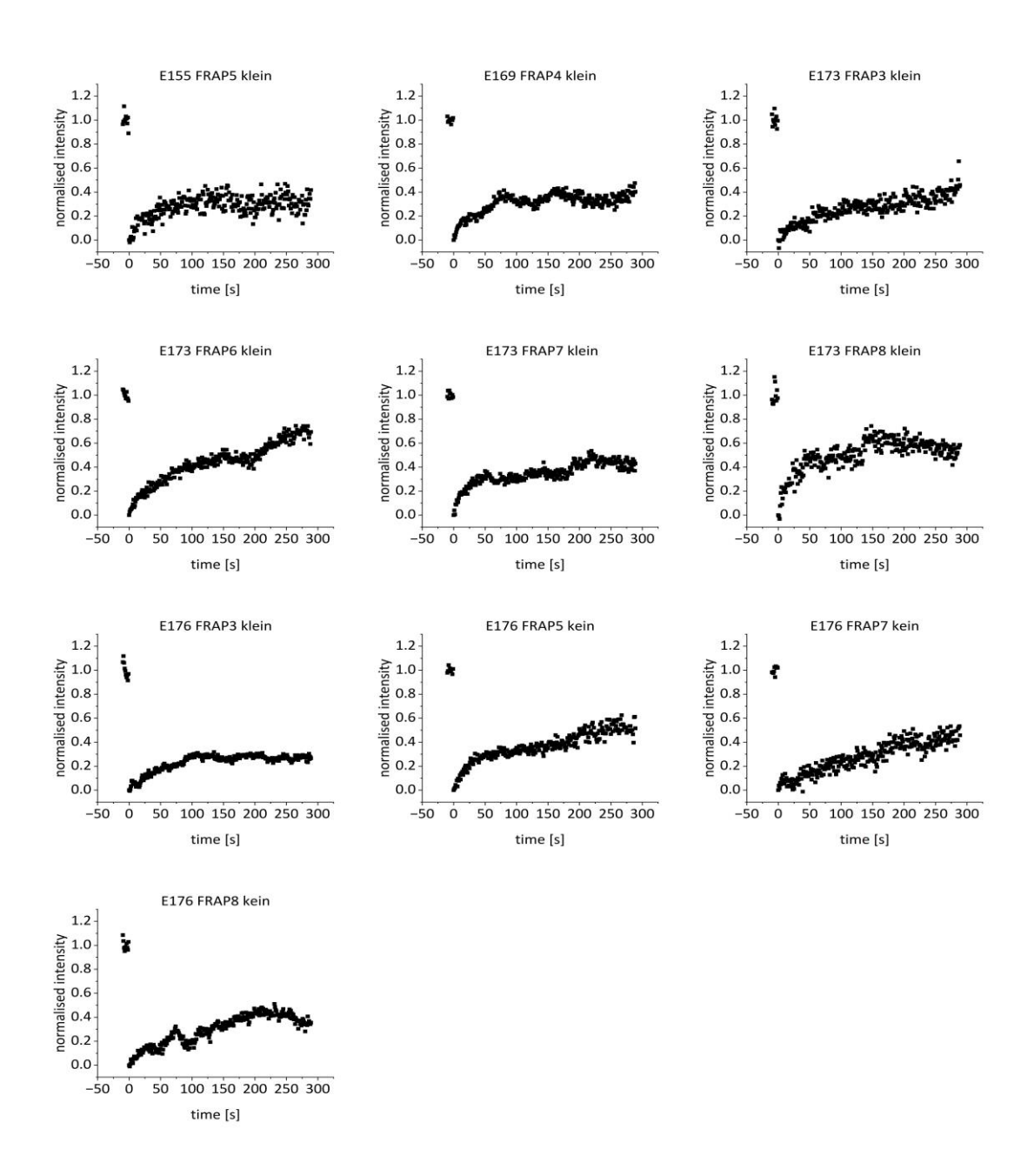


Figure 6: The individual recovery curves of the PG stretch FRAP experiments. All recovery curves were fitted with the exponential fit.

# PG stretch+24 h-samples

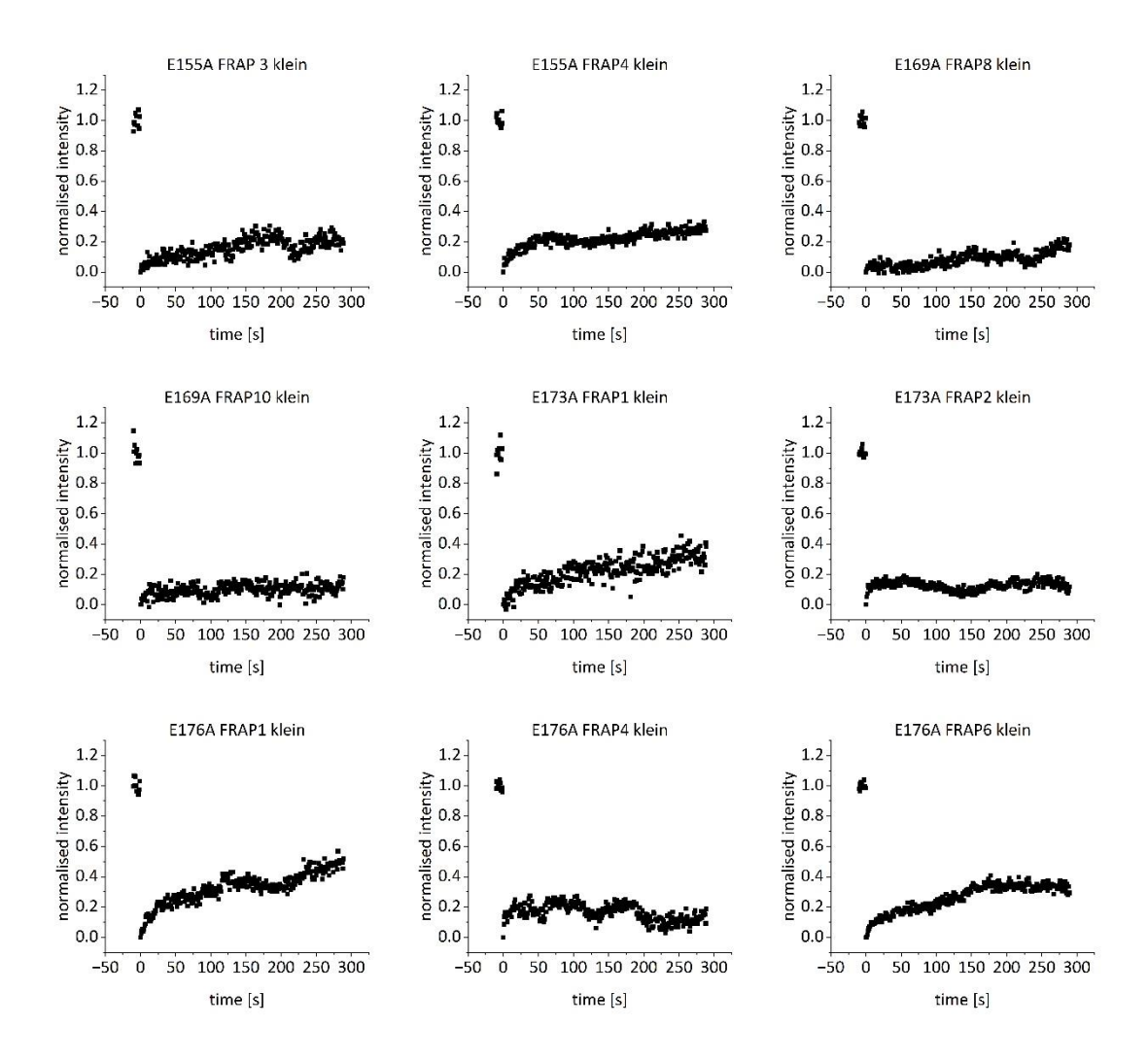


Figure 7: The individual recovery curves of the PG stretch+24h FRAP experiments. The recovery curves E169A FRAP8 klein and E169A FRAP10 klein were fitted with the linear fit. The recovery curves were E155A FRAP3 klein, E155A FRAP4 klein, E173A FRAP1 klein, E173A FRAP2 klein, E176A FRAP1 klein, E176A FRAP4 klein and E176A FRAP6 klein, fitted with the exponential fit.

# PG CTRL+24 h-samples

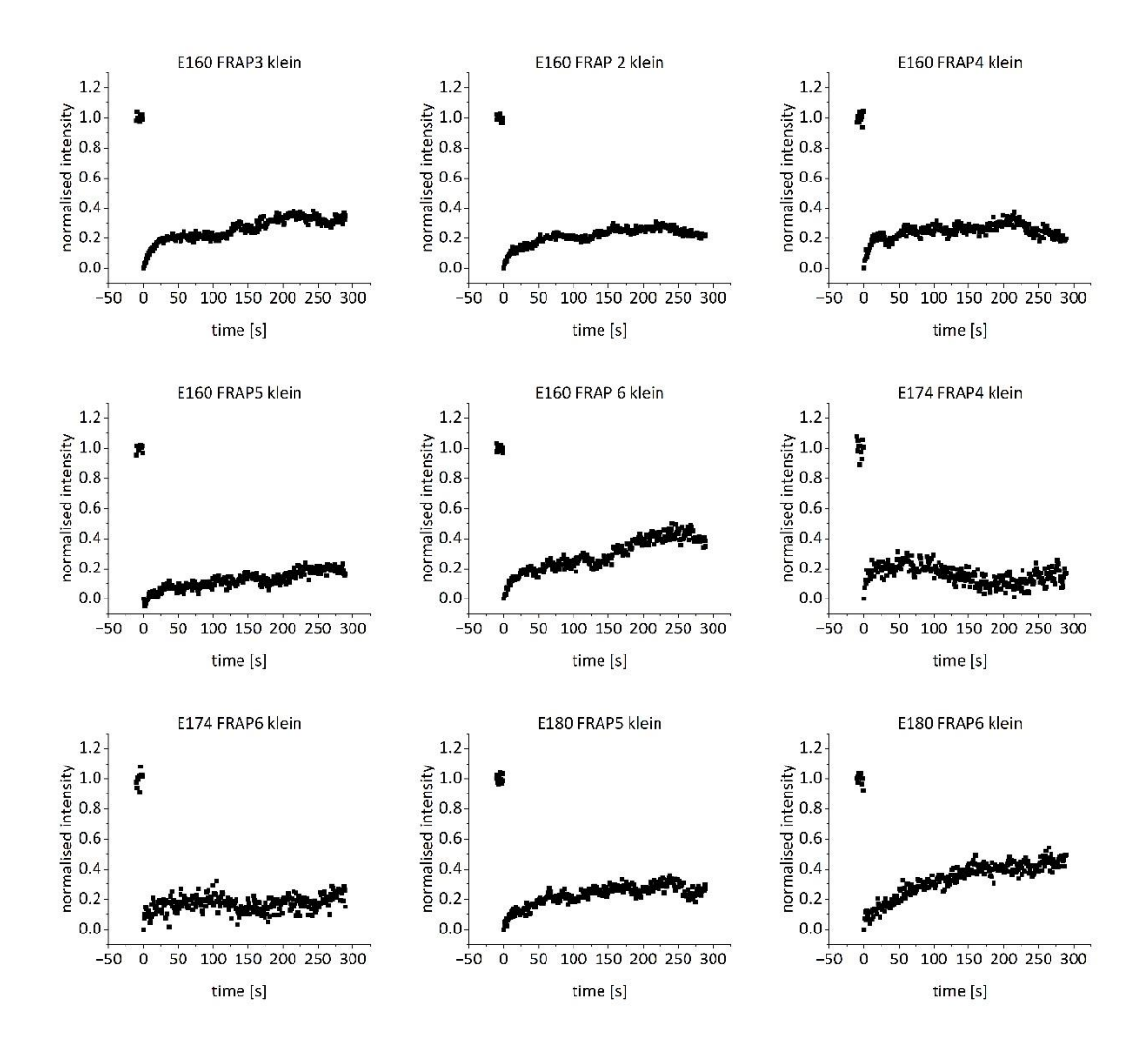


Figure 8: The individual recovery curves of the PG CTRL+24h FRAP experiments. All recovery curves were fitted with the exponential fit except E160 FRAP5 klein, which was fitted with the linear fit.

#### **Dsc2aNG** CTRL-samples

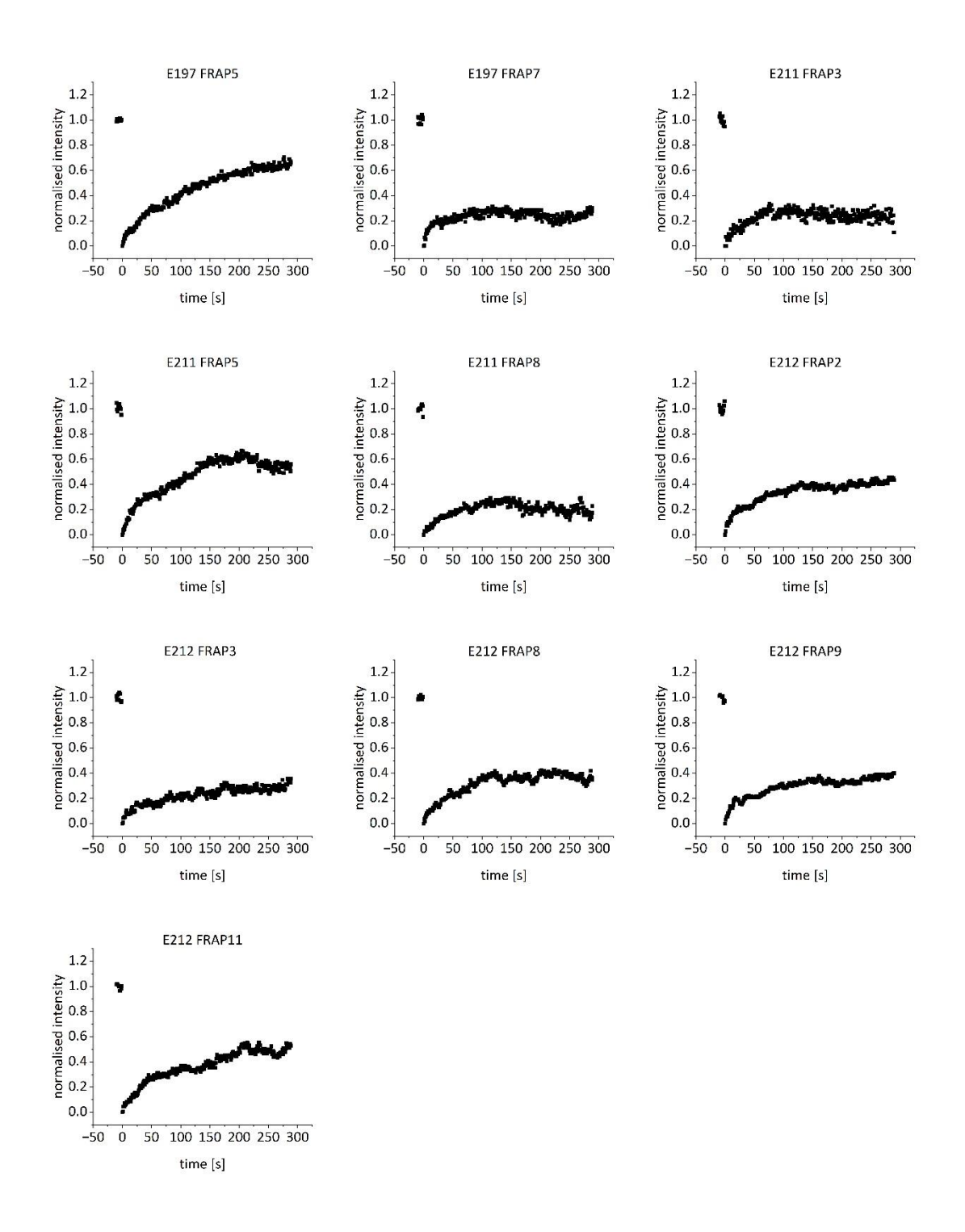
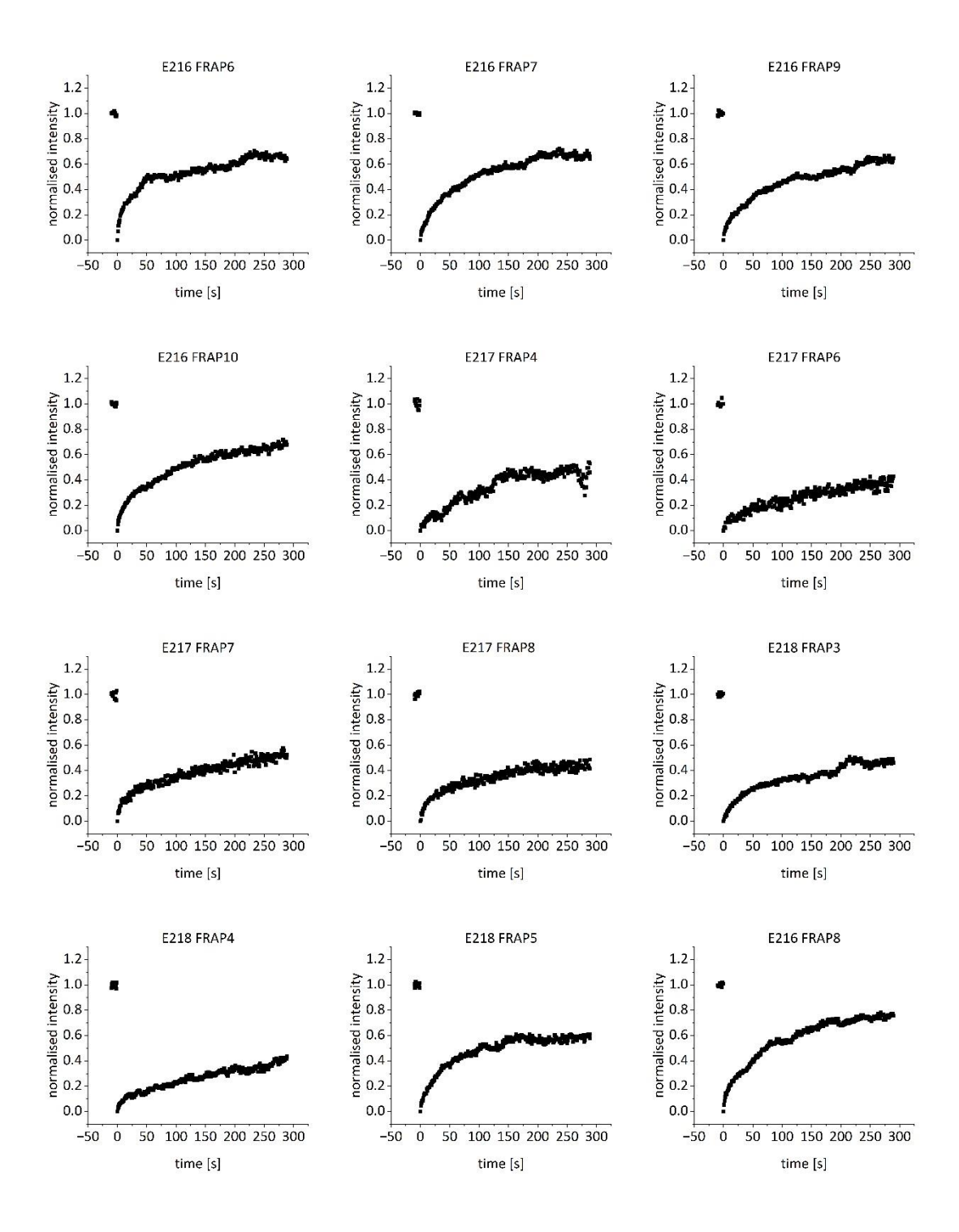


Figure 9: The individual recovery curves of the Dsc2aNG CTRL FRAP experiments. All recovery curves were fitted with the exponential fit.

#### **Dsc2aNG** stretch-samples



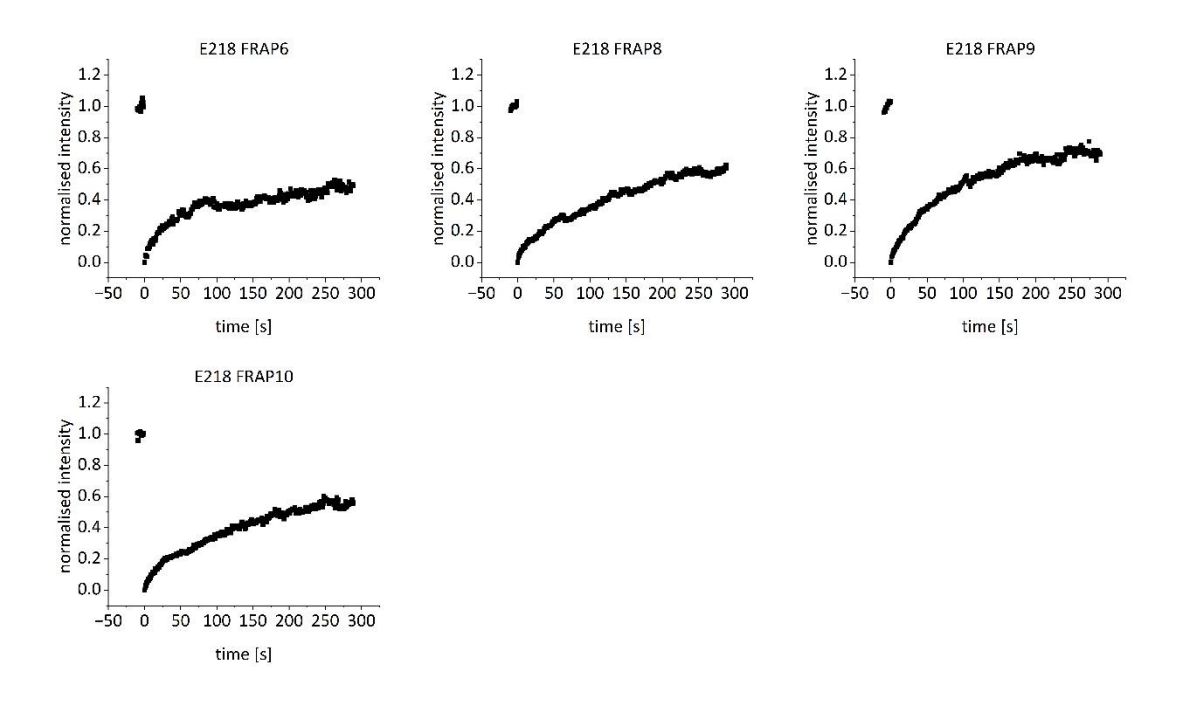


Figure 10: The individual recovery curves of the Dsc2aNG stretch FRAP experiments. All recovery curves were fitted with the exponential fit.

#### Dsc2aNG stretch+24 h-samples

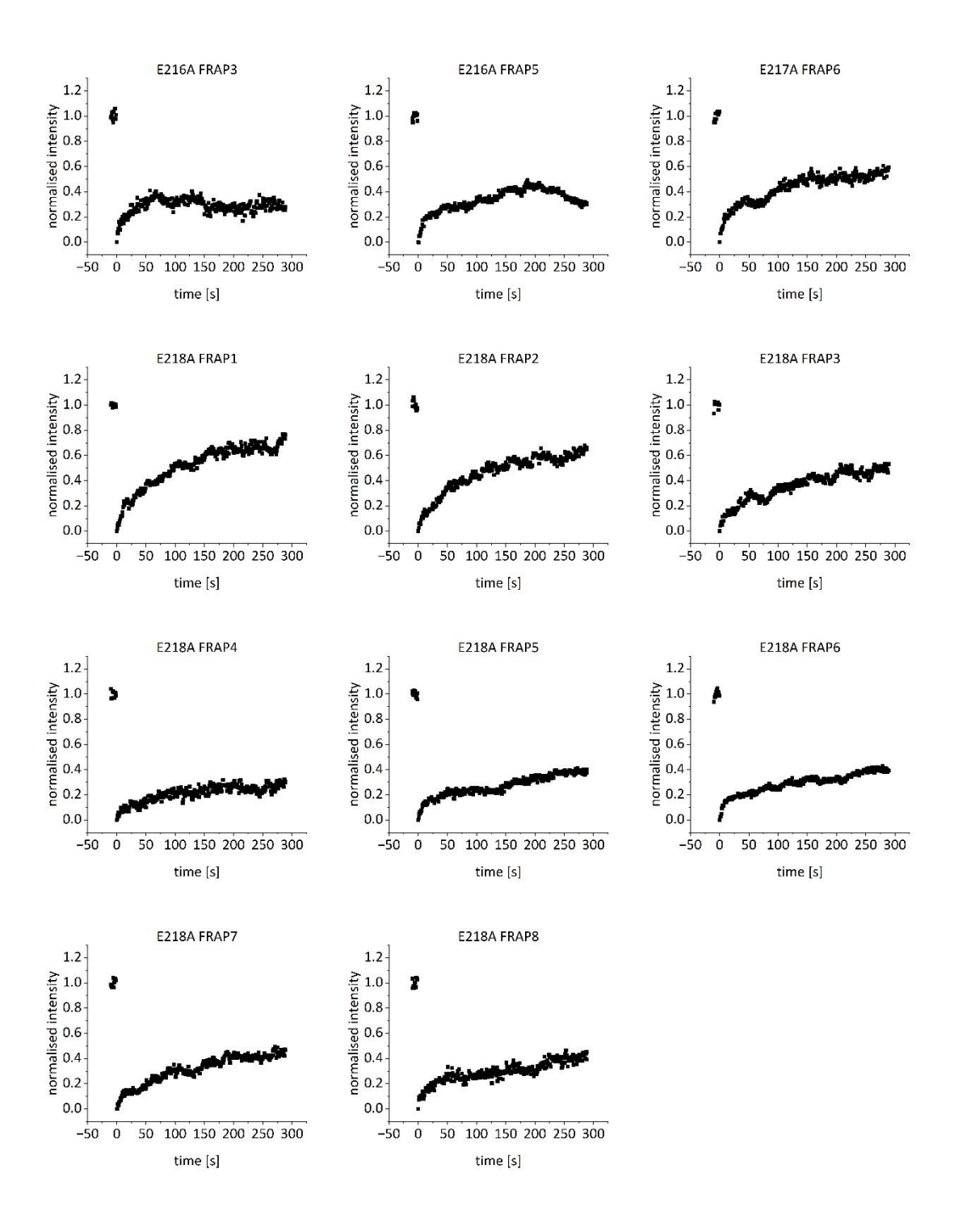


Figure 11: The individual recovery curves of the Dsc2aNG stretch+24h FRAP experiments. All recovery curves were fitted with the exponential fit.

#### Dsc2aNG CTRL+24 h-samples

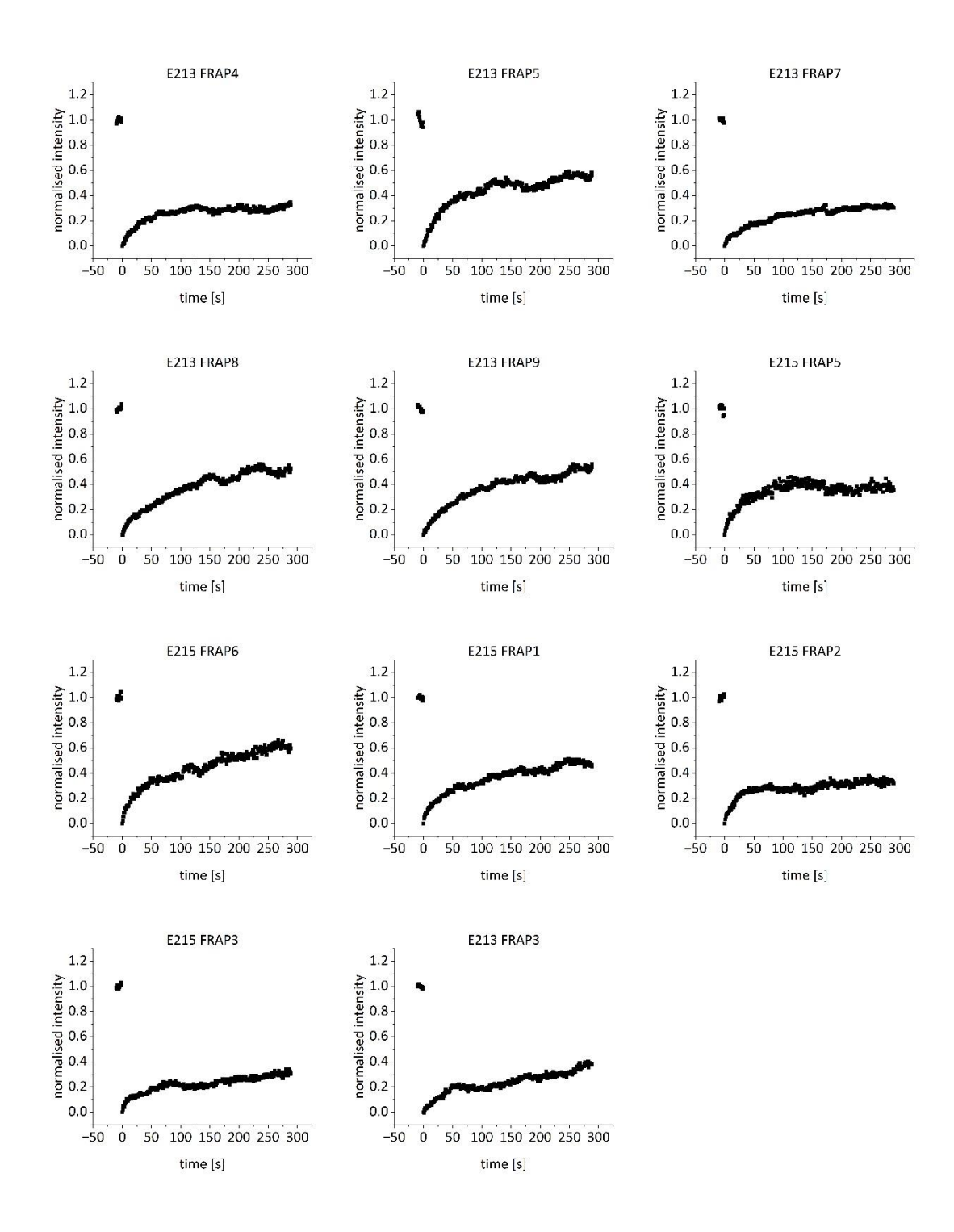


Figure 12: The individual recovery curves of the Dsc2aNG CTRL+24h FRAP experiments. All recovery curves were fitted with the exponential fit.

#### **Dsc2aGFP** CTRL-samples

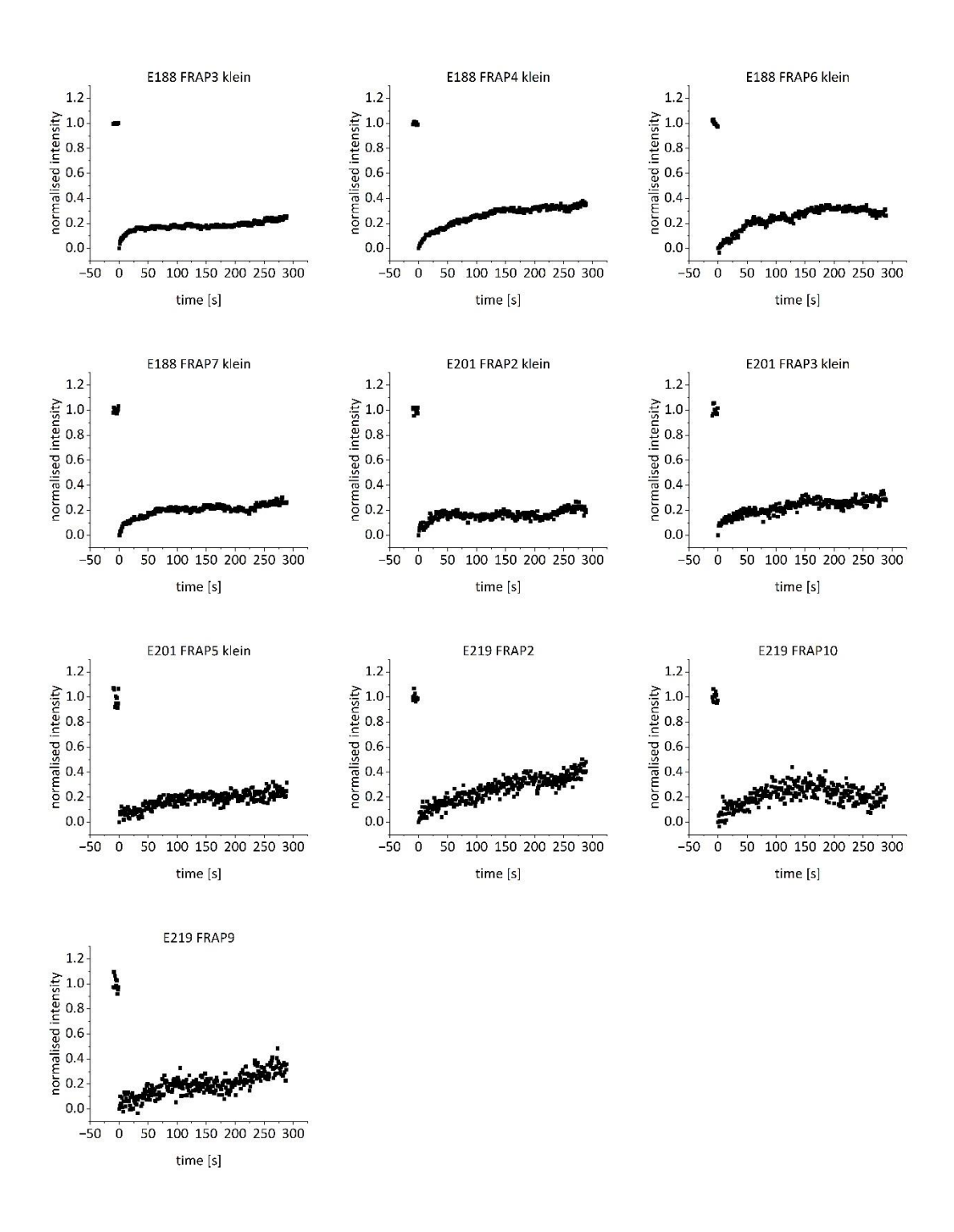


Figure 13: The individual recovery curves of the Dsc2aGFP CTRL FRAP experiments. All recovery curves were fitted with the exponential fit except E219 FRAP9, which was fitted with the linear fit.

#### **Dsc2aGFP** stretch-samples

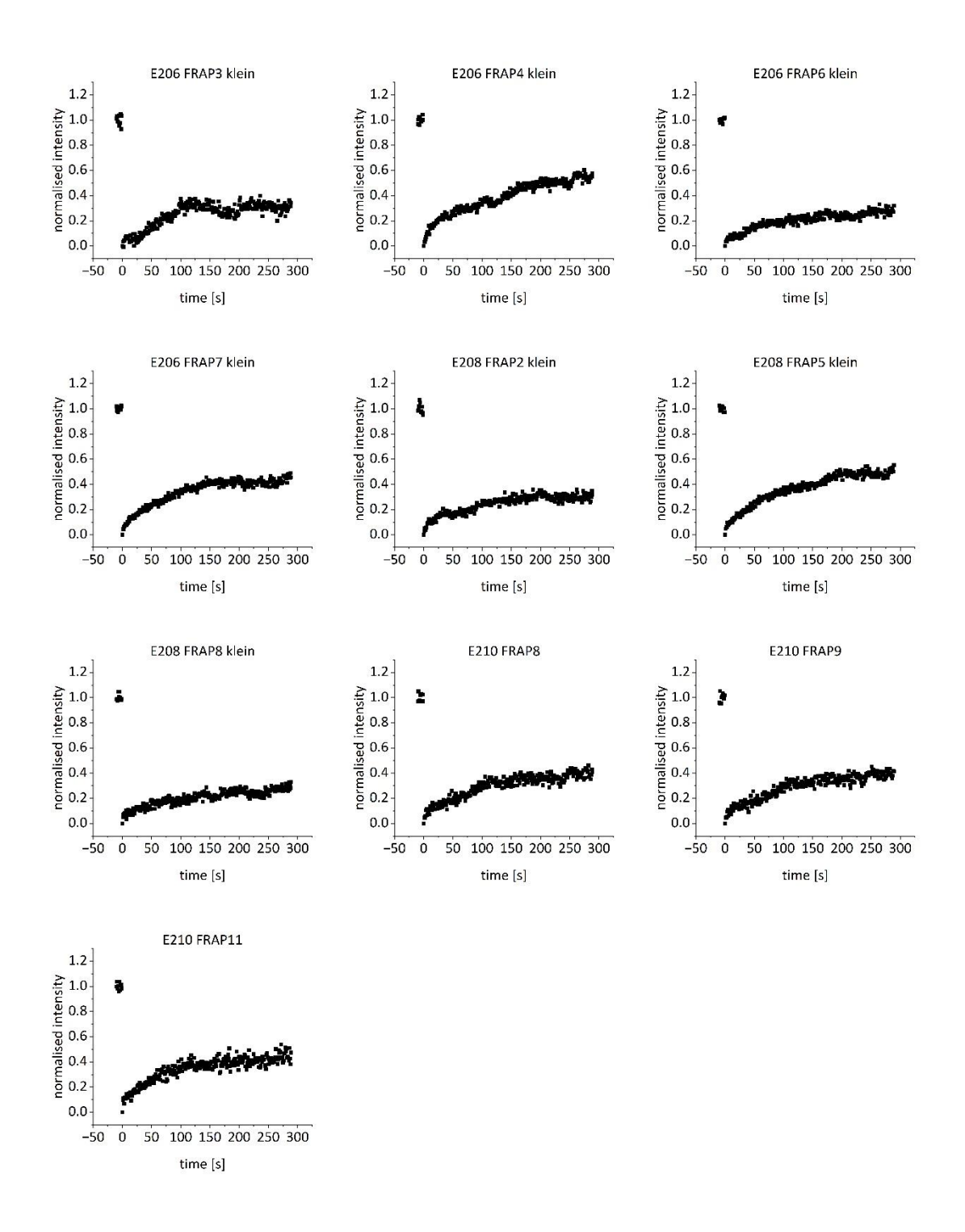


Figure 14: The individual recovery curves of the Dsc2aGFP stretch FRAP experiments. All recovery curves were fitted with the exponential fit.

### Dsc2aGFP stretch+24 h-samples

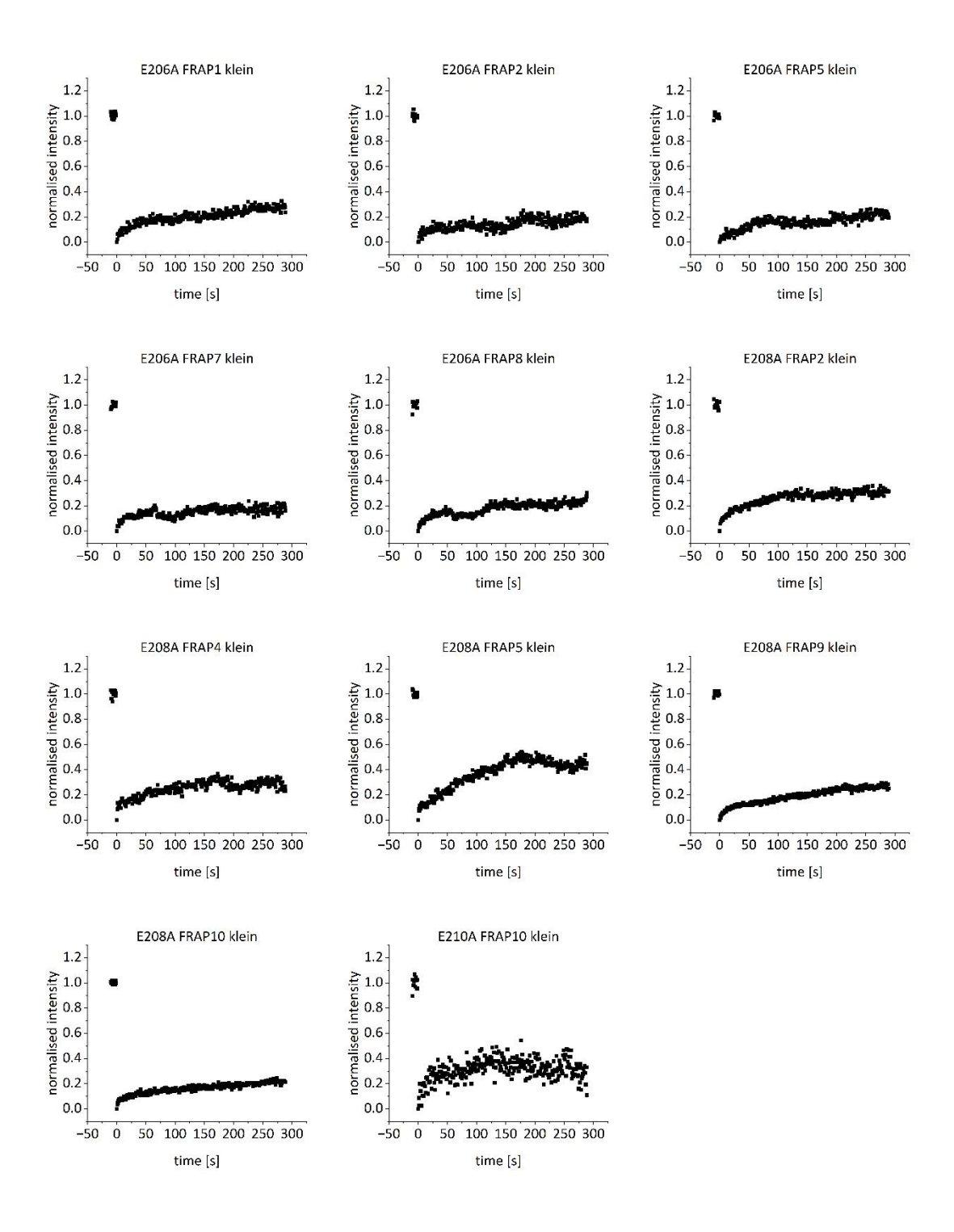


Figure 15: The individual recovery curves of the Dsc2aGFP stretch+24h FRAP experiments. All recovery curves were fitted with the exponential fit except E206A FRAP2 klein, which was fitted with the linear fit.

#### Dsc2aGFP CTRL+24 h-samples

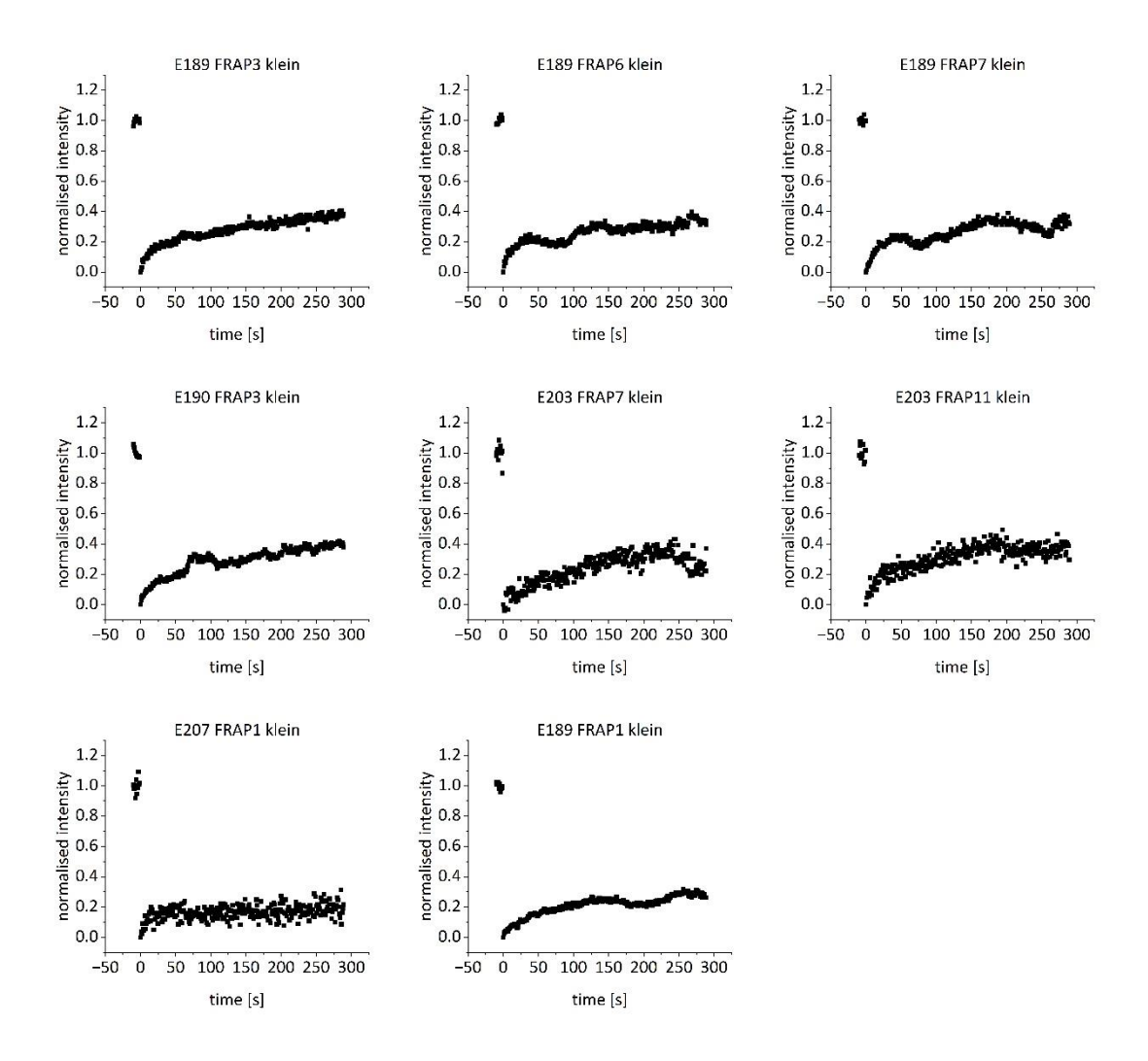


Figure 16: The individual recovery curves of the Dsc2aGFP CTRL+24h FRAP experiments. All recovery curves were fitted with the exponential fit.

## **Applied fit function**

In the following section, the respective fit function applied to the recovery curves is presented sorted by desmosomal protein and mechanical state. The parameter  $f_{max}$  represents the maximal distance between the exponential fit and a straight drawn between the first and the last point of the exponential fit result. If  $f_{max}$  was exceeding the standard deviation of the noise originating from the recovery curve, the recovery curve was fitted with the exponential fit function, otherwise, it was fitted with the linear function.

protein/mechanical state	name	standard deviation of noise	f_max	applied fit function
DP CTRL	E159 FRAP2 klein	0.029	0.027	
	E167 FRAP4 klein	0.091	0.025	linear
	E171 FRAP5 klein	0.024	0.16	exponential
	E171 FRAP6 klein	0.040	0.13	exponential
	E182 FRAP2 klein	0.030	0.049	exponential
	E193 FRAP3 klein	0.033	0.060	exponential
	E193 FRAP4 klein	0.055	0.13	exponential
	E193 FRAP5 klein	0.038	0.028	linear
	E193 FRAP6 klein	0.081	0.029	linear
DP stretch	E163 FRAP2 klein	0.080	0.16	exponential
	E163 FRAP3 klein	0.035	0.13	exponential
	E163 FRAP5 klein	0.073	0.11	exponential
	E186 FRAP1 klein	0.094	0.010	linear
	E186 FRAP2 klein	0.12	0.27	exponential
	E186 FRAP5 klein	0.15	0.11	linear
	E186 FRAP8 klein	0.11	0.057	linear
	E186 FRAP9 klein	0.16	0.12	linear
	E209 FRAP1 klein	0.032	0.061	exponential
	E209 FRAP2 klein	0.041	0.028	linear
DP stretch+24 h	E163A FRAP3 klein	0.070	0.13	exponential
	E163A FRAP5 klein	0.069	0.0033	linear
	E186A FRAP5 klein	0.14	0.051	linear
	E186A FRAP6 klein	0.062	0.13	exponential
	E186A FRAP7 klein	0.098	0.24	exponential
	E209A FRAP10 klein	0.025	0.011	linear

protein/mechanical state	name	standard deviation of noise	f_max	applied fit function
DP stretch+24 h	E209A FRAP11 klein	0.023	0.036	exponential
DP CTRL+24 h	E172 FRAP1 klein	0.069	0.089	exponential
	E172 FRAP3 klein	0.041	0.028	linear
	E172 FRAP4 klein	0.057	0.13	exponential
	E172 FRAP5 klein	0.032	0.046	exponential
	E172 FRAP6 klein	0.042	0.054	exponential
	E191 FRAP4 klein	0.049	0.093	exponential
	E191 FRAP5 klein	0.032	0.062	exponential
	E191 FRAP6 klein	0.033	0.18	exponential
	E205 FRAP2 klein	0.056	0.13	exponential
	E205 FRAP4 klein	0.089	0.038	linear
Osc2aGFP <i>CTRL</i>	E188 FRAP3 klein	0.0083	0.094	exponential
	E188 FRAP4 klein	0.0094	0.10	exponential
	E188 FRAP6 klein	0.015	0.11	exponential
	E188 FRAP7 klein	0.011	0.11	exponential
	E201 FRAP2 klein	0.018	0.11	exponential
	E201 FRAP3 klein	0.022	0.057	exponential
	E201 FRAP5 klein	0.029	0.067	exponential
	E219 FRAP2	0.039	0.063	exponential
	E219 FRAP9	0.045	0.037	linear
	E219 FRAP10	0.051	0.13	exponential
Osc2aGFP stretch	E206 FRAP3 klein	0.027	0.15	exponential
	E206 FRAP4 klein	0.019	0.077	exponential
	E206 FRAP6 klein	0.018	0.078	exponential
	E206 FRAP7 klein	0.017	0.15	exponential
	E208 FRAP2 klein	0.019	0.076	exponential
	E208 FRAP5 klein	0.018	0.10	exponential
	E208 FRAP8 klein	0.020	0.058	exponential
	E210 FRAP8	0.025	0.104	exponential
	E210 FRAP9	0.026	0.094	exponential
	E210 FRAP11	0.031	0.14	exponential
Osc2aGFP stretch+24 h	E206A FRAP1 klein	0.019	0.033	exponential
	E206A FRAP2 klein	0.025	0.013	linear

protein/mechanical state	name	standard deviation of noise	f_max	applied fit function
Dsc2aGFP stretch+24h	E206A FRAP5 klein	0.020	0.080	exponential
	E206A FRAP7 klein	0.019	0.024	exponential
	E206A FRAP8 klein	0.016	0.030	exponential
	E208A FRAP2 klein	0.017	0.11	exponential
	E208A FRAP4 klein	0.023	0.086	exponential
	E208A FRAP5 klein	0.022	0.14	exponential
	E208A FRAP9 klein	0.011	0.024	exponential
	E208A FRAP10 klein	0.012	0.036	exponential
	E210A FRAP10 klein	0.057	0.16	exponential
Dsc2aGFP CTRL+24h	E189 FRAP1 klein	0.0091	0.10	exponential
	E189 FRAP3 klein	0.015	0.073	exponential
	E189 FRAP6 klein	0.015	0.058	exponential
	E189 FRAP7 klein	0.015	0.060	exponential
	E190 FRAP3 klein	0.015	0.109	exponential
	E203 FRAP7 klein	0.035	0.069	exponential
	E203 FRAP11 klein	0.035	0.11	exponential
	E207 FRAP1 klein	0.037	0.13	exponential
Dsc2aNG <i>CTRL</i>	E197 FRAP5	0.016	0.13	exponential
	E197 FRAP7	0.021	0.14	exponential
	E211 FRAP3	0.028	0.16	exponential
	E211 FRAP5	0.019	0.17	exponential
	E211 FRAP8	0.019	0.15	exponential
	E212 FRAP2	0.013	0.15	exponential
	E212 FRAP3	0.018	0.067	exponential
	E212 FRAP8	0.017	0.16	exponential
	E212 FRAP9	0.012	0.12	exponential
	E212 FRAP11	0.017	0.091	exponential
Dsc2aNG stretch	E216 FRAP6	0.016	0.18	exponential
	E216 FRAP7	0.012	0.19	exponential
	E216 FRAP8	0.012	0.20	exponential
	E216 FRAP9	0.011	0.17	exponential
	E216 FRAP10	0.013	0.16	exponential
	E217 FRAP4	0.021	0.12	exponential

protein/mechanical state	name	standard deviation of noise	f_max	applied fit function
Dsc2aNG stretch	E217 FRAP6	0.024	0.048	exponential
	E217 FRAP7	0.022	0.085	exponential
	E217 FRAP8	0.021	0.11	exponential
	E218 FRAP3	0.011	0.089	exponential
	E218 FRAP4	0.013	0.055	exponential
	E218 FRAP5	0.014	0.23	exponential
	E218 FRAP6	0.015	0.18	exponential
	E218 FRAP8	0.010	0.081	exponential
	E218 FRAP9	0.013	0.20	exponential
	E218 FRAP10	0.011	0.093	exponential
Dsc2aNG stretch+24 h	E216A FRAP3	0.028	0.21	exponential
	E216A FRAP5	0.017	0.098	exponential
	E217A FRAP6	0.024	0.13	exponential
	E218A FRAP1	0.023	0.18	exponential
	E218A FRAP2	0.022	0.20	exponential
	E218A FRAP3	0.021	0.091	exponential
	E218A FRAP4	0.025	0.084	exponential
	E218A FRAP5	0.017	0.10	exponential
	E218A FRAP6	0.013	0.068	exponential
	E218A FRAP7	0.019	0.085	exponential
	E218A FRAP8	0.025	0.051	exponential
Dsc2aNG <i>CTRL+24 h</i>	E213 FRAP3	0.011	0.061	exponential
	E213 FRAP4	0.010	0.17	exponential
	E213 FRAP5	0.014	0.25	exponential
	E213 FRAP7	0.0093	0.099	exponential
	E213 FRAP8	0.012	0.11	exponential
	E213 FRAP9	0.012	0.17	exponential
	E215 FRAP5	0.023	0.23	exponential
	E215 FRAP6	0.018	0.10	exponential
	E215 FRAP1	0.012	0.11	exponential
	E215 FRAP2	0.014	0.19	exponential
	E215 FRAP3	0.011	0.066	exponential
PG CTRL	E156 FRAP 1 klein	0.019	0.037	exponential

protein/mechanical state	name	standard deviation of noise	f_max	applied fit function
PG <i>CTRL</i>	E156 FRAP 3 klein	0.012	0.031	exponential
	E156 FRAP 4 klein	0.019	0.11	exponential
	E177 FRAP2 klein	0.018	0.16	exponential
	E179 FRAP1 klein	0.027	0.27	exponential
	E179 FRAP3 klein	0.023	0.18	exponential
	E204 FRAP1 klein	0.042	0.049	exponential
PG stretch	E155 FRAP4 klein	0.055	0.19	exponential
	E169 FRAP4 klein	0.025	0.18	exponential
	E173 FRAP3 klein	0.039	0.098	exponential
	E173 FRAP6 klein	0.026	0.13	exponential
	E173 FRAP7 klein	0.024	0.18	exponential
	E173 FRAP8 klein	0.052	0.23	exponential
	E176 FRAP3 klein	0.015	0.15	exponential
	E176 FRAP5 kein	0.023	0.17	exponential
	E176 FRAP7 kein	0.044	0.044	exponential
	E176 FRAP8 kein	0.026	0.041	exponential
PG stretch+24 h	E155A FRAP 3 klein	0.032	0.052	exponential
	E155A FRAP4 klein	0.020	0.11	exponential
	E169A FRAP8 klein	0.022	0.016	linear
	E169A FRAP10 klein	0.031	0.027	linear
	E173A FRAP1 klein	0.046	0.073	exponential
	E173A FRAP2 klein	0.018	0.12	exponential
	E176A FRAP1 klein	0.028	0.12	exponential
	E176A FRAP4 klein	0.030	0.16	exponential
	E176A FRAP6 klein	0.020	0.064	exponential
PG CTRL+24 h	E160 FRAP3 klein	0.018	0.023	exponential
	E160 FRAP2 klein	0.013	0.072	exponential
	E160 FRAP4 klein	0.022	0.091	exponential
	E160 FRAP5 klein	0.021	0.020	linear
	E160 FRAP 6 klein	0.022	0.097	exponential
	E174 FRAP4 klein	0.036	0.16	'
	E174 FRAP6 klein	0.040	0.091	·
	E180 FRAP5 klein	0.021	0.078	'
PG CTRL+24 h	E180 FRAP6 klein	0.029	0.12	'

# **Table parameter values (exponential fits)**

In the following section, the values of the parameter *a, b* and *k* originating from the exponential fit function applied to the recovery curves are presented sorted by desmosomal protein and mechanical state. The indicated error values correspond to the standard error of the individual fits and were returned in python with *pcov2-D array* (SciPy Version 1.11.1, for more details see section 2.2.5.2).

protein/ mechanical state	name	а	b	k	a error	b error	k error
DP CTRL	E171 FRAP5 klein	0.048	0.21	0.075	0.015	0.015	0.0083
	E171 FRAP6 klein	0.15	0.19	0.040	0.017	0.016	0.0056
	E182 FRAP2 klein	0.12	0.20	0.0095	0.0080	0.0099	0.0015
	E193 FRAP3 klein	0.088	0.29	0.0081	0.0082	0.013	0.0011
	E193 FRAP4 klein	-0.0059	0.24	0.027	0.020	0.020	0.0042
DP stretch	E163 FRAP2 klein	0.20	0.24	0.036	0.033	0.033	0.0081
	E163 FRAP3 klein	0.067	0.20	0.041	0.019	0.019	0.0064
	E163 FRAP5 klein	0.22	0.25	0.018	0.022	0.021	0.0036
	E186 FRAP2 klein	-0.025	0.37	0.053	0.055	0.055	0.013
	E209 FRAP1 klein	0.068	0.24	0.0097	0.0087	0.010	0.0013
DP stretch	E163A FRAP3 klein	0.033	0.22	0.026	0.024	0.023	0.0050
+24 h	E186A FRAP6 klein	0.032	0.15	0.14	0.042	0.042	0.062
	E186A FRAP7 klein	-0.066	0.27	0.26	0.081	0.081	0.13
	E209A FRAP11 klein	0.059	0.13	0.011	0.0059	0.0062	0.0017
DP CTRL	E172 FRAP1 klein	0.084	0.12	0.051	0.032	0.032	0.021
+24 h	E172 FRAP4 klein	0.093	0.26	0.023	0.022	0.021	0.0037
	E172 FRAP5 klein	0.067	0.14	0.012	0.0093	0.0090	0.0024
	E172 FRAP6 klein	0.11	0.18	0.011	0.011	0.012	0.0023
	E191 FRAP4 klein	0.12	0.25	0.014	0.014	0.013	0.0020
	E191 FRAP5 klein	-0.017	0.12	0.021	0.012	0.012	0.0042
	E191 FRAP6 klein	0.0051	0.34	0.023	0.013	0.012	0.0016
	E205 FRAP2 klein	0.13	0.33	0.014	0.016	0.015	0.0018
Dsc2aGFP	E188 FRAP3 klein	0.049	0.13	0.047	0.0057	0.0056	0.0032
CTRL	E188 FRAP4 klein	0.038	0.30	0.013	0.0031	0.0030	0.00037
	E188 FRAP6 klein	0.0070	0.33	0.013	0.0058	0.0054	0.00064
	E188 FRAP7 klein	0.030	0.19	0.028	0.0054	0.0053	0.0014

protein/ mechanical	name	a	b	k	a error	b error	k error
state Dsc2aGFP	E201 FRAP2 klein	0.018	0.14	0.070	0.011	0.011	0.0087
CTRL	E201 FRAP3 klein	0.091	0.19	0.011	0.0068	0.0070	0.0013
	E201 FRAP5 klein	0.038	0.18	0.014	0.0084	0.0078	0.0017
	E219 FRAP2	0.055	0.35	0.0072	0.0094	0.020	0.0010
	E219 FRAP10	0.0090	0.25	0.024	0.019	0.018	0.0034
Dsc2aGFP	E206 FRAP3 klein	-0.027	0.35	0.017	0.012	0.011	0.0013
stretch	E206 FRAP4 klein	0.10	0.54	0.0060	0.0063	0.019	0.00049
	E206 FRAP6 klein	0.033	0.23	0.013	0.0053	0.0050	0.00085
	E206 FRAP7 klein	0.042	0.40	0.014	0.0055	0.0051	0.00050
	E208 FRAP2 klein	0.064	0.26	0.011	0.0059	0.0062	0.00081
	E208 FRAP5 klein	0.070	0.49	0.0083	0.0050	0.0079	0.00039
	E208 FRAP8 klein	0.061	0.20	0.011	0.0059	0.0062	0.0011
	E210 FRAP8	0.055	0.34	0.012	0.0074	0.0074	0.00080
	E210 FRAP9	0.055	0.35	0.010	0.0071	0.0080	0.00074
	E210 FRAP11	0.068	0.35	0.016	0.0089	0.0082	0.0010
Dsc2aGFP	E206A FRAP1 klein	0.088	0.21	0.0064	0.0055	0.015	0.0011
stretch +24 h	E206A FRAP5 klein	0.019	0.16	0.021	0.0077	0.0072	0.0020
	E206A FRAP7 klein	0.084	0.11	0.0085	0.0061	0.0091	0.0021
	E206A FRAP8 klein	0.077	0.18	0.0068	0.0057	0.014	0.0013
	E208A FRAP2 klein	0.071	0.23	0.018	0.0054	0.0050	0.00090
	E208A FRAP4 klein	0.091	0.21	0.016	0.0081	0.0075	0.0015
	E208A FRAP5 klein	0.051	0.46	0.012	0.0085	0.0084	0.00066
	E208A FRAP9 klein	0.065	0.32	0.0039	0.0029	0.023	0.00049
	E208A FRAP10 klein	0.070	0.14	0.010	0.0032	0.0036	0.00085
	E210A FRAP10 klein	0.089	0.25	0.033	0.023	0.022	0.0051
Dsc2aGFP	E189 FRAP1 klein	0.020	0.23	0.019	0.0051	0.0048	0.00089
CTRL+24 h	E189 FRAP3 klein	0.088	0.28	0.0099	0.0048	0.0056	0.00063
	E189 FRAP6 klein	0.11	0.21	0.010	0.0069	0.0076	0.0012
	E189 FRAP7 klein	0.10	0.25	0.0091	0.0082	0.011	0.0012
	E190 FRAP3 klein	0.056	0.30	0.014	0.0074	0.0069	0.00088
	E203 FRAP7 klein	0.024	0.41	0.0069	0.0085	0.019	0.00084
	E203 FRAP11 klein	0.082	0.30	0.014	0.011	0.0099	0.0013

protein/ mechanical state	name	а	b	k	a error	b error	k error
Dsc2aGFP CTRL+24 h	E207 FRAP1 klein	0.009	0.16	0.12	0.024	0.024	0.027
Dsc2aNG	E197 FRAP5	0.056	0.68	0.0074	0.0045	0.0086	0.00026
CTRL	E197 FRAP7	0.052	0.20	0.047	0.013	0.012	0.0048
	E211 FRAP3	0.012	0.24	0.040	0.013	0.013	0.0037
	E211 FRAP5	0.064	0.60	0.011	0.0087	0.0092	0.00053
	E211 FRAP8	-0.0069	0.23	0.034	0.012	0.012	0.0029
	E212 FRAP2	0.067	0.33	0.018	0.0055	0.0051	0.00064
	E212 FRAP3	0.061	0.23	0.011	0.0057	0.0060	0.00087
	E212 FRAP8	0.029	0.37	0.017	0.0069	0.0064	0.00072
	E212 FRAP9	0.070	0.28	0.017	0.0054	0.0050	0.00076
	E212 FRAP11	0.076	0.51	0.0071	0.0072	0.015	0.00055
Dsc2aNG	E216 FRAP6	0.18	0.44	0.016	0.010	0.0096	0.00087
stretch	E216 FRAP7	0.092	0.61	0.012	0.0055	0.0055	0.00032
	E216 FRAP8	0.11	0.67	0.011	0.0049	0.0050	0.00027
	E216 FRAP9	0.090	0.51	0.012	0.0057	0.0055	0.00040
	E216 FRAP10	0.11	0.56	0.011	0.0047	0.0049	0.00030
	E217 FRAP4	0.016	0.53	0.0086	0.0077	0.011	0.00055
	E217 FRAP6	0.063	0.41	0.0052	0.0058	0.025	0.00064
	E217 FRAP7	0.12	0.41	0.0081	0.0061	0.0099	0.00057
	E217 FRAP8	0.095	0.35	0.011	0.0063	0.0064	0.00064
	E218 FRAP3	0.084	0.42	0.0081	0.0067	0.011	0.00060
	E218 FRAP4	0.064	0.36	0.0064	0.0036	0.0096	0.00042
	E218 FRAP5	0.066	0.51	0.018	0.0059	0.0055	0.00045
	E218 FRAP6	0.056	0.37	0.021	0.0076	0.0072	0.00087
	E218 FRAP8	0.075	0.70	0.0052	0.0035	0.015	0.00023
	E218 FRAP9	0.050	0.68	0.011	0.0046	0.0047	0.00025
	E218 FRAP10	0.067	0.60	0.0065	0.0035	0.0093	0.00024
Dsc2aNG	E216A FRAP3	0.036	0.27	0.072	0.022	0.022	0.0092
stretch +24 h	E216A FRAP5	0.11	0.34	0.011	0.0076	0.0081	0.00081
	E217A FRAP6	0.13	0.43	0.012	0.0088	0.0088	0.00075
	E218A FRAP1	0.083	0.64	0.010	0.0073	0.0080	0.00041
	E218A FRAP2	0.043	0.56	0.013	0.0073	0.0069	0.00047

protein/ mechanical	a	b	k	a error	b error	k error	name
state	F2404 FD 4 D2	0.005	0.45	0.0070	0.0072	0.012	0.00000
Dsc2aNG stretch	E218A FRAP3	0.085	0.45	0.0078	0.0072	0.012	0.00060
+24 h	E218A FRAP4	0.038	0.22	0.014	0.0075	0.0070	0.0012
Dsc2aNG stretch	E218A FRAP5	0.041	0.20	0.040	0.0076	0.0073	0.0029
+24 h	E218A FRAP6	0.11	0.27	0.0094	0.0052	0.0065	0.00069
	E218A FRAP7	0.055	0.44	0.0077	0.0061	0.011	0.00054
	E218A FRAP8	0.13	0.27	0.0074	0.0083	0.016	0.0012
Dsc2aNG	E213 FRAP3	0.056	0.27	0.0085	0.0056	0.0082	0.00077
CTRL +24 h	E213 FRAP4	0.0075	0.28	0.030	0.0050	0.0048	0.00091
	E213 FRAP5	0.029	0.48	0.022	0.0086	0.0081	0.00077
	E213 FRAP7	0.033	0.28	0.013	0.0032	0.0030	0.00041
	E213 FRAP8	0.048	0.54	0.0082	0.0049	0.0078	0.00034
	E213 FRAP9	0.017	0.47	0.014	0.0043	0.0040	0.00034
	E215 FRAP5	0.026	0.36	0.034	0.011	0.011	0.0018
	E215 FRAP6	0.13	0.52	0.0077	0.0069	0.013	0.00052
	E215 FRAP1	0.086	0.40	0.010	0.0050	0.0056	0.00046
	E215 FRAP2	0.027	0.27	0.044	0.010	0.010	0.0027
	E215 FRAP3	0.074	0.20	0.012	0.0053	0.0050	0.0010
PG CTRL	E156 FRAP 1 klein	0.051	0.084	0.017	0.0098	0.0091	0.0045
	E156 FRAP 3 klein	0.034	0.19	0.0068	0.0032	0.0074	0.00068
	E156 FRAP 4 klein	0.021	0.15	0.061	0.012	0.011	0.0073
	E177 FRAP2 klein	0.0081	0.19	0.096	0.022	0.022	0.017
	E179 FRAP1 klein	0.051	0.38	0.052	0.016	0.016	0.0035
	E179 FRAP3 klein	0.0095	0.37	0.020	0.0082	0.0077	0.00091
	E204 FRAP1 klein	0.14	0.12	0.015	0.012	0.011	0.0037
PG stretch	E155 FRAP4 klein	0.0057	0.31	0.032	0.021	0.021	0.0037
	E169 FRAP4 klein	0.034	0.32	0.027	0.013	0.012	0.0019
	E173 FRAP3 klein	0.028	0.33	0.011	0.010	0.011	0.0011
	E173 FRAP6 klein	0.076	0.55	0.0088	0.010	0.014	0.00069
	E173 FRAP7 klein	0.027	0.30	0.052	0.014	0.013	0.0041
	E173 FRAP8 klein	0.11	0.49	0.019	0.019	0.018	0.0016
	E176 FRAP3 klein	-0.0085	0.29	0.021	0.0070	0.0067	0.0010
	E176 FRAP5 kein	0.0030	0.34	0.037	0.0096	0.0091	0.0020

protein/ mechanical state	a	b	k	a error	b error	k error	name
PG stretch	E176 FRAP7 kein	0.031	0.64	0.0037	0.010	0.093	0.00089
	E176 FRAP8 kein	0.049	0.76	0.0032	0.0080	0.10	0.00065
PG stretch	E155A FRAP 3 klein	0.032	0.17	0.011	0.011	0.011	0.0022
+24 h	E155A FRAP4 klein	0.051	0.18	0.033	0.011	0.010	0.0033
	E173A FRAP1 klein	0.039	0.25	0.011	0.012	0.012	0.0017
	E173A FRAP2 klein	-0.0000029	0.13	0.55	0.027	0.027	0.21
	E176A FRAP1 klein	0.073	0.32	0.015	0.011	0.0098	0.0012
	E176A FRAP4 klein	0.0064	0.17	0.60	0.050	0.050	0.34
	E176A FRAP6 klein	0.059	0.36	0.0071	0.0061	0.013	0.00066
PG CTRL	E160 FRAP3 klein	0.12	0.42	0.0032	0.0061	0.075	0.00087
+24 h	E160 FRAP 2 klein	0.071	0.20	0.014	0.0053	0.0050	0.0010
	E160 FRAP4 klein	0.11	0.17	0.024	0.010	0.0095	0.0026
	E160 FRAP 6 klein	0.044	0.21	0.032	0.0098	0.0092	0.0032
	E174 FRAP4 klein	-0.00062	0.16	0.61	0.058	0.058	0.40
	E174 FRAP6 klein	0.056	0.11	0.091	0.025	0.025	0.032
	E180 FRAP5 klein	0.060	0.24	0.012	0.0069	0.0067	0.0010
	E180 FRAP6 klein	0.052	0.40	0.011	0.0080	0.0082	0.00073

## **Table parameter values (linear fits)**

In the following section, the values of the parameter  $a_{lin}$  and  $b_{lin}$  originating from the linear fit function applied to the recovery curves are presented sorted by desmosomal protein and mechanical state. The indicated error values correspond to the standard error of the individual fits and were returned in python with pcov2-D array (SciPy Version 1.11.1, for more details see section 2.2.5.2).

protein/mechanical state	name	a <sub>lin</sub>	b <sub>lin</sub>	a <sub>lin</sub> error	b <sub>lin</sub> error
DP CTRL	E159 FRAP2 klein	0.11	0.00030	0.0044	0.000030
	E167 FRAP4 klein	0.21	0.00017	0.012	0.000084
	E193 FRAP5 klein	0.12	0.0010	0.0058	0.000040
	E193 FRAP6 klein	0.16	0.0010	0.011	0.000075
DP stretch	E186 FRAP1 klein	0.25	0.00043	0.013	0.000087
	E186 FRAP5 klein	0.35	0.00038	0.021	0.00014
	E186 FRAP8 klein	0.39	0.00051	0.014	0.00010
	E186 FRAP9 klein	0.43	0.00054	0.022	0.00015
	E209 FRAP2 klein	0.091	0.00057	0.0054	0.000037
DP stretch+24 h	E163A FRAP5 klein	0.28	0.00027	0.0095	0.000066
	E186A FRAP5 klein	0.31	0.00082	0.019	0.00013
	E209A FRAP10 klein	0.073	0.00058	0.0034	0.000023
DP CTRL+24 h	E172 FRAP3 klein	0.21	0.00042	0.0069	0.000048
	E205 FRAP4 klein	0.22	0.00092	0.012	0.000084
Dsc2aGFP CTRL	E219 FRAP9	0.076	0.00079	0.0067	0.000047
Dsc2aGFP stretch+24 h	E206A FRAP2 klein	0.086	0.00039	0.0040	0.000028
PG stretch+24 h	E169A FRAP8 klein	0.029	0.00035	0.0037	0.000025
	E169A FRAP10 klein	0.073	0.00018	0.0046	0.000032
PG CTRL+24 h	E160 FRAP5 klein	0.036	0.00060	0.0035	0.000024

# **Table parameter values (joint evaluation)**

In the following table, the values of the product of the two individual parameters  $b^*k$  for the joint evaluation of the recovery curves are presented sorted by desmosomal protein and mechanical state. To estimate the error, the standard deviation  $s_{b^*k}$  was determined using quadratic propagation of error (see section 2.2.5.3). The individual values for  $a_i$   $a_{lin}$  and  $b_{lin}$  including their error values can be found in the table parameter values (exponential fits), respective in the table parameter values (linear fits).

protein/mechanical state	name	b*k	b*k error
DP CTRL	E171 FRAP5 klein	0.015	0.0020
	E171 FRAP6 klein	0.0078	0.0013
	E182 FRAP2 klein	0.0019	0.00031
	E193 FRAP3 klein	0.0023	0.00033
	E193 FRAP4 klein	0.0064	0.0011
DP stretch	E163 FRAP2 klein	0.0087	0.0023
	E163 FRAP3 klein	0.0080	0.0015
	E163 FRAP5 klein	0.0044	0.00095
	E186 FRAP2 klein	0.019	0.0054
	E209 FRAP1 klein	0.0023	0.00033
DP stretch+24 h	E163A FRAP3 klein	0.0058	0.0013
	E186A FRAP6 klein	0.020	0.011
	E186A FRAP7 klein	0.069	0.040
	E209A FRAP11 klein	0.0014	0.00022
DP CTRL+24 h	E172 FRAP1 klein	0.0063	0.0031
	E172 FRAP4 klein	0.0058	0.0011
	E172 FRAP5 klein	0.0017	0.00035
	E172 FRAP6 klein	0.0020	0.00044
	E191 FRAP4 klein	0.0035	0.00053
	E191 FRAP5 klein	0.0027	0.00058
	E191 FRAP6 klein	0.0078	0.00063
	E205 FRAP2 klein	0.0048	0.00063
Dsc2aGFP CTRL	E188 FRAP3 klein	0.0062	0.00050
	E188 FRAP4 klein	0.0039	0.00012
	E188 FRAP6 klein	0.0043	0.00022

protein/mechanical state	name	b*k	b*k error
Dsc2aGFP CTRL	E188 FRAP7 klein	0.0052	0.00031
	E201 FRAP2 klein	0.010	0.0015
	E201 FRAP3 klein	0.0021	0.00026
	E201 FRAP5 klein	0.0026	0.00033
	E219 FRAP2	0.0025	0.00040
	E219 FRAP10	0.0060	0.00094
Dsc2aGFP stretch	E206 FRAP3 klein	0.0060	0.00049
	E206 FRAP4 klein	0.0032	0.00029
	E206 FRAP6 klein	0.0029	0.00020
	E206 FRAP7 klein	0.0056	0.00021
	E208 FRAP2 klein	0.0029	0.00022
	E208 FRAP5 klein	0.0040	0.00020
	E208 FRAP8 klein	0.0022	0.00022
	E210 FRAP8	0.0039	0.00028
	E210 FRAP9	0.0036	0.00027
	E210 FRAP11	0.0056	0.00036
Dsc2aGFP stretch+24 h	E206A FRAP1 klein	0.0014	0.00024
	E206A FRAP5 klein	0.0034	0.00035
	E206A FRAP7 klein	0.00093	0.00024
	E206A FRAP8 klein	0.0012	0.00025
	E208A FRAP2 klein	0.0042	0.00023
	E208A FRAP4 klein	0.0034	0.00033
	E208A FRAP5 klein	0.0054	0.00032
	E208A FRAP9 klein	0.0012	0.00018
	E208A FRAP10 klein	0.0014	0.00012
	E210A FRAP10 klein	0.0085	0.0015
Dsc2aGFP CTRL+24 h	E189 FRAP1 klein	0.0043	0.00022
	E189 FRAP3 klein	0.0028	0.00018
	E189 FRAP6 klein	0.0022	0.00026
	E189 FRAP7 klein	0.0023	0.00032
	E190 FRAP3 klein	0.0041	0.00028
	E203 FRAP7 klein	0.0028	0.00037
	E203 FRAP11 klein	0.0043	0.00041

protein/mechanical state	name	b*k	b*k error
Dsc2aGFP CTRL+24 h	E207 FRAP1 klein	0.018	0.0051
Dsc2aNG CTRL	E197 FRAP5	0.0051	0.00019
	E197 FRAP7	0.0092	0.0011
	E211 FRAP3	0.0098	0.0010
	E211 FRAP5	0.0064	0.00033
	E211 FRAP8	0.0080	0.00079
	E212 FRAP2	0.0060	0.00023
	E212 FRAP3	0.0025	0.00021
	E212 FRAP8	0.0063	0.00029
	E212 FRAP9	0.0047	0.00023
	E212 FRAP11	0.0037	0.00030
Dsc2aNG stretch	E216 FRAP6	0.0070	0.00042
	E216 FRAP7	0.0072	0.00021
	E216 FRAP8	0.0076	0.00019
	E216 FRAP9	0.0063	0.00022
	E216 FRAP10	0.00619	0.00018
	E217 FRAP4	0.0045	0.00030
	E217 FRAP6	0.0022	0.00029
	E217 FRAP7	0.0033	0.00025
	E217 FRAP8	0.0040	0.00024
	E218 FRAP3	0.0034	0.00027
	E218 FRAP4	0.0023	0.00016
	E218 FRAP5	0.0095	0.00025
	E218 FRAP6	0.0078	0.00036
	E218 FRAP8	0.0036	0.00018
	E218 FRAP9	0.0076	0.00017
	E218 FRAP10	0.0039	0.00016
Dsc2aNG stretch+24 h	E216A FRAP3	0.019	0.0029
	E216A FRAP5	0.0037	0.00029
	E217A FRAP6	0.0050	0.00033
	E218A FRAP1	0.0067	0.00028
	E218A FRAP2	0.0074	0.00028
	E218A FRAP3	0.0036	0.00029

protein/mechanical state	name	b*k	b*k error
Dsc2aNG stretch+24 h	E218A FRAP4	0.0032	0.00029
	E218A FRAP5	0.0078	0.00064
	E218A FRAP6	0.0026	0.00020
	E218A FRAP7	0.0033	0.00025
	E218A FRAP8	0.0020	0.00035
Dsc2aNG CTRL+24 h	E213 FRAP3	0.0023	0.00022
	E213 FRAP4	0.0086	0.00030
	E213 FRAP5	0.011	0.00041
	E213 FRAP7	0.0037	0.00012
	E213 FRAP8	0.0044	0.00020
	E213 FRAP9	0.0066	0.00017
	E215 FRAP5	0.012	0.00076
	E215 FRAP6	0.0039	0.00028
	E215 FRAP1	0.0041	0.00019
	E215 FRAP2	0.012	0.00086
	E215 FRAP3	0.0025	0.00020
PG CTRL	E156 FRAP 1 klein	0.0015	0.00041
	E156 FRAP 3 klein	0.0013	0.00014
	E156 FRAP 4 klein	0.0091	0.0013
	E177 FRAP2 klein	0.018	0.0039
	E179 FRAP1 klein	0.020	0.0015
	E179 FRAP3 klein	0.0074	0.00037
	E204 FRAP1 klein	0.0019	0.00049
PG stretch	E155 FRAP4 klein	0.0099	0.0013
	E169 FRAP4 klein	0.0086	0.00069
	E173 FRAP3 klein	0.0037	0.00039
	E173 FRAP6 klein	0.0048	0.00040
	E173 FRAP7 klein	0.016	0.0014
	E173 FRAP8 klein	0.0093	0.00085
	E176 FRAP3 klein	0.0063	0.00033
	E176 FRAP5 kein	0.013	0.00077
	E176 FRAP7 kein	0.0024	0.00067
	E176 FRAP8 kein	0.0024	0.00059

### XXXIII Appendix

protein/mechanical state	name	b*k	b*k error
PG stretch+24 h	E155A FRAP 3 klein	0.0020	0.00041
	E155A FRAP4 klein	0.0060	0.00068
	E173A FRAP1 klein	0.0028	0.00045
	E173A FRAP2 klein	0.069	0.031
	E176A FRAP1 klein	0.0047	0.00042
	E176A FRAP4 klein	0.10	0.064
	E176A FRAP6 klein	0.0026	0.00026
PG CTRL+24 h	E160 FRAP3 klein	0.0014	0.00044
	E160 FRAP 2 klein	0.0028	0.00021
	E160 FRAP4 klein	0.0041	0.00050
	E160 FRAP 6 klein	0.0066	0.00072
	E174 FRAP4 klein	0.099	0.075
	E174 FRAP6 klein	0.010	0.0042
	E180 FRAP5 klein	0.0029	0.00026
	E180 FRAP6 klein	0.0045	0.00030

### **Calibration elastomer chamber**

For the calibration of the elastomer chambers, fluorescent beads (FluoSpheres 540/560, carboxillated, 100 nm from Invitrogen) were physiosorbed to the surface in the area designated for cell seeding. Their displacement was then measured during the gradual stretching of the elastomer chambers (figure 17). For this purpose, the beads were first sonicated for 5 min at 4°C. Afterwards, 0.5 µl beads were added to 500 µl PBS and applied onto the area designated for cell seeding. The surface was incubated for 1.5 h at room temperature. Afterwards, the surface was washed thrice with ultrapure water. The calibration was carried out immediately at an upright microscope with an EC Plan-Neofluar 5x/0.16 M27 objective. For analysis, the institute's internal Matlab program AffineBeadsTracking (R2021b) was used (software development Dr. R. Springer).

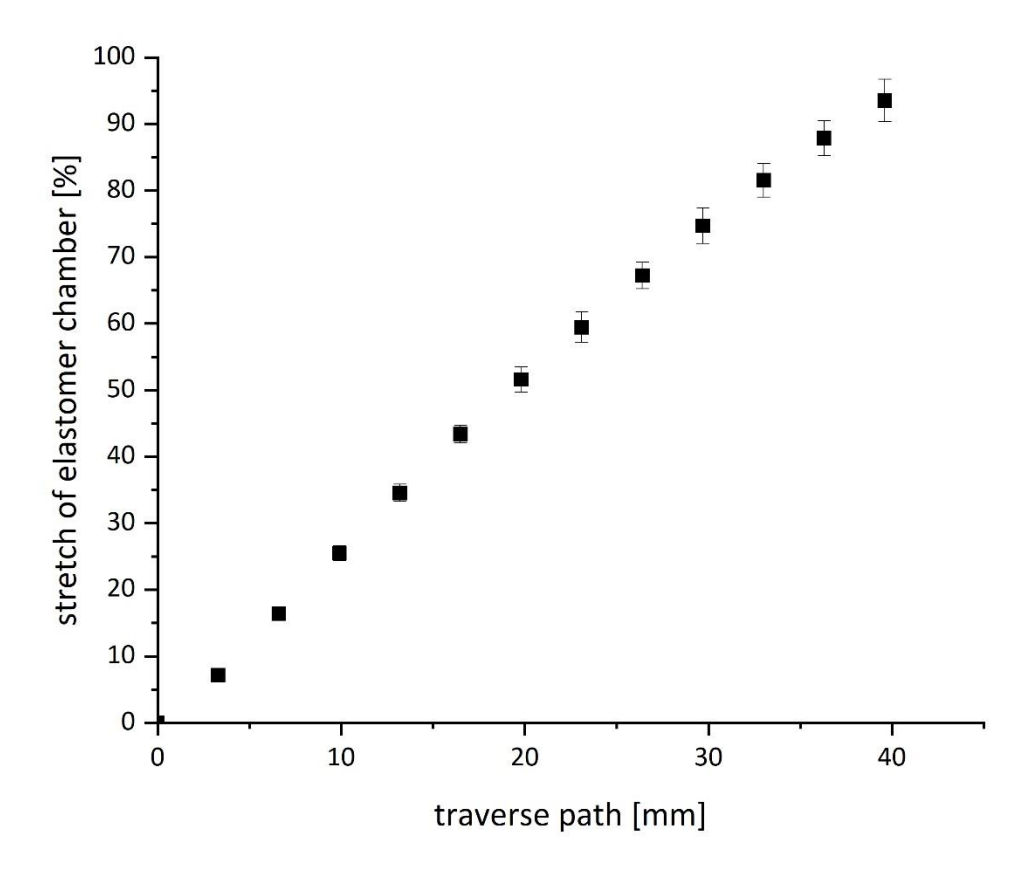


Figure 17: Calibration of the elastomer chambers (see section 3.2.1 for more details). The traverse path was covered in 3.3 mm increments.